

1. Report No. FHWA/TX-84/04+257-1F		2. Government Accession No.		3. Recipient's Catalog No.	
4. Title and Subtitle INTEGRITY EVALUATION OF DRILLED PIERS BY STRESS WAVES				5. Report Date January 1984	
				6. Performing Organization Code	
7. Author(s) A. Scot Harrell and Kenneth H. Stokoe II				8. Performing Organization Report No. Research Report 257-1F	
9. Performing Organization Name and Address Center for Transportation Research The University of Texas at Austin Austin, Texas 78712-1075				10. Work Unit No.	
				11. Contract or Grant No. Research Study 3-5-80-257	
12. Sponsoring Agency Name and Address Texas State Department of Highways and Public Transportation; Transportation Planning Division P. O. Box 5051 Austin, Texas 78763				13. Type of Report and Period Covered Final	
				14. Sponsoring Agency Code	
15. Supplementary Notes Study conducted in cooperation with the U. S. Department of Transportation, Federal Highway Administration Research Study Title: "Evaluation of Drilled Shaft Integrity by Stress Waves"					
16. Abstract The theory of elastic wave propagation in solid rods is presented in terms of using elastic waves to evaluate the integrity of drilled piers. Equipment and instrumentation as well as experimentally determined advantages and disadvantages of previously established wave propagation methods used to evaluate the integrity of drilled piers are also discussed. Recent advancements in recording equipment are examined, particularly digital recording equipment. Measurements with receivers embedded in piers were conducted on previously constructed piers near Granger, Texas, to assess the use of new digital recording equipment. Four drilled piers were constructed and tested in Houston, Texas; one sound pier and three with planned defects. These tests were designed to study the effects of the cross-sectional area of the defect on wave propagation measurements. Wave propagation measurements were performed on the piers in Houston with both surface and embedded receivers. In addition, various sources and receivers were used. Analyses of the time-domain measurements are presented, and wave velocity and reflected wave arrival assessments are emphasized. Finally, analyses of wave attenuation in sound and defective drilled piers are presented and shown to be an important parameter in detecting defective piers.					
17. Key Words compression waves, compression wave velocity, source, receiver, wave propagation with embedded receiver (WAPER), attenuation, direct wave arrival			18. Distribution Statement No restrictions. This document is available to the public through the National Technical Information Service, Springfield, Virginia 22161.		
19. Security Classif. (of this report) Unclassified		20. Security Classif. (of this page) Unclassified		21. No. of Pages	22. Price

INTEGRITY EVALUATION OF DRILLED PIERS BY STRESS WAVES

by

A. Scot Harrell
Kenneth H. Stokoe, II

Research Report Number 257-1F

Evaluation of Drilled Shaft Integrity by Stress Waves
Research Project 3-5-80-257

conducted for

Texas Department of Highways
and Public Transportation

in cooperation with the
U.S. Department of Transportation
Federal Highway Administration

by the

Center for Transportation Research
Bureau of Engineering Research
The University of Texas at Austin

January 1984

The contents of this report reflect the views of the authors, who are responsible for the facts and the accuracy of the data presented herein. The contents do not necessarily reflect the official views or policies of the Federal Highway Administration. This report does not constitute a standard, specification, or regulation.

There was no invention or discovery conceived or first actually reduced to practice in the course of or under this contract, including any art, method, process, machine, manufacture, design or composition of matter, or any new and useful improvement thereof, or any variety of plant which is or may be patentable under the patent laws of the United States of America or any foreign country.

PREFACE

This report summarizes the results of an experimental study to evaluate the use of the stress wave propagation method in the verification of shaft integrity and identification of defects in shafts.

The project was conducted at the Center for Transportation Research, Research Program sponsored by the Texas State Department of Highways and Public Transportation (TSDHPT) and the Federal Highway Administration.

Special appreciation is due H.D. Butler of TSDHPT, Glyen Farmer of Farmer Foundation Co., and J. Scott Heisey, Richard Hoar and Jimmy Allen of the University of Texas for their assistance concerning this project.

A. Scot Harrell

Kenneth H. Stokoe, II

ABSTRACT

The theory of elastic wave propagation in solid rods is presented in terms of using elastic waves to evaluate the integrity of drilled piers. Equipment and instrumentation as well as experimentally determined advantages and disadvantages of previously established wave propagation methods used to evaluate the integrity of drilled piers are also discussed. Recent advancements in recording equipment are examined, particularly digital recording equipment. Measurements with receivers embedded in piers were conducted on previously constructed piers near Granger, Texas, to assess the use of new digital recording equipment. Four drilled piers were constructed and tested in Houston, Texas; one sound pier and three with planned defects. These tests were designed to study the effects of the cross-sectional area of the defect on wave propagation measurements. Wave propagation measurements were performed on the piers in Houston with both surface and embedded receivers. In addition, various sources and receivers were used. Analyses of the time-domain measurements are presented, and wave velocity and reflected wave arrival assessments are emphasized. Finally, analyses of wave attenuation in sound and defective drilled piers is presented and shown to be an important parameter in detecting defective piers.

KEYWORDS: Compression waves, compression wave velocity, source, receiver, wave propagation with embedded receiver (WAPER), wave propagation with surface receiver (WAPS), attenuation, direct wave arrival, reflected wave arrival, interval travel time

SUMMARY

The use of wave propagation methods to evaluate the integrity of drilled piers was studied experimentally. Wave propagation methods generally involve assessing travel time and amplitudes of direct and reflected compression waves. Test methods investigated in this study included wave-propagation-with-embedded-receivers (WAPER) and wave-propagation-with-surface-receivers (WAPS) methods. These wave propagation methods were used to investigate both sound and defective drilled piers at two sites in Texas. Initially, WAPER tests were performed on drilled piers constructed at a site near Granger, Texas. The piers, one having no planned defects and two implanted with various irregularities, were constructed and instrumented by Arias (1977) as part of a previous research project. Primary goals of this series of tests were to confirm the previously reported results and to evaluate new recording equipment. The results showed that both wave propagation methods, WAPS and WAPER, could be used successfully to evaluate the integrity of drilled piers. Comparisons of previous test records with those obtained from this series of tests show that the digital oscilloscope is clearly superior to analog oscilloscopes as a recording/analyzing device, particularly in the areas of waveform resolution and data manipulation.

Wave propagation measurements were also performed on test piers constructed at a site in Houston, Texas. Four test piers were constructed at this site, three of which were implanted with defects consisting of soil inclusions of varying cross-sectional areas. Primary goals of this study were to evaluate further new equipment (monitoring instruments, sources, and receivers) and to investigate the effects of the cross-sectional area of the

defect on wave propagation measurements. Results of these measurements again confirmed the ability to assess drilled pier integrity using wave propagation methods. Both test methods (WAPER and WAPS) provided conclusive data on pier integrity, although the WAPER method provided information necessary for assessment of defect characteristics. In addition, the surface receiver method suffered from surface wave noise present at the top of the pier and problems associated with filtering of this noise. Velocity transducers performed well as embedded receivers, although ceramics transducers also yielded conclusive data and warrant further research. The surface source configuration utilizing a hand sledge and embedded nail consistently provided a clear wave signature when compared to drop-hammer and stud-gun sources. Use of multiple receivers in the WAPER method provides a clearer picture of direct and reflected wave propagation and allows study of wave attenuation, an important variable when reflected wave arrivals are indistinguishable in recorded wave output.

IMPLEMENTATION STATEMENT

Wave propagation methods, utilizing both embedded and surface receivers, have been further shown to be effective techniques in assessing drilled pier integrity. The methods are easily implemented in the field, quick to perform, and relatively inexpensive aside from the initial cost of the recording equipment. However, although the theory of wave propagation is quite simple and the field technique inelaborate, well-trained, conscientious field personnel are required to obtain useful field data for successful interpretation at a later date.

In this study the following observations were made. The digital oscilloscope was found to be a far superior recording device relative to the analog storage oscilloscope used in previous investigations. Advantages of the digital oscilloscope include: high resolution of wave signatures; easy interpretation of identified wave arrivals for velocity and boundary location computations; ability to show pre-trigger information; ability to show waveforms with digital scale expansion; ability to superimpose waveforms; and, magnetic disk recording capabilities for compact, lightweight ease of data storage. To generate compression waves, impact-type hammers proved most suitable for the techniques utilized, with the hand sledge and embedded nail configuration repeatedly providing excellent wave signatures. Vertical velocity transducers are still considered the optimum choice for embedded receivers while accelerometers are the best choice for surface receivers.

Of the two techniques tested, the wave-propagation-with-embedded-receivers (WAPER) method is clearly the best suited for definitively

assessing drilled pier integrity. The WAPER method, utilizing two or more embedded receivers, provides an abundance of wave propagation parameters (such as wave velocity, reflected wave arrivals, and wave attenuation) that allow a more precise assessment of drilled pier integrity. Conversely, the wave-propagation-with-surface-receiver (WAPS) method, while successfully detecting some pier defects, has several inherent disadvantages that limit the use of this technique. It is, therefore, the opinion of the authors that the WAPS method only be used to supplement the WAPER method in testing large numbers of piers, or to test previously constructed piers suspected of being defective.

With regard to wave propagation tests performed on the four test piers constructed in Houston, it was concluded that a defect on the order of 20 to 25 percent of the cross-sectional area of the pier may go undected by assessing wave excitation records solely for reflected waves. In these instances, a study of wave amplitude attenuation can prove extremely valuable in evaluating pier integrity.

Further research should be performed to investigate the frequency content and response of reflected stress waves propagating in the drilled pier. By performing a frequency analysis of the recorded waveform, revealing information regarding pier integrity may be extracted from the data that was not apparent from the time domain representation of the signal.

TABLE OF CONTENTS

PREFACE	iii
ABSTRACT	v
SUMMARY	vii
IMPLEMENTATION STATEMENT	ix
CHAPTER 1. INTRODUCTION	1
CHAPTER 2. ELASTIC WAVE PROPAGATION THEORY	
Introduction	5
Wave Propagation Theory	5
Wave Equation	5
Rods in Longitudinal Vibration	6
Boundary Conditions	9
Experimental Investigations	14
Summary	16
CHAPTER 3. WAVE PROPAGATION METHODS APPLIED TO EVALUATING DRILLED PIER INTEGRITY	
Introduction	17
Wave Propagation Method	17
Background	17
Wave Propagation Method with Embedded Receivers (WAPER)	18
Velocity Measurements with Embedded Receivers	21
Wave Propagation Method with Surface Receivers (WAPS)	27
Wave Propagation Measurements	33
Initial and Reflected Wave Arrivals	33
Non-Defective Drilled Piers	33
Summary	45

CHAPTER 4. WAVE GENERATION AND MEASUREMENT EQUIPMENT

Introduction	49
Recording Equipment	49
Receivers	55
Embedded Receivers	55
Surface Receivers	57
Sources	58
Triggering Systems	60
Filters	62

CHAPTER 5. DESIGN CONSIDERATIONS AND PIER CONSTRUCTION

Introduction	67
Discussion	68
First Test Site Near Granger, Texas	69
Second Test Site; Houston, Texas	77
Number and Dimensions of Piers	79
Construction Materials	80
Planned Irregularities	81
Instrumentation	88
Subsurface Stratigraphy	93
Pier Construction	93
Summary	94

CHAPTER 6. WAVE PROPAGATION ON SOUND DRILLED PIERS

Introduction	115
Wave Propagation Using Embedded Receivers (WAPER Method)	115
Direct Wave Arrivals	115
Reflected Wave Arrivals	126
Receivers	133
Wave Propagation Using Surface Receivers (WAPS Method)	145
Accelerometer Receiver	146
Velocity Transducer Receiver	150
Wave Attenuation	150
Theory	150
Measurements	154
Sources	168
WAPER Tests	168
Summary	173

CHAPTER 7. MEASUREMENTS ON DEFECTIVE PIERS

Introduction	175
Time Domain Measurements at Granger Site	175
Time Domain Measurements at Houston Site	183
Shaft B	183
Shaft C	205
Shaft D	234
Summary	255
CHAPTER 8. Conclusions	259
REFERENCES	265

CHAPTER 1. INTRODUCTION

The use of drilled pier foundations for the support of buildings and bridges has become widespread within the last century, due in part to the growth in population and advancements in construction equipment. Lack of space in larger cities has created the need for the construction of higher and, consequently, heavier buildings. Over the years, high capacity drilled pier foundations have been used with increasing frequency, especially when settlement design considerations require that the heavy structure be supported on deep hard soils or bedrock. In regard to the transportation industry, the growth in population has spawned new cities and towns, creating the need for a larger network of interconnecting highways. Along with the growth in cities comes an increase in undesirable highway routes, resulting in an increased necessity for highway bridges and, consequently, for drilled pier foundations.

Unfortunately, along with the increased use of drilled piers and the complicated soil and groundwater conditions often encountered during their construction comes an uncertainty concerning the integrity of the structural members. Various papers and articles (Feld, 1968; Baker and Khan, 1971; Reese, 1976; Reese and Wright, 1977) have been written acknowledging that the presence of defects or irregularities within drilled piers may be detrimental to the performance of the foundation system. In their paper on drilled pier construction, Baker and Khan (1971) present a list of twelve conditions that may lead to defective drilled piers, these being:

- (1) Excess water at cold joints resulting in weak concrete;
- (2) Migration of water, washing out of cement, or segregation resulting in weak concrete at the top of the shaft;
- (3) Side cave-in of soil resulting in contaminated concrete;
- (4) Surface cave-in of soil resulting in contaminated concrete;
- (5) Development of voids in the shaft;
- (6) Casing collapse;
- (7) Improperly poured tremie concrete;
- (8) Concrete poured into surface water;
- (9) Inadequate bell sizes;
- (10) Inadequate bearing material;
- (11) Squeeze in or necking of the shaft, and
- (12) Poor concrete delivered to the site.

Ten of the twelve conditions listed above are related to field construction practices, greatly increasing the chances of one or more occurring at some point during the foundation construction sequence. Due to the uncertainty often surrounding drilled pier integrity, an economical, reliable test method is needed whereby the structural soundness of a pier may be determined in situ, with minimal interference with normal construction operations.

In the recent past, several nondestructive methods (meaning to test without jeopardizing structural performance) have been developed and used to evaluate the structural integrity of drilled piers. These methods include coring and percussive drilling, borehole camera inspection, caliper logging and acoustic recordings, sonics, nuclear radiation (gamma ray transmission and neutron backscatter), shaft prestressing and compression, vibration testing, and stress wave propagation (Gardner and Moses, 1973; Mitchell, 1973; Whitaker, 1974; Davis and Dunn, 1974; Steinbach and Vey, 1975;

Robertson, 1976; Davis and Robertson, 1976; Arias, 1977; Preiss, et al, 1978; van Koten and Middendorp, 1978; Hearne, et al, 1981).

An excellent literature survey and detailed discussion of many of the methods listed above is presented in Arias` (1977) report. To substantiate the findings of his survey, Arias constructed three test piers, one sound and two defective, and performed integrity evaluation experiments on the piers utilizing the more promising techniques (in terms of reported effectiveness and economics). Based on his experiments, Arias singled out two methods that he deemed overall superior to the others in assessing drilled pier integrity. Referred to in his report as the TNO basic method and the Direct Arrival-Reflection method, both require the assessment of stress wave propagation methods in evaluating drilled pier integrity. Each method employs the same basic equipment, is quick to perform, and is relatively inexpensive aside from the initial one-time cost of the recording equipment.

Unfortunately, the TNO basic method only provides a quantitative evaluation of overall cast in situ pile integrity, due to the use of a surface receiver. Detection of waveform displacements other than those resulting from reflected wave energy off the pile bottom indicate possible defects, but no conclusions can be drawn from the wave signature regarding defect characteristics. Furthermore, this method would likely not detect a defect such as weak concrete at the base of the pile caused by placing the concrete in water.

Conversely, the Direct Arrival-Reflection method shows promise not only in detecting pier defects, but also in providing insight into the characteristics of the defect, such as nature and overall magnitude. Arias provided proof of the significance of this method in his experiments on defective test piers. However, several important questions remained

unresolved in Arias` study, and further research was recommended to improve current test equipment and enhance recorded stress waves.

Therefore, in an attempt to discover new applications and improve upon this promising method of evaluating drilled pier integrity, a research program was initiated in the Center for Transportation Research at The University of Texas at Austin. The following sections of this report present the findings of this study. Because the technique requires an understanding of stress wave propagation, theoretical considerations of wave propagation are discussed in Chapter 2. The general mechanics of wave propagation as they relate to drilled pier evaluation are then presented in Chapter 3, along with descriptions of test equipment and field testing techniques. Equipment advancements and modifications are examined in Chapter 4, and the construction and instrumentation of additional test piers at a site in Houston are described in detail in Chapter 5. Results and interpretations of field experiments conducted at both sites are presented in Chapters 6 and 7. Finally, conclusions and recommendations for further study are given.

CHAPTER 2. ELASTIC WAVE PROPAGATION THEORY

INTRODUCTION

Stress wave propagation methods of evaluating drilled pier integrity are based on the theory of waves propagating in elastic solids. The theory concerning wave propagation in an elastic media was developed during the last century by Stokes, Rayleigh, Kelvin and others as an extension of the theory of elasticity applied to the problem of vibrating systems. In this chapter, wave propagation theory developed by these and other investigators is presented. Boundary conditions are imposed on the theoretical solution to allow application of the theory to methods of drilled pier evaluation. Finally, experimental evidence is provided supporting the wave propagation concepts.

WAVE PROPAGATION THEORY

Wave Equation.

The partial differential equation governing wave propagation in a bounded elastic medium, referred to as the wave equation, may be expressed as follows:

$$\frac{\partial^2 \mathbf{u}}{\partial t^2} = v^2 \left(\frac{\partial^2 \mathbf{u}}{\partial x^2} \right) \quad (2.1)$$

where

- u = displacement in the x-direction,
- v = wave propagation velocity,
- x = horizontal distance, and
- t = time.

In the discipline of mechanics, a variety of vibrating systems are mathematically represented by the wave equation. Examples of such systems include solid rods in longitudinal and torsional vibration and pressure waves in an ideal fluid along the container axis [Richart et al (1970)]. In this study, discussion of theoretical considerations is limited to solid rods, due to their physical similarities with drilled piers.

Rods in Longitudinal Vibration.

Wave propagation in cylindrical elastic media was initially investigated by Pochhammer (1876) [Love (1944)] and by Chree (1886). The formulas and concepts derived from their theoretical studies are the basis for wave propagation methods of evaluating drilled pier integrity. For purposes of comparison with the structural member under investigation, consider the theoretical case of an infinite elastic rod of cross-sectional area, A , and Young's Modulus, E , as shown in Fig. 2.1. The elastic rod may experience three independent types of vibration: longitudinal, torsional, and flexural. Of the three types of vibration, only longitudinal and torsional motions resolve mathematically to the wave equation. Because only longitudinal motion was employed in this drilled pier study, only longitudinal vibration of the rod is treated in the theoretical discussion.

If the stress acting on plane Q in Fig. 2.1 is σ_x , then the stress acting on plane R is $\sigma_x + (\partial u_x / \partial x) \Delta x$ for the rod under free longitudinal

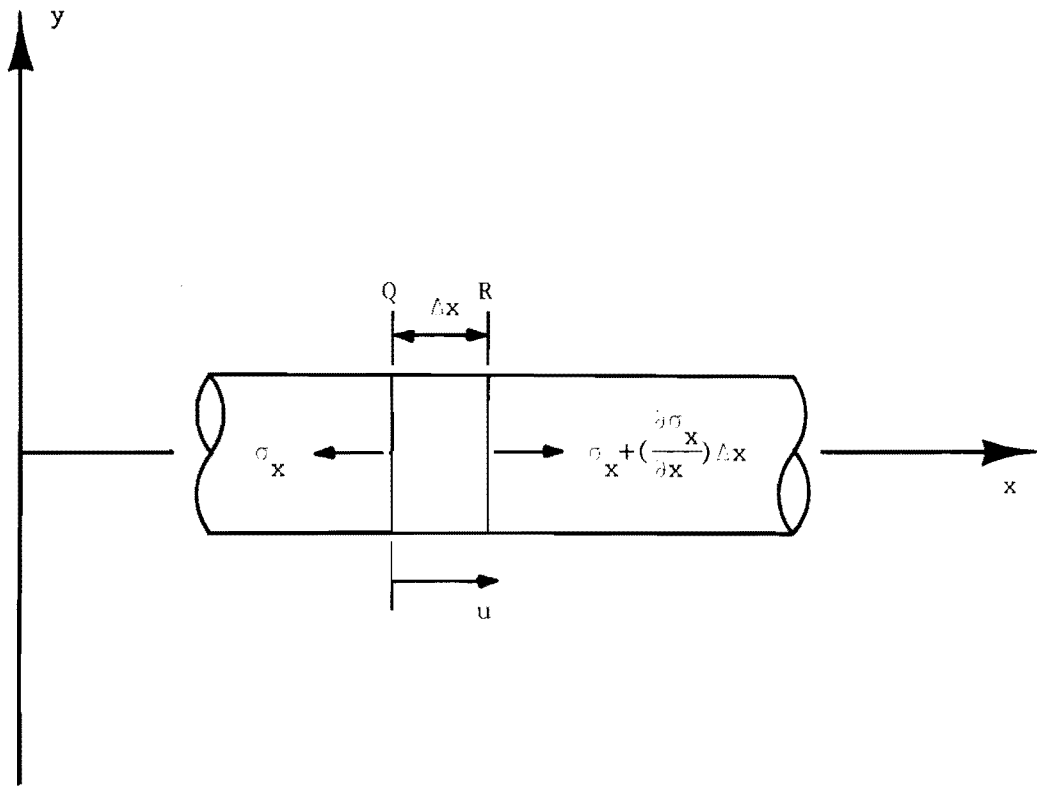


Fig. 2.1. Forces acting on an element of a rod undergoing longitudinal vibration.

vibration. For a longitudinal displacement of u in the x -direction, Newton's second law of motion results in:

$$\rho A \Delta x (\partial^2 u / \partial t^2) = A (\partial u_x / \partial x) \Delta x \quad (2.2)$$

where

- ρ = mass density of rod material ($\rho = \gamma / g$),
- γ = unit weight of rod material,
- g = acceleration of gravity (32.2 ft/sec^2), and
- Δx = incremental length along the rod.

However, Young's modulus is equivalent to the ratio between the stress σ_x and the strain $\partial u / \partial x$ in the rod element, and Equation 2.2 may therefore be rewritten as:

$$\rho (\partial^2 u / \partial t^2) = E (\partial^2 u / \partial x^2) \quad (2.3)$$

The above expression is of the same form as the wave equation (Eq. 2.1) with:

$$v_c^2 = E / \rho \quad (2.4)$$

In Eq. 2.4, v_c is defined as the propagation velocity of a longitudinal wave in the elastic rod. The longitudinal wave is also the compression wave or P-wave. The compression wave velocity primarily depends on the material properties through which the P-wave is travelling and is a fundamental value in stress wave propagation methods of evaluating drilled pier integrity.

The solution to the wave equation developed for the infinite elastic rod (Eq. 2.3) may be written in the form:

$$u = f(v_c t + x) + h(v_c t - x) \quad (2.5)$$

where f and h are arbitrary functions depending on the initial boundary conditions (Timoshenko and Goodier, 1934). Equation 2.5 mathematically represents the displacement resulting from stress waves propagating in an elastic rod at constant velocity v_c . It can be shown that the first term on the right side of Eq. 2.5 represents a tensile stress wave travelling in the negative x -direction and the second term on the right represents a compressive stress wave travelling in the positive x -direction.

To derive the general solution of Eq. 2.5, it was assumed that plane transverse sections of the rod remain plane during passage of the stress wave. In addition, it was assumed that the stress acts uniformly over the area, implying that inertia forces caused by lateral motions of particles can be neglected. These limiting assumptions render the general solution approximate, but accurate results may be obtained provided the wavelength of the longitudinal wave is large compared with the cross-sectional dimensions of the rod.

Boundary Conditions.

The theory developed thus far is based on the wave equation describing the propagation of stress waves in infinite elastic rods. However, drilled piers have finite lengths. Therefore, to apply the wave equation theory to the study of drilled piers, boundary conditions must be imposed on the general solution.

When an elastic rod of finite length is subjected to an impulse at one end, a stress wave is generated that travels the length of the rod at the velocity of v_c . Upon arrival at the end of the rod, the stress wave is reflected, with the nature of the wave reflection dependent on conditions at the end of the rod. Kolsky (1963) presents a theoretical study of wave propagation in finite rods, applying various boundary conditions to the wave equation (Eq. 2.3).

Consider the case of a pulse reaching the free end of an elastic rod. For free-end conditions, the appropriate boundary condition is to assume no normal stress is present at the end of the rod. If the displacement due to the incident wave is represented by:

$$u_1 = f(v_c t + x) \quad (2.6)$$

and that due to the reflection wave is:

$$u_2 = h(v_c t - x) \quad (2.7)$$

the stresses produced by the two waves will be $E(\partial u_1 / \partial x)$ and $E(\partial u_2 / \partial x)$, respectively. The resultant of these stresses will be:

$$E\{(\partial u_1 / \partial x) + (\partial u_2 / \partial x)\} = E\{f'(v_c t + x) - h'(v_c t - x)\} \quad (2.8)$$

By measuring a distance, x , from the end of the rod and satisfying the boundary condition of no normal stress acting on the free end of the rod, Eq. 2.8 becomes:

$$f'(v_c t) - h'(v_c t) = 0 \quad (2.9)$$

Equation 2.9 mathematically states that the shape of the reflected wave is the same as that of incident wave but is of the opposite sign. In other words, a compression wave will be reflected from the free end of a rod as a tension wave of identical magnitude and shape. Similarly, a tension wave propagating in an elastic rod will be reflected from a free end as a compression wave of the same magnitude and shape. Wave reflection in an elastic rod with free-end conditions is illustrated in Fig. 2.2.

By a similar analysis, it can be shown that the total displacement at the end of a rod is given by:

$$u_1 + u_2 = f(v_c t + x) + h(v_c t - x) \quad (2.10)$$

For a stress wave reflected at the fixed end of an elastic rod, the appropriate boundary condition is that the displacement is zero at x equal 0. Applying the boundary condition to Eq. 2.10 reveals that the displacement of the reflected wave is equal and opposite to the displacement of the incident wave, and $E(\partial u_1 / \partial x)$ is now equal to $E(\partial u_2 / \partial x)$. Therefore, a stress wave, either tension or compression, is reflected from the fixed end of a rod unaltered, experiencing only a reversal in direction of propagation, as illustrated in Fig. 2.3.

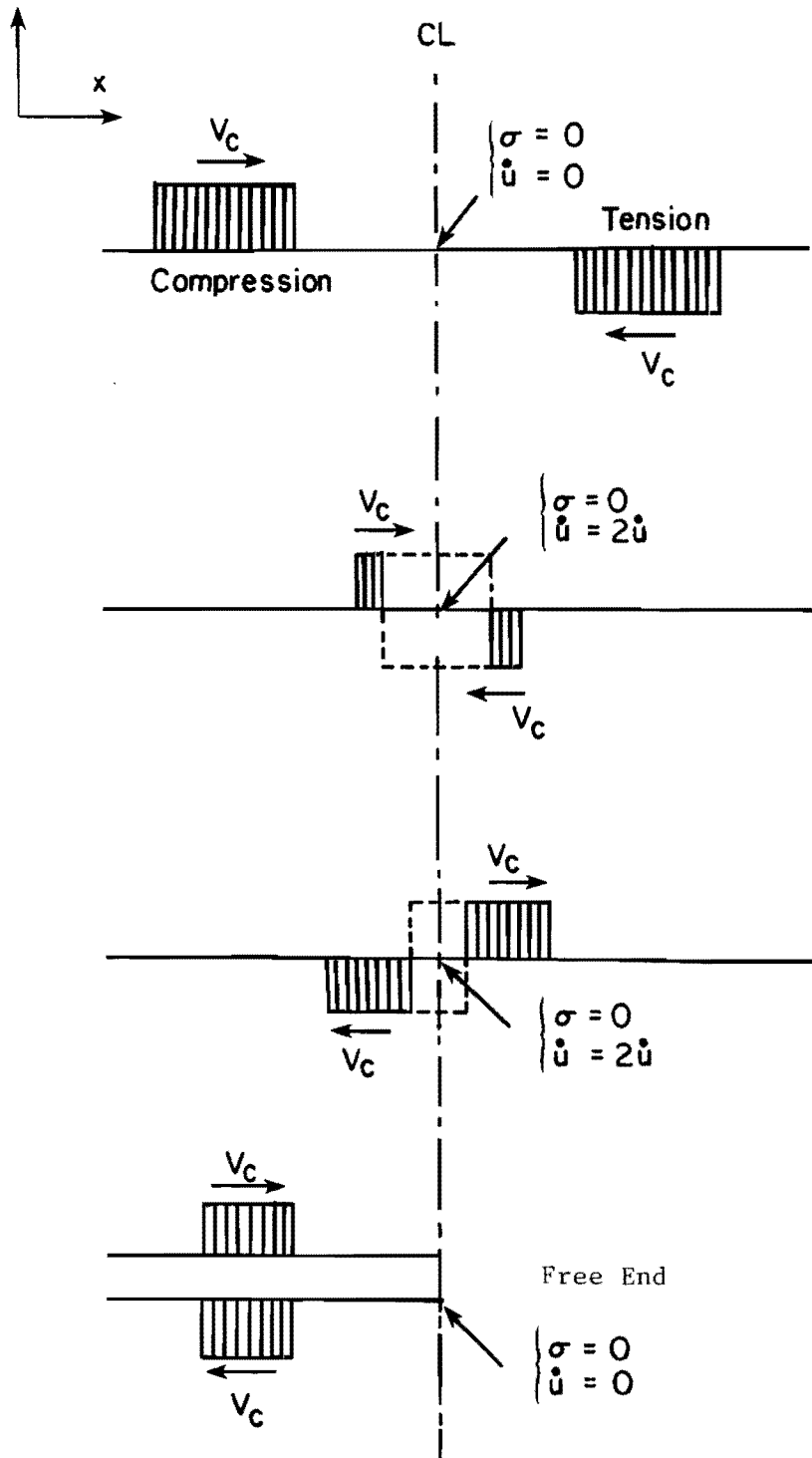


Fig. 2.2. Elastic waves in a rod illustrating a free-end condition.

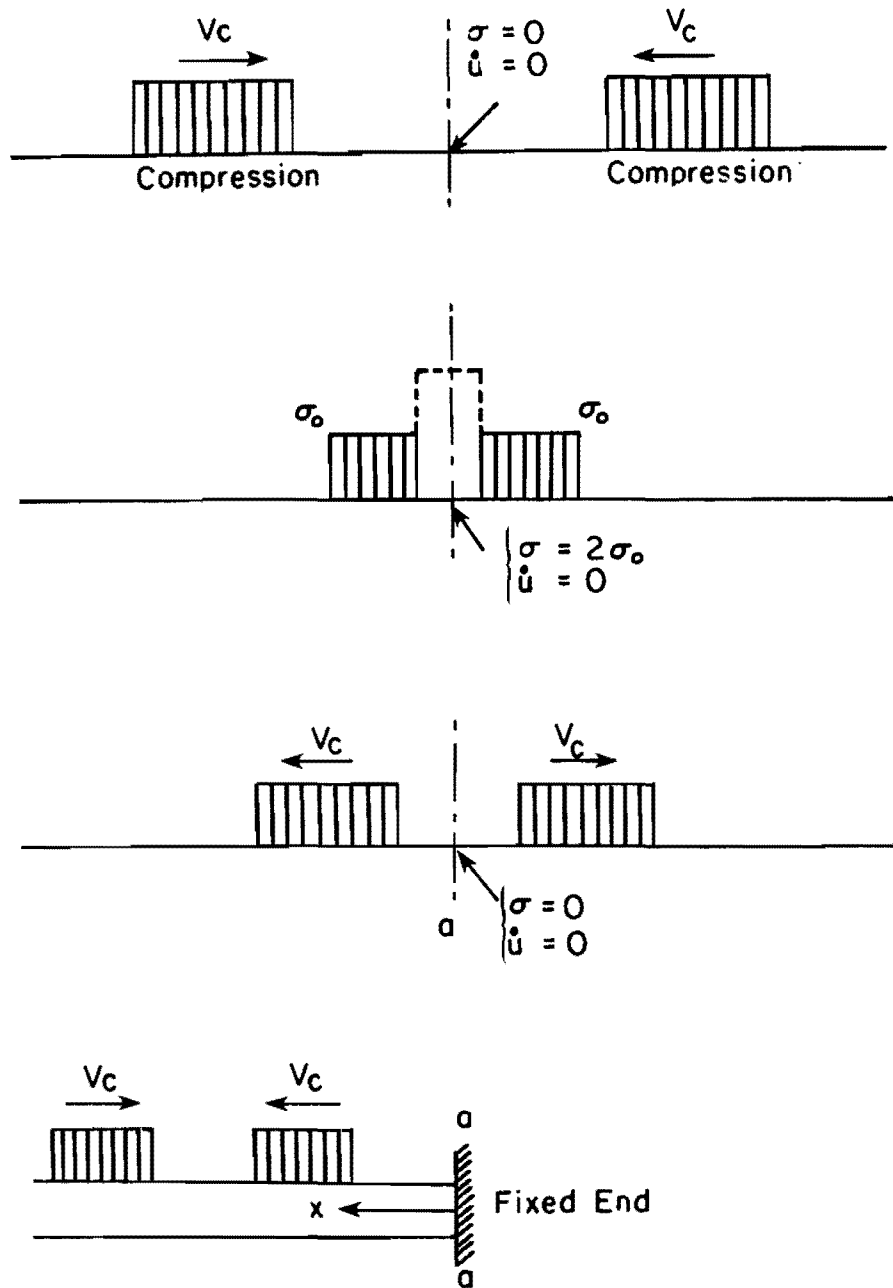


Fig. 2.3. Elastic waves in a rod illustrating a fixed-end condition.

In wave propagation methods used to evaluate the integrity of drilled piers, the ends of the drilled piers are considered free boundaries. Therefore, from theory, a compression wave propagating through the pier should be reflected as a tensile wave at the appropriate shaft interfaces. However, the magnitude of the reflected wave at the embedded end of the pier should not remain unchanged, as predicted in wave propagation theory. This difference in reflected wave magnitude experienced in practice is discussed in greater detail in Chapter 6.

EXPERIMENTAL INVESTIGATIONS

Although theoretical investigations concerning the propagation of stress waves in elastic solids date back to the end of the nineteenth century, it was only comparatively recently that technology became sophisticated enough to allow comparisons between experimental evidence and theory.

In 1940, Shear and Focke performed ultrasonic velocity and wavelength measurements on polycrystalline silver, nickel, and magnesium cylinders dusted with lycopodium powder. The wavelength was determined by direct measurement of the standing wave pattern produced on the coated rods at resonance. By knowing the excitation frequency and resulting wavelength, it was possible to compute the phase velocity in the cylinders. Shear and Focke concluded that the theoretical solution was sufficiently accurate for prediction of material velocities, provided that the wavelength of the stress wave is several times greater than the diameter of the rod.

Further evidence supporting the accuracy of the theoretical solution of stress wave propagation was provided by Davies (1948). Davies devised a pressure bar similar in principle to the Hopkinson bar, whereby continuous electronic measurements could be recorded of the longitudinal displacement

produced by a pressure pulse at the free end of a cylindrical bar. Davies concluded from his experiments that the velocities predicted in theory were in excellent agreement with velocities measured in the pressure bar.

Steinbach and Vey (1975) conducted a similar laboratory investigation employing a measuring system closely resembling the set-up used in this drilled pier study. By performing tests on a 31.5 in. (80 cm) long aluminum bar that was freely suspended horizontally, Steinbach and Vey found that the velocity predicted in theory was approximately four percent greater than the velocity measured in the aluminum bar. Although the authors provide no explanation for this difference, one possible reason is the high frequencies associated with the "hammer" employed as the impulsive source. As previously mentioned, wave propagation theory developed for cylindrical elastic solids is accurate provided the wavelength of the longitudinal wave is several times greater than the diameter of the rod. Early investigators observed that at high frequencies, when the wavelengths become of the same order as the rod diameter, the measured velocities were found to be lower than those predicted from theory. An examination of the oscilloscope record provided in Steinbach and Vey's paper reveals that the stress wave is propagating at a velocity of 16,100 ft/sec (4,907 m/sec) through the 3.75 in. (9.53 cm) diameter aluminum bar and oscillating at a frequency of approximately 20 kHz. The wavelength corresponding to a frequency of this magnitude is 0.8 ft (0.03 m) which results in a wavelength to diameter ratio of approximately 2.6. The wavelength-to-diameter ratio computed from the data provided by Steinbach and Vey is not of the same magnitude as that suggested by the early investigators and could cause some of the difference exhibited in the theoretical and experimentally measured velocities.

SUMMARY

Wave propagation theory, the basis for methods employed in this drilled pier study, mathematically describes the propagation of stress waves through cylindrical elastic solids by use of the wave equation. The theory predicts that compression waves propagate through an elastic solid at a velocity that is a function of the material properties, specifically the mass density and Young's modulus. The behavior of stress waves reflected in finite cylinders, such as drilled piers, can be predicted by applying boundary conditions to the wave equation solution. For plane ends that are free from constraints, the theory predicts that a compression wave will be reflected as a tension wave and a tension wave will be reflected as a compression wave, with the reflected wave remaining unchanged in magnitude and shape. For a fixed-end condition, the incident stress wave remains unaltered in state, magnitude, and shape after reflection at the constrained boundary. Although embedded in soil, drilled pier members more closely represent a free-end condition than a fixed end. However, unlike theory, the embedded condition of the pier alters the magnitude of reflected waves.

Experimental investigations performed on rods of various materials prove the wave propagation theory to be accurate, provided the wavelength of the pulse is several times greater than the cross-sectional dimension of the rod.

CHAPTER 3. WAVE PROPAGATION METHODS APPLIED TO EVALUATING DRILLED PIER INTEGRITY

INTRODUCTION

The theoretical solution derived for the propagation of stress waves in elastic solids has experimentally been shown to be valid for homogeneous, elastic rods. Wave propagation velocities, determined in the laboratory on cylindrical specimens of material that behaved essentially elastically, were found to agree with theoretical values based on material properties. Drilled pier foundations, on the other hand, consist primarily of concrete, a nonhomogeneous construction material. Several inherent properties of concrete, including compressive strength, unit weight, and water/cement ratio, exhibit an influence on the wave propagation velocity. In addition, supplemental construction materials are often present in drilled piers, such as varying amounts of reinforcing steel, which tend to further complicate measurements in this medium. To evaluate the effects of these conditions on records obtained from field measurements, a general understanding is required of stress wave propagation methods as applied to the evaluation of drilled pier integrity.

WAVE PROPAGATION METHOD

Background.

The wave propagation method of evaluating drilled pier integrity principally involves time domain measurements of stress wave arrivals; that is, impulsively induced stress waves propagating vertically through the pier

are monitored by instruments (referred to as receivers) measuring wave amplitude with respect to time. The waveform monitored by each receiver during passage of the stress wave is evaluated visually and analytically for information such as source-to-receiver travel time, propagation velocity, amplitude and attenuation characteristics, frequency content, and wave length. The resulting values of these parameters are used in conjunction with the recorded output to determine arrival times of reflected waves which are used in the detection of possible discontinuities or irregularities present in the drilled pier.

Numerous source-receiver configurations may be employed for collecting wave propagation data. In this study, two source-receiver configurations which have been used with limited success in the past are investigated. The two configurations are classified according to the location of the receivers relative to the pier as: (1) receivers embedded in the pier, and (2) receivers placed on the top surface of the pier. The decision of which configuration to use in practice depends upon the time the pier is instrumented with respect to pier construction. If instrumentation is performed prior to or during drilled pier construction, then embedded receivers can be used. Conversely, tests conducted on previously constructed piers almost always necessitates the use of surface receivers. The uses, advantages and limitations of each method are discussed in the following sections.

Wave Propagation Method with Embedded Receivers(WAPER).

The monitoring of stress waves may be accomplished by placing receivers at known elevations within the drilled pier during construction of the foundation (Hearne, et al, 1981). With receivers mounted at predetermined elevations within the pier, wave propagation velocity can be determined once

the source-to-receiver travel time is measured. A schematic representation of the Wave Propagation with Embedded Receiver (WAPER) method is presented in Fig. 3.1, in which the source-receiver configuration and necessary equipment are illustrated.

Detection instruments which may be used as embedded receivers include displacement transducers, velocity transducers, and accelerometers. Vertical velocity transducers have been utilized as embedded receivers exclusively in the past due to their economic advantage over accelerometers (about \$40 versus \$200). Regardless of which instrument is selected, the receivers must be protected from possible moisture contamination by suitable waterproofing or casing. A sufficient quantity of electrical cable (preferably shielded) must be attached to each receiver to allow transmission of the receiver signal to the recording device located at the top of the pier. The receivers are generally secured at predetermined elevations within the piers by attaching them to the steel reinforcing cage prior to installation of the cage. Steel hose clamps are usually employed to secure the receivers to the reinforcing cage. Verticality of the embedded receivers must be ensured to prevent reduction and distortion of the output signal. The receivers should be shielded from possible extraneous wave energy propagating through the accompanying reinforcing steel, which can present problems in velocity calculations due to the greater propagation of the P-wave velocity in steel compared with concrete. Proper insulation is achieved by placing a suitable dampening material, such as a 1.0 in. (2.5 cm) thick silicon rubber pad, between the reinforcing steel and the attached receiver. A sufficient number of receivers should be placed in the drilled pier for accurate assessment of pier integrity. Although the number of receivers per pier is dependent on such factors as pier length, total number of piers to be constructed, and

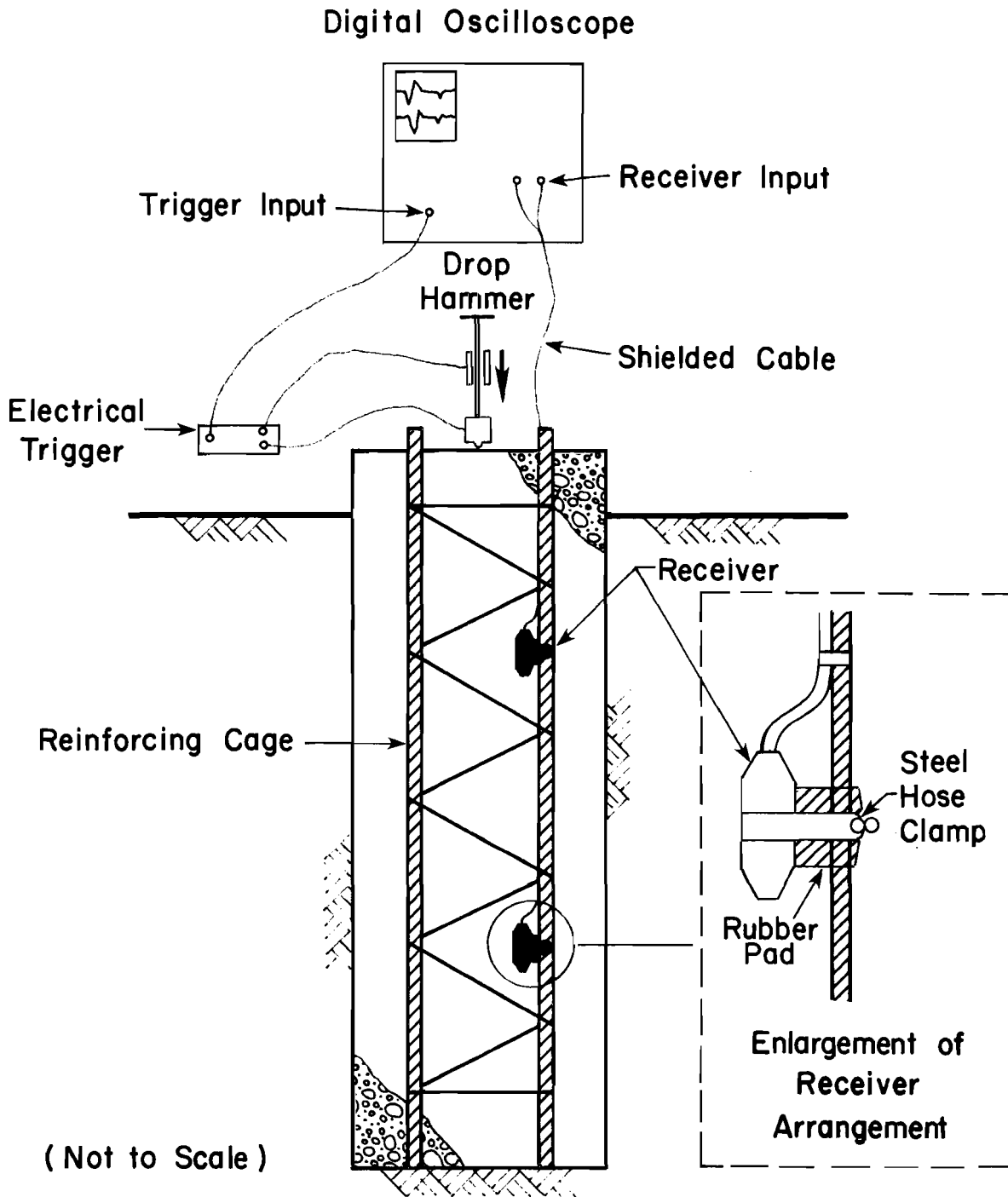


Fig. 3.1. Schematic of wave propagation testing with embedded receivers.

economic considerations, a minimum of two receivers is desirable for comparison of interval travel times and attenuation characteristics of the recorded output.

The compression wave pulse is typically generated by a source located at the top of the drilled pier as illustrated in Fig. 3.1. The surface source configuration is usually employed with the embedded receiver set-up because it is economical and easily accessible. Typical compression wave sources include drop hammers, sledge hammers of various weights, nail-shooting stud guns, and explosive charges.

A time domain record of the embedded receiver output is visually displayed on the viewing screen of a storage or digital oscilloscope located at the top of the pier. The displayed wave signature may be permanently recorded for further evaluation at a later time by equipping the storage oscilloscope with a Polaroid camera or by taking advantage of the magnetic disc recording capabilities associated with the digital oscilloscope. An electrical trigger connecting the source to either oscilloscope is used to activate the oscilloscope recording process. A detailed discussion of the test equipment employed in the WAPER method is provided in Chapter 4.

Velocity Measurements with Embedded Receivers.

At the time of impact or detonation, the surface source triggers the oscilloscope which initiates monitoring of the embedded receiver output. The time required for the resulting compression wave to propagate from the top of the pier down to the monitoring receiver is referred to as the direct travel time. Figure 3.2 illustrates the direct travel times for wave signatures captured during a typical wave propagation measurement performed on a 36 in. (91.4 cm) diameter, 92 ft (28.0 m) long drilled pier instrumented with

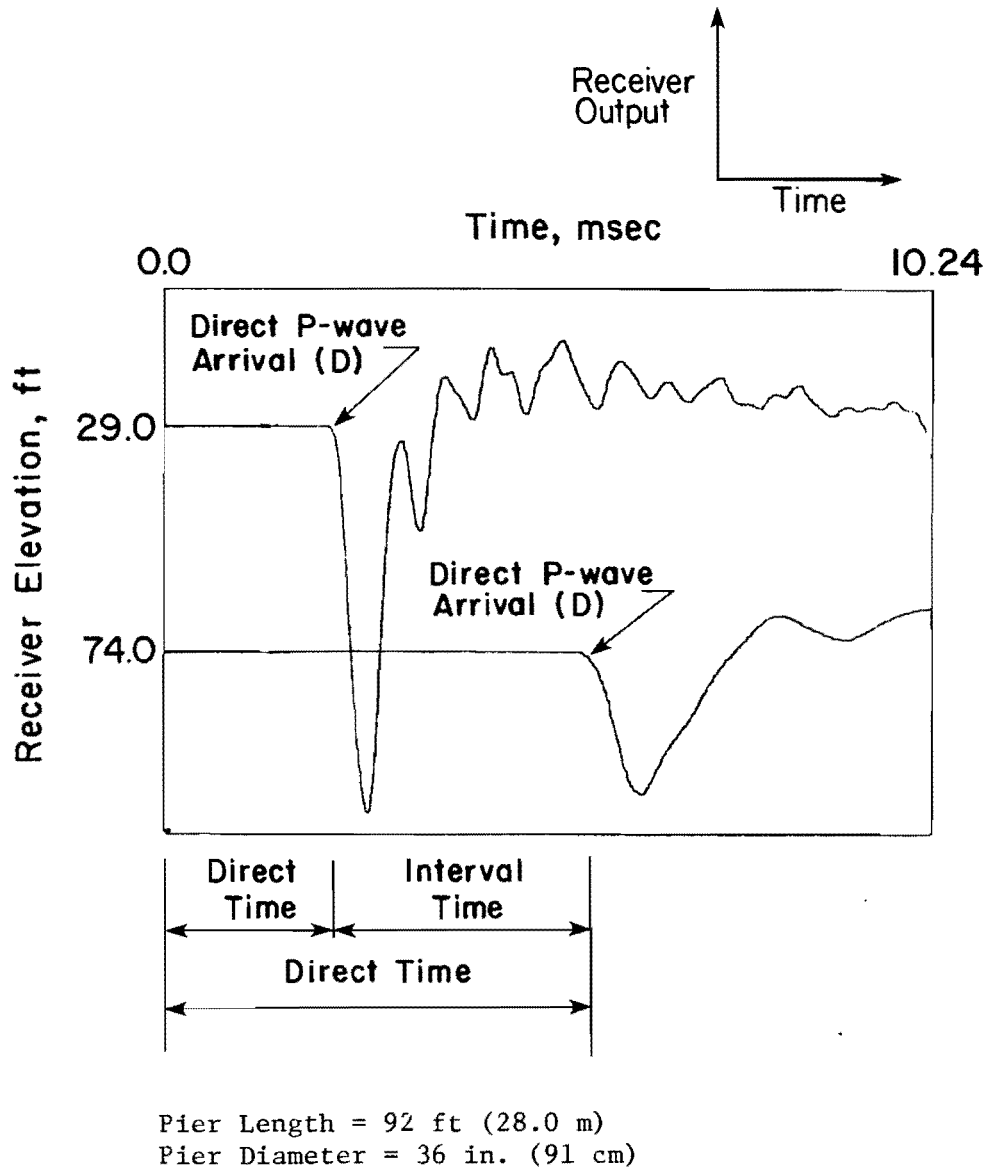


Fig. 3.2. Direct and interval travel times measured in a drilled pier instrumented with embedded receivers.

receivers embedded 29 ft (8.8 m) and 74 ft (22.6 m) below the top of the pier. With the receivers mounted at predetermined elevations within the pier, the direct travel time can be used to determine the compression wave propagation velocity in the following manner:

$$v_c = \frac{\text{travel distance}}{\text{travel time}} \quad (3.1)$$

Equation 3.1 is the fundamental equation of the wave propagation method for determining the elevations of wave reflection points in drilled piers.

With the wave propagation velocity known, Young's modulus (elastic modulus) of the shaft material may be computed by:

$$E = \rho v_c^2 \quad (3.2)$$

where

- E = Young's modulus,
- v_c = P-wave velocity,
- ρ = mass density of shaft material (= γ/g),
- γ = unit weight of shaft material, and
- g = acceleration of gravity (32.2 ft/sec²).

Young's modulus determined by this procedure is the modulus of elasticity at low strain levels. Strain levels resulting from P-waves propagating down piers are typically less than 0.001 percent. As a result, the modulus of elasticity determined by this method represents the maximum value of E, and moduli of elasticity measured at higher strain levels such as those determined in a standard compression test will be much lower.

Evidence of concrete quality may be ascertained from direct velocity measurements made with embedded receivers. Although compression wave velocity cannot be directly related to concrete strength (due to mix design variations), measured P-wave velocity for a given mix design provides a relative indication of concrete quality of the pier. A suggested rating of concrete quality based on P-wave velocity is provided in Table 3.1 (Malhotra, 1976). The rating scale shown in Table 3.1 is based on ultrasonic pulse tests (high frequency tests) which were used to measure P-wave velocity through a concrete medium. Wave propagation velocity in a rod differs from the wave propagation velocity in a continuous medium of an identical material if the wavelength of the pulse is greater than the rod diameter. Since a drilled pier acts like a rod-like structure, in this testing, wave propagation velocity as determined herein will be less than the velocity measured at ultrasonic frequencies, the reduction being approximately ten percent for a Poisson's ratio of 0.25 (Richart, et al, 1970). Therefore, velocities listed in Table 3.1 have been reduced by 10 percent and presented in Table 3.2 so that they can be compared with velocities determined by the methods discussed herein.

For accurate computation of wave velocity utilizing direct travel time, it is essential that triggering of the recording equipment occurs at a known time (hopefully essentially zero time) after the source impulse is applied. A trigger delay of unknown magnitude will result in the calculation of an erroneously high direct velocity, with the magnitude of the error dependent on the extent of the time delay and the depth of the embedded receiver.

One method of eliminating possible triggering problems is to install two or more receivers within the drilled pier and to measure the interval travel time between receivers. Interval travel time is defined as the time required

TABLE 3.1. SUGGESTED COMPRESSION WAVE VELOCITY RATINGS FOR CONCRETE FROM ULTRASONIC TESTS (FROM MALHOTRA, 1976).

Compression Wave Velocity.		General Conditions
ft/sec	m/sec	
Above 15,000	Above 4570	Excellent
12,000 to 15,000	3660 to 4570	Good
10,000 to 12,000	3050 to 3660	Questionable
7,000 to 10,000	2133 to 3050	Poor
Below 7,000	Below 2130	Very Poor

TABLE 3.2. SUGGESTED COMPRESSION WAVE VELOCITY RATINGS FOR CONCRETE FROM WAVE PROPAGATION METHOD*

P-Wave Velocity, fps	E, psi**	General Condition
Above 13,500	5.90	Excellent
10,800 to 13,500	3.77 to 5.90	Good
9,000 to 10,800	2.62 to 3.77	Questionable
6,300 to 9,000	1.28 to 2.62	Poor
Below 6,300	1.28	Very Poor

*Assuming wavelength is greater than two times diameter of pier

**Assuming of concrete equals 150 pcf

for the stress wave to propagate from one receiver to another for the same impulse. For the wave propagation measurements illustrated in Fig. 3.2, the interval travel time is shown as the difference in the initial arrival times of the P-wave at the embedded receivers. For measurements of interval travel times to be relevant, the output of both embedded receivers must be recorded for the same impulse. It is recommended that the receivers be spaced at intervals of 10 ft (3.0 m) or more to minimize the influence of slight variations in interpretations of the initial P-wave arrival.

The impact-type source, such as a drop hammer, generates other types of waves in addition to compression waves. Rayleigh waves, or surface waves, are also produced by the hammer blow, and there is usually no control over the division of input energy among the resulting compression and surface waves. Surface waves produced by the hammer propagate radially outward from the point of impact, with the path of the surface particle motion associated with the Rayleigh wave described as a retrograde ellipse. It can be shown that for the case of an elastic half-space, the amplitude of the Rayleigh waves decreases in proportion to the ratio $1/\sqrt{r}$, where r is the radial surface distance from the impulse (Ewing, Jardetzky, and Press, 1957). Unfortunately, the side of the cylindrical drilled pier acts as a reflection boundary, causing the Rayleigh wave to propagate back and forth across the surface of the pier, creating a "noisy" environment in the near-surface region of the pier.

Rayleigh wave amplitude decreases rapidly with depth in an elastic half-space, with the decrease in magnitude dependent on the wavelength of the surface wave. The length of the surface wave in an elastic medium is dependent on the propagation velocity and the frequency of excitation. This relationship can be expressed as:

$$V_R = f \cdot L_R \quad (3.3)$$

where

V_R = Rayleigh wave velocity,

f = frequency, and

L_R = Rayleigh wavelength.

Figure 3.3 shows theoretical curves representing attenuation of the vertical and horizontal components of Rayleigh wave motion. On the basis of these attenuation curves, it is reasonable to assume that the bulk of the Rayleigh wave travels within a depth of approximately one wavelength of the top of the drilled pier. In his study on drilled pier integrity, Hearne (1984) experimentally observed that the effect of surface waves on wave propagation measurements is most severe in the upper 10 ft (3.1 m) of the pier. Due to the "noisy" environment produced by surface waves in the upper portions of the pier which tend to complicate identification of P-wave arrivals, Hearne recommended that receivers be embedded within the pier at a depth of 10 ft (3.1 m) or more when using this method.

Wave Propagation Method with Surface Receiver (WAPS).

Evaluation of drilled pier integrity by the wave propagation method employing a surface receiver (WAPS) has been used with varying degrees of success in the past (Mitchell, 1973; Steinbach and Vey, 1975; Arias, 1977; Hearne, 1984). The surface receiver method is very similar in principle to the wave propagation method utilizing embedded receivers. The procedures

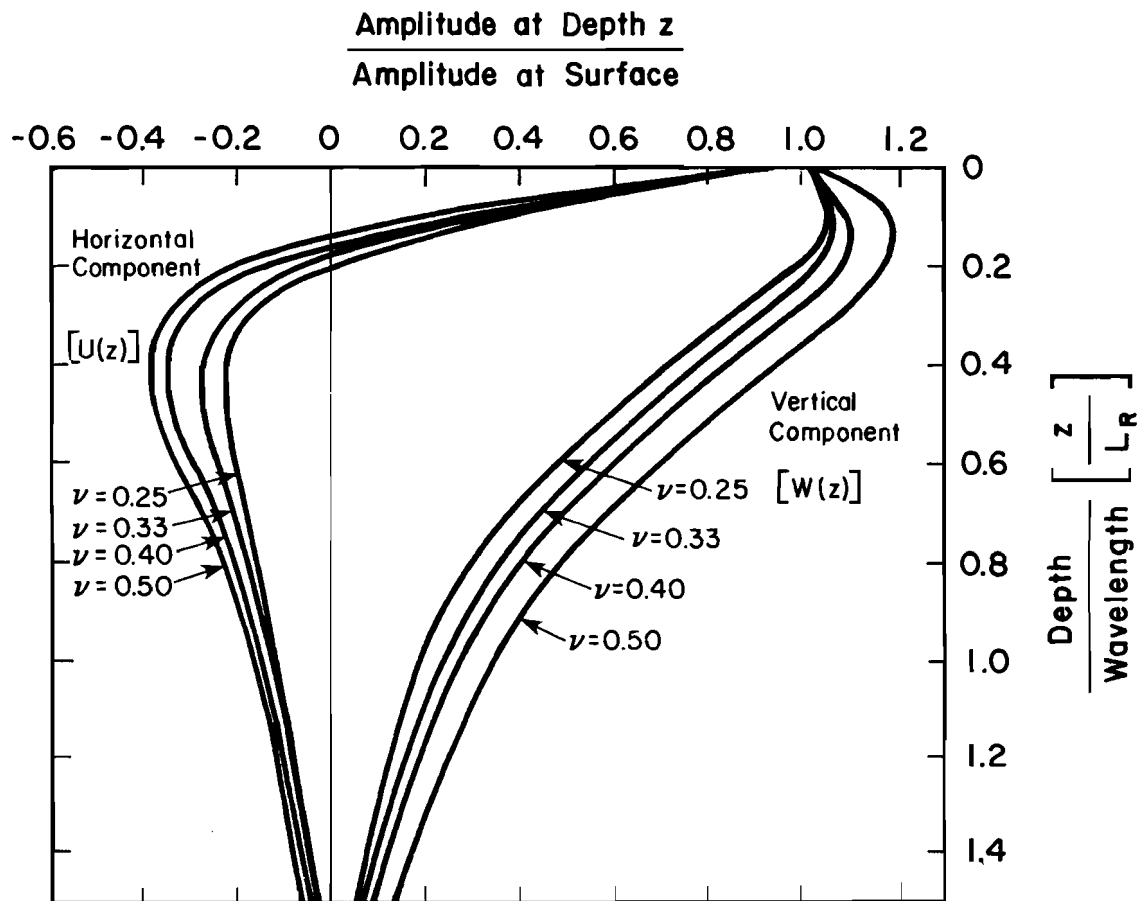


Fig. 3.3. Variation in amplitude with depth of particle motions associated with the Rayleigh wave (from Richart, et al, 1970).

used in generating and recording stress waves propagating in the drilled pier are essentially identical for both methods. However, when a surface receiver is used instead of embedded receivers, several important differences occur between the two methods related to receiver output. These differences as well as the basic WAPS method are discussed in the follow paragraphs.

Testing equipment employed and the source-receiver configuration used in the WAPS method are illustrated in Fig. 3.4. The receiver is lightly cemented in some fashion to the top of the pier (epoxy provides an adequate coupling) rather than being embedded at some depth within the pier. The receiver may be either a vertical velocity transducer or an accelerometer, although use of an accelerometer results in greater ease in monitoring wave reflections. If an accelerometer is used as the surface receiver, a charge amplifier must be included in the wave propagation measuring system. The charge amplifier conditions the accelerometer output prior to monitoring of the signal by the oscilloscope.

The WAPS method has several distinct advantages over the embedded receiver method (WAPER) in evaluating drilled pier integrity. First, the surface receiver configuration is extremely economical, due to the fact that a single receiver is used throughout the entire testing program. Second, use of a surface receiver does not require instrumentation of the pier prior to or during construction of the foundation which also represents a cost savings.

In spite of these advantages, several severe limitations are associated with the surface receiver method. One major disadvantage is that the wave propagation velocity cannot be measured directly using the surface receiver configuration. Steinbach (1971) developed an indirect method for estimating the compression wave velocity utilizing the Rayleigh waves present in the

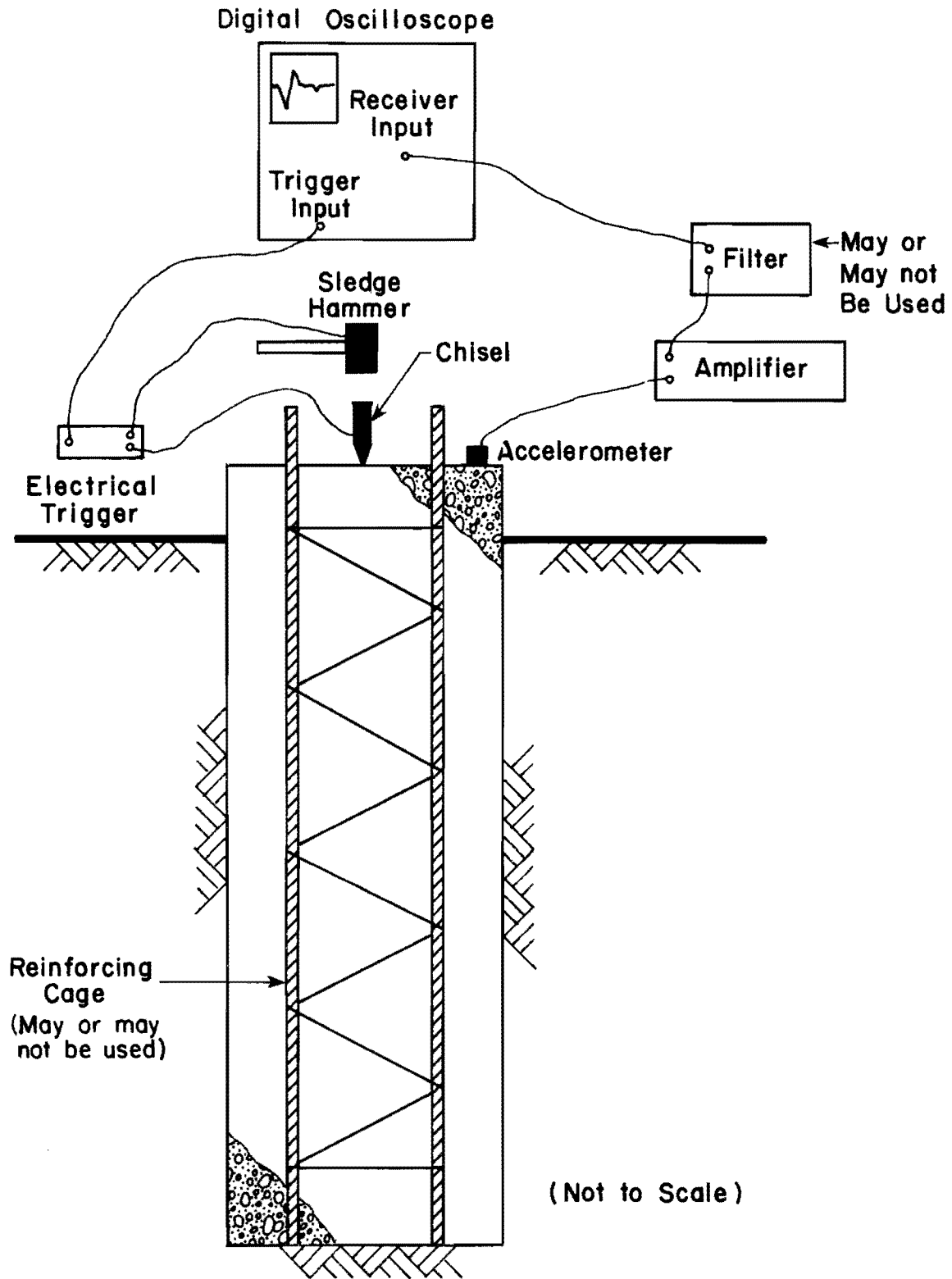


Fig. 3.4. Schematic of wave propagation testing with a surface receiver.

upper portion of the drilled pier. By measuring the frequency of the surface wave captured in the initial time period of the surface receiver output, the Rayleigh wave velocity can be determined by:

$$V_R = f \cdot d \quad (3.4)$$

where

f = the measured excitation frequency, and

d = the diameter of the pier.

If Rayleigh wave velocity is determined in this manner and if Poisson's ratio for concrete is assumed, an estimation of the compression wave velocity may be obtained from:

$$v_c^2 = K^2 v_R^2 \{ [2(1-\nu)] / (1-2\nu) \} \quad (3.5)$$

where ν is Poisson's ratio and $K = 1.03$ and 1.08 , when $\nu = 0.3$ and 0.2 , respectively. Steinbach and Vey (1975) provided test records of surface receiver output from field tests with drilled piers supporting the indirect method of determining P-wave velocities. However, the authors concluded that for surface receiver measurements on drilled piers posing irregularly shaped surfaces or protruding reinforced steel (conditions common in practice) no appreciable Rayleigh waves develop or the waves are often non-periodic.

Therefore, the indirect method of determining P-wave velocity is crude, at best, and often times the compression wave velocity must be assumed in order to determine the depth from which reflections occur.

Additional problems associated with the surface receiver method are created by the Rayleigh waves propagating back and forth across the top of the drilled pier. As mentioned previously, Rayleigh waves generated by the impact of the source are confined to the near-surface region of the drilled pier and act as background noise which complicates the surface receiver output. Surface waves can continue to propagate across the top of the pier for a period of time that extends well beyond the arrival time of the P-wave reflection off the pier bottom, thus masking the reflected wave arrival. If a reflection cannot be monitored or identified, the results of the test are inconclusive, and no accurate information can be obtained to judge concrete quality or pier integrity.

The noise created in the upper region of the drilled pier by the Rayleigh wave may be minimized by use of a variable filter. The purpose of the filter is to eliminate the unwanted Rayleigh wave frequencies from the surface receiver output. However, filtering of the surface wave may cause additional problems, many times unrecognized, by altering amplitudes and travel times of wave reflections. Furthermore, if the P-wave frequency generated by the surface source is close to that of the Rayleigh wave, filtering will not be advantageous because the P-wave will be attenuated along with the surface noise resulting in little or no improvement in the monitored receiver output. To alleviate this potential problem, attempts should be made to maximize the variance between the two generated frequencies. Since the surface wave frequency is a function of the wave propagation velocity and the pier diameter, two factors that are fixed for

any given pier, all attempts in maximizing the frequency variance must be concentrated at altering the P-wave frequency. The P-wave frequency is a component of the input pulse; therefore, various surface sources should be experimented with in hopes of producing a P-wave pulse that has a low frequency in comparison with the typically high frequency surface wave.

WAVE PROPAGATION MEASUREMENTS

Initial and Reflected Wave Arrivals.

Regardless of the source-receiver configuration employed, the success of the stress wave propagation method depends on recording and identification of reflected wave arrivals. The travel times corresponding to reflected wave arrivals identified in the P-wave record are used with the computed or estimated compression wave velocity to assess points of reflection in the drilled pier. Reflection points for sound, straight-sided piers are the concrete-air and concrete-soil interfaces at the top and bottom of the pier, respectively. For drilled piers with discontinuities or irregularities, additional reflection points occur, and it is the monitoring of reflections from these additional points which allow identification of defective piers.

Non-Defective Drilled Piers.

To develop these concepts further, consider the case of a wave propagation test performed on a 84 in. (213.4 cm) diameter, 92 ft (28.0 m) long drilled pier constructed on a site in Beaumont, Texas. The structurally sound pier was instrumented with a vertical velocity transducer embedded at a depth of 29.2 ft (8.9 m) within the pier. Figure 3.5(a) illustrates the source-receiver configuration employed in the test, as well as the local

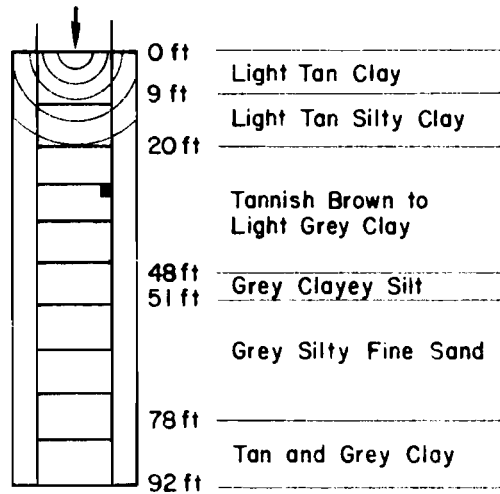


Fig. 3.5(a). Schematic of 92 ft. long drilled pier with embedded receiver and surrounding soil conditions.

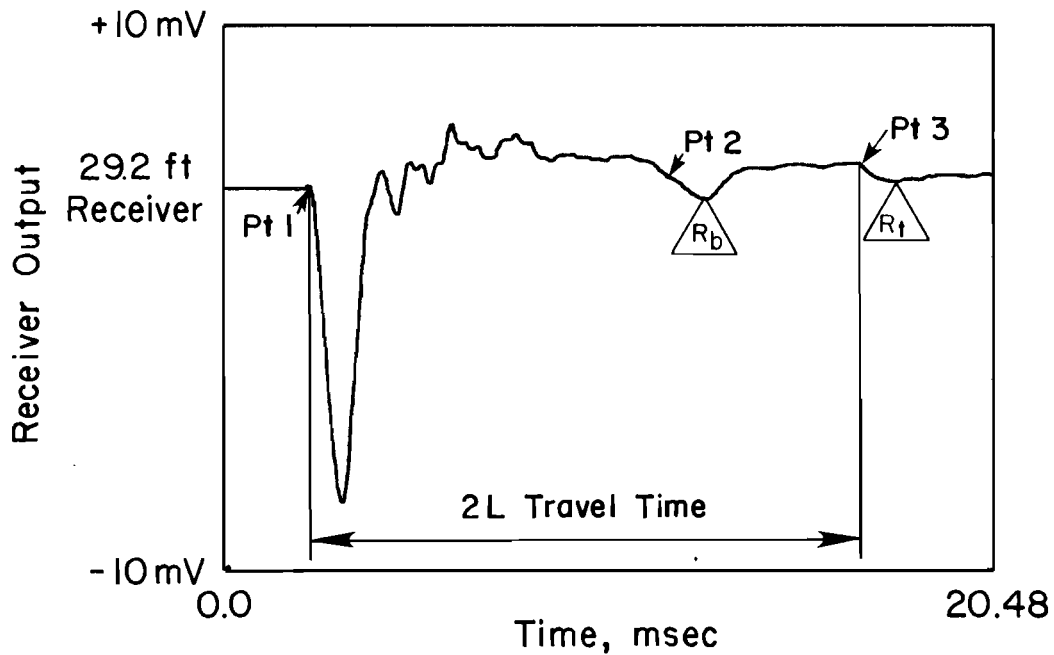


Fig. 3.5(b). Receiver output for velocity transducer embedded at a depth of 29.2 ft. in 92 ft. long drilled pier on site in Beaumont, Texas.

subsurface conditions. The monitored receiver output caused by the propagating stress wave is given in Fig. 3.5(b).

The surface source, as mentioned previously, provides a dual purpose. In addition to generating a compression wave, the hammer impact triggers the oscilloscope to begin monitoring the receiver output. As illustrated in Fig. 3.5(a), the compression wave resulting from the impact initially propagates radially outward from the source along a hemispherical wave front. However, the wave front quickly becomes nearly plane and perpendicular to the longitudinal axis of the pier. As the stress wave propagates past the embedded receiver, excitation of the velocity transducer causes an electrical signal to be produced, with initiation of the movement of the transducer being recorded on the oscilloscope display as point 1 in Fig. 3.5(b). The travel time associated with the initial arrival of the stress wave is then used to compute the wave propagation velocity. For sound, straight-sided drilled piers, the stress wave will continue to travel through the pier until it contacts the concrete-soil interface at the tip. At this point, a certain percentage of the amplitude of the incident stress wave will be reflected, with the magnitude dependent on the soil conditions present at the bottom of the pier. The arrival of the reflected stress wave as it passes the embedded receiver is again monitored in the output signal shown as point 2 in Fig. 3.5(b). Upon arrival at the top of the pier, the propagating stress wave is again reflected and monitored by the receiver, as point 3 in Fig. 3.5(b). This reflection process continues and is recorded as long as there is sufficient wave amplitude to excite the receiver.

Several significant points concerning wave propagation measurements in drilled piers can be emphasized by inspection of the time domain record in Fig. 3.5(b). First, a visual examination of the receiver output reveals that

the amplitudes of the initial and reflected wave arrivals decrease, or attenuate, with respect to time. Attenuation of the stress wave pulse as it propagates within the drilled pier depends on many variables including: (1) concrete quality, (2) the presence of discontinuities or irregularities, (3) the size and nature of such defects, (4) material damping within the pier, (5) surrounding soil conditions, (6) the bond between the surrounding soil and pier, and (7) the geometry of the structural member. Because stress wave attenuation is caused by such factors as soil inclusions, voids, changes in cross-sectional area, and changes in concrete quality, a relative indication of the structural integrity of the pier can be obtained by performing an attenuation study of the monitored receiver output. Initial and reflected wave amplitudes measured from receiver output should be compared for a number of drilled piers on a single site in order to distinguish possible discrepancies in the recorded data resulting from suspect piers. The subject of stress wave attenuation in drilled piers is discussed in greater detail in Chapters 6 and 7.

It is of interest to note the polarity of the wave arrivals monitored in the receiver output. The polarity of the reflected wave arrivals is identical to that of the initial wave arrival, signifying that the drilled pier is performing in accordance with wave propagation theory for a free-free rod. Theory predicts that for a finite rod with both ends free, a compression wave will be reflected as a tension wave and a tension wave will be reflected as a compression wave at the ends of the rod. As shown in Fig. 3.5(b), the pushing motion of the compression wave input causes an initial downward motion of the vertical velocity transducer upon arrival of the initial wave at the embedded receiver. As the compression wave reaches the "free" end at the bottom of the pier, the P-wave is reflected as a tension

wave, the pulling motion of the tension wave likewise results in a downward motion of the velocity transducer upon arrival. The propagating tension wave is reflected at the top of the pier as a compression wave, and the process is repeated. This represents a typical reflection pattern for sound drilled piers with their bases founded in soil.

It is possible to compute the effective length of a drilled pier without prior knowledge of the embedded receiver depth, provided that the reflection from the top of the pier can be identified in the receiver output. If a significant portion of the incident P-wave is reflected from the concrete-soil interface at the bottom of the pier, chances are favorable for identifying a reflection from the top of the pier, where essentially total reflection of energy occurs. Figure 3.5(b) illustrates such a case, where the $2L$ travel time is determined from the output record and used with the direct wave propagation velocity to determine L , the effective pier length.

Furthermore, the record presented in Fig. 3.5(b) indicates that the WAPER method can be used successfully in evaluating the integrity of large-diameter piers of substantial lengths as well as piers of small dimensions. The reflected wave arrivals are distinctly identifiable in the wave propagation record, providing ample amount of data for determining the integrity of the drilled pier.

Defective Drilled Piers.

In regard to structural stability, the presence of a discontinuity or irregularity in a drilled pier contributes to a reduction in pier integrity which can affect the overall performance of the foundation. In their paper on drilled pier construction, Baker and Khan (1971) present a list of twelve conditions that can lead to the construction of defective piers. Baker and

Khan's list of causes can be condensed into the following five major categories:

- (1) The presence of excess water in the borehole at various times during the pier construction process, resulting from negligent inspection and/or poor construction practices.
- (2) The presence of soil inclusions, resulting from a soil cave-in when constructing uncased piers or a soil cave-in during removal of the casing.
- (3) The presence of voids, created by concrete temporarily hanging up in the casing during removal or by inadequate vibration of low-slump concrete.
- (4) A reduction in the cross-sectional dimension of a segment of the pier, termed necking, whereby water and soil pressure collapse the casing.
- (5) Poor concrete delivered to the project site.

One or a number of these conditions could occur simultaneously at the time of foundation construction, resulting in a number of possible combinations of defects in drilled piers.

For wave propagation tests performed on defective drilled piers, the discontinuity or irregularity present in the pier provides an additional reflection boundary for the stress wave to strike. This additional boundary results in an early arrival of a reflected wave in the receiver output relative to the reflection of the pulse off the concrete-soil interface at the bottom of the pier. Successful determination of defective piers depends on positive identification of early reflected wave arrivals in the records.

For illustrative purposes, consider the case of a WAPER test performed on a defective pier in Granger, Texas. The pier, part of a research program conducted by Arias (1977), was constructed with a planned soil inclusion. A schematic representation of the 30 in. (76.2 cm) diameter, 39 ft (11.9 m) long drilled pier is given in Fig. 3.6, along with the receiver output

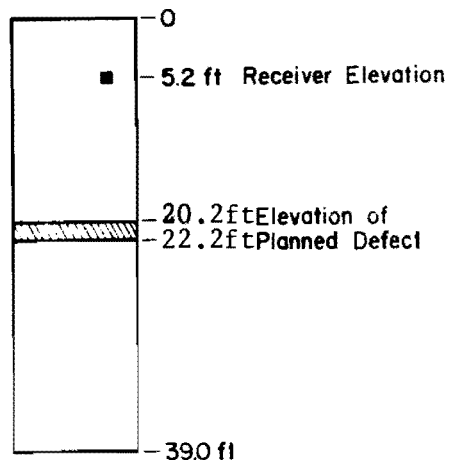


Fig. 3.6(a). Schematic of 39.0 ft (11.9m) drilled pier with embedded receiver.

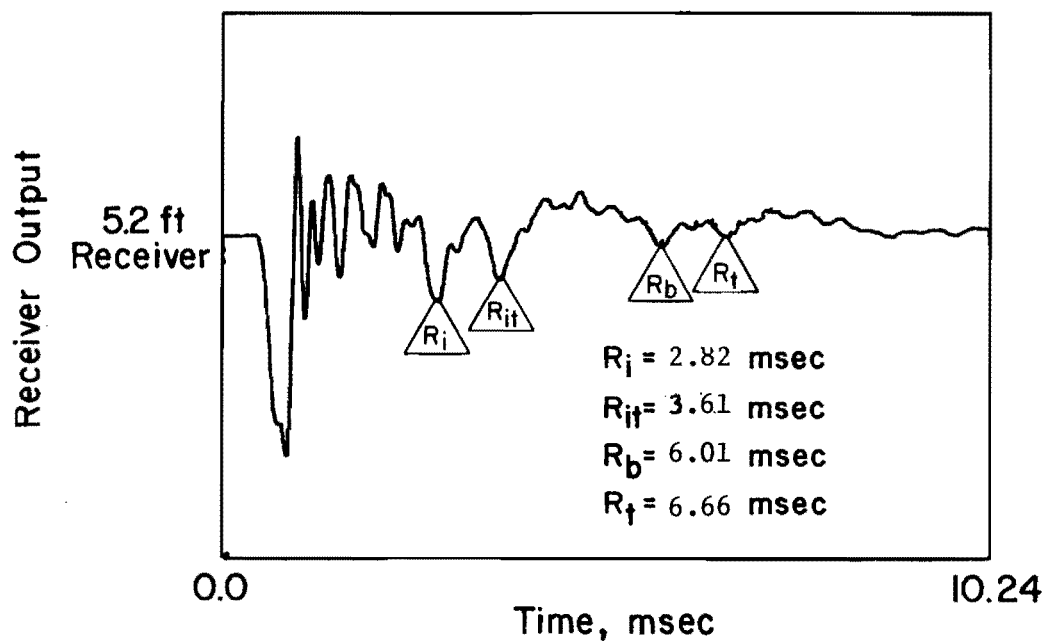


Fig. 3.6(b). Receiver output from velocity transducer embedded at a depth of 5.2 ft (1.6m).

captured during one of the measurements in this study. The wave propagation velocity in the drilled pier, computed directly from the travel time of the compression wave as it propagated from the top of the pier to the embedded velocity transducer, at a depth of 5.2 ft (1.6 m), is approximately 12,400 fps (3,780 mps). With the wave velocity determined and the length of the pier known, the arrival time of the tension wave reflected off the bottom of the pier can be computed, which in this case is 5.87 ms. An examination of the monitored receiver output reveals an apparent tension wave reflected off the bottom of the pier (designated as R_b in Fig. 3.6(b)) at the approximate time corresponding to the computed arrival of the reflected stress wave. In a similar manner, the arrival time of the reflected compression wave off the top of the pier (designated as R_t in Fig. 3.6(b)) can be computed. This method of determining reflected wave arrivals is identical to the procedure used on sound, straight-sided drilled piers.

However, a closer examination of the receiver output illustrated in Fig. 3.6(b) reveals wave arrivals (designated R_i and R_{it}) occurring prior to any arrival of a wave reflected off the bottom of the pier. The early reflected wave arrivals indicate that an additional reflection boundary, a discontinuity or irregularity, is present in the pier. Since the reflected wave arrival is displayed in the output signal at a time which is greater than three times the direct travel time (meaning greater than the time for the stress wave to travel from the pier surface down to the receiver, back to the surface, and back down to the receiver again), the irregularity is located at some depth below the embedded receiver.

The elevation of the discontinuity or irregularity is determined in a manner similar to that used for determining the length of a sound drilled pier:

$$[(R_i \text{ arrival time}) + (\text{initial arrival time})]v_c/2 = \text{elevation of irregularity} \quad (3.6)$$

which in this case calculates to be approximately 20 ft (6.1 m) below the top of the pier. Due to the shallow depth of the embedded receiver and the high degree of reflected wave energy off the irregularity, the reflection off the concrete-air interface at the top of the pier (R_{it}) can also be easily identified in the wave signature.

Since it has now been determined that a defect exists in the pier at a depth of about 20 ft (6.1 m), reexamination of the reflections thought to come from the bottom of the pier is appropriate. It is possible that those reflections also came from the defect. By using points R_b and R_t , a $2L$ travel time of 32 msec is measured which represents a reflection depth of 19.8 ft (6.0 m). This depth compares very closely to the depth of the defect, and it is therefore likely that the reflections labeled R_b and R_t in the figure resulted from the defect and not the bottom of the pier as originally assumed. This result also confirms the severity of the defect; that is, very little energy passes the defect indicating it probably covers the cross-section of the pier.

To draw accurate conclusions concerning the integrity of a drilled pier, it is extremely important that the engineer performing the tests be informed of "special" construction procedures utilized on the foundation member under investigation. Certain drilled pier designs, such as step-tapered shafts and partial casings left in place, can alter the output signature and result in an erroneous conclusion regarding the pier integrity. For a case in point,

consider the wave propagation test performed on a 56 in. (142 cm) diameter, 93 ft (28.4 m) long drilled pier constructed at a site in Beaumont, Texas. The drilled pier, constructed by the slurry displacement method, was instrumented with a vertical velocity transducer embedded at an elevation of 29.2 ft (8.9 m) within the pier. Figure 3.7 shows a schematic representation of the instrumented drilled pier, local subsurface conditions, and the receiver output for a typical wave propagation measurement performed on the pier.

An examination of the receiver output shown in Fig. 3.7(b) reveals that the wave arrival of the reflection off the bottom of the pier (R_b) can be identified in the wave signature; methods presented previously for calculating the arrival time of the reflected wave confirm this finding. However, an additional wave arrival (designated as R_1) can be identified in the record. Contrary to the finding in Fig. 3.6(b), the reflected wave arrival is displayed in the output signal at a time which is less than three times the direct travel time between the pier surface and the receiver and, therefore, the irregularity may exist either above or below the embedded receiver.

Assuming that the additional reflection boundary lies below the embedded receiver, use of the method described previously (Eq. 3.6) for location of irregularities results in a depth of approximately 47 ft (14.3 m) below the top of the pier. However, if it is assumed that the additional reflection boundary is located above the 29.2 ft (8.9 m) depth of the receiver, the method of pinpointing the irregularity elevation is as follows:

$$[(R_1 \text{ arrival time}) - (\text{initial arrival time})] v_c / 2 = \text{elevation of irregularity} \quad (3.7)$$

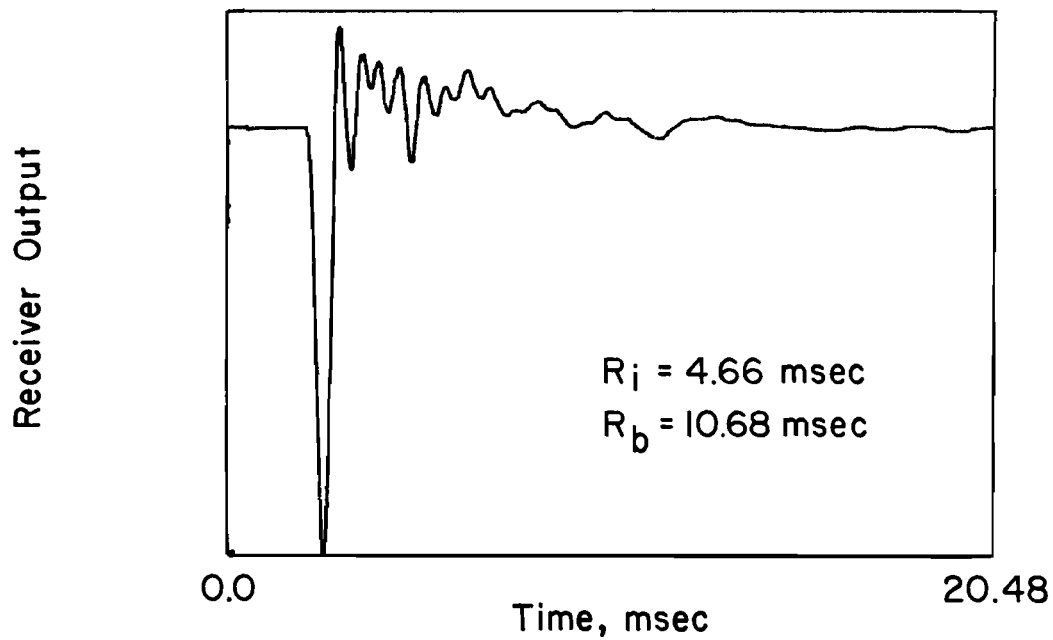
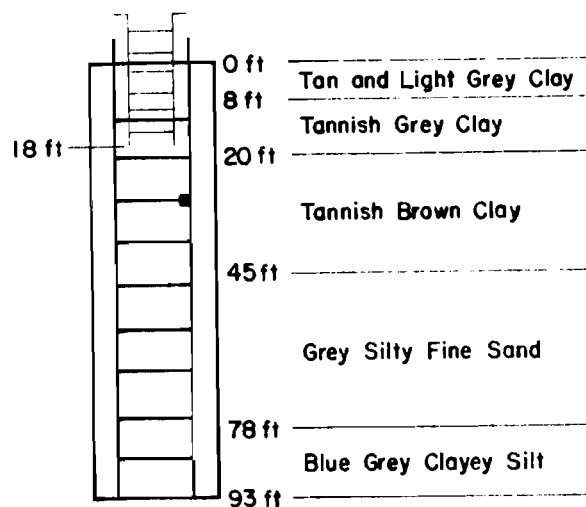


Fig. 3.7. WAPER Test on 93-foot (28.1 in) long, drilled pier in Beaumont, Texas.

For the receiver output shown in Fig. 3.7(b), the elevation of the irregularity calculates to be 17.5 ft (5.3 m) below the top of the pier.

To determine the elevation of the irregularity, attempts must be made to: (1) identify possible additional reflected wave arrivals in the receiver output and, (2) identify possible discrepancies in wave attenuation by comparing the questionable output record with records obtained from wave propagation tests on adjacent drilled piers proven to be of sound integrity. If the irregularity is located below the embedded receiver, a wave reflection off the top of the pier resulting from the irregularity should be identifiable in the output signature at a time corresponding to 8.90 msec, provided the wave energy is not attenuated appreciably during reflection. However, no discernible wave arrival is present in the receiver output (Fig. 3.7(b)) at the designated time. For the case of the irregularity located above the receiver, the wave arrival shown as R_1 would represent a reflection off the top of the pier, and the subsequent reflection from the irregularity would be another reflection off the top of the pier at a time corresponding to 7.19 msec. An examination of the receiver output reveals that a possible arrival may be detected at the designated time, confirming the belief that the irregularity of unknown nature is located at a depth of approximately 17.5 ft (5.3 m) within the drilled pier. The small magnitude of the second wave arrival is due to attenuation of the pulse caused by the repeated reflections off the irregularity and the top of the pier.

Without prior knowledge of the drilled pier design, it could be concluded from the above analysis that an irregularity is present in the pier at a depth of 17.5 ft (5.3 m). However, examination of wave propagation records obtained from measurements on additional drilled piers at the site revealed an identical wave arrival occurring in each signature at

approximately the same time. After consulting with the project engineer, it was concluded that the early wave arrivals were the result of the inner reinforcing steel. It was learned that the interior tie rod cage, which possessed an extremely high percentage of steel, extended down to a depth of approximately 18 ft (5.5 m) within the pier. The large amount of closely spaced reinforcing steel acted as a poor, but nonetheless effective, reflection boundary for the stress wave.

The example cited above indicates the importance of being aware of all "special" construction procedures and designs incorporated in the foundation structure under investigation. Had the tie rod cage not been realized as the source of the early wave arrival, a serious error in judging the pier integrity could have occurred.

SUMMARY

Stress wave propagation methods for evaluating drilled pier integrity rely on time domain measurements of initial and reflected wave arrivals. Two wave propagation methods are employed in this study, the methods differing in the source-receiver configuration. The embedded-receiver-wave-propagation (WAPER) method involves attaching receiver(s) to the steel reinforcing cage prior to construction of the pier. With the receiver(s) located within the pier at pre-determined elevations, the times corresponding to reflected wave arrivals identified in the output can be used to determine wave propagation velocity and elevations of reflection boundaries. The wave propagation velocity, computed using either the direct or interval travel time, can be employed to determine Young's modulus for the concrete as well as give a relative indication of the quality of the concrete. To eliminate problems related to "noise" in the recorded output (caused by Rayleigh waves generated

in the upper region of the drilled pier), it is recommended that the receiver(s) be located at a depth of approximately a wavelength (of the Rayleigh wave) or more below the top of the pier.

The surface-receiver-wave-propagation (WAPS) method of evaluating drilled pier integrity requires the receiver (preferably an accelerometer) to be secured to the upper surface of the pier. Advantages of employing a surface receiver rather than an embedded receiver include: (1) economy (only one receiver instrument is required for testing an entire site), and (2) convenience (procedure does not require installation prior to drilled pier construction). However, major disadvantages of the WAPS method are: (1) the wave propagation velocity cannot be determined directly, and (2) Rayleigh waves propagating across the top of the pier often hinder identification of reflected wave arrivals. A filter can be used to eliminate the undesired frequencies associated with the "noisy" surface waves, but the user should be aware of the fact that filtering can alter wave arrival amplitudes and travel times monitored by the receiver. Filtering is also ineffective if the frequencies of the compression and Rayleigh waves are similar.

The success of either wave propagation method employed in this study is dependent upon identification of reflected wave arrivals in the receiver output. Reflection boundaries for sound, straight-sided piers are the concrete-air and concrete-soil interfaces at the top and bottom of the piers, respectively. Discontinuities or irregularities present in the drilled pier represent additional reflection boundaries for the propagating stress wave to strike, resulting in the occurrence of early reflected wave arrivals in the output signal.

By examining the polarity of the initial and reflected wave arrivals in various wave propagation measurement records, it was concluded that drilled

piers bearing on soil behave in accordance with wave propagation theory regarding rods with free-end conditions. However, examination of various receiver output records also revealed that the propagating stress wave attenuates with respect to time, the dissipation of wave energy caused by such factors as material damping in the pier, pier geometry, and surrounding soil conditions. In addition, reference was made to the importance of realizing all special design and construction procedures incorporated in the drilled pier foundation to interpret properly the records and to eliminate possible erroneous conclusions regarding pier integrity.

CHAPTER 4. WAVE GENERATION AND MEASUREMENT EQUIPMENT

INTRODUCTION

Recent advances in electronic technology and computer software have greatly enhanced the users capability in recording and assessing wave signatures. For example, digital oscilloscopes possess distinct advantages over older analog storage oscilloscopes, particularly in the areas of resolution and waveform analysis. As one of the objectives of this study is to improve existing wave propagation techniques, various modifications and substitutions in test equipment and apparatus were experimented with in an effort to obtain easily interpretable wave signatures. Equipment utilized in this study is collectively shown in Figs. 4.1 and 4.2. The equipment can be divided into the following general categories: recording equipment, receivers, sources, triggering systems and filters. Brief descriptions of the equipment, with pertinent information regarding specifications and advantages and disadvantages as they pertain to wave propagation measurements, are presented in this chapter.

RECORDING EQUIPMENT

Oscilloscope

The primary function of the recording equipment is to accurately and precisely measure, record and display time-varying stress wave signals. Accurate and precise recording of receiver output requires recording

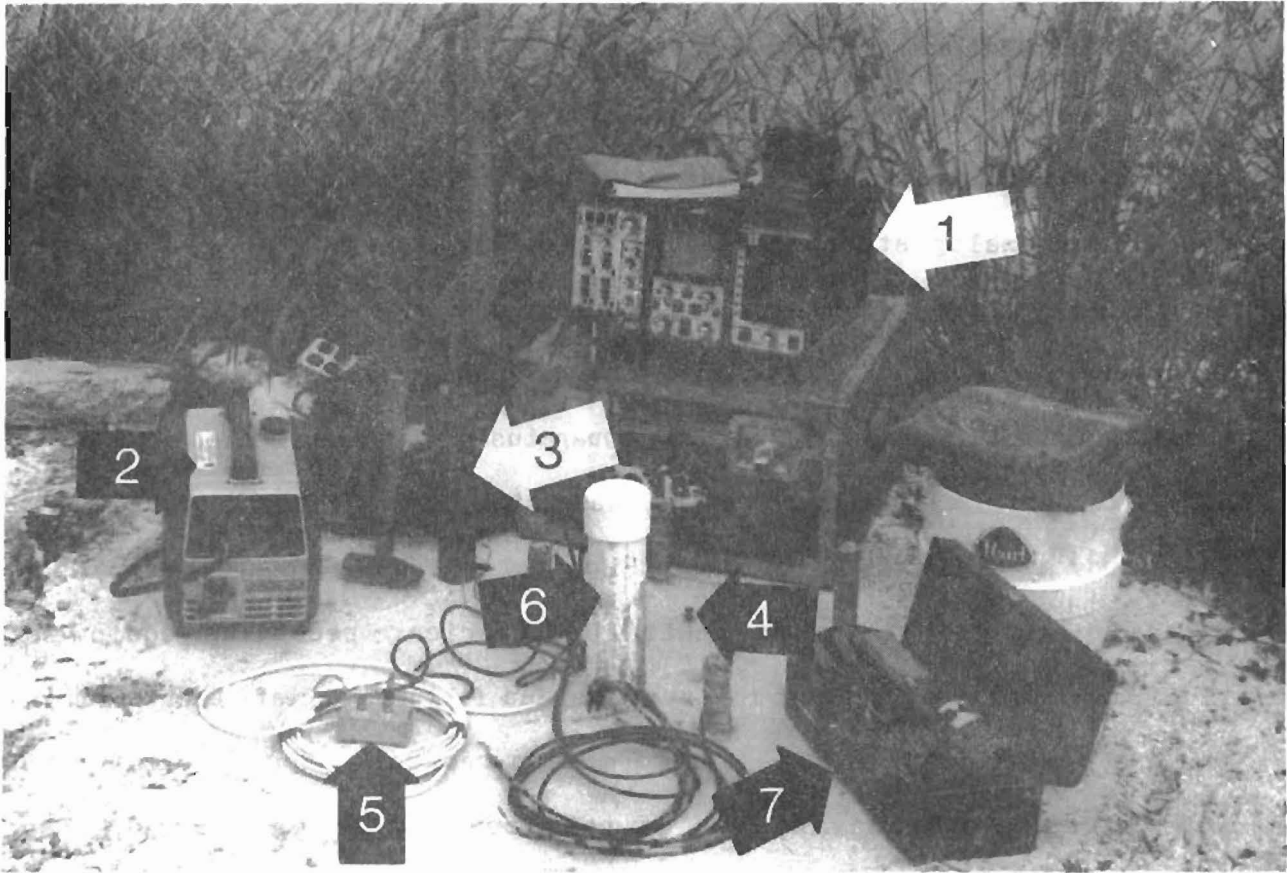


Fig 4.1. Equipment used in evaluating drilled pier integrity by stress wave propagation.

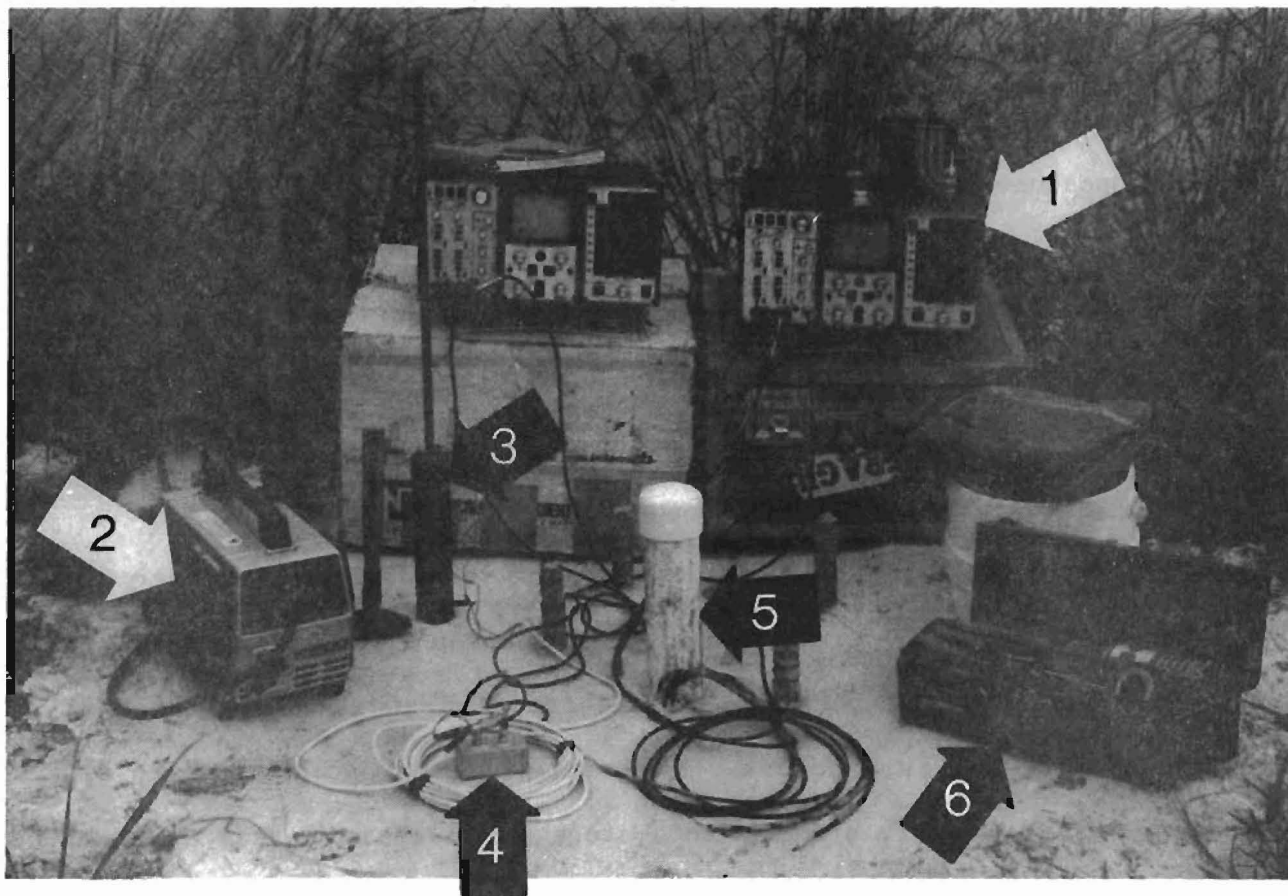


Fig 4.2. Equipment used for attenuation study of stress waves in evaluating drilled pier integrity.

equipment with the proper frequency response and timing accuracy. Travel time measurements in these tests are in the millisecond range and wave frequencies are in the range of kilohertz. An oscilloscope is an excellent recording device for these time and frequency ranges. For this study, a digital oscilloscope was selected for recording and measurement purposes. Advantages of digital oscilloscopes over conventional analog storage oscilloscopes used in the past include: (1) greater accuracy; (2) ability to show pretrigger information; (3) ability to expand waveforms; (4) ability to superimpose waveforms (both live and stored signals); (5) sweep durations which can range from microseconds to days; (6) digital display of values of voltage and time for any selected point on the waveform; and (7) ability to interface with calculators or computers.

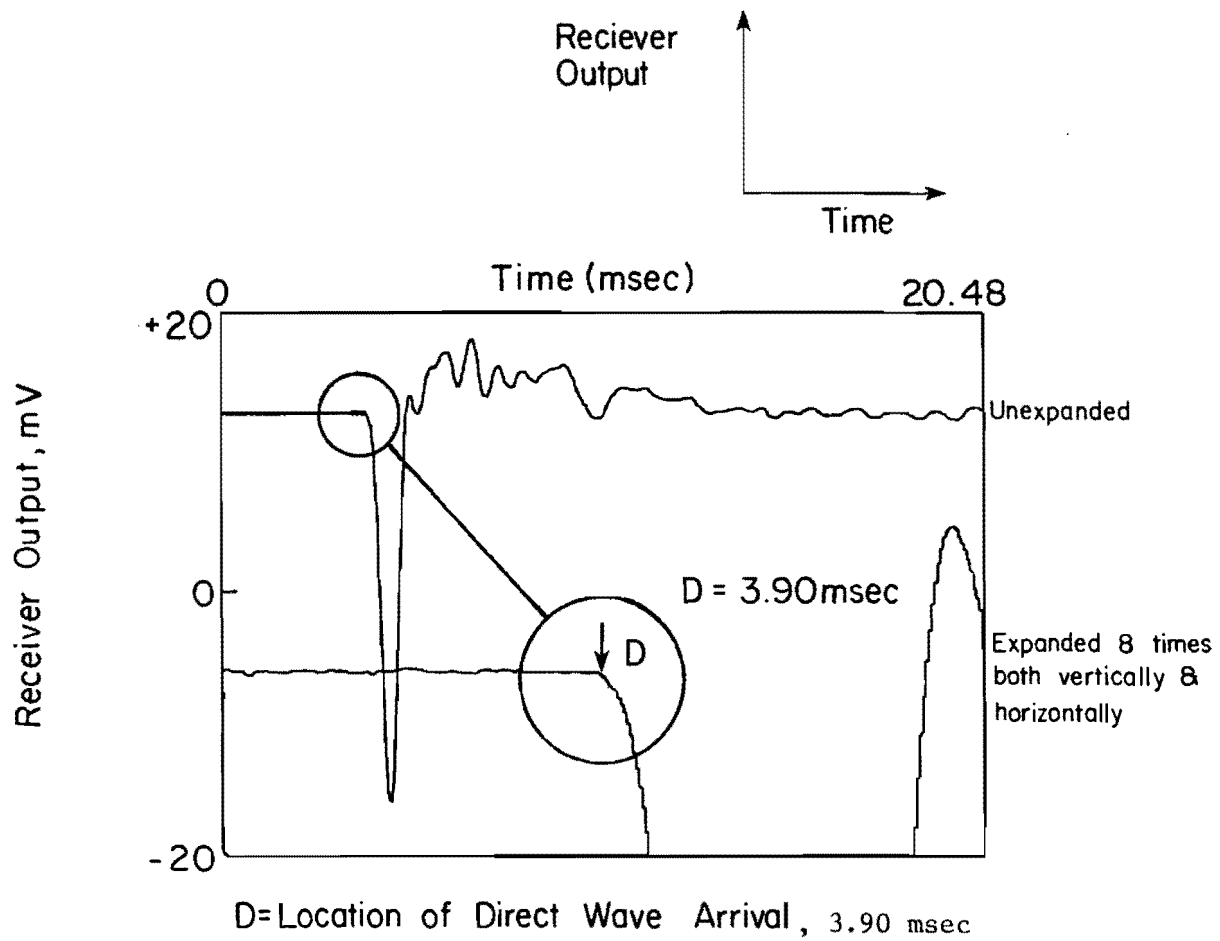
The digital oscilloscope used in this study is an Explorer III, manufactured by Nicolet Oscilloscopes and is shown as item one in Figs. 4.1 and 4.2. The Explorer III is a modular oscilloscope with a three-bay mainframe which allows the use of various plug-ins and a magnetic disk recorder. Functionally similar to a storage oscilloscope, this instrument also has: (1) a movable cursor with an autocenter switch that allows automatic vertical centering of the waveform; (2) a zeroing switch which allows determination of the time and voltage values of any point on the waveform with respect to any other waveform point; and (3) the ability to dump the waveform to recorders for hard copy graphics.

A Model 201 differential amplifier was selected for use with the Explorer III mainframe because of the frequency and time ranges of this plug-in. This unit is a two-channel amplifier with high resolution (4096 points by 12 bits) and high sensitivity (± 10 mV full scale) in the low frequency range (less than 25 kHz). In addition, the special mid-signal trigger mode

allows assessment of pretrigger information as well as capturing of the desired waveform.

The magnetic disk recorder used with the mainframe can store eight, 4096-point records, along with information indicating the voltage and time settings used in each of the measurements. In addition, the recorder can subdivide the storage registers so that up to 32 waveforms of 1024 points each can be stored. Standard magnetic disks with a diameter of 5.25 in. are used.

In regard to wave propagation measurements on drilled piers, the major advantages of the Explorer III digital oscilloscope are the accuracy (0.1 percent of full scale) and high resolution (0.025 percent) of the unit and the capability to display both vertically and horizontally expanded waveforms. The success of determining locations of reflected wave boundaries in drilled piers depends upon the accuracy of computed compression wave velocities, which is directly dependent upon accurate assessment of wave arrival times. The digital oscilloscope allows precise determination of wave arrival times and, therefore, compression wave velocities. This feature is illustrated in Fig. 4.3, where the direct wave arrival portion of a typical WAPER wave signature has been expanded horizontally and vertically. In the expanded mode, the point in time of the initial wave arrival can be easily and precisely identified. This time can then be used with the known distance to the embedded receiver to compute the compression wave velocity. With the actual P-wave velocity known, accurate conclusions can be reached concerning possible reflection boundaries identified in the wave propagation records.



Receiver depth = 55 ft (16.8 m)
 Pier Length = 92 ft (28.0 m)
 Pier Diameter = 36 in. (91 cm)

Fig. 4.3. WAPER test on drilled pier illustrating wave expansion capability of digital oscilloscope.

All oscilloscopes require electrical power. It was found convenient in this study to use a portable generator. Generally, a Honda EM500 portable generator was used as shown in Figs. 4.1 and 4.2 (item 2).

RECEIVERS

The primary purpose of receivers is to track wave particle motion resulting from wave energy propagating through the drilled pier medium. Three different instruments were utilized as receivers in this study, two types which were embedded within the drilled piers and one which was affixed to the pier surface.

Embedded Receivers.

Velocity Transducers. Small, vertical velocity transducers were selected as the primary detectors in this study due to their proven success in previous investigations (Arias, 1977; Hearne et al, 1981). The transducers were Model 15B land geophones, which are manufactured by Mark Products, Inc. These electro-mechanical units are subminiature, digital grade, dual coil geophones with a natural frequency of about 8 Hz, a damping ratio of approximately 30 percent and a weight of several hundred grams. The velocity transducers were housed in sealed plastic cases referred to as marsh cases and equipped with varying lengths of shielded conductor cables. The transducers were sealed in the plastic cases to protect the units against contamination resulting from the harsh conditions of the embedded environment. Typical unit prices for the velocity transducers, including the plastic marsh cases and shielded cable, range between \$35 and \$45 each. (One unit is shown in Fig. 5.12.)

Ceramic Transducers. Piezoelectric ceramic transducers were included in this study as embedded receivers on an experimental basis. This was done because piezoelectric transducers are less expensive than velocity transducers, and, if they could be used successfully, piezoelectric transducers would allow for a greater number of drilled piers to be evaluated to a greater extent on a project for a given amount of funds.

As in the case of velocity transducers, piezoelectric transducers are electro-mechanical transducers; that is, mechanical motion is used to generate an electric charge. With a velocity transducer, movement of the coil in the magnetic field generates an electrical output. With a ceramic transducer, straining of the transducer produces a change in cross-sectional area which results in an electrical charge across the electrodes. A piezoceramic is, therefore, capable of acting as a sensing element. Piezoceramic transducers, commonly made of lead zirconate titanate, are manufactured by pressing, firing and machining the ceramics into specified geometries. Silver electrodes are fired-on in thin coats on opposing sides of the ceramics, and the elements are polarized in the final process. Polarization is established within the ceramic during manufacturing by application of a high D.C. voltage between the pair of electrode faces.

Relationships between applied forces and resultant voltages in piezoceramic transducers depend upon: (1) the piezoelectric properties of the ceramic, (2) the size and shape of the ceramic, and (3) the direction of the electrical and mechanical vector quantities. For this study, it was decided to vary two of the three variables stated above, hopefully to determine the ceramic properties and shapes most compatible as receivers in wave propagation testing. The piezoceramic transducers used as embedded receivers in this study were manufactured by Transducer Products, Inc. Although all

were manufactured of lead zirconate titanate, different dielectric constants were selected for the ceramics on an experimental basis. Models LTZ-2 and LTZ-2H were used, with the 2H ceramics possessing higher dielectric constants (3500 compared to 1800). The cross-sectional areas of the ceramics were also varied for varying electro-mechanical capacitance, with the following cross-sectional dimensions used: 0.33 by 0.25 in. (0.85 by 0.64 cm); 0.50 by 0.13 in. (1.25 by 0.32 cm); and 0.50 by 0.25 in (1.25 by 0.64 cm). All ceramics were cast in 1.0 in. (2.5 cm) lengths.

The piezoceramic transducers were polarized for use in transverse compression. For protection against contamination or deterioration in the concrete environment, each piezoceramic transducer was sealed in a protective case. The sealant was applied in a three-stage process. First, the ceramic was coated with a thin skin of Dow Corning Silicone Rubber Sealant. The rubber sealant was used to act as a waterproofing membrane and to provide some flexibility to resist cracking. Second, the waterproofed ceramic was "potted" using a high density liquid fiberglass compound and (thirdly) placed in a 0.75 in. (1.91 cm) diameter aluminum cylinder. The piezoceramic transducers were supplied with shielded cable similar to that used with the velocity transducers. Several units are shown in Fig. 5.13.

Unit cost for the small number of piezoceramics ordered for this study was on the order of \$20 each. A considerable reduction in unit cost could be realized if the ceramics were purchased in bulk quantities of 100 or more.

Surface Receivers

Accelerometer and Charge Amplifier. An accelerometer and charge amplifier were utilized during evaluation of surface receivers. An accelerometer was used as the surface receiver due to its proven superiority over velocity transducers as a stress wave monitor (Steinbach et al, 1975;

Arias, 1977; Hearne et al, 1981). Only cost prohibits the use of accelerometers as embedded receivers.

The accelerometer used in this study is a Model 302-6, manufactured by Columbia Research Laboratories. Specifications for the accelerometer include a resonant frequency of 30 kHz, a crystal capacitance of 460pf, and a range of 0.005g to 10kg (g equals acceleration of gravity). The charge amplifier (necessary for amplification of the accelerometer signal) is a Model 4102M, manufactured by Columbia Research Laboratories.

SOURCES

As mentioned previously, the purpose of the source is to generate stress waves within the drilled pier. Various mechanical sources, classified as either impulsive or steady-state, have been used in previous investigations with varying success. In the study by Steinbach and Vey (1975), various lengths of steel rods were used to generate compression waves. Although the authors reported favorable results, interpretation of surface receiver output was difficult due to generated surface waves inherent in this set-up. The use of embedded receivers positioned at sufficient depths in the drilled pier will eliminate the "masking" effects of surface wave noise on wave propagation output. Hearne et al (1981) and Arias (1977) evaluated various drop hammers and hammer-and-chisel combinations as compression wave sources with equally favorable results. Arias (1977), in an attempt to generate lower velocity stress waves, experimented with horizontally impulsive mechanical sources in hopes of producing shear waves. Although general conclusions could be drawn from the computed shear wave velocities concerning pier integrity, the shear wave records revealed little in regard to the

magnitude or location of the "identified" defects. Robertson (1976) and Van Koten and Middendorp (1977) reported favorable results for integrity tests using electrodynamic vibrators as steady-state mechanical sources placed on top of driven and cast in-situ concrete piles.

In this study, wave generators were limited to vertical impulsive sources due to their simplicity and past success as P-wave sources. Vertical impulsive sources used in this study included rods and trigger plates of various lengths and diameters, drop hammers employing various weights, and various hammer-and-chisel combinations. In addition, various source striking points consisting of steel bars, rods, plates, nails and balls embedded in the concrete pier top were experimented with in an attempt to produce more easily interpretable wave signatures. Advantages of these various mechanical sources include: (1) the ability to produce stress waves rich in P-wave generation; (2) the ability to vary wave amplitudes and occasionally wave frequencies for varying pier parameters (such as length and diameter); (3) repeatability; and (4) accessibility (when used as surface sources).

As a final note, drilled pier defects that are small in relation to the stress wave length may possibly go undetected during testing. A source generating higher frequency stress waves (and consequently shorter wave lengths) would effectively sample smaller regions of concrete, possibly resulting in reflected waves from small defects. A stud gun was also used as a P-wave source in this study, in an attempt to produce higher frequency compression waves. The results of comparison tests between the various mechanical sources included in this wave propagation study are presented in Chapter 6.

TRIGGERING SYSTEMS

The device used to initiate recording of the receiver output by the digital oscilloscope is referred to as the trigger. The function of the trigger is to produce a voltage change when activated, usually as a result of applying an impulse at the source. This voltage change causes the oscilloscope to begin the recording process some finite amount of time after the impulse. Knowledge of this time delay is critical for proper assessment of the wave signatures, particularly in comparing drilled pier lengths with depths of probable defects.

Triggering systems used in this study included electrical circuits and velocity transducers. The electrical trigger, a resistance-capacitance (RC) circuit, is the simplest system and best suited for the present stress wave testing technique. A diagram of an RC circuit with appropriate connections to activate the oscilloscope is shown in Fig. 4.4. The trigger packaged in a small aluminum box, is shown as item 5 in Fig. 4.1.

Velocity transducers were utilized as triggers only in instances when the electrical circuitry was not possible, as in the instance when the stud gun was being tested as a source. Under these conditions, the velocity transducer is glued to the top of the concrete shaft, and the source impact is applied as close as possible to the transducer trigger. The impact from the source excites the nearby velocity transducer, which in turn produces a signal that triggers the oscilloscope. A triggering system employing a velocity transducer is not as accurate as an electrical trigger, with time delays in the transducer dependent upon such factors as the distance between impulse application and transducer and the amplitude and frequency of the generated impulse.

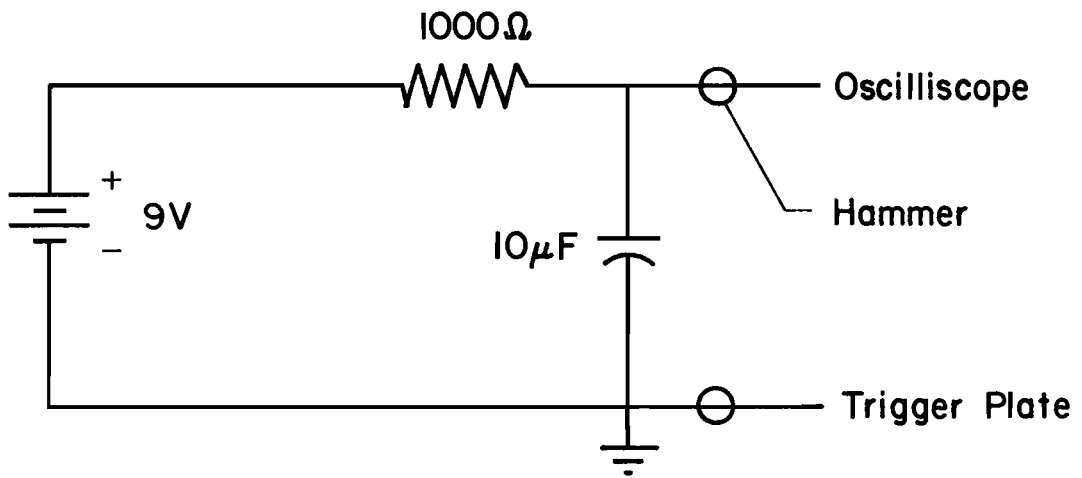


Fig. 4.4. Circuit diagram of resistance-capacitance (RC) trigger used in field tests.

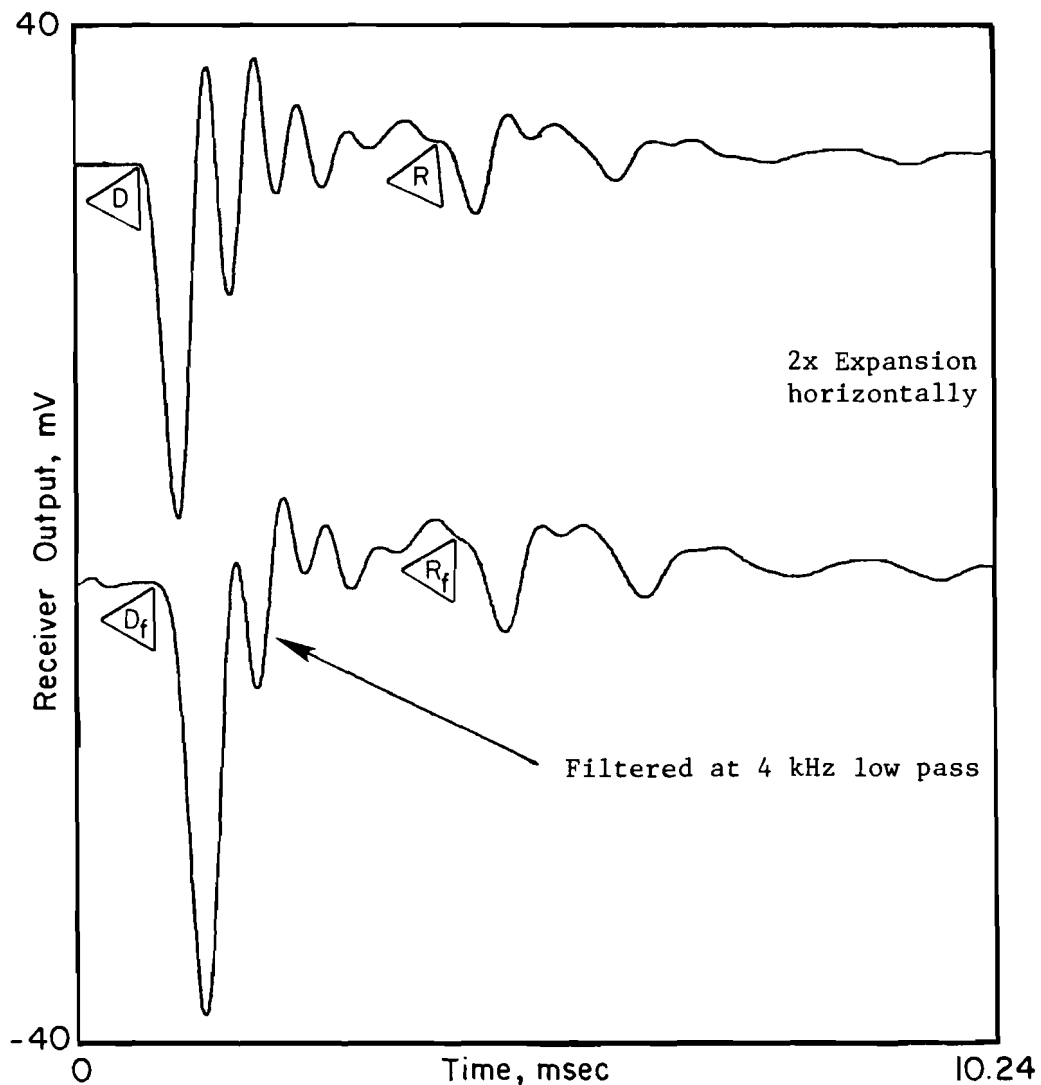
Regardless of the triggering device, the effectiveness of the triggering system depends on how the oscilloscope is set to be activated, i.e., either a-c or d-c coupling and positive or negative slope setting. The characteristics of the triggering system in use and how it interacts with the monitoring instrument must be thoroughly understood by the user. A more detailed discussion of the application and accuracy of the two triggering systems used in this study has been previously presented by Hoar and Stokoe (1978).

FILTERS

The purpose of a filter is to eliminate undesirable frequencies or "noise" in the recorded wave signature which tend to mask reflected wave arrivals. A filter was used in the evaluation of testing with surface receivers (WAPS) The filter was used in an attempt to screen the surface waves that are inherent in this source-receiver configuration.

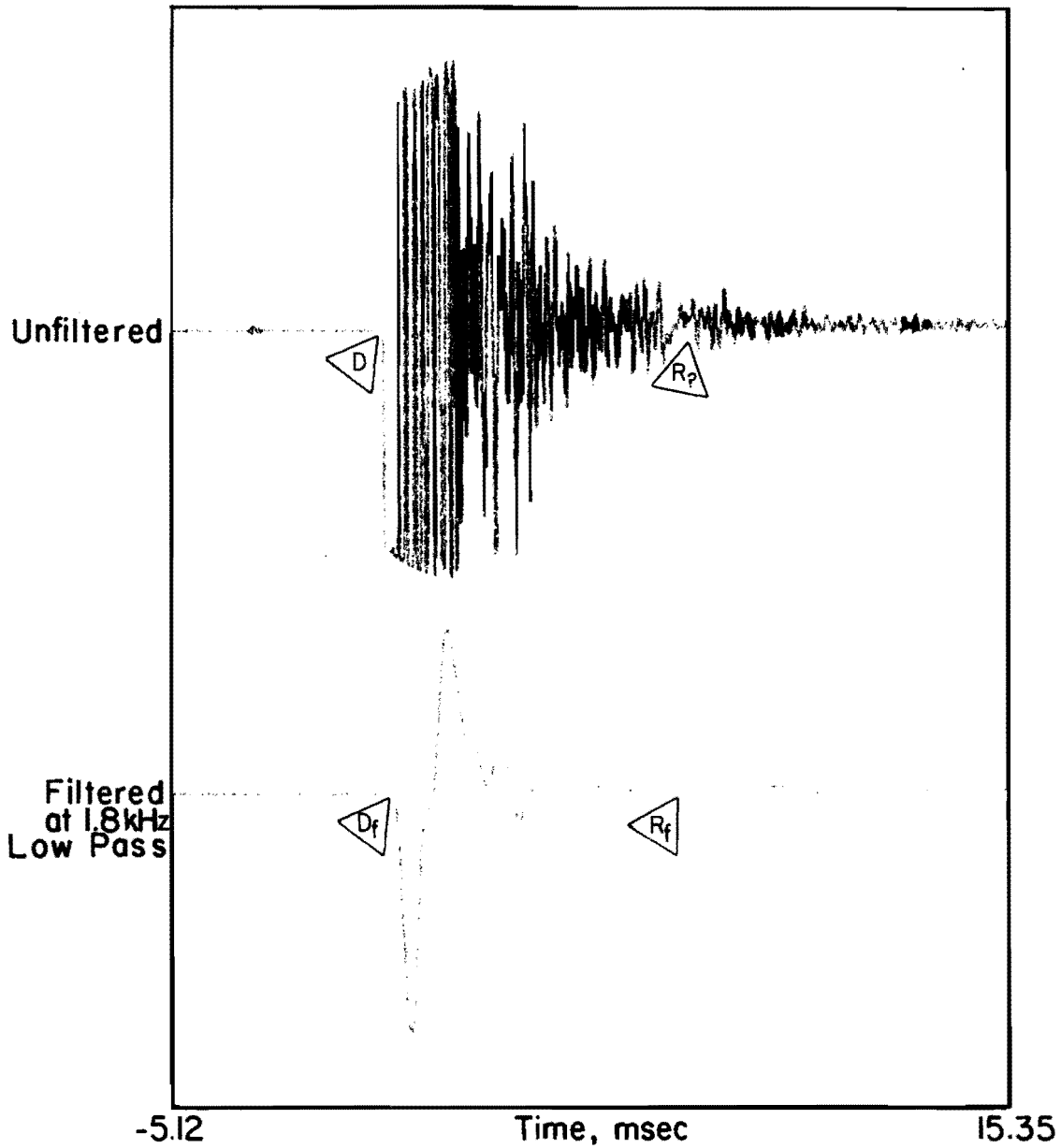
The filter used in this study is a Model 3342, manufactured by Krohn-Hite. It is a two channel variable filter designed with cut-off frequencies ranging from 0.001 Hz to 99.9 kHz. The pass-band gain is unity (0 db) or 10 (20db), with an attenuation rate of 96 db per octave and output hum and noise less than 500 microvolts. With the channels connected in series, the Model 3342 has the capability of functioning as a low-pass, high-pass, or band-pass filter.

Caution should be exercised when using a filter in conjunction with time-domain measurements. Incorrect filtering can increase apparent travel times and change apparent wave amplitudes as illustrated in Figs. 4.5 and 4.6. In general, filtering effects begin when cut-off filter frequencies are



D = Direct wave arrival, 0.73 msec
 D_f = Direct wave arrival (filtered), 0.91 msec
 R = Reflected wave arrival, 4.08 msec
 R_f = Reflected wave arrival (filtered), 4.30 msec
 Receiver Elevation = 10 ft (3.0m)
 Pier Length = 50 ft (15.2m)
 Pier Diameter = 32 in. (81.3 cm)

Fig. 4.5. WAPER Test illustrating effects of filtering time domain output.



Sensitivity: $\pm 10V$ (unfiltered trace)
 $\pm 4V$ (filtered trace)

D = Direct Wave Arrival (Unfiltered), 0.01 msec
 D_f = Direct Wave Arrival (Filtered), 0.16 msec
 $R_?$ = Reflected Wave Arrival off Bottom of Pier (Unfiltered), ?
 R_f = Reflected Wave Arrival off Bottom of Pier (Filtered), 7.22 msec

Fig. 4.6. WAPS tests on drilled pier illustrating effects of filtering on receiver output.

less than about a factor of ten away from the predominant wave frequency (Stokoe and Hoar, 1978). These effects are dependent upon many variables such as wave frequencies, cut-off filter frequencies, and wave travel distance. Under most conditions, there is no need to filter the recorded signal when performing measurements using the WAPER test method. This is shown in Fig. 4.5 , where both direct and reflected wave arrivals are easily identifiable in the unfiltered as well as filtered signatures. Conversely, as shown in Fig. 4.6, use of a filter is helpful, and often necessary, in extracting meaningful output when performing measurements using the WAPS test method.



CHAPTER 5. DESIGN CONSIDERATIONS AND PIER CONSTRUCTION

INTRODUCTION

As discussed in Chapter 3, the primary justification for this study is the inability of present evaluation methods to determine definitively the characteristics of pier irregularities or discontinuities (i.e., type and magnitude). To determine the effects of various drilled pier irregularities on stress wave propagation measurements in an attempt to improve current evaluation methods, it was deemed necessary to conduct full-scale field investigations of defective piers constructed under carefully controlled conditions. The testing program was divided into two parts: first, evaluation of previously constructed drilled piers on a site located near Granger, Texas, and second, instrumentation, construction and evaluation of test piers at a site located in Houston, Texas. In this chapter, a discussion is presented of design considerations adopted for the drilled piers, along with descriptions of the sites and local geological profiles. A description of the instrumentation and construction of the piers at the Houston site is also presented, including a pictorial documentation of the construction sequence. Results of stress wave propagation measurements performed on these drilled piers are then presented in Chapters 6 and 7.

DISCUSSION

The primary objective of any nondestructive test is accurate determination of the structural integrity of the pier. In evaluating drilled piers with stress waves, the structural integrity of the foundation is determined by identifying and assessing reflected wave arrivals. As discussed in Chapter 3, stress wave reflections occur in sound, straight-sided drilled piers at the concrete-air and concrete-soil interfaces at the top and bottom of the pier, respectively. Additional reflected wave arrivals indicate the possible presence of an additional boundary or boundaries in the drilled pier. Excluding the possibility of special drilled pier designs, such as a step tapered cross-section or an underreamed interface, additional wave arrivals most likely indicate discontinuities or irregularities in the pier. The success of wave propagation methods in determining defective drilled piers is dependent on identification of these additional reflected wave arrivals in the monitored receiver output. In instances when additional wave arrivals may be "masked" by spurious noise in the recorded signal, an attenuation study of multiple receiver output may prove to be a successful method of identifying defective drilled piers.

Regardless of the method of wave signature analysis, once it has been established that a discontinuity or irregularity is present in a drilled pier, questions invariably change to concern over the nature and magnitude of the defect and what influence the defect will have on the structural performance of the foundation system. Unfortunately, the state-of-the-art in regard to evaluation of drilled pier integrity by wave propagation methods allows few conclusions to be drawn concerning the characteristics and resulting effects of "identified" pier irregularities. At the present time, analysis of receiver output exhibiting additional or early reflections

discloses little in regard to the nature of the discontinuity or irregularity, and only a vague indication of the magnitude of the defect may be obtained from an attenuation study of the wave signatures. Therefore, for drilled piers evaluated by stress wave propagation methods, the geotechnical engineer currently must base decisions concerning alternatives for piers of questionable integrity on intuition and engineering judgement.

To eliminate some of the indecision and confusion surrounding identification of defective drilled piers and, in addition, to contribute to the advancement of drilled pier technology, it was decided to conduct an investigation of defective drilled piers with stress waves, concentrating on the influence of various pier irregularities on wave propagation measurements. To ensure accumulation of pertinent and realistic data, it was concluded that wave propagation measurements (as described in Chapter 3) would be performed on full-scale drilled piers constructed under carefully controlled conditions. The test piers would be equipped with known irregularities, with varying properties and locations. Then, with all other drilled pier parameters held constant, an analysis of measurements performed on these defective piers should reflect the influence of the different irregularities on wave propagation measurements and should act as a library of signatures for future use.

FIRST TEST SITE NEAR GRANGER, TEXAS

Initially, stress wave propagation measurements were performed on drilled piers previously designed and analyzed by Arias (1977) in an integrity study conducted for the Association of Drilled Shaft Contractors. Three drilled piers, each 30 in. (76.2 cm) in diameter and 39 ft (11.9 m)

long, were constructed adjacent to a highway bridge embankment near Granger, Texas. Authorization to construct the piers at this site was granted by the Texas State Department of Highways and Public Transportation.

Diagrams of the three test piers, illustrating the general configuration of the instrumentation and planned defects selected by Arias, are presented in Figs. 5.1 through 5.3. The piers were instrumented with both vertical and horizontal velocity transducers. (Because the scope of the study performed by the present authors was limited solely to the generation and monitoring of compression waves propagating through drilled piers, only the vertical velocity transducers were of importance in this investigation.) The transducers were positioned at various depths within the piers by attachment to a 2.5 in. (6.35 cm) I.D. PVC pipe extending along the vertical axis of each shaft. The PVC pipes were centered in the piers by 0.25 in. (0.64 cm) thick, circular pieces of plywood located at the bottom of the shafts and 0.25 in. (0.64 cm) by 0.50 in. (1.27 cm) metal bars spaced 120 degrees apart around the pipe circumference and attached at 10 ft (3.0 m) intervals along the length of the pipe.

In terms of pier irregularities, Shaft 1 had no defects and hence was considered the control pier. Shafts 2 and 3 were constructed with various irregularities representing possible problems resulting during construction. The irregularities planned for Shaft 2 consisted of a 2 ft (0.61 m) thick defect, composed of soil from the augered borehole and a styrofoam-filled bag positioned at a depth of 20.2 ft (6.2 m) below the top of the pier. This defect was selected to simulate possible entrapment of slurry caused by elevating the concrete tremie above the concrete-slurry interface when utilizing the slurry displacement method of drilled pier construction.

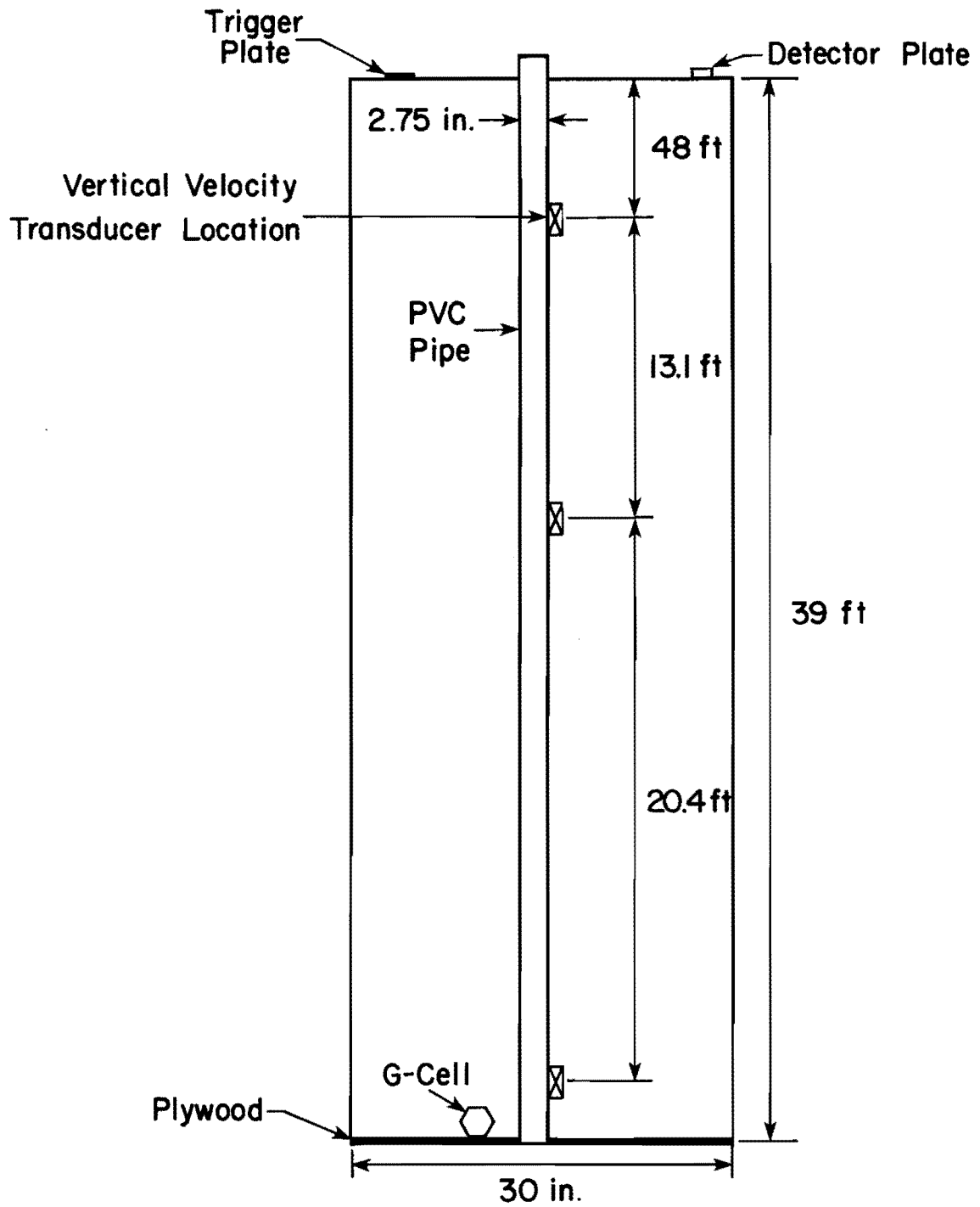


Fig. 5.1. Test shaft No. 1; sound shaft (Arias, 1977).

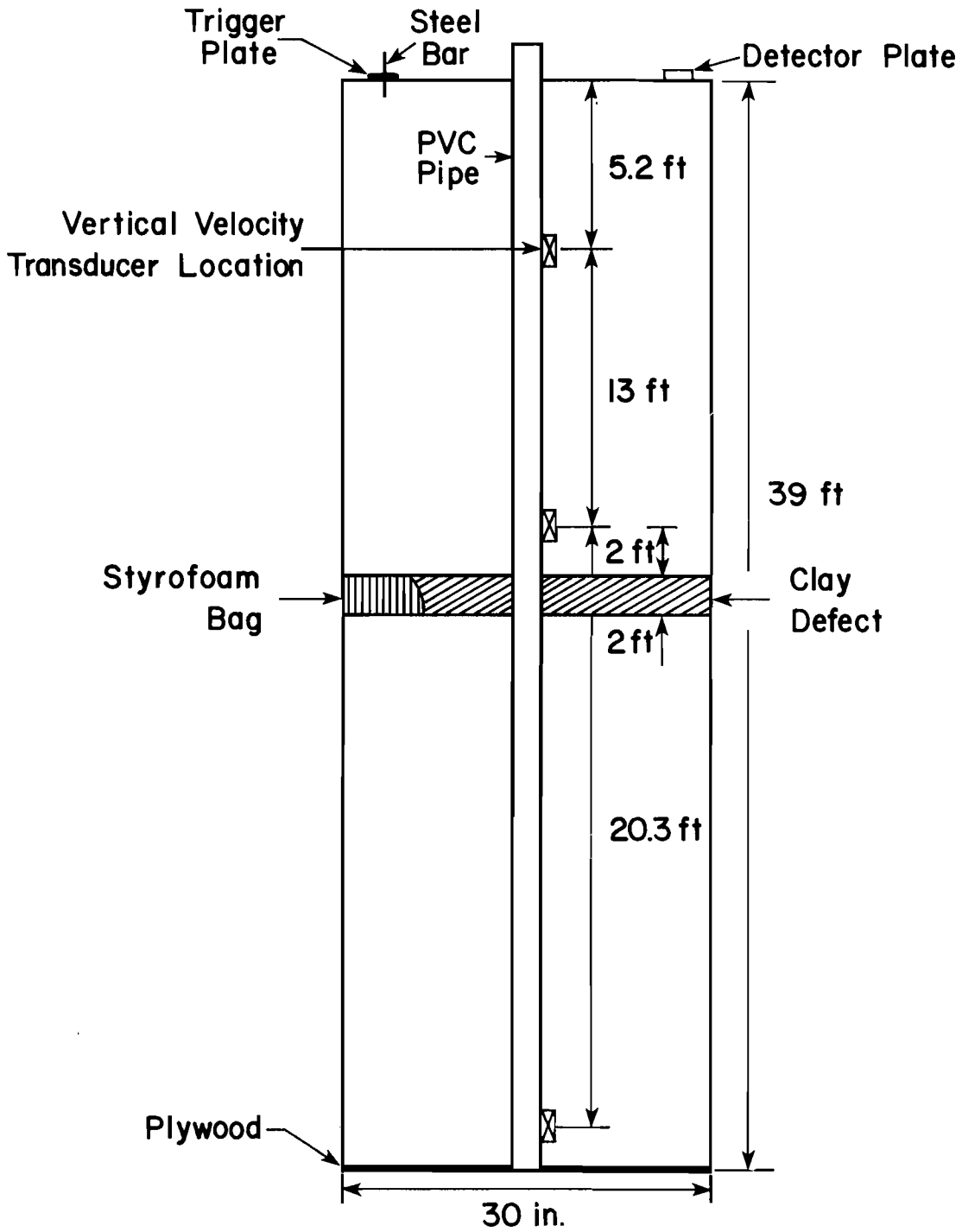


Fig. 5.2. Test shaft No. 2; defective shaft (Arias, 1977).

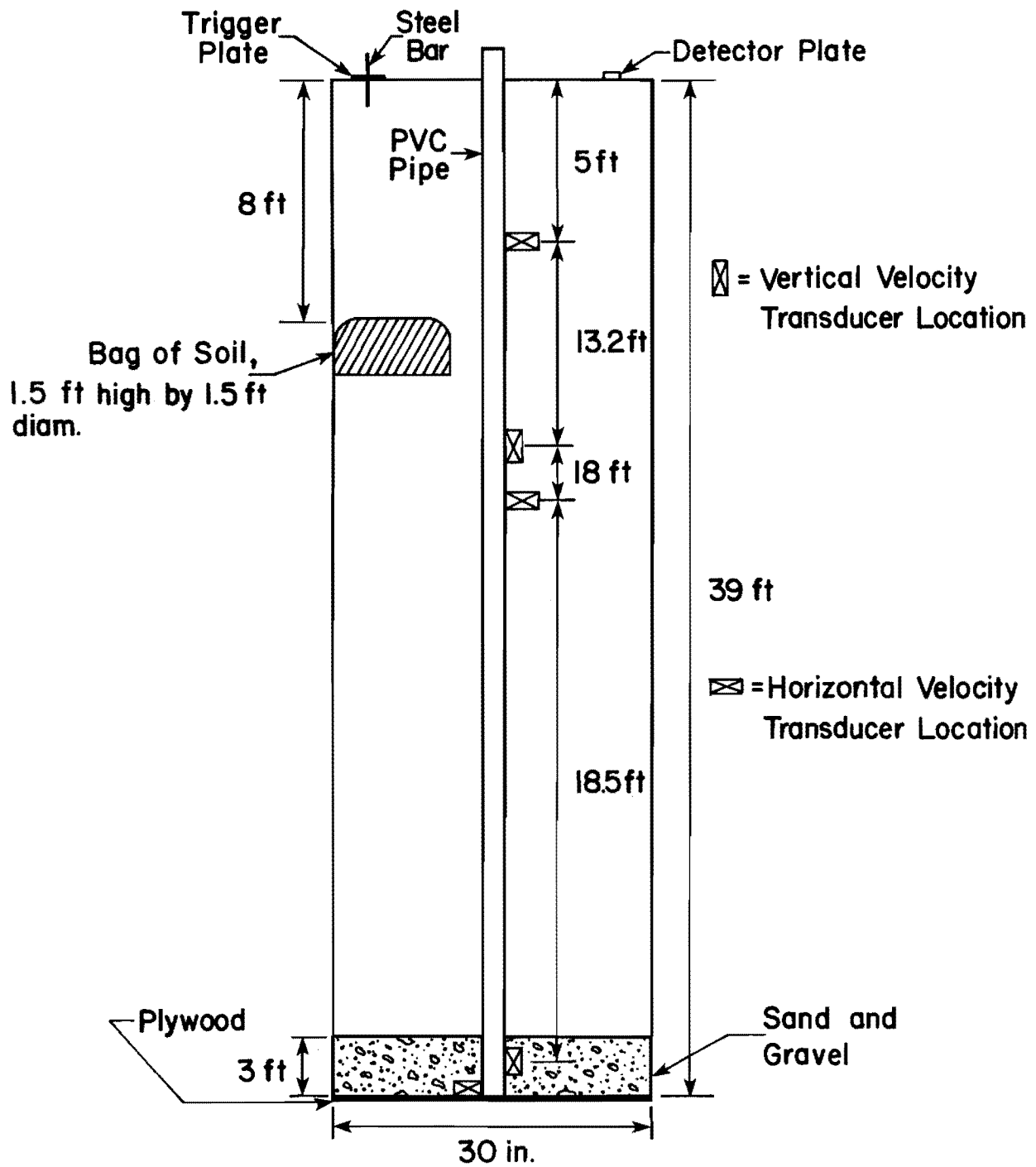
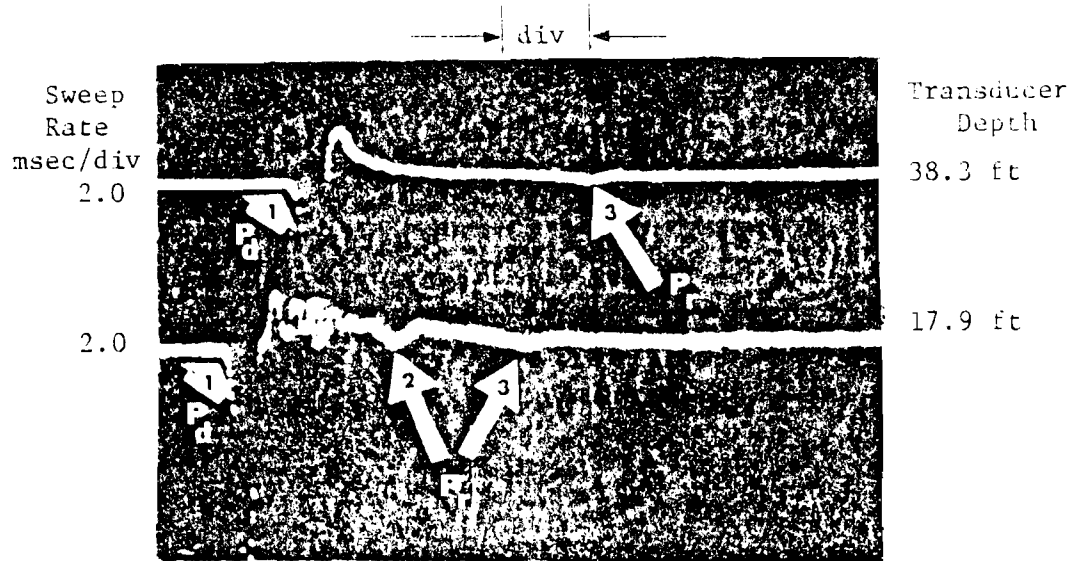


Fig. 5.3. Test shaft No. 3; defective shaft (Arias, 1977).

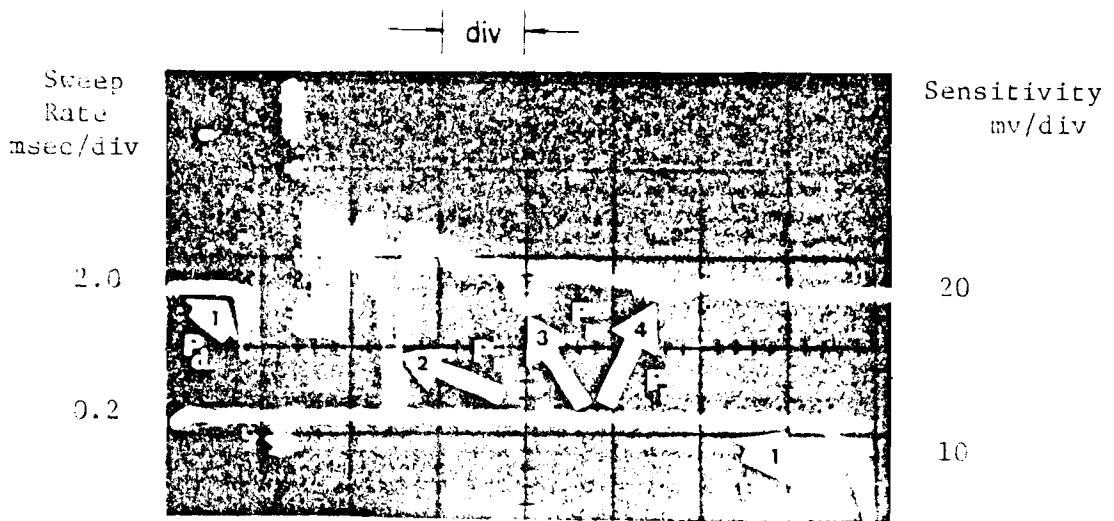
Shaft 3 was constructed with two irregularities, consisting of: (1) a 1.5 ft (0.46 m) diameter by 1.5 ft (0.46 m) thick bag of soil, and (2) a 2.5 ft (0.76 m) diameter by 3 ft (0.91 m) thick sand and gravel seam at the bottom of the shaft. The soil-filled bag, located at a depth of 8 ft (2.4 m) below the top of the pier, represents a soil inclusion possibly resulting from a cave-in of the borehole sidewall during concreting operations. The sand and gravel seam was positioned at the extreme bottom of the test pier, and was an attempt to simulate a possible cement wash-out resulting from flowing ground water.

In his study, Arias concluded that the stress wave propagation method (which he termed the direct arrival-reflection method) yielded satisfactory results, provided the transducers are located at the bottom of the drilled piers and exact elevations of both the bottom and top of the piers and any special configurations or differences in pier dimensions are known. Stress wave measurements conducted on Shaft 1 (free of planned defects) and Shaft 2 (full cross-sectional defect at 20.2 ft (6.2 m) below pier top) substantiated the above statement as shown in Fig. 5.4. However, regarding his analysis of the wave signatures recorded for Shaft 3, few conclusions could be drawn from a review of the recorded wave signatures concerning the type, magnitude or depth of the two defects in the pier. A reduction in the velocity of the direct P-wave (computed from the embedded receiver at a depth of 18 ft (5.5 m)) was the only indication of an irregularity in the upper portion of the pier (soil inclusion). The weak wave signature recorded at the 38.5 ft (11.7 m) embedded receiver in Shaft 3, shown in Fig. 5.5, was correctly attributed to the sand and gravel seam located at the elevation of the receiver. However, under normal field conditions, the weak wave signature could be due to a contaminated or faulty receiver, which could have been damaged during



Sensitivity = 10 mV/div.
 Pd = direct compression wave arrival
 Pr = reflected compression wave arrivals

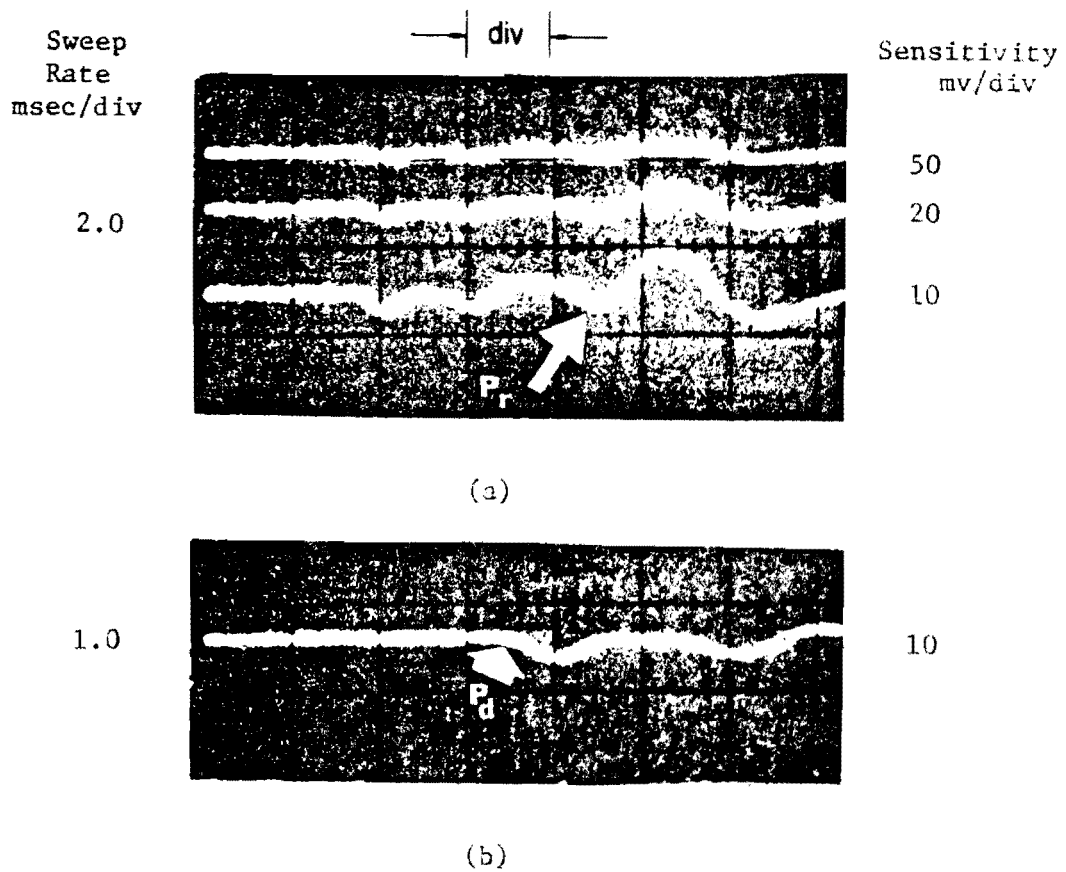
a. Signatures of stress wave recorded by vertical velocity transducers located in shaft No. 1.



Pd = direct compression wave arrival
 Pr = reflected compression wave arrivals

b. Signatures of stress waves recorded by the vertical transducer embedded in shaft No. 2 at a depth of 18.2 ft. (4.8m) showing reflections.

Fig. 5.4. Wave propagation measurements conducted on sound and defective shafts at Granger test site (Arias, 1977).



P_d = direct compression wave arrival

P_r = reflected compression wave arrival

Fig. 5.5. Signatures of stress waves recorded by the vertical transducer embedded in shaft No. 3 at a depth of 38.5 ft. (11.7m) (Arias, 1977).

pier construction or by corrosive agents (cement, water, etc.). Under actual field conditions, identification of the lower sand and gravel defect in this pier would be unlikely without additional receiver information.

Uncertainty surrounding identification of the physical properties and depths of the planned defects in Shaft 3 may be attributed to a number of variables. It may be concluded from the results of Arias' investigation that determination of drilled pier integrity is difficult, at best, when two or more irregularities are present in the pier. Evaluation is further complicated when irregularities differ in nature and magnitude. Although a general indication of the planned defects was obtained from an attenuation study of the monitored wave output, a better understanding of the pier integrity may have been possible had the test pier been equipped with a greater number of receivers or the receiver configuration been altered. Due to the unanswered questions raised by Arias' study, an additional study was planned and conducted at a site in Houston, Texas.

SECOND TEST SITE; HOUSTON, TEXAS

Additional stress wave propagation measurements were performed on test piers constructed at a site located in southeast Houston, Texas. This integrity study was sponsored by the Texas State Department of Highways and Public Transportation through a contract with The University of Texas at Austin, Center for Transportation Research. Four test piers were constructed in the equipment stockyard of Farmer Foundation Company, the foundation contractor that constructed the drilled piers. A site vicinity map of the area is shown in Fig. 5.6.

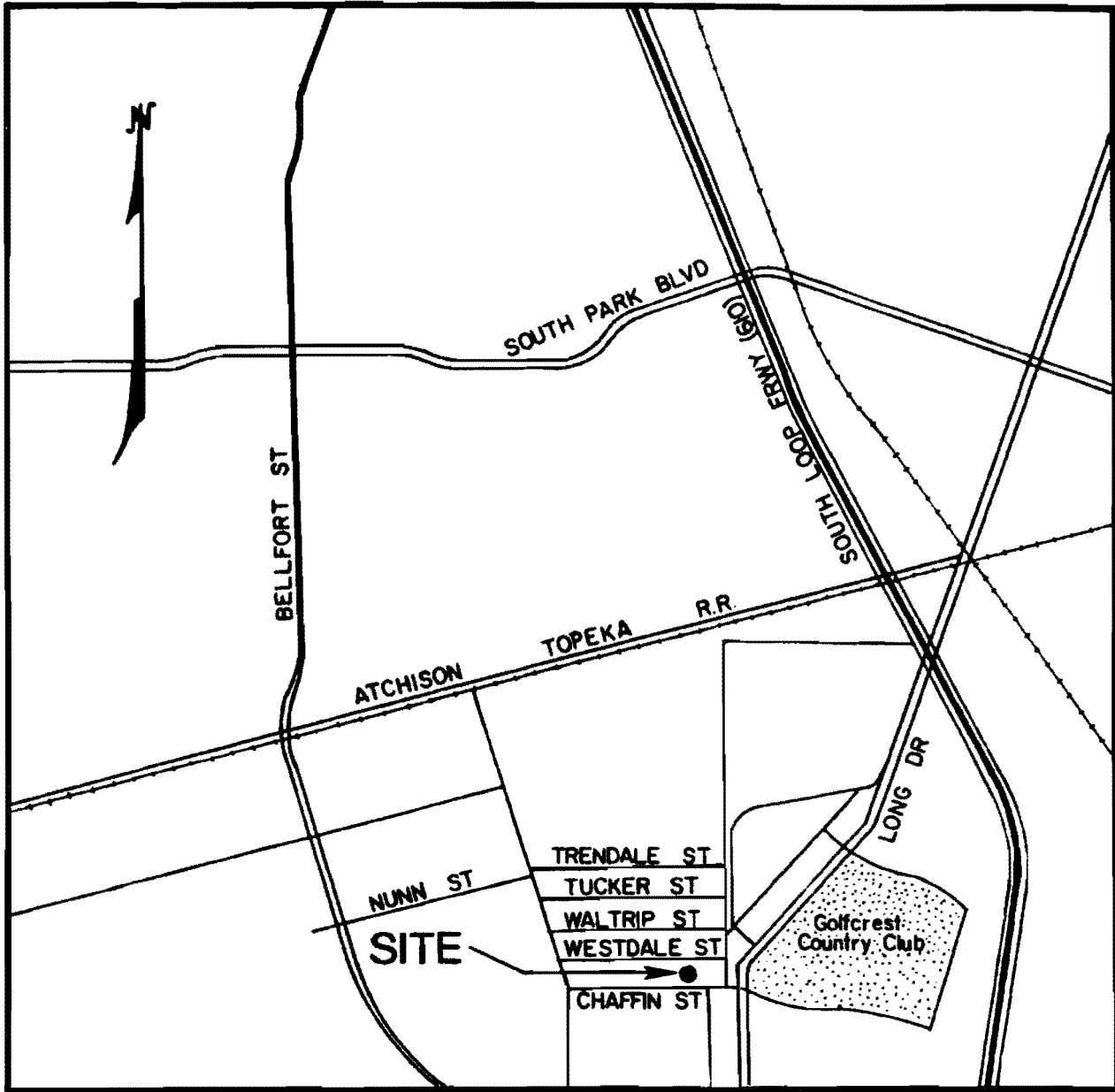


Fig. 5.6. Map of second test site in Houston, Texas.

Number and Dimensions of Piers.

Throughout the design stages, decisions concerning the various defects to be investigated were dependent on the number of drilled piers incorporated in the test program and their respective dimensions. In turn, the size and number of test piers to be constructed was governed by the expense of construction and the allotted research funds. In addition, two interrelated criteria influenced the pier dimensions. The piers were designed so the length simulated actual field members and, thereby, allowed performance of pertinent wave propagation and attenuation studies. However, the pier length was dependent on the second criteria, which involved the length-to-diameter ratio, commonly referred to as the slenderness ratio. In practice, typical slenderness ratios for drilled piers range between 20 and 30. To satisfy these criteria and remain within economic limitations, a slenderness ratio of 20 was deemed appropriate.

Based on this analysis, the decision was made to construct four drilled piers, each pier being 50 ft (15.2 m) in length and 2.5 ft (0.76 m) in diameter. Identical dimensions were selected for each pier so that pier geometry did not influence wave propagation measurements, only the implanted irregularities.

In addition to the number and dimension of the piers, the topic of pier spacing surfaced during the early stages of the design process. Upon deliberation, it was concluded that the arrangement of the four test piers would bear an insignificant influence on wave propagation measurements, regardless of the properties of the irregularities selected for investigation. In view of this decision, a center-to-center spacing of two diameters was selected, based on the local subsurface conditions and pre-existing boundary constraints at the construction site.

Construction Materials.

Materials utilized in the construction of drilled pier foundations, such as concrete and reinforcing steel, are selected on the basis of predetermined structural design requirements. Concrete compressive strength and hardening rate can be varied, as well as the size and quantity of reinforcing steel, to satisfy the structural design requirements. In addition, selection of construction materials is dependent on local subsurface conditions and the method employed to construct the foundation members.

Concrete. Since the test piers would not support a structure, the compressive strength of the concrete was not critical. However, the quality of the concrete was of importance. As mentioned previously, poor quality concrete can result in low compression wave velocities and/or additional reflection boundaries, which could impair the findings of the proposed wave propagation measurements. Therefore, to avoid possible complications attributable to concrete quality, a mix design of 3,000-psi compressive strength concrete was selected for use in constructing the test piers. The concrete mix, a standard design selected by the supplier, consisted of five sacks of Type I cement per cubic yard of concrete and 1.5 in. (3.8 cm) nominal size coarse aggregate. Representative samples of the concrete were secured during placement for field inspection and evaluation. In addition, standard specimens for compressive strength tests were fabricated during concrete placement, allowing for future comparisons and correlations between P-wave velocity and concrete quality. Results of the compressive strength tests and comparisons with P-wave velocities are presented in Chapter 6.

Reinforcing Steel. In practice, reinforcing steel is commonly included in drilled piers to resist lateral loads or tensile uplift forces and to tie the piers to the structure. In this study, reinforcing steel was designed to

extend down the entire length of each pier. This was done so that embedded receivers could be positioned at various depths, resulting in increased instrumentation capabilities and, consequently, an abundance of experimental attenuation data. The reinforcing, designed identically for each individual test pier, consisted of a 22 in. (55.9 cm) diameter cage comprised of four number 9 bars extending vertically down the pier. Circular steel bands welded to the bars at 10 ft (3.05 m) intervals form the reinforcing cage and insure even spacing of the steel rods along the length of the drilled pier. The cages are shown in Figs. 5.12 through 5.18, documenting the construction sequence.

Planned Irregularities.

The greatest difficulties encountered during the design stages concerned the selection of planned irregularities. As mentioned previously, a number of undesirable conditions can occur during construction of a drilled pier which can result in a discontinuity or irregularity. Furthermore, the possibility exists of a number of these adverse conditions occurring simultaneously, greatly increasing the number of possible combinations of defects. Variable properties of each defect include: (1) type (air void, soil inclusion, slurry entrapment, or cement washout); (2) nature (cohesive soil, cohesionless soil, or combination soil inclusion); and (3) dimensions. It was impossible to perform a detailed investigation of all possible irregularities in the number of test piers designated for this study; the resulting wave propagation data would only be inconclusive. Therefore, to obtain wave propagation data pertinent to the objective of the study, that being the understanding and advancement of integrity evaluation for major defects, the only feasible alternative was to limit the scope of the study and concentrate on a single phase of the overall problem.

Dimensions. Questions often arise following the discovery of a defective drilled pier concerning the size and nature of the purported irregularity. Although knowledge of the type of irregularity present in the pier would be helpful in decisions concerning possible alternatives, it was reasoned that knowledge of the magnitude of the "identified" defect would be of greater benefit to the engineer in the decision making process. Therefore, for this study, the decision was made to vary the dimensions of a single type of irregularity and evaluate only the effects of defect magnitude on wave propagation measurements.

Again, there are a number of possible choices regarding size and geometry of drilled pier irregularities to be investigated. However, the dimension of principal importance to the structural performance of the foundation member is the cross-sectional area of the drilled pier dominated by an irregularity. As the cross-sectional area of the defect increases with respect to the drilled pier cross section, the greater the risk of structural failure under the designed load. Due to the importance of the cross-sectional area of the irregularity on the structural integrity of the drilled pier, the decision was made to investigate variations in this defect dimension on wave propagation measurements.

To acquire pertinent information concerning the effects of cross-sectional dimensions of the irregularity on wave propagation measurements, especially in the attenuation phase of this investigation, it was necessary to design all defects to be of identical thickness. With this in mind, the following choices were made concerning the dimensions of the irregularities. Of the four test piers designed for this study, one pier would be absent of any irregularity. This sound pier, designated as Shaft A in Fig. 5.7, would be employed as a control pier with which to base comparisons with the

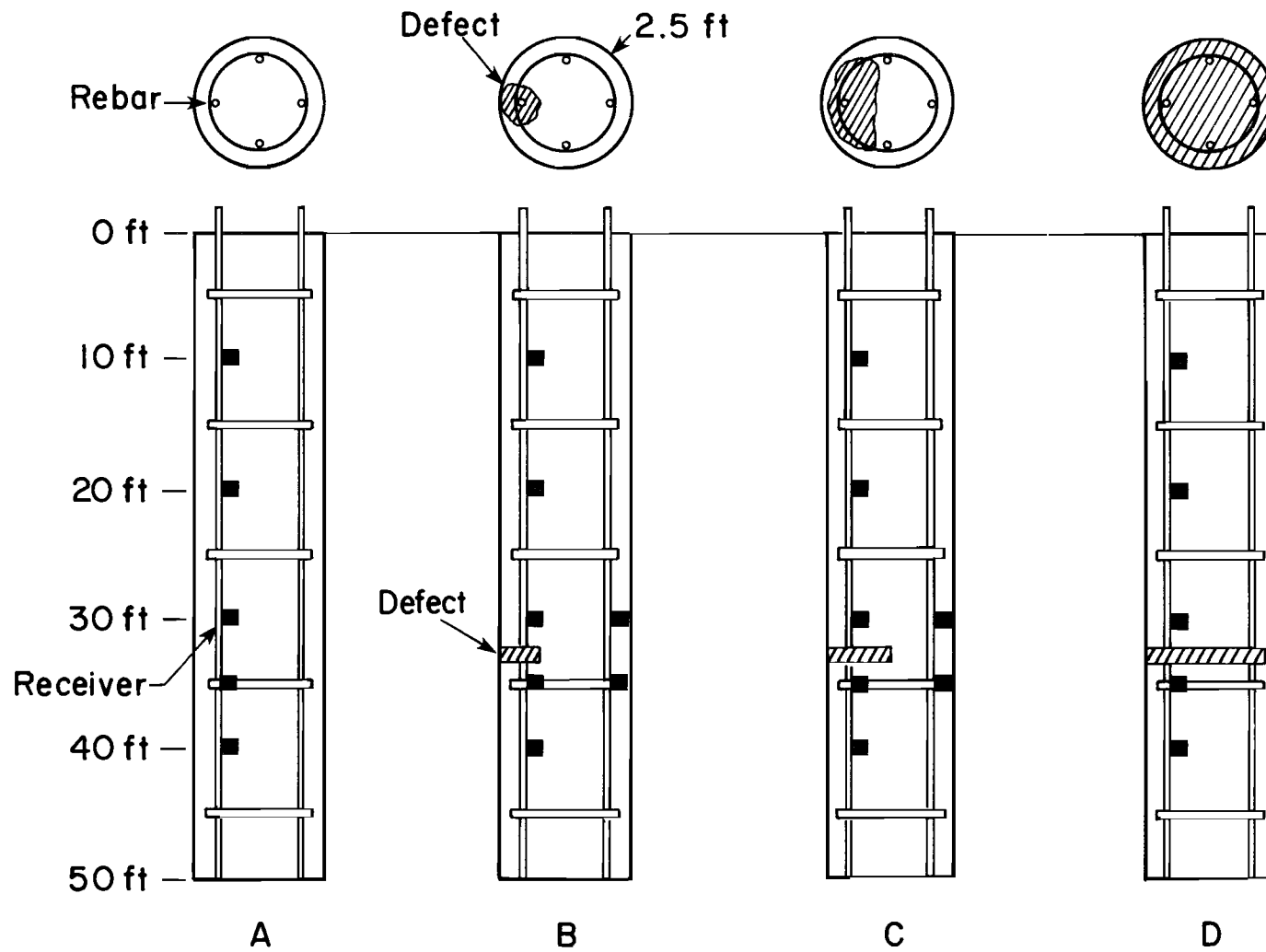


Fig. 5.7 Test piers constructed at second test site (Houston, Texas), showing defect and embedded receiver configurations.

defective piers. The remaining three piers, designated as Shafts B, C, and D in Fig. 5.7, would contain irregularities of varying cross-sectional areas, ranging from $1/4$ to $1/2$ to the full cross-sectional area of the piers, respectively. Although dynamic vibration test methods have successfully "identified" irregularities as thin as cracks in driven piles, all irregularities in this study were designed to be 1 ft (0.3 m) thick across their total cross section, to assure wave reflections from the imposed boundaries.

Nature. To insure the collection of wave propagation data solely related to irregularity cross-sectional magnitude, the scope of this study had to be further limited to evaluating the effects of various sizes of defects of identical nature. Because the nature of the irregularity would not vary, it was decided that the type of defect should be typical of those most often encountered in practice. Irregularities referenced frequently in drilled pier literature include shaft "necking," cement "washout" and soil inclusions. Based on such factors as number of case histories and ease of construction, the decision was made to investigate the effects of soil inclusions on wave propagation measurements.

Location. Prior to committing to a specific installation method for the drilled pier irregularities, it was necessary to establish the locations of defects within the drilled piers. Initially, it was decided that the various soil inclusions would be located at the same elevation within their respective piers, regardless of the final elevation chosen. Positioning the soil inclusions at the same elevation would allow relevant comparisons to be made between the various wave propagation measurements performed on each test shaft.

It was shown in Arias' study (1977) and similar investigations that substantial defects located within the upper regions of drilled piers are identified by assessing reflected wave arrivals and attenuation characteristics of wave signatures. However, near-surface irregularities typically attenuate the input pulse significantly during the early stages of wave propagation, resulting in a limited amount of data obtainable from lower embedded receivers. Likewise, irregularities positioned near the bottom of the test piers result in a reduction of wave propagation/attenuation data. In this case, wave reflections off the bottom of drilled piers are typically "masked" in the monitored receiver output by wave excitation resulting from the wave reflecting off the irregularity. Because of their limiting effect on wave propagation data and the fact that both conditions were addressed and evaluated in Arias' (1977) and Hearne's (1984) studies, irregularities positioned in the upper and lower regions of the test piers were eliminated from consideration in this study.

Thus, it was decided that the irregularities should be positioned within the test piers at a depth which was deep enough to provide an abundance of wave propagation data, yet at a sufficient height above the pier bottom to assure collection of pertinent incident/reflected wave attenuation data from the concrete-soil interface. The ideal defect elevation for optimization of wave propagation measurements was controlled by the wavelength of the generated compression wave. Assuming the wavelength of the incident P-wave to be long (at least 2 to 3 times the pier diameter) compared to the distance between the irregularity and the pier bottom, output registered from receivers positioned in the vicinity of the irregularity would be confusing due to overlapping of the incident and reflected waves. Because of problems associated with this overlapping phenomenon, the irregularities planned for

the test shafts were located at a depth above the bottom of the piers corresponding to approximately one-half the wavelength of the generated P-wave. In his integrity study, Hearne (1984) reported wavelengths in drilled piers ranging between 10 and 25 ft (3.2 and 7.6 m), depending on the type of hammer employed as the source. Since a variety of compression wave sources were scheduled for investigation in this study, a conservative wavelength of 30 ft (9.1 m) was selected for locating the defect. Therefore, the irregularities were positioned 15 ft (4.6 m) above the bottom of the test piers, or at a depth of 35 ft (10.7 m) below the top of the piers. However, to simplify the receiver arrangements and corresponding data reduction, the 1 ft (0.3 m) thick soil inclusions were located within the test piers at a depth of 32 to 33 ft (9.8 to 10.1 m) below the top of the piers, as shown in Fig. 5.7.

Installation. During preliminary discussions, it was established that the method employed to install the soil inclusions within the test piers was dependent on the method of drilled pier construction, which in turn was dependent on local subsurface conditions. Unfortunately, information concerning the nature of subsurface conditions at the test site was unavailable during the preliminary design phase. To avoid possible problems associated with drilled piers constructed in areas consisting of loose sands, soft clays, and/or a shallow water table, the conservative decision was made to utilize steel casing in constructing the test shafts, regardless of the soil conditions encountered at the site. The use of steel casing in constructing the test piers reduced the possibility of entrapping additional irregularities within the test piers.

The decision to case the piers influenced the method of installing the defects. Steel casing placed in the test piers during the construction

process eliminated all possibilities of constructing the planned soil inclusion as extensions of the surrounding soil. A simple method of defect installation employed in the past and adaptable to cased drilled piers utilizes bags filled with sand or clay. The drilled shaft is filled with concrete to a predetermined elevation, the sand or clay-filled bags are dropped down the hole, and concrete placement is continued to the ground surface. Steinbach and Vey (1975) reported wave propagation measurements with surface receivers performed on a 60 ft (18.2 m) long pier constructed with irregularities installed in the manner described above. This crude method of irregularity installation proved to be effective. However, the test pier incorporated in their study was absent of reinforcing steel which could obstruct falling bags and, furthermore, the defect was designed to occupy the full cross section of the shaft at the designated elevation. The test piers in this study were planned to contain steel reinforcing cages for the purpose of attaching receivers. Furthermore, the soil inclusions to be investigated varied in cross-sectional area, and it was reasoned that the smaller defects warranted anchoring to avoid displacement from the designated elevation during concrete placement.

A number of installation methods, more precise in nature, were devised and discussed before a final procedure was selected. To eliminate the problems associated with the interior reinforcing cages, the irregularities were constructed and positioned on the cages prior to installation of the cages within the drilled shafts. The irregularities, comprised of large burlap bags filled with clay obtained from the auger cuttings during construction, were attached to the reinforcing cages at the desired elevation with heavy gauge bailing wire, as shown in Fig. 5.14 in the construction

sequence. The cross-sectional area of the irregularity governed the size and number of bags to be attached to each reinforcing cage.

The remaining problem in constructing the defective test piers concerned concrete placement. Early in the design stages, it was suggested that a tremie would reduce the possibility of concrete segregation, which could result in additional reflection boundaries in the test piers or altered wave propagation measurements due to low P-wave velocities. Use of a 12 in. (30.5 cm) diameter tremie would allow continuous concrete placement throughout the entire length of Shaft B, the test pier containing the soil inclusion covering 1/4 of the total cross-sectional area. However, problems were anticipated prior to placing concrete in Shafts C and D, which contained the soil inclusions covering 1/2 and all of the cross-sectional area, respectively, due to the impassability of the tremie created by the defects and accompanying reinforcing cages. To remedy this situation, it was decided to initially place concrete in Shafts C and D to the level corresponding to the bottom elevation of the defects (elevation of - 33 ft (- 10.0 m)), then remove the tremie and install the reinforcing cages complete with attached defects. The reinforcing cages were forced through the small amount of concrete located in the bottom of the piers until contact of the cage bottom on the concrete-soil interface was assured. With the reinforcing cages in place, the concrete placement operation was resumed.

Instrumentation.

It was stated in Chapter 4 that monitoring of stress waves in this investigation would be accomplished by transducers positioned in various configurations in the test piers. The transducers utilized in this study as receivers consisted of vertical velocity transducers, ceramic piezoelectric transducers, and accelerometers. Of the two categories of receiver

configurations investigated in this study, the surface receiver method (Fig. 3.4) of monitoring stress waves required little consideration prior to construction of the test piers. However, the embedded receiver configuration (Fig. 3.1) required pre-construction consideration in order to position the receivers within the drilled piers for optimum utilization.

Vertical Velocity Transducers. Vertical velocity transducers embedded within drilled piers have been shown to be effective monitors of direct and reflected stress waves (Arias, 1977; Hearne et al, 1981). For this investigation, the decision was made to equip the test piers with a number of vertical velocity transducers, so that information about the nature of wave motions could be generated. Additionally, the large number of velocity transducers would provide an excellent means of studying the attenuation characteristics of propagating stress waves.

It was decided that each pier would be instrumented with a string of vertical velocity transducers for the direct purpose of monitoring stress wave arrivals. To ensure the performance of a comprehensive integrity investigation, each string consisted of five velocity transducers embedded within each pier at depths of 10-, 20-, 30-, 34.5- and 40-ft (3.0-, 6.1-, 9.1-, 10.5- and 12.2-m) as shown in Fig. 5.7. The velocity transducers were located at these predetermined elevations by attachment to the steel reinforcing cages prior to installation of the cages (see Fig. 5.12). Each velocity transducer, encased in a plastic marsh case to prevent moisture contamination, was shielded from extraneous waves propagating down the reinforcing steel by placing lengths of 0.5 in. (1.3 cm) thick, foam pipe insulation between the receiver and rebar.

In addition to the string of embedded velocity transducers installed in each test pier, Shafts B and C were supplemented with other vertical velocity

transducers. These additional receivers, identical in make to the others, were attached to the steel reinforcing rods directly opposite the 30 and 34.5 ft (9.1 and 10.5 m) velocity transducers in the string of embedded receivers. These supplemental velocity transducers were added to Shafts B and C due to the fact that these piers contained defects averaging only part of the cross-sectional area, and it was desired to augment information concerning the nature of initial and reflected stress waves propagating through shafts of varying cross-sectional areas.

As a sideline to this study, the special case of unreinforced drilled piers was planned for investigation. Under certain soil conditions, lateral loads and/or uplift forces acting on a drilled pier foundation are of such small magnitude that reinforcing steel is unnecessary in the structural design. Unfortunately, the absence of reinforcing steel in the drilled pier creates a problem for wave propagation testing with embedded receivers. At the present time, the WAPER method requires receivers to be attached to steel reinforcing installed in the drilled piers. To investigate the possibility of using embedded receivers in unreinforced drilled piers, Shafts B and D were instrumented with vertical velocity transducers which were not attached to the reinforcing. These "floating" receivers were positioned in the test piers by securing the instruments to the kelly bar of the drilling rig and pushing the receivers down through the concrete to the desired elevation. The receivers were secured to the kelly bar in such a manner that the instruments would remain embedded within the concrete shafts upon removal of the bar (see Figs. 5.24 and 5.25). The floating velocity transducers were located at a depth of 10 ft (3.0 m) within Shafts B and D in order to allow comparisons between them and the embedded receivers attached to the reinforcing steel at a depth of 10 ft (3.0 m).

Ceramic Piezoelectric Transducers. As discussed in Chapter 4, two ceramic materials differing in piezoelectric coefficients and dielectric constants were selected for use as embedded transducers in this study. Designated as LTZ-2 and LTZ-2H, with the 2H material possessing the higher dielectric constant, the two materials were ordered directly from the manufacturer as "finished" transducer elements of varying cross-sectional dimensions. The cross-sectional areas of the ceramic transducers were varied in order to determine the dimension of optimum performance in wave propagation measurements, since the cross-sectional area of the ceramic transducer is directly related to the electro-mechanical capacity of the sensors.

Once shielded electrical wires were soldered to the electrodes of the ceramic transducers and the elements were encased in suitable epoxy, the piezoelectric receivers were ready for installation in the drilled piers. Installation was performed in a manner identical to the methods employed for the velocity transducer (see Fig. 5.13). The ceramics were secured to the reinforcing cage at predetermined elevations prior to insertion of the cage into the drilled shaft. However, due to the limited number of piezoelectric transducers utilized as receivers in this study, the location scheme differed from that planned for the velocity transducers. All ceramic transducers were positioned in the designated piers at a depth of 20 ft (6.1 m). A listing of the transducers is given in Table 5.1. The majority of the ceramic transducers were placed in Shafts A and C. This scheme was adopted to obtain individual and comparative information concerning the effectiveness of the ceramic transducers in monitoring propagating stress waves in sound piers (Shaft A) and piers containing sizable discontinuities (Shaft C). The elevation for the ceramic transducers was selected to provide a suitable time

TABLE 5.1. DIMENSIONS AND DISTRIBUTION OF PIEZOELECTRIC TRANSDUCERS
WITHIN TEST PIERS

Shaft	Ceramic Transducer Type	
	LTZ-2 Dimensions, in.	LTZ-2H Dimensions, in.
A	$1/3 \times 1/4 \times 1$	$1/3 \times 1/4 \times 1$
	$1/2 \times 1/8 \times 1$	$1/2 \times 1/8 \times 1$
	$1/2 \times 1/4 \times 1$	$1/2 \times 1/4 \times 1$
B	$1/3 \times 1/4 \times 1$	$1/3 \times 1/4 \times 1$
C	$1/3 \times 1/4 \times 1$	$1/3 \times 1/4 \times 1$
	$1/2 \times 1/8 \times 1$	$1/2 \times 1/8 \times 1$
	$1/2 \times 1/4 \times 1$	$1/2 \times 1/4 \times 1$

*all transducers oriented with 1-in. length parallel to the longitudinal axis of the pier

interval between the arrival of the initial wave pulse and the subsequent reflection from the planned defect, aiding in ease of analysis of the wave propagation records. Furthermore, the piezoelectric transducers were located within the test piers at an elevation instrumented with vertical velocity transducers, which also permitted comparisons between the contrasting receivers.

Subsurface Stratigraphy

The Houston site is located in a region consisting predominately of highly plastic clays. Based upon visual classification of the subsurface soils performed during pier drilling operations, stiff to very stiff, brown and gray, ferrous-stained, silty clays were encountered to a depth of 27 ft (8.2 m) below the existing ground surface. A 2 ft (0.6 m) thick, medium dense, uniform fine silty sand stratum was encountered within the silty clay stratum at a depth of approximately 16 ft (4.9 m) below grade. These near-surface silty clays appear to belong to a group geologically referred to as the Lake Charles Formation. These soils, classified under the Pleisocene epoch of the Quaternary period, are typically highly plastic clays, generally possessing plasticity indices on the order of 50 to 60.

Below the Lake Charles clays, very stiff to hard, reddish-brown and dark gray clays were encountered to the 50 ft (15.2 m) termination depths of the piers. These clays appear to be part of a massive formation geologically classified as the Beaumont Formation, comprised of highly swelling clays with plasticity indices typically in the range of 65 to 80 percent.

Pier Construction.

The drilled piers were constructed on consecutive days in late March, 1981. Shafts A and C were constructed on March 24, while Shafts B and D were

completed the following day. A pictorial documentation of the construction sequence for the piers is presented in chronological order in Figs. 5.8 through 5.26.

SUMMARY

Full-scale field investigations of defective drilled piers were deemed necessary to determine the effects of various pier irregularities on stress wave propagation measurements. Two sites were selected for study. Initially, wave propagation measurements were performed on drilled piers previously constructed at a site near Granger, Texas (Arias, 1971). Three drilled piers, each 30 in. (76.2 cm) in diameter and 39 ft (12.2 m) in length, were constructed at the Granger site, with two of the piers instrumented with various irregularities representing possible pier integrity problems resulting from poor construction practices. Tests performed on these drilled piers were used to evaluate advanced signal recording and processing equipment in conjunction with previously established wave propagation measurement techniques.

Additional drilled piers were constructed at a second site in southeast Houston, Texas, to assess modifications in both wave propagation equipment and measurement techniques. Four drilled piers, each 32 in. (81.3 cm) in diameter and 50 ft (15.2 m) in length, were constructed at the site.

Irregularities in the form of soil inclusions were constructed in three of the four drilled piers, with the soil inclusions varying in cross-sectional areas in the test shafts. Various modifications to the previously established wave propagation measurement techniques, including embedded piezoelectric ceramic transducer receivers, different sources and surface impact mediums, and source-receiver configurations, were proposed for the



Fig 5.8. Drilling 50 ft. (15.2 m) pier shaft using 32 in. (81.3 cm) diameter auger.



Fig 5.9. Mixing bentonite slurry in pier shaft to seal off permeable, water-bearing, sand stratum at depth of 16 ft. (4.9 m) and to stabilize soil along sides of shaft.



Fig. 5.10. Installing 30-in. (76.2 cm) diameter steel casing in augered hole.



Fig. 5.11. Extracting bentonite slurry from within steel casing using plunger-type bucket.

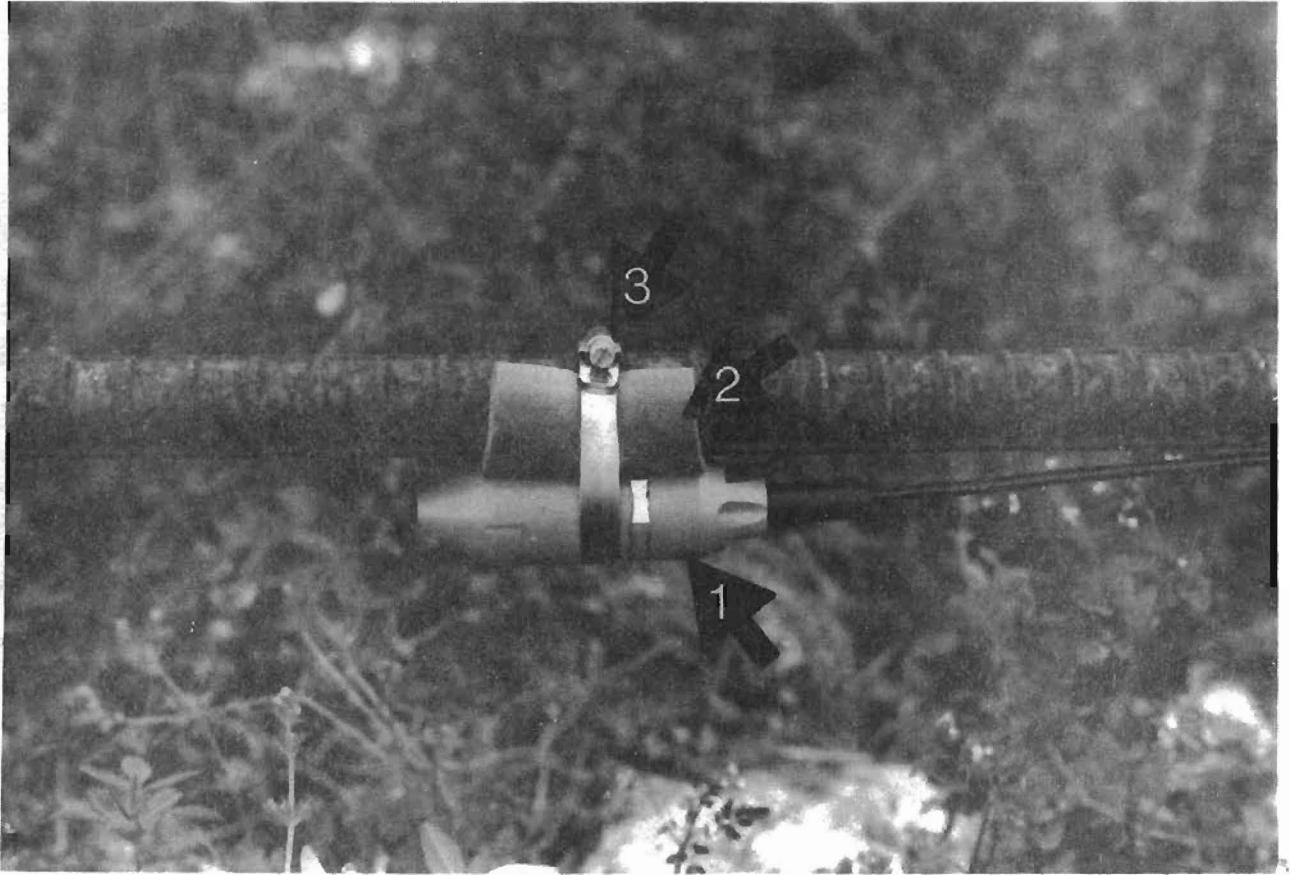


Fig 5.12. Vertical velocity transducer attached to steel reinforcing cage prior to installation.



Fig 5.13. Ceramic transducers attached to steel reinforcing cage prior to installation.



Fig. 5.14. Soil inclusion (1/4 cross-sectional area) attached to steel reinforcing cage prior to installation.



Fig. 5.15. Soil inclusion (1/2 cross-sectional area) attached to steel reinforcing cage prior to installation.



Fig. 5.16. Soil inclusion (full cross-sectional area) attached to steel reinforcing cage immediately prior to installation.



Fig. 5.17. Installing instrumented reinforcing cage with attached soil inclusion "defect".



Fig. 5.18. Installing 2.5 in. (6.4 cm) diameter PVC pipe in test shaft.



Fig. 5.19. Installing concrete tremie.



Fig. 5.20. Placing concrete for lower portion of pier.



Fig. 5.21. Placing concrete through side of tremie as concrete level rises in pier.



Fig. 5.22. Placing concrete in upper portion of pier by partially removing steel casing and utilizing concrete bucket.

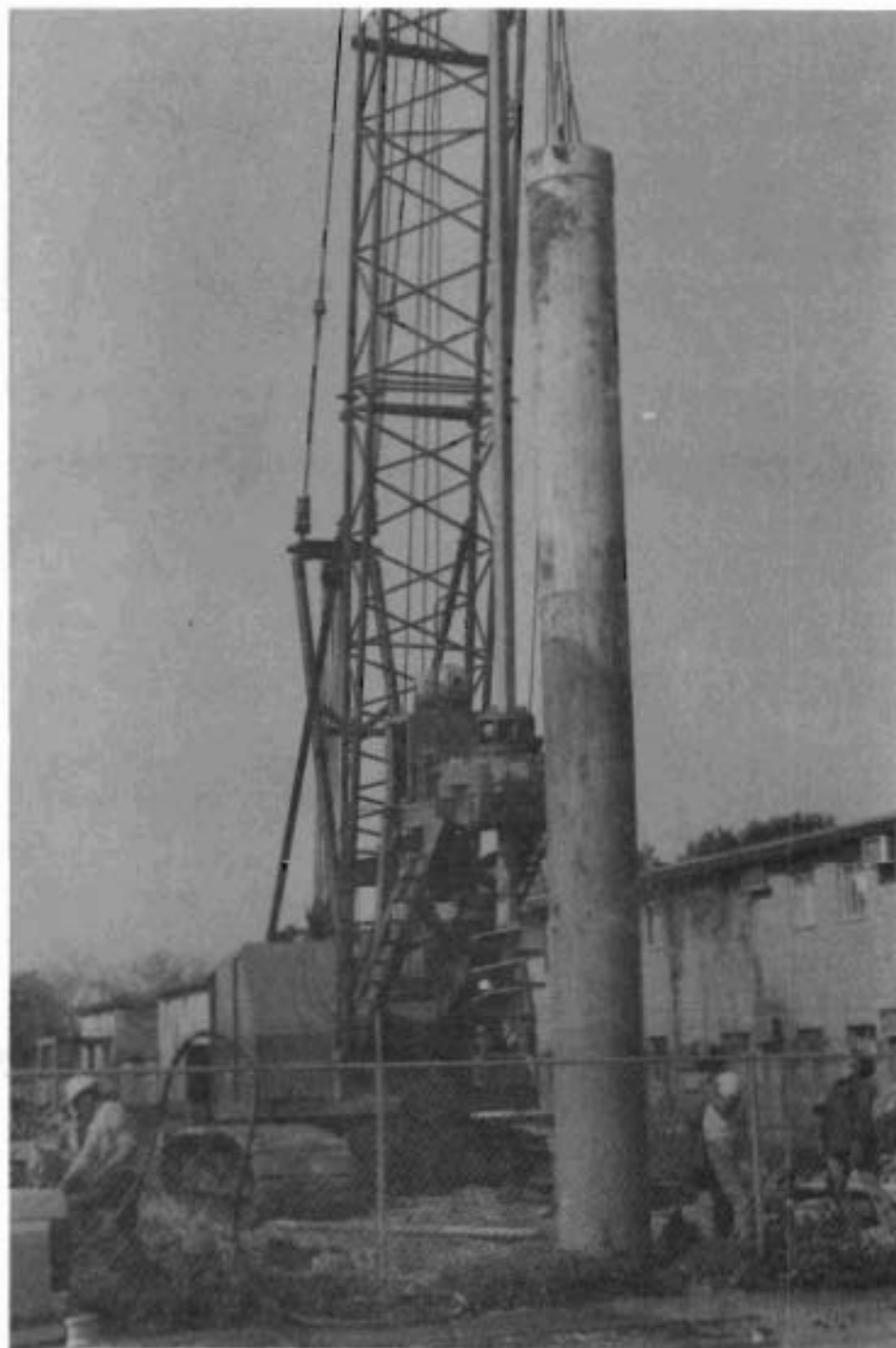


Fig. 5.23. Removing steel casing.

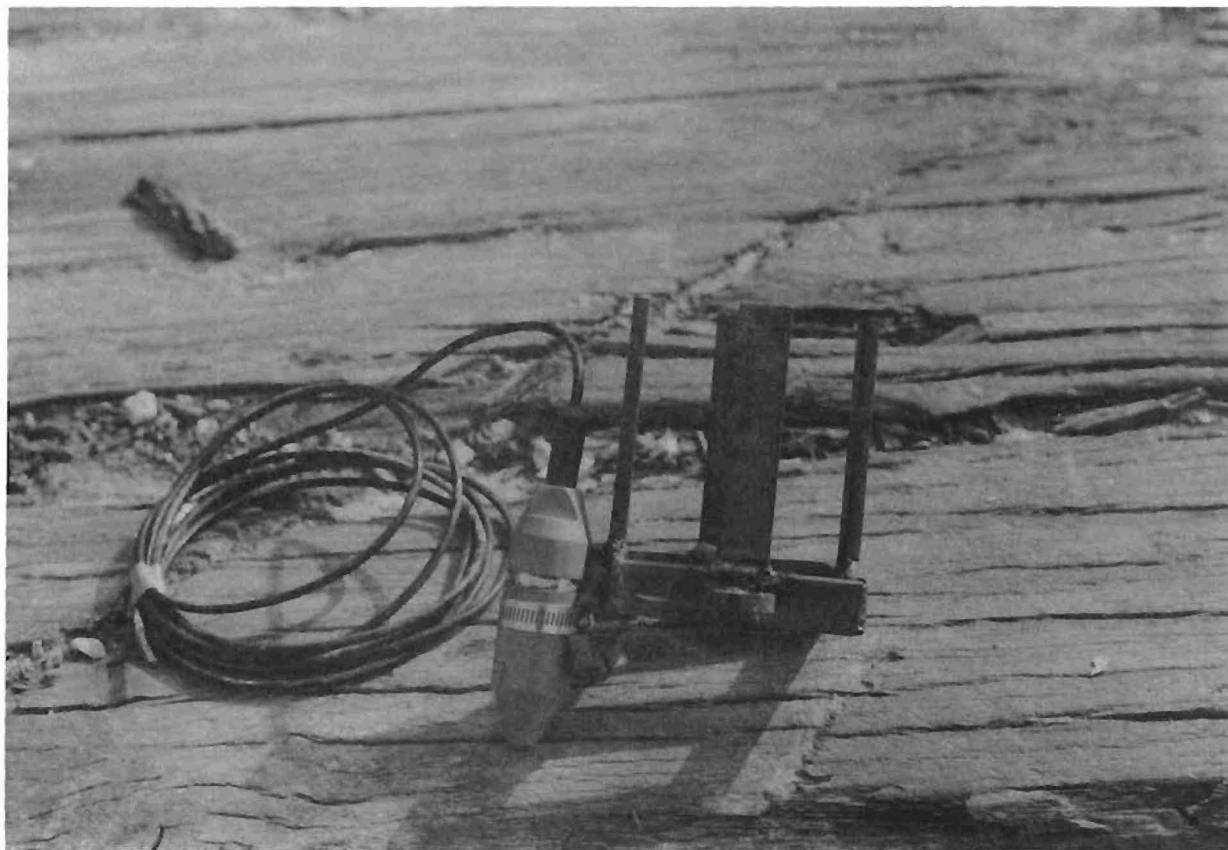


Fig. 5.24. "Floating" velocity transducer and harness used for placement.



Fig. 5.25. Positioning "floating" velocity transducer (shafts B and D only).



Fig. 5.26. Finishing pier surface and installing various source contact surfaces in fresh concrete.

drilled piers constructed at the Houston site. The findings of the wave propagation measurements performed at both sites are discussed in Chapters 6 and 7.

CHAPTER 6. WAVE PROPAGATION MEASUREMENTS ON SOUND DRILLED PIERS

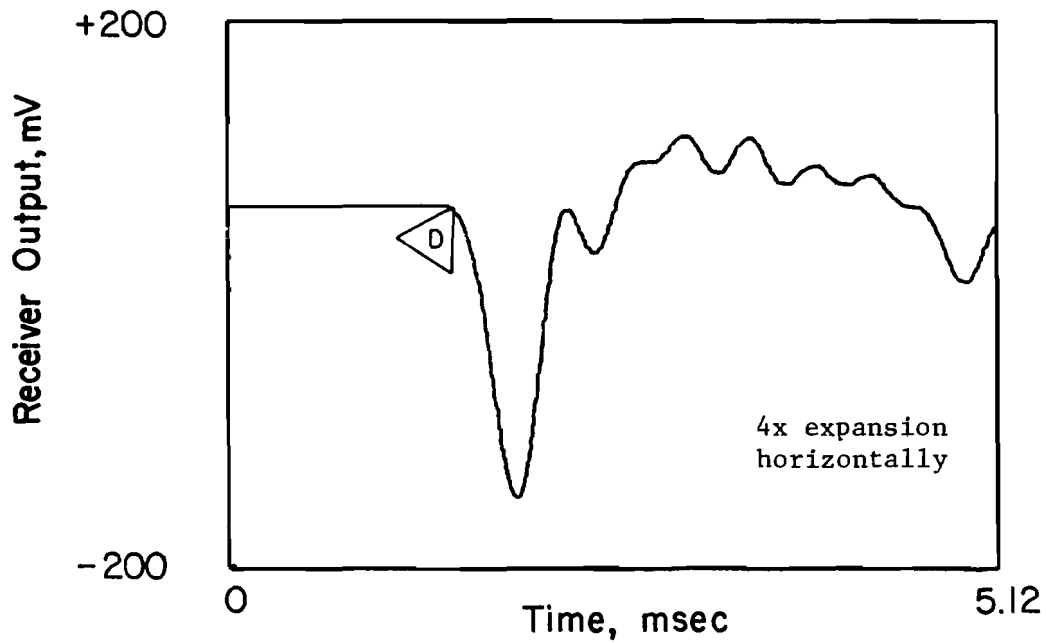
INTRODUCTION

In this chapter, wave propagation measurements are presented for tests conducted on sound drilled piers (containing no planned defects) at both test sites. Both embedded receiver (WAPER method) and surface receiver (WAPS method) measurements are presented. Discussions of the time domain measurements pertaining to direct and reflected wave identification, compression wave velocities, and determination of pier length are given. An attenuation study of wave energy in sound drilled piers is also included. Finally, comparisons are presented of the various sources and receivers investigated. Wave propagation measurements resulting from tests conducted on the various defective piers are presented in Chapter 7.

WAVE PROPAGATION USING EMBEDDED RECEIVERS (WAPER METHOD)

Direct Wave Arrivals.

First Test Site; Granger, Texas. A typical wave signature for a WAPER test performed on Shaft 1 is shown in Fig. 6.1. As described in Chapter 5, Shaft 1 was a 2.5 ft (0.76 m) diameter, 39 ft (11.9 m) long drilled pier, free of planned defects. As shown in Fig. 5.1, the pier was instrumented by Arias (1977) with three vertical velocity transducers positioned at depths of 4.8 ft (1.5 m), 17.9 ft (5.5 m), and 38.3 ft (11.7 m) below the top of the



D = Direct Wave Arrival, 1.44 msec
Receiver Depth = 17.9 ft (5.5 m)
Pier Length = 39 ft (11.9 m)
Pier Diameter = 30 in. (76.2 cm)

Fig. 6.1. WAPER test conducted on Shaft 1 showing direct wave arrival.

pier. The wave signature shown in Fig. 6.1 is the output generated by the 17.9 ft (5.5 m) embedded receiver and was produced by a 15 lb (6.8 kg) drop hammer. The waveform has been expanded horizontally by four times to accentuate the direct wave arrival that is denoted by the arrow in the figure.

As discussed in Chapter 3, the time of the direct wave arrival is the time it takes for the compression wave to propagate from the top of the pier to the receiver. The direct arrival of the compression wave at the 17.9 ft (5.5 m) velocity transducer is shown by the downward turn from the initial straight-line portion of the wave signature in Fig. 6.1 (denoted by D). This downward excursion is the result of the pushing action of the particle motion of the compression wave as it propagates past the receiver. The arrival time of the direct wave for the sound pier is 1.44 msec. With the travel time and distance (depth to receiver) known, the velocity of the direct compression wave can be computed using Eq. 3.1, which in this case is 12,430 ft/sec (3,790 m/sec). This value compares favorably with the 12,100 ft/sec (3,690 m/sec) P-wave velocity reported by Arias (1977). The difference in reported P-wave velocities is most likely attributable to differences in oscilloscope resolutions and selected wave arrival times and possibly a slight increase in concrete strength over the years. Regardless, based on the compression wave velocities, the quality of the concrete would be considered good.

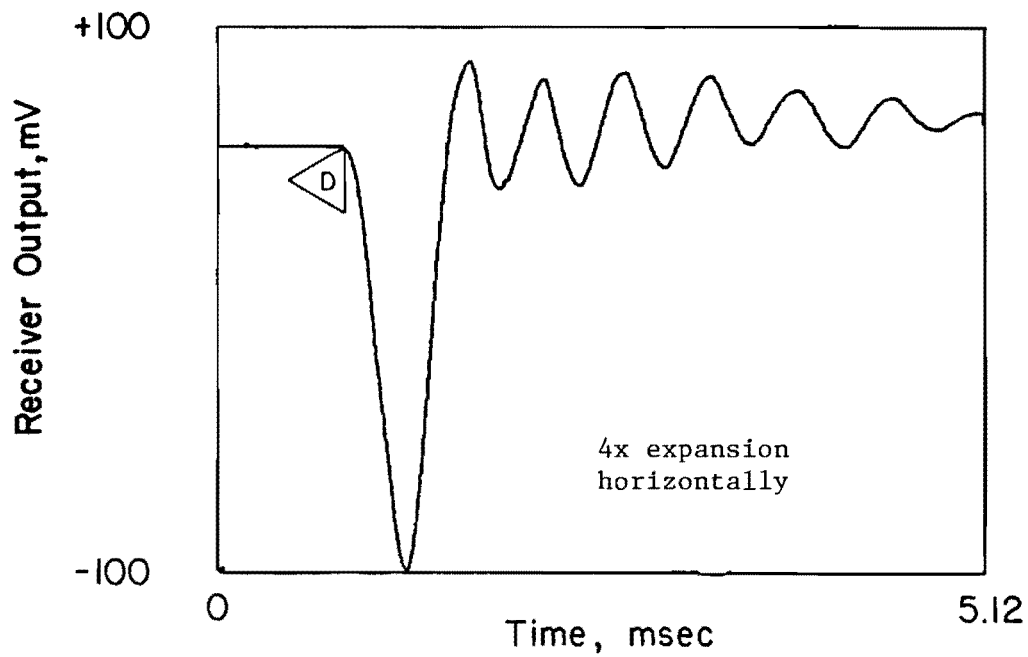
Several important points are highlighted in Fig. 6.1. First, a comparison of the digital oscilloscope record with a record from an analog storage oscilloscope for the same shaft and receiver (shown in Fig. 5.4(a)) reveals the superiority of the digital record. Although both records resulted in similar time domain measurements, the higher resolution of the digital oscilloscope record and the clarity and ease of waveform manipulation

of the digital equipment are major assets in assessing reflection boundaries and wave attenuation. Second, the amplitude of the direct wave arrival shown in Fig. 6.1 is dependent upon oscilloscope sensitivity settings and source impact, but the initial arrival shown in Fig. 6.1 is independent of wave amplitude. Only the initial downturn in the wave signature is important in determination of the direct compression wave velocity. However, the amplitude of the direct wave arrival is important in wave attenuation studies, as discussed earlier. Furthermore, correct evaluation of the direct compression wave velocity is dependent on proper triggering of the oscilloscope. Unknown time delays in triggering result in lower P-wave velocities, which in turn could result in erroneous assessments of reflection boundaries and concrete quality. The use of multiple embedded receivers to eliminate the effects of triggering problems on determination of compression wave velocity is discussed below.

As a final note, Fig. 6.1 provides proof of the durability of cased vertical velocity transducers as embedded receivers, as the transducer used to produce the wave signature had been in place for over four years.

Second Test Site; Houston, Texas. A typical wave signature for a WAPER test conducted on the 32 in. (81.3 cm) diameter, 50 ft (15.2 m) long sound pier (Shaft A) is shown in Fig. 6.2. The wave signature shows the output recorded by the 10 ft (3.0 m) embedded receiver, with the waveform expanded 4 times horizontally to emphasize the direct wave arrival. Again, wave excitation was generated by a 15 lb (6.8 kg) drop hammer.

A comparison of Figs. 6.1 and 6.2 reveals that the initial shape of the wave signatures is basically the same. The initial downturn of the wave signature, again denoted by D, occurs at a time of 0.80 msec, resulting in a direct Pwave velocity of 12,500 ft/sec (3,810 m/sec). By comparing this



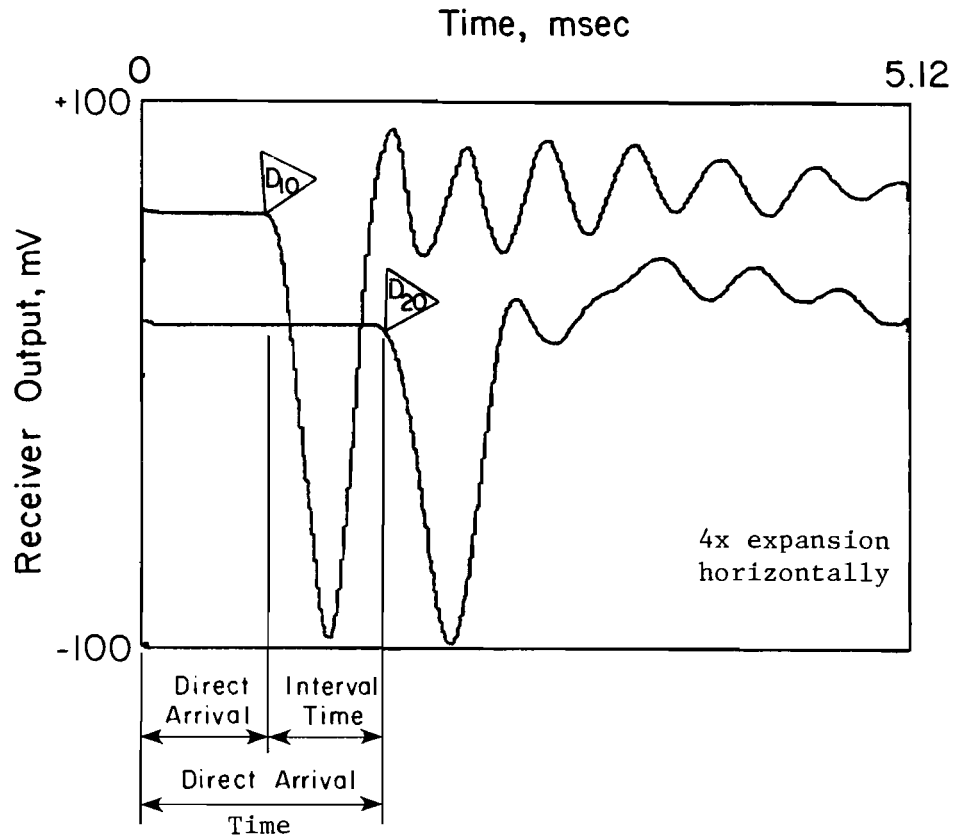
D = Direct Wave Arrival, 0.80 msec
Receiver Depth = 10 ft (3.0 m)
Pier Length = 50 ft (15.2 m)
Pier Diameter = 32 in. (81.3 cm)

Fig. 6.2. WAPER test conducted on Shaft A showing direct wave arrival.

velocity with values listed in Table 3.2, the quality of the concrete would be considered good. This observation is further substantiated by compressive strength tests performed on standard test cylinders sampled during construction of Shaft A. The 28-day compressive strengths of the 3,000-psi concrete mix averaged 3,650 psi.

As mentioned previously, triggering of the oscilloscope can have a direct effect on measured travel times of direct and reflected waves. Improper triggering, either early or delayed, results in erroneous compression wave velocities. The problem of erroneous P-wave velocities resulting from improper triggering can be eliminated by the use of two or more embedded receivers, as illustrated in Fig. 6.3. In Fig. 6.3, wave excitation recorded at the 10 ft (3.1 m) and 20 ft (6.1 m) velocity transducers embedded in Shaft A are shown. To eliminate the effects of triggering, the interval travel time is used to calculate P-wave velocity. The interval travel time is defined as the time it takes for the compression wave to propagate from one receiver to another. In Fig. 6.3, the interval travel time is the difference in the direct wave arrival times of the two receivers, which in this instance is 0.79 msec. Since the embedded receivers are positioned 10 ft (3.1 m) apart, the interval P-wave velocity is 12,660 ft/sec (3,860 m/sec). This value, although somewhat higher, compares favorably with the direct compression wave velocities of the two receivers, an indication that the triggering system was performing properly. It should be noted that correct assessment of interval velocities requires that the output recorded at the monitored receivers be generated by the same impulse.

Because numerous velocity transducers were embedded in Shaft A, assessment of P-wave velocity throughout the sound pier could be done. In Fig. 6.4, initial wave excitation recorded at the 10 ft (3.0 m), 20 ft (6.1



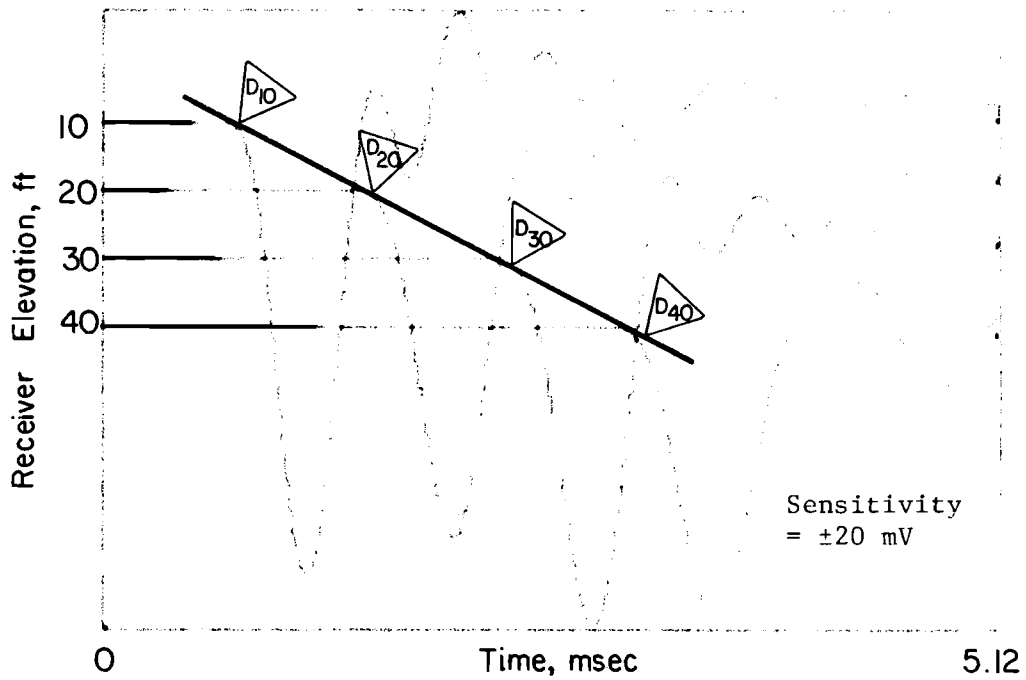
D_{10} = Direct Wave Arrival at 10 ft (3.0 m) receiver, 0.80 msec

D_{20} = Direct Wave Arrival at 20 ft (6.1 m) receiver, 1.59 msec

Pier Length = 50 ft (15.2 m)

Pier Diameter = 32 in. (81.3 cm)

Fig 6.3. WAPER test conducted on Shaft A illustrating determination of interval travel time with multiple receivers.



D_{10} = Direct wave arrival at 10 ft (3.0 m) receiver, 0.74 msec
 D_{20} = Direct wave arrival at 20 ft (6.1 m) receiver, 1.47 msec
 D_{30} = Direct wave arrival at 30 ft (9.1 m) receiver, 2.22 msec
 D_{40} = Direct wave arrival at 40 ft (12.2 m) receiver, 2.92 msec
 Pier Length = 50 ft (15.2 m)
 Pier Diameter = 32 in. (81.3 cm)

Fig. 6.4. WAPER test conducted on Shaft A illustrating constant velocity of concrete.

m), 30 ft (9.1 m) and 40 ft (12.2 m) embedded velocity transducers in Shaft A are shown. For this record, two digital oscilloscopes were used in series, and the output is the result of a single impulse of the drop hammer. The output has been positioned along the ordinate at equal voltage differentials, reflecting the equi-distance positioning of the receivers in the pier. By viewing multiple receiver output in this manner, several significant conclusions can be drawn concerning P-wave velocity throughout a sound pier.

The direct and interval P-wave velocities for the embedded receiver output shown in Fig. 6.4 have been tabulated in Table 6.1. A review of Table 6.1 reveals that the direct P-wave velocity increases slightly with depth in Shaft A (approximately 3 percent over the monitoring depth of 40 ft), with the exception of the velocity from the 30 ft (9.1 m) receiver. The same is true, but to a larger percent, of the interval P-wave velocities, again with the exception of the interval velocity associated with the 20 ft (6.1 m) and 30 ft (9.1 m) embedded receivers. Furthermore, a comparison of the tabulated velocities reveals that the interval velocity is generally higher than the respective direct P-wave velocities, the difference between the interval and corresponding direct P-wave velocities becoming greater with depth within the pier.

The increase in both direct and interval P-wave velocities with depth within a sound pier may be attributed to at least two effects. First, increased consolidation of the concrete occurs with depth because of an increase in surcharge with depth. Second, the concrete curing environment becomes more favorable in the lower regions of the drilled pier. The phenomena of higher interval velocities and increased difference in interval and corresponding direct P-wave velocities with depth are the result of both the physical characteristics of the drilled pier as described above and the

Table 6.1. Direct and Interval Compression Wave Velocities
for Shaft A.

<u>Receiver</u> <u>Depth</u> <u>f_t</u>	<u>Compression Wave Velocity</u> <u>ft/sec</u>	
	<u>Direct</u>	<u>Interval</u>
10	13,510	13,700
20	13,610	13,330
30	13,510	14,290
40	<u>13,700</u>	
	Avg. 13,580	

effective sampling depth. Whereas the interval velocities are representative of segmental portions of the pier [10 ft (3.0 m) increments in this case], the direct P-wave velocities effectively sample a larger portion of the pier, that being from the top of concrete to the embedded receiver depth. With concrete consistency slightly increasing in quality with depth within the pier, P-wave velocities representative of wave propagation over incremental portions of the pier should increase in magnitude at a greater rate than velocities representing the total travel path of the wave excitation.

By assessing direct and interval velocities of piers instrumented with multiple embedded receivers, an indication of both overall and incremental concrete quality can be obtained. This assessment is extremely valuable in detecting weak areas of concrete within the pier resulting from cement washout or material segregation, areas that may go undetected when evaluating receiver output solely from reflected wave arrivals. Direct and interval P-wave velocities substantially lower than the average value should be considered suspect. Subsequent evaluation of wave attenuation in the questionable pier is often helpful in confirming weak areas in the pier. The direct and interval P-wave velocities tabulated for Shaft A in Table 6.1 indicate good to excellent concrete quality. The small decrease in P-wave velocity between the 20 ft (6.1 m) and 30 ft (9.1 m) embedded receivers is thought to be caused by slight differences in equipment triggering (two oscilloscopes were used in series) and not by some slight discrepancy in concrete quality.

The relatively small differences in direct P-wave velocities tabulated in Table 6.1 shows that the simplifying assumption of constant P-wave velocity with depth within a sound pier is reasonable. In Fig. 6.4, a line has been drawn through the direct arrivals of the compression wave registered

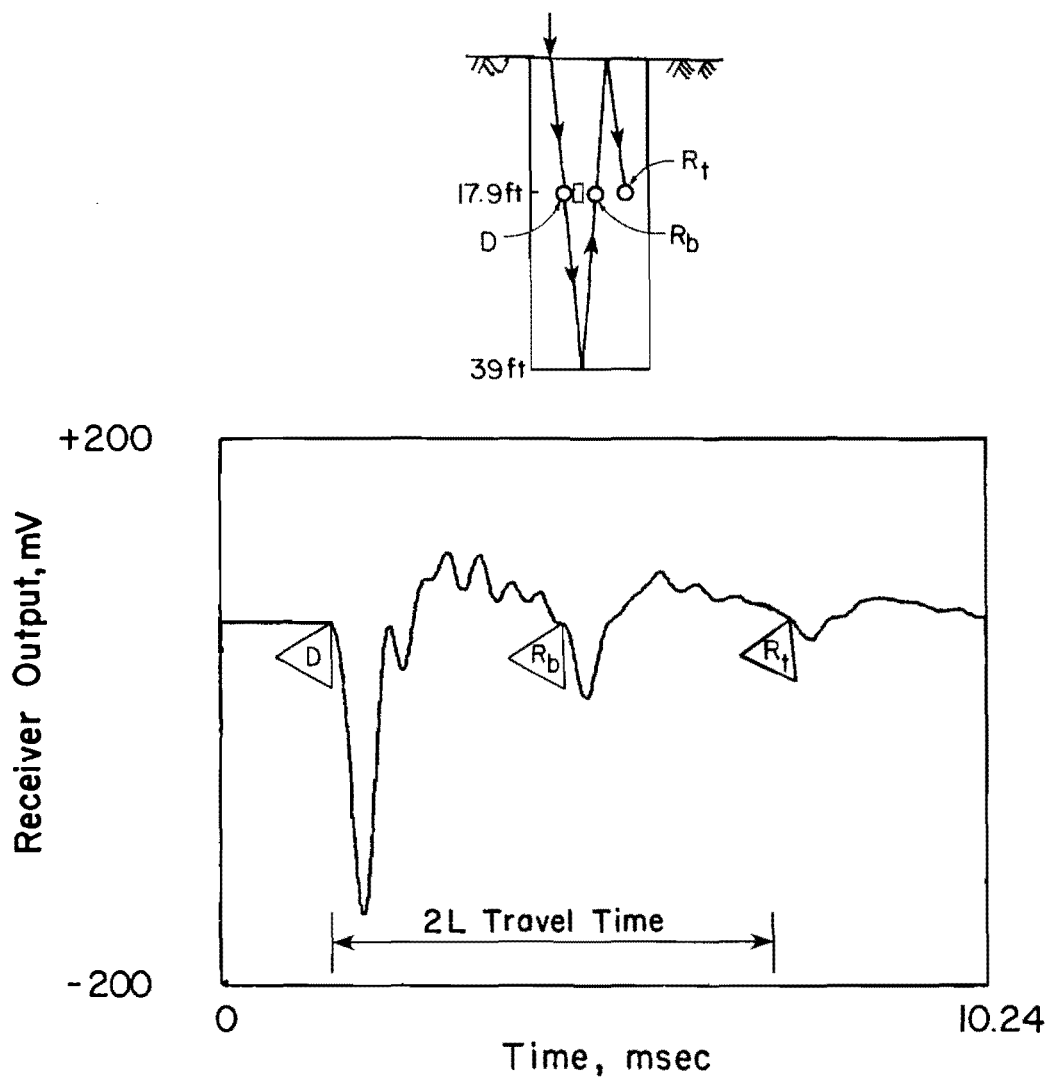
at the respective receivers. The slope of the line represents the average P-wave velocity in the concrete, which in this instance is approximately 13,580 ft/sec (4,140 m/sec). This simplifying assumption of linearity of travel time with distance will be utilized in the following sections to assess reflection boundaries.

As a final note, it can be seen that discrepancies exist in the direct wave arrival times shown in Figs. 6.3 and 6.4. The differences in travel times are attributable to the different test dates and changes in concrete properties during this interval. The receiver output presented in Fig. 6.3 was collected from tests conducted seven days after pier concrete placement, whereas the receiver output in Fig. 6.4 was collected from tests conducted eighteen days after concrete placement. Concrete hardening and strengthening that occurred subsequent to the initial test date resulted in an increase in P-wave velocity and, consequently, a decrease in P-wave travel time at the time of the second phase of testing. It is also interesting to note that substantive wave propagation measurements can be conducted a week after construction of the drilled piers, providing an indication of concrete quality and pier integrity.

Reflected Wave Arrivals

First Test Site; Granger, Texas. To view reflected wave arrivals, proper oscilloscope settings, including sweep times and sensitivity ranges, must be selected. This was accomplished for the wave signature shown in Fig. 6.5. The waveform is the output recorded at the 17.9 ft (5.5 m) velocity transducer embedded in Shaft 1.

This record provides an excellent study of wave propagation in a sound drilled pier. As discussed in Chapter 3, the source, in this case a 15 lb (6.8-kg) drop hammer, provides an impact at the top of the pier. The impact



D = Direct wave arrival, 1.44 msec

R_b = Reflection arrival from bottom of pier, 4.72 msec

R_t = Reflection arrival from top of pier, 7.59 msec

Receiver Depth = 17.9 ft (5.5 m)

Pier Length = 39 ft (11.9 m)

Pier Diameter = 30 in (76.2 cm)

Fig 6.5. WAPER test on Shaft 1 (Granger site) showing reflected wave arrivals for sound pier.

results in a compression wave which propagates down the pier. As the compression wave first passes the monitoring receiver, the pushing action of the P-wave results in a downward excursion in the wave signature. The start of this excursion, denoted by D in Fig. 6.5, gives a direct arrival time of 1.44 msec and a direct P-wave velocity of 12,430 ft/sec (3,790 m/sec). The compression wave continues to propagate down the pier until it encounters the concrete-soil interface at the bottom of the pier. Here, a certain amount of wave energy is transmitted into the bearing stratum while the remaining energy is reflected back up the pier. The amount of reflected energy is dependent upon the properties of the materials on either side of the interface and is the topic of discussion in a later section of this chapter.

If the bottom of the pier behaves in accordance with a free-end condition, the wave is reflected as a tensile wave. By knowing the pier length and assuming constant P-wave velocity, the arrival time of the reflected wave off the bottom can be computed. Using the average P-wave velocity of 12,570 ft/sec (3,830 m/sec) reported by Arias (1977), the reflected wave should arrive at the monitored receiver at 4.80 msec. This is confirmed in Fig. 6.5 as the reflected wave off the pier bottom, denoted as R_b , arrives at a time of 4.72 msec. Slight differences in computed and assessed arrival times are more common with reflected waves, due to attenuation in wave energy during the propagation and reflection processes,

and due to difficulties in identifying initial arrivals of reflected waves. The shape of the reflected wave arrival off the pier bottom is indicative of a tensile wave, the initial downward excursion resulting from the pulling action of particle motion associated with tensile waves.

If ample wave energy is supplied by the source and wave attenuation is minimal, the possibility exists of identifying additional reflections in the

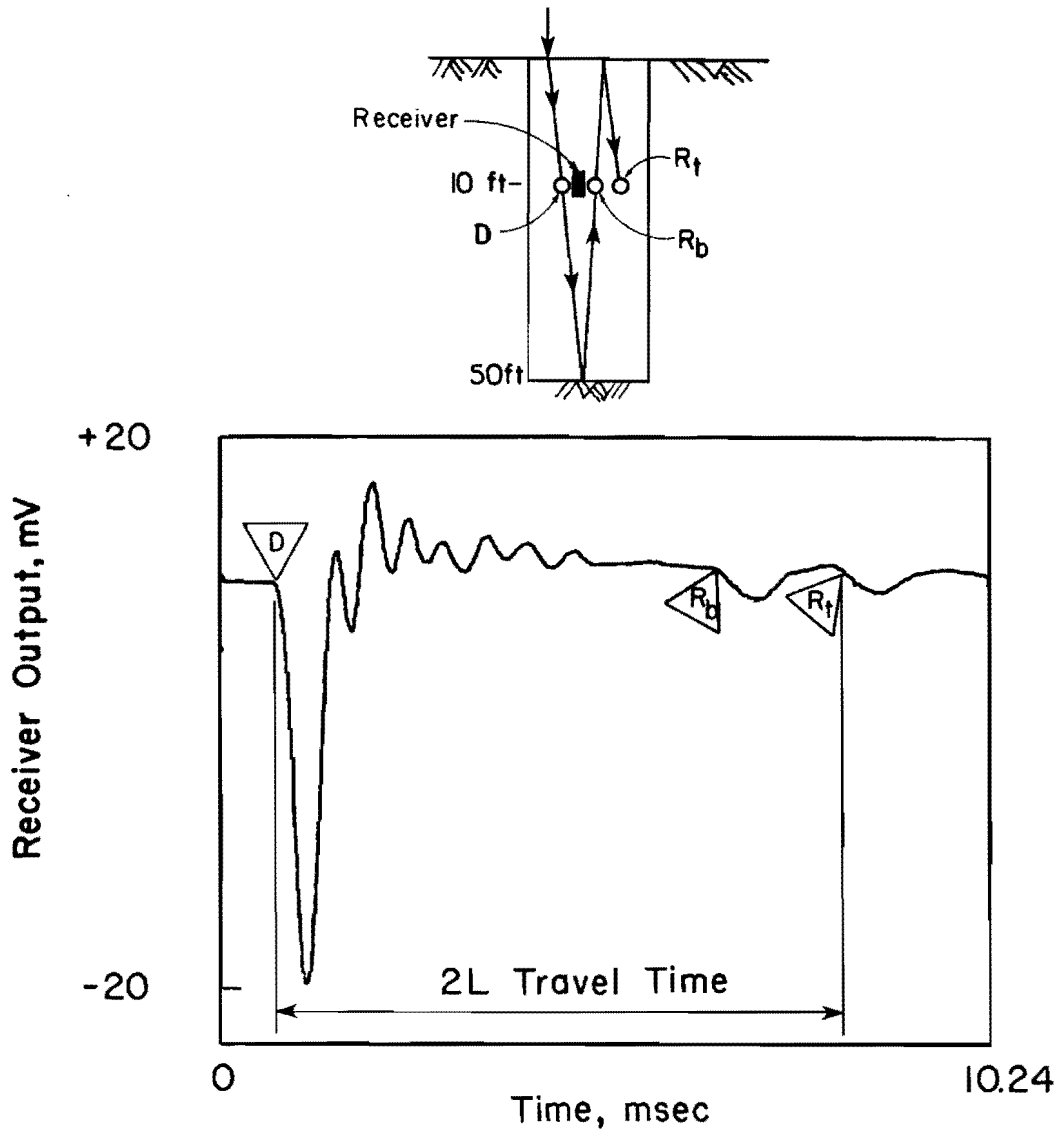
recorded output. This is the case in Fig. 6.5, where the reflected wave off the top of the pier is identifiable, denoted by R_t in the figure. The interval time between the reflected wave arrival off the pier bottom (R_b) and the reflected wave arrival off the top of the pier (R_t) should be equal to twice the time of the direct wave arrival. The computed arrival time of the reflection off the pier top is then of 7.68 msec ($4.80 \text{ msec} + 2 \times 1.44 \text{ msec}$). An examination of the wave signature resulted in an arrival time of 7.59 msec, the difference in computed and measured arrival times again attributable to difficulties in assessing the exact arrival time of reflected waves.

The analysis presented in the previous paragraphs should be sufficient to substantiate the sound integrity of the pier tested. Although computed and assessed reflected wave arrivals were not identical, the differences were small and within reasonable error for proper integrity evaluation.

As a final note, the ability to identify the reflected wave arrival off the top of the pier (R_t) allows easy determination of the effective pier length. By using the average P-wave velocity and the travel time between the direct wave arrival and the second reflected wave arrival (R_t), referred to as the $2L$ travel time in Fig. 6.5, the pier length can be estimated. The length in this case is 38.7 ft (11.8 m) compared to the planned construction length of 39 ft (11.9 m).

Test Site 2; Houston, Texas . Output recorded at the 10 ft (3.0 m) embedded velocity transducer in Shaft A is shown in Fig. 6.6. A 15 lb (6.8 kg) drop hammer was used to generate the compression wave signature.

Analysis of the wave signature for the sound shaft is identical to that discussed in the previous section for Shaft 1 at the Granger site. The direct wave arrival of the compression wave occurs at 0.73 msec, resulting in



D = Direct wave arrival, 0.73 msec

R_b = Reflection arrival from bottom of pier, 6.56 msec

R_t = Reflection arrival from top of pier, 8.03 msec

Receiver Depth = 10 ft (3.0 m)

Pier Length = 50 ft (15.2 m)

Pier Diameter = 32 in. (81.3 cm)

Fig 6.6. Reflected wave arrivals for Shaft A at Houston Site using WAPER method.

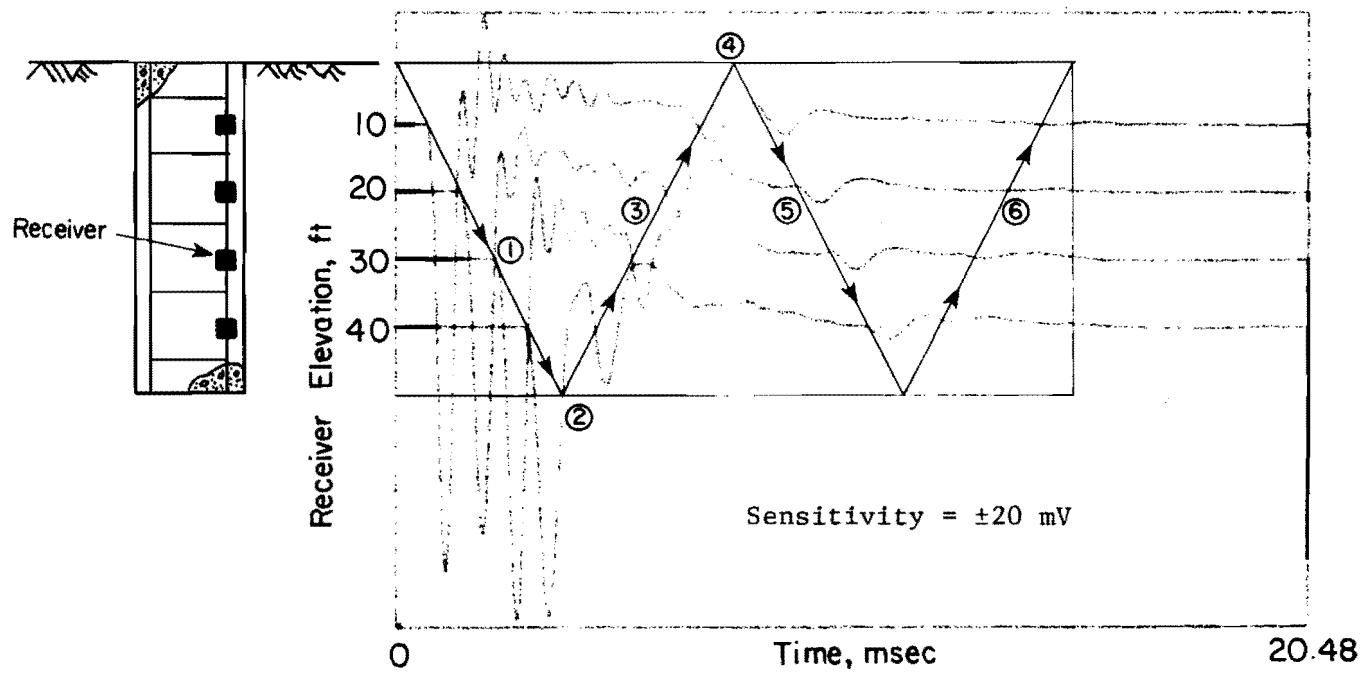
a direct compression wave velocity of 13,700 ft/sec (4,180 m/sec). A reflected wave arrival is identified in the wave signature (R_b) at an approximate time of 6.56 msec. Using the interval travel time between the reflected and direct wave arrivals and the computed direct P-wave velocity, the total travel distance of the P-wave is

$$[(6.56 \text{ msec}) - 0.73 \text{ msec}] \cdot 13,700 \text{ ft/sec} \div 2 = 39.9 \text{ ft (12.2 m)}$$

When adding the 10 ft (3.1 m) depth of the receiver is accounted for, a pier length of 49.9 ft (15.2 m), which compares favorably with the construction length of 50 ft (15.2 m). Based on this computation, the pier would be assessed as being sound.

As in Fig. 6.5, wave energy was of sufficient amplitude to provide a visible reflection off the top of the pier. In Fig. 6.6, this reflection (R) occurs at an approximate time of 8.03 msec in the wave signature. By using this reflection to measure the $2L$ travel time, an effective pier length of 50 ft (15.2 m) is determined.

Again, the numerous velocity transducers embedded in Shaft A allow a more definitive assessment of reflected wave arrivals in the sound pier. In Fig. 6.7, wave propagation recorded at the 10-, 20-, 30-, and 40-ft (3.1-, 6.1-, 9.1-, and 12.1-m) embedded receivers is shown. As before, two digital oscilloscopes were connected in series and a single impulse was used to generate the waveforms. The wave signatures have been positioned along the ordinate in equal voltage increments to simulate the receiver positioning in the drilled pier. For illustrative purposes, the drilled pier has been



Pier Length = 50 ft (15.2 m)
Pier Diameter = 32 in. (81.3 cm)

Fig. 6.7. Reflected wave arrivals as recorded using WAPER test on Shaft A (Houston site).

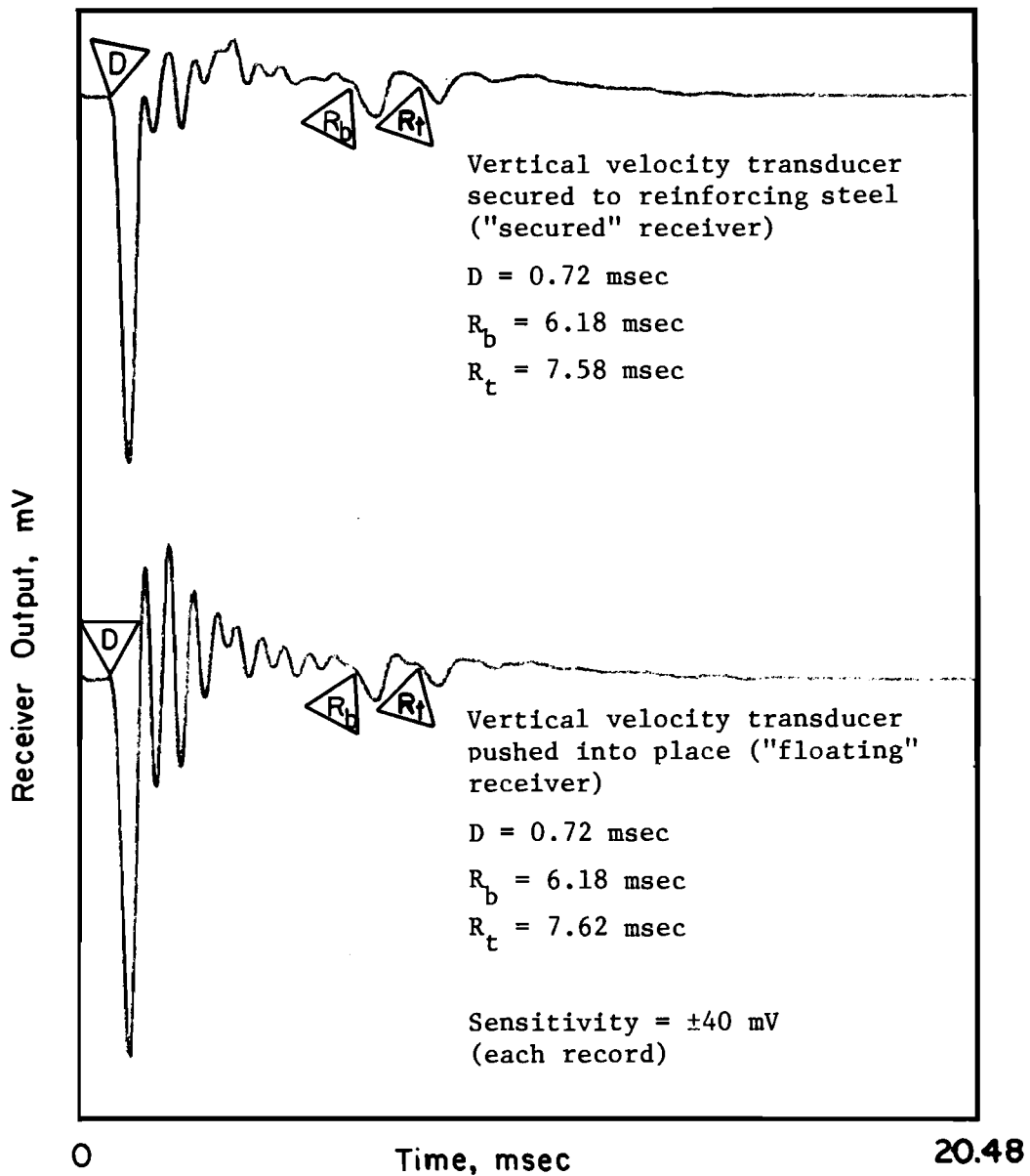
drafted alongside the wave record, with individual receivers opposite their respective wave signatures.

Direct and reflected wave arrivals have been identified in Fig. 6.7 by lines drawn through the arrival times. Arrows have been placed on the lines to illustrate the propagation path of the direct and reflected compression wave. As described previously, the slopes of the lines represent the average P-wave velocity of the wave. It can be seen from the figure that the generated compression wave propagates down the pier and past the embedded receivers (1), is reflected off the concrete-soil interface at the pier bottom (2), propagates back past the receivers as a tensile wave (3), is reflected at the concrete-air interface at the pier top (4), and propagates back past the receivers as a compression wave once again (5). The wave energy is such that the second reflection off the bottom of the pier is visible in the wave records (6). The advantage of plotting the output from multiple receivers in this manner is that it allows the viewer to obtain a better understanding of wave propagation in the pier, while allowing the evaluator ease in assessing reflected wave arrivals and pier integrity.

Embedded Receivers. Two types of instruments were utilized as embedded receivers in this study, these being vertical velocity transducers and piezoelectric ceramic transducers. Both types of receivers were discussed in detail in Chapter 4. Vertical velocity transducers have repeatedly been shown throughout this chapter to be effective monitors of wave propagation within drilled piers. Therefore, with respect to vertical velocity transducers, only the special case of "floating" embedded receivers is addressed in this section. The major highlights of piezoelectric ceramic transducers and their effectiveness as embedded receivers is also presented.

Vertical Velocity Transducers. As discussed in Chapter 5, the special case of evaluating unreinforced drilled piers with embedded receivers was included in this investigation. At the present time, the WAPER method of pier evaluation requires that receivers be attached to steel reinforcing installed in the pier. To investigate the possibility of using embedded receivers in unreinforced drilled piers, vertical velocity transducers were positioned in two test piers by securing the instruments to special sleeves (shown in Fig. 5.24) and pushing the receivers with the kelly bar of the drilling rig down through the fresh concrete to the desired elevation. Floating velocity transducers were located at a depth of 10 ft (3.0 m) in Shafts B and D to allow comparisons between them and the corresponding embedded receivers attached to the reinforcing steel (hereafter referred to as secured receivers) at a depth of 10 ft (3.0 m). Shafts B and D were selected for instrumentation with floating embedded receivers due to the defects present in these piers, allowing an assessment of the ability of these receivers to detect pier discontinuities. In this section, discussion is limited to a basic comparison of secured and floating embedded receiver output from WAPER tests conducted on Shaft B, concentrating solely on direct and reflected wave arrivals off the concrete-air and concrete-soil interfaces at the top and bottom of the pier, respectively. A detailed evaluation of the floating embedded receivers of Shafts B and D, specifically as detectors of pier discontinuities, is reserved for Chapter 7.

Output recorded at both the floating embedded receiver and corresponding secured receiver in Shaft B is shown in Fig. 6.8. Both velocity transducer receivers are positioned at a depth of 10 ft (3.0 m). A 5 lb (2.3 kg) hand-held sledge hammer and embedded nail combination was used to generate P-waves. Although the output shown in Fig. 6.8 is the result of two separate



Receiver Elevation = 10 ft (3.0 m) (both traces)

Pier Length = 50 ft (15.2 m)

Pier Diameter = 32 in. (81.3 cm)

Fig. 6.8. Comparison of secured and floating velocity transducer records for WAPER test conducted on Shaft B (Houston site).

WAPER tests, the wave signatures were found to be repeatable for a number of the tests.

The receiver output presented in Fig. 6.8 provides proof of the ability to assess the integrity of unreinforced drilled piers using floating embedded velocity transducers. Both records show a clearly defined direct arrival occurring at 0.72 ms. This travel time corresponds to a direct P-wave velocity of 13,890 ft/sec (4,230 m/sec). Further analysis of the wave signatures reveals that the reflected wave arrivals off the bottom and top of the pier are easily identifiable in both the floating and secured receiver outputs. The reflected wave arrival off the bottom of the pier occurs at approximately 6.20 ms in both wave signatures. This travel time corresponds to a P-wave velocity of 14,520 ft/sec (4,430 m/sec), a reasonable value when accounting for the previously discussed phenomena of pier consolidation and variable curing environments which tend to improve concrete quality and, consequently, increase P-wave velocity with depth within a pier.

An apparent disadvantage of the floating embedded receiver is "noise" in the output following the direct arrival of the P-wave. This "noise" is absent from the secured receiver output. The reason for this noise is unknown and is not thought to be a function of the receivers or embedded material properties. One possible reason would be concrete shrinkage

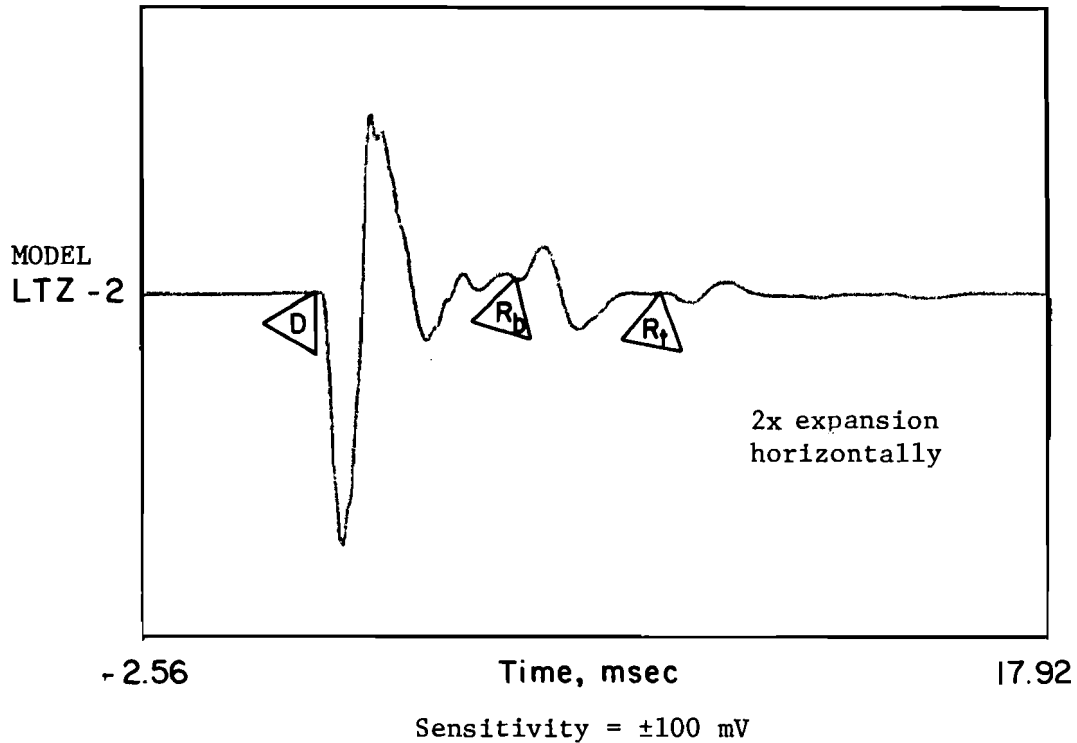
around the unsecured receiver. In any case, the inherent noise in the initial portion of the floating receiver output is a detriment to pier integrity assessment because reflected waves off discontinuities located a short distance below the receiver may be "masked" in the recorded output. It may be possible to position two floating receivers within the pier to be tested, the distance between the receivers made as large as possible, which would greatly increase the chances of detecting pier discontinuities.

Piezoelectric Ceramic Transducers. As discussed in Chapter 1, piezoelectric ceramic transducers were included in this study to determine their effectiveness as monitors of wave propagation in drilled piers. If successful, the economics of these receivers would allow testing a greater number of piers on a project or increased instrumentation of a given number of piers.

Piezoelectric ceramic transducers are electro-mechanical transducers, using mechanical motion to generate an electric charge. Resultant voltages in the piezoceramic transducers are dependent upon: (1) the piezoelectric properties of the ceramic, (2) ceramic dimensions and shape, and (3) the direction of the electrical and mechanical vector quantities. For this study, it was decided to vary ceramic dielectric constants and cross-sectional areas, in an attempt to find an appropriate ceramic transducer. The piezoelectric transducers selected were made of lead zirconate titanate and were manufactured by Transducer Products, Inc., (models LTZ-2 and LTZ-2H). LTZ-2H ceramics possessed higher dielectric constants than the model LTZ-2 (3500 compared to 1800). Ceramic cross-sectional dimensions selected for this study were as follows: 0.33 by 0.25 in (0.85 by 0.61 cm); 0.50 by 0.13 in (1.25 by 0.32 cm); and 0.50 by 0.25 in (1.25 by 0.61 cm). All ceramics were cast in 1.0 in (2.54 cm) lengths and were polarized for use in tranverse compression.

Piezoelectric transducers were positioned at a depth of 20 ft (6.1 m) in Shafts A, B and C to allow comparisons with the vertical velocity transducers at the same depths and to assess the ability of the ceramics to monitor sound and defective drilled piers.

A typical wave propagation record for a piezoelectric transducer embedded in Shaft A (Houston site) is shown in Fig. 6.9. The output shown in



D = Direct wave arrival, 1.48 msec

R_b = Reflected wave from bottom of pier, 5.90 msec

R_t = Reflected wave from top of pier, 8.72 msec

Receiver elevation = 20 ft (6.1 m)

Pier Length = 50 ft (15.2 m)

Pier Diameter = 32 in. (81.3 cm)

Fig. 6.9. WAPER test on Shaft A (Houston site) using drop hammer source and 1/2 in. x 1/4 in. x 1 in. (1.27 cm x 0.64 cm x 2.54 cm) piezoelectric ceramic transducer.

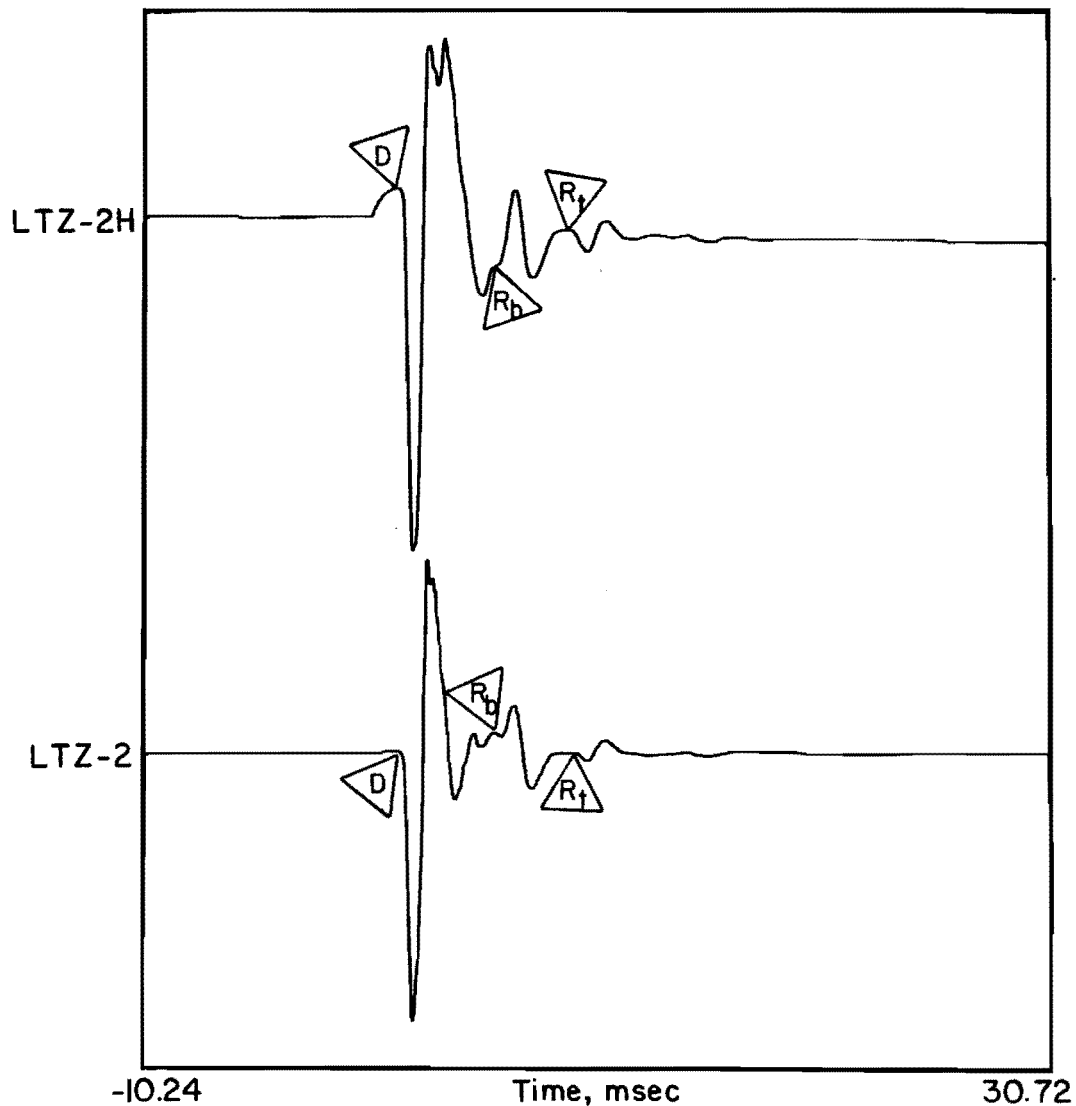
Fig. 6.9 was recorded with the 0.50 by 0.25 in. (1.25 by 0.64 cm) model LTZ-2 transducer. The source used to generate the P-waves was a 15 lb (6.8 kg) drop hammer. The oscilloscope mid-signal trigger was utilized for recording purposes to allow assessment of pre-trigger and early waveform data.

A review of the wave signature in Fig. 6.9 reveals a clearly defined direct P-wave arrival occurring at 1.48 msec. With an the receiver depth of 20 ft (6.1 m), this travel time corresponds to a P-wave velocity of 13,510 ft/sec (4120 m/sec). Assuming constant P-wave velocity, the estimated arrival time of the reflected wave off the bottom of the 50 ft (15.2 m) long sound pier is 5.92 msec. An examination of the output in Fig. 6.9 shows a wave arrival (denoted as R_p) occurring at approximately 5.90 msec. However, instead of the typical downward excursion of the signal exhibited by the velocity transducers, the reflected wave arrival in Fig. 6.9 is identified as an upward excursion in the wave signature. This deviation is the result of the alteration of wave energy at the free-end condition of a drilled pier and the polarization of the piezoelectric ceramic transducer. As discussed previously, the piezoelectric transducers used in this study were polarized in transverse compression, meaning compressive strain of the ceramics along their longitudinal axis will produce a positive voltage output. Conversely, a tensile strain along the longitudinal axis of the piezoelectric transducer causes an elongation of the ceramic, resulting in a negative voltage output. Therefore, the change in reflected wave energy as the result of the free-end conditions inherent of a drilled pier will in turn result in alternating upward and downward excursions of the wave signature. Because the oscilloscope was connected so that the initial P-wave would be downward, the reflected tensile wave off the bottom of the pier is registered in the recorded output as an upward excursion of the wave signature.

Similarly, the reflected compression wave off the top of Shaft A should result in a downward excursion of the wave signature, the arrival of the reflected wave estimated to occur at 8.76 msec in Fig. 6.9. The initial impulse was of sufficient energy such that a reflected wave off the top of the pier (denoted by R_t) is visible at the estimated arrival time. The downward trough of the reflected compression wave arrival in the wave signature confirms the effects of ceramic polarity on recorded receiver output.

Not all of the piezoelectric transducers included in this study performed as well as the model shown in Fig. 6.9. Comparisons of the various piezoelectric transducers embedded in Shaft A are presented in Figs. 6.10 through 6.12. Examination of the output presented in these figures reveals that all records have the same basic waveform, with the exception of the 0.50 by 0.13 in. (1.25 by 0.32 cm) LTZ-2H transducer, which apparently was damaged during pier construction. Direct and reflected wave arrivals are identifiable in all records shown, with the exception of the above mentioned transducer, and arrival times are consistent throughout. However, the Model LTZ-2 transducers (possessing the lower dielectric constant) generally provided a more well defined wave signature when compared to the LTZ-2H receiver records for the same impulse. Ceramic cross-sectional area does not have a significant affect on wave propagation output for the dimensions and ceramic models studied.

The output shown in Figs. 6.9 through 6.12 is evidence that piezoelectric ceramic transducers show promise as wave propagation receivers in integrity testing of drilled piers. For comparison purposes, wave propagation records of both piezoelectric ceramic and velocity transducer receivers positioned in Shaft A are provided in Fig. 6.13. Both records show



Sensitivity = $\pm 100\text{mV}$

D = Direct wave arrival, 1.44 msec

R_b = Reflected wave from bottom of pier, 5.75 msec

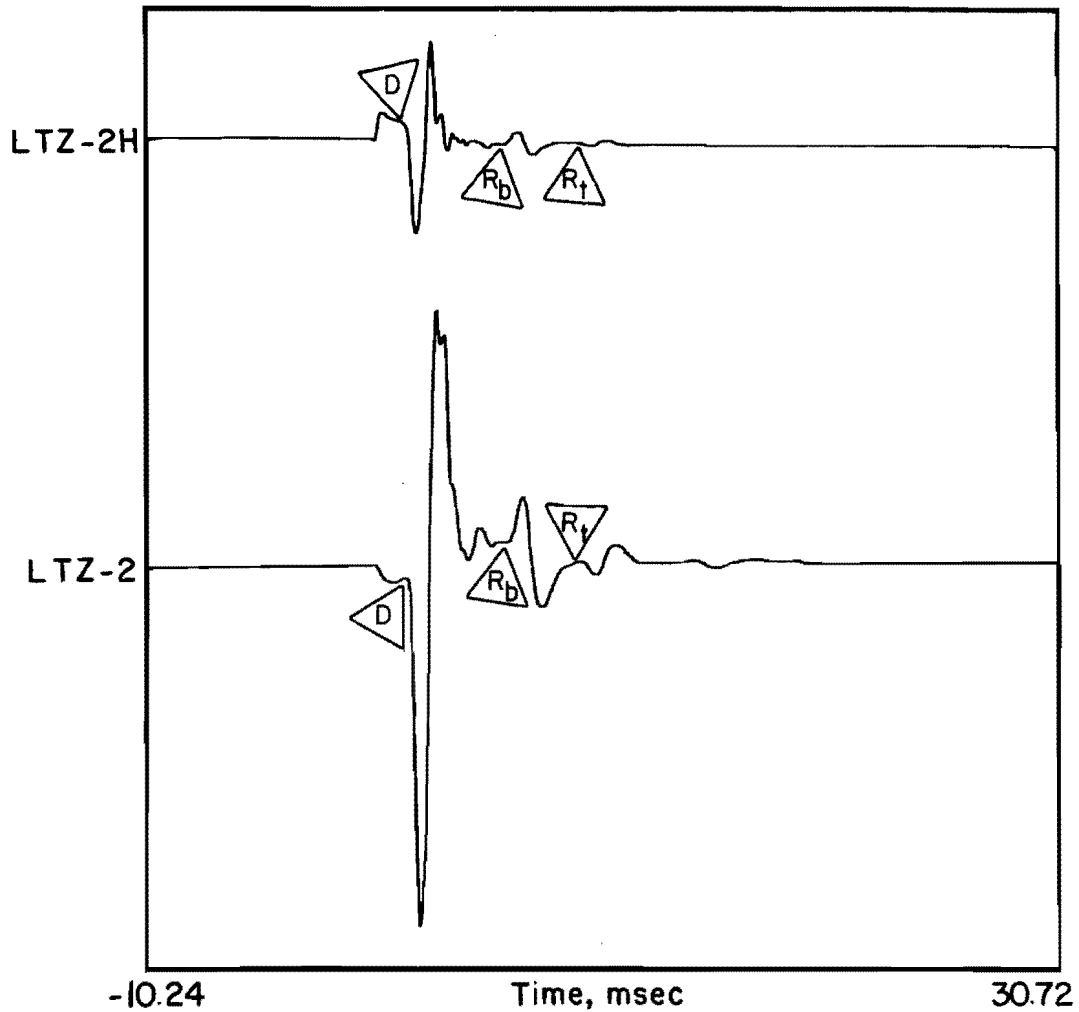
R_t = Reflected wave from top of pier, 8.72 msec

Receiver Elevation = 20 ft (6.1 m)

Pier Length = 50 ft (15.2 m)

Pier Diameter = 32 in. (81.3 cm)

Fig. 6.10. WAPER test on Shaft A (Houston site) using drop hammer source and 1/2 in x 1/4 in x 1 in piezo-electric ceramic transducers.



Sensitivity = \pm 100mV

D = Direct wave arrival, 1.48 msec

R_b = Reflected wave from bottom of pier, 5.90 msec

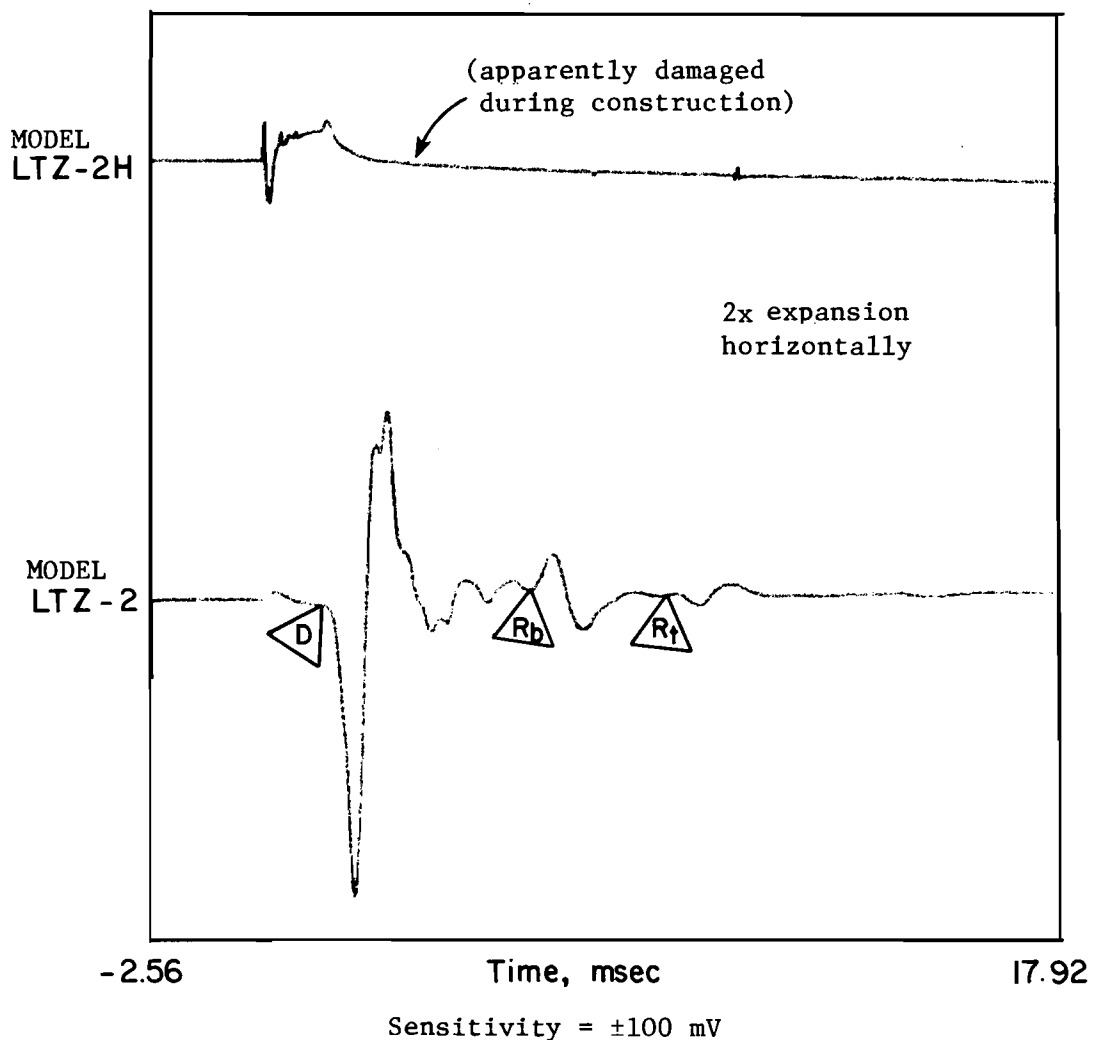
R_t = Reflected wave from top of pier, 8.86 msec

Receiver Elevation = 20 ft (6.1 m)

Pier Length = 50 ft (15.2 m)

Pier Diameter = 32 in. (81.3 cm)

Fig. 6.11. WAPER Test on Shaft A (Houston site) using drop hammer source and 1/2 in x 1/8 in x 1 in piezoelectric ceramic transducers.



D = Direct wave arrival, 1.48 msec

R_b = Reflected wave from bottom of pier, 5.90 msec

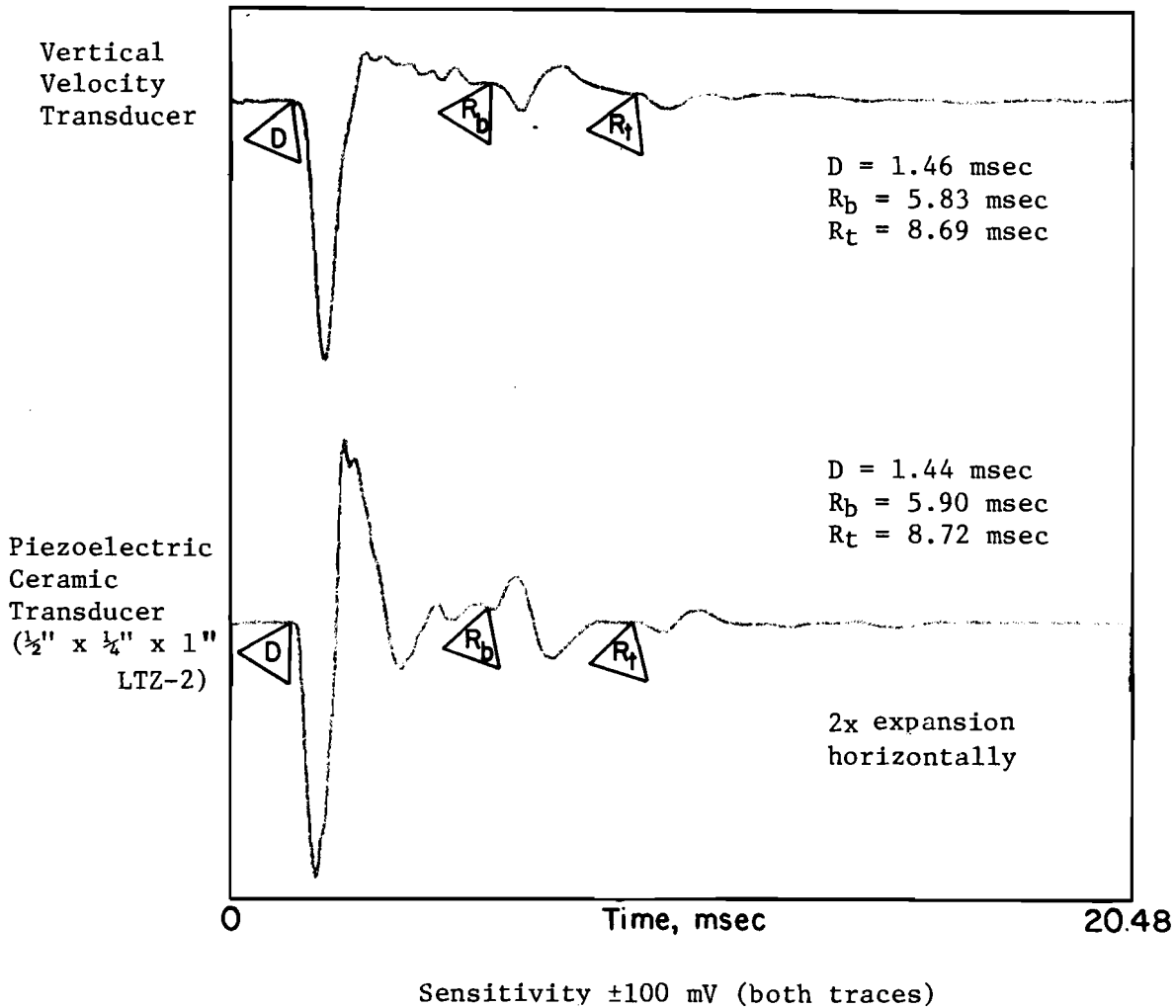
R_t = Reflected wave from top of pier, 8.86 msec

Receiver Elevation = 20 ft (6.1 m)

Pier Length = 50 ft (15.2 m)

Pier Diameter = 32 in. (81.3 cm)

Fig 6.12. WAPER test on Shaft A (Houston site) using drop hammer source and 1/3 in. x 1/4 in. x 1 in. (0.85 cm x 0.64 cm x 2.54 cm) piezoelectric ceramic transducers.



D = Direct wave arrival

R_b = Reflected wave from bottom of pier

R_t = Reflected wave from top of pier

Receiver Elevation = 20 ft (6.1 m)

Pier Length = 50 ft (15.2 m)

Pier Diameter = 32 in. (81.3 cm)

Fig. 6.13. Comparison of velocity transducer and piezoelectric ceramic transducer records for WAPER test conducted on Shaft A (Houston site).

clearly defined direct and reflected wave arrivals. The major advantage of using velocity transducers receivers instead of piezoelectric transducers is in evaluating reflected wave arrivals. The downward excursion of the velocity transducer signature for both compression and tension waves, whether direct or reflected, is less complicated than the alternating upward and downward excursions of the piezoelectric transducer record, providing the evaluator ease in signal interpretation and reduced chances of error. Irregardless, piezoelectric ceramic transducers have been shown to monitor successfully drilled piers that are sound. Their ability to distinguish defective drilled piers is investigated in Chapter 7.

WAVE PROPAGATION USING SURFACE RECEIVERS (WAPS METHOD)

As discussed in Chapter 3, the procedures involved in generating and recording stress waves in drilled piers are similar for both embedded receiver and surface receiver measurements. Surface receiver (WAPS) measurements differ from embedded receiver measurements in that the receiver, typically an accelerometer, is lightly bonded to the top of the pier rather than being embedded, and a filter is typically required to reduce noise in the (accelerometer) output.

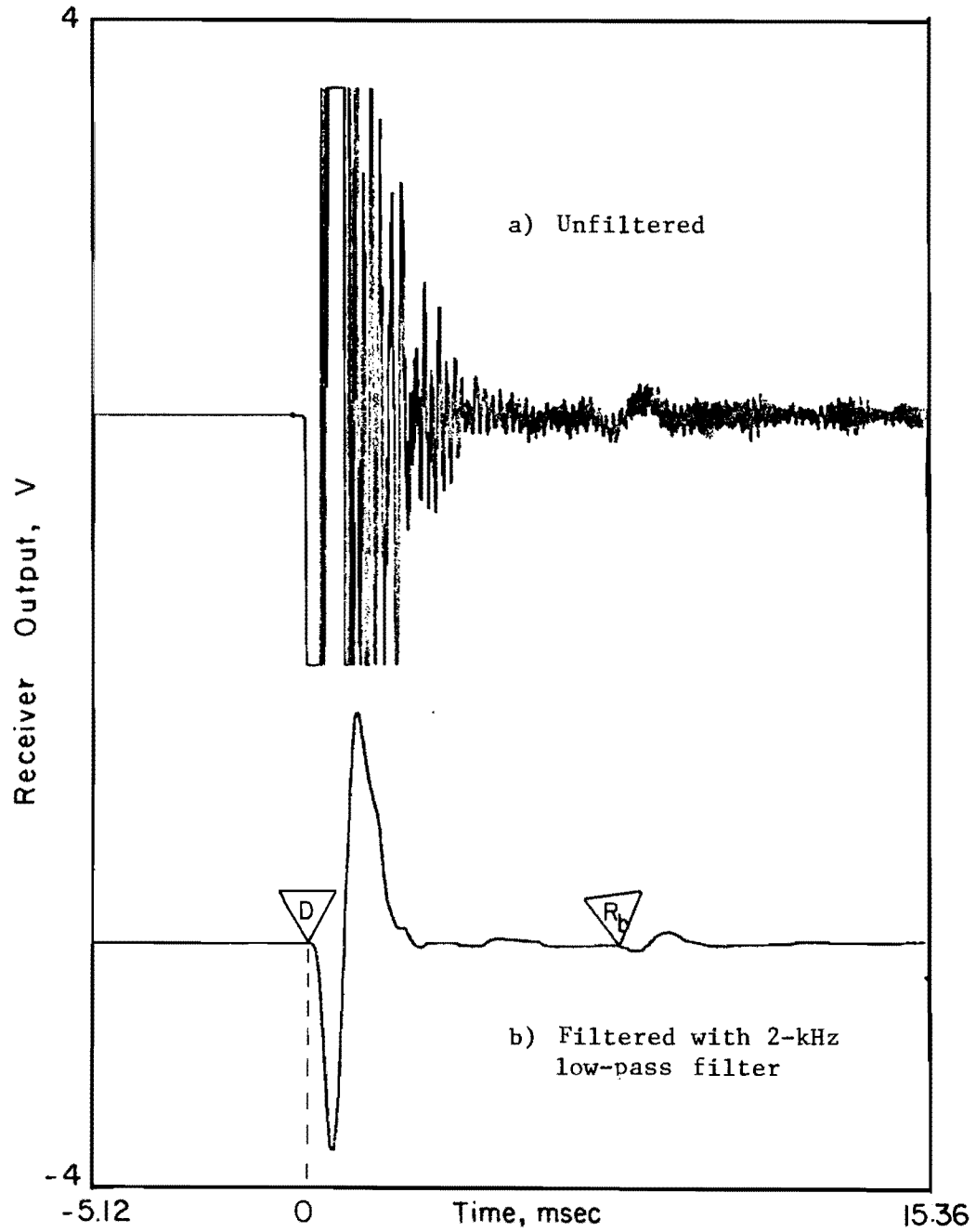
Advantages of the WAPS method include convenience (no preconstruction installation required), economy (one receiver can be used to test all shafts), and ease of testing (both source and receiver are located at the top of the pier). Disadvantages include the inability to measure P-wave velocity directly and problems associated with source-generated surface waves. If the surface wave and reflected wave frequencies are similar, or if surface wave excitation occurs over an extended period of time, reflected wave arrivals may be "masked" in the receiver output resulting in inconclusive data

regarding concrete quality and integrity. These topics are addressed in the following sections.

Accelerometer Receiver.

As mentioned previously, surface waves tend to complicate the wave signature recorded with a surface receiver. Reinforcing steel projecting out of the top of the pier tends to alter surface wave excitation, further complicating the recorded waveform. This is illustrated in the P-wave record shown in Fig. 6.14(a). The wave signature shown is the unfiltered output recorded for a WAPS test conducted on Shaft A (Houston site). A 15 lb (6.8 kg) drop hammer was used as the source. It can be seen that surface waves propagating across the top of the pier greatly affect the recorded output. No reflected wave arrivals are clearly visible in the wave signature, allowing no conclusions concerning pier integrity.

To obtain interpretable wave propagation records, a filter must be used to eliminate undesirable surface wave excitation. This is illustrated in the P-wave record shown in Fig. 6.14(b). This record is identical to the WAPS record shown in Fig. 6.14(a), with the exception that the output was filtered using 2-kHz low-pass filter. The mid-signal trigger feature of the digital oscilloscope was utilized for this trace. This feature is extremely valuable when evaluating filtered output, due to the affects of filtering on time measurements. A comparison of Figs. 6.14(a) and (b) reveals that the majority of the "noise" evident in (a) has been eliminated in (b) by the filtering process. As a result, a reflected wave arrival is identifiable in the filtered trace, denoted by R_b . The reflected wave arrival occurs at approximately 7.5 msec on the filtered record. This arrival time corresponds to the 2L travel time of the compression wave previously discussed. Using



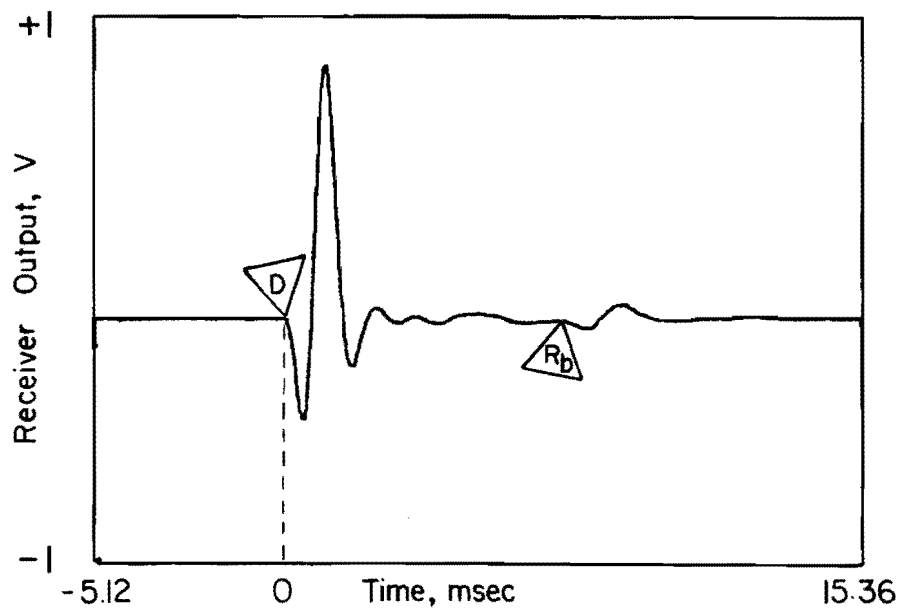
R_b = Reflected wave arrival from bottom of pier, 7.50 msec
 Pier Length = 50 ft (15.2 m)
 Pier Diameter = 32 in. (81.3 cm)

Fig. 6.14. WAPS test on Shaft A (Houston site) using drop hammer and a surface accelerometer.

the average P-wave velocity of 13,600 ft/sec (4,150 m/sec) obtained in the direct wave arrival analysis, a 2L travel distance of 102 ft (31.1 m) is obtained, resulting in a pier length of 51 ft (15.5 m). The difference in actual and computed pier length can be attributed to the difficulty in determining the exact arrival of the reflected wave and to the effects of filtering. As discussed in Chapter 3, filtering of the receiver output can affect wave amplitudes and time measurements, and the user should be aware of these possible alterations when assessing filtered waveforms.

Similar results were obtained in Fig. 6.15. This figure is identical to Fig. 6.14(b), with the exceptions that the impulse was provided by a 5 lb (2.3 kg) hand sledge and embedded nail source, and the receiver output was filtered using a low pass filter set at 1 kHz.

Based on Figs. 6.14(b) and 6.15 and the above analysis, it would appear that the WAPS method using an accelerometer is a viable method for assessing pier integrity. However, the slenderness ratio for this test pier is 20. Steinbach (1971) observed that when the pier diameter is relatively large with respect to the pier length, surface waves will not attenuate enough to allow observation of the reflected waves. Furthermore, for piers with diameters greater than about 5 ft (1.5 m), the surface wave frequency (dependent upon the wave velocity and pier diameter, both fixed factors) may be close to the reflected wave frequency. Attempting to filter the surface wave would also result in attenuation of the reflected wave. Both of these factors render identification of reflected wave arrivals difficult, at best. Therefore, integrity testing of drilled piers using the WAPS method seems to be best reserved for small diameter piers.



R_b = Reflected wave arrival from bottom of pier, 7.48 msec
Pier Length = 50 ft (15.2 m)
Pier Diameter = 32 in. (81.3 cm)

Fig. 6.15. WAPS test on Shaft A (Houston site) using hand sledge and embedded nail as a source and surface accelerometer filtered at 1-kHz low pass.

Velocity Transducer Receiver

WAPS measurements using a velocity transducer as the surface receiver proved to be less successful than measurements conducted using an accelerometer. Wave propagation measurements on Shaft A using a velocity transducer (natural frequency of 8-Hz) as the surface receiver are shown in Figs. 6.16 and 6.17. The recorded output shown in Fig. 6.16 was generated using a 15 lb (6.8 kg) drop hammer, while the output shown in Fig. 6.17 was the result of a 5 lb (2.3 kg) hand sledge and embedded nail setup. In both figures, the unfiltered wave excitation registered by the surface receiver is shown in the upper traces, while the lower records show receiver output filtered at 2.5- kHz low pass.

A review of the traces in Figs. 6.16(b) and 6.17(b) reveals that filtering was again successful in eliminating the majority of the surface wave excitation. However, no reflected wave arrivals are visible at the approximate arrival time (7.35 msec) computed using the previously obtained P-wave velocity. Because the reflected wave frequency may have been attenuated at the 2.5-kHz, low-pass, filter setting, filter settings (1 to 5- kHz) were experimented with in an attempt to obtain a wave signature with identifiable reflected waves. Unfortunately, all results were similar to the previous findings shown in Figs. 6.16(b) and 6.17(b).

WAVE ATTENUATION

Theory

As the compression wave travels through the concrete pier during a measurement, wave energy is dissipated or attenuated during the propagation process. As discussed in Chapter 3, wave attenuation is influenced by such factors as concrete quality, the presence of irregularities in the pier and

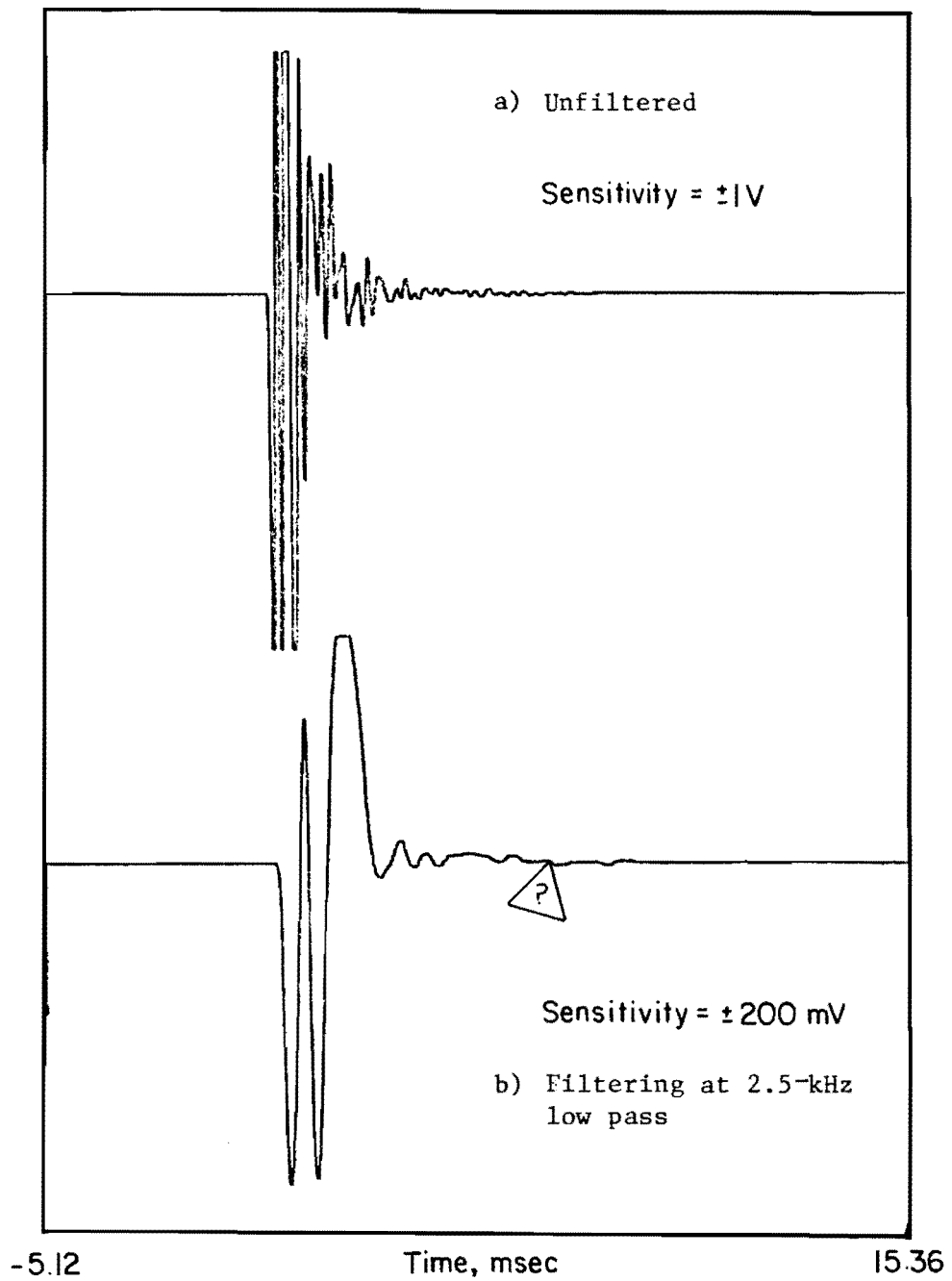


Fig. 6.16. WAPS test on Shaft A (Houston site) using drop hammer source and a velocity transducer as a surface receiver.

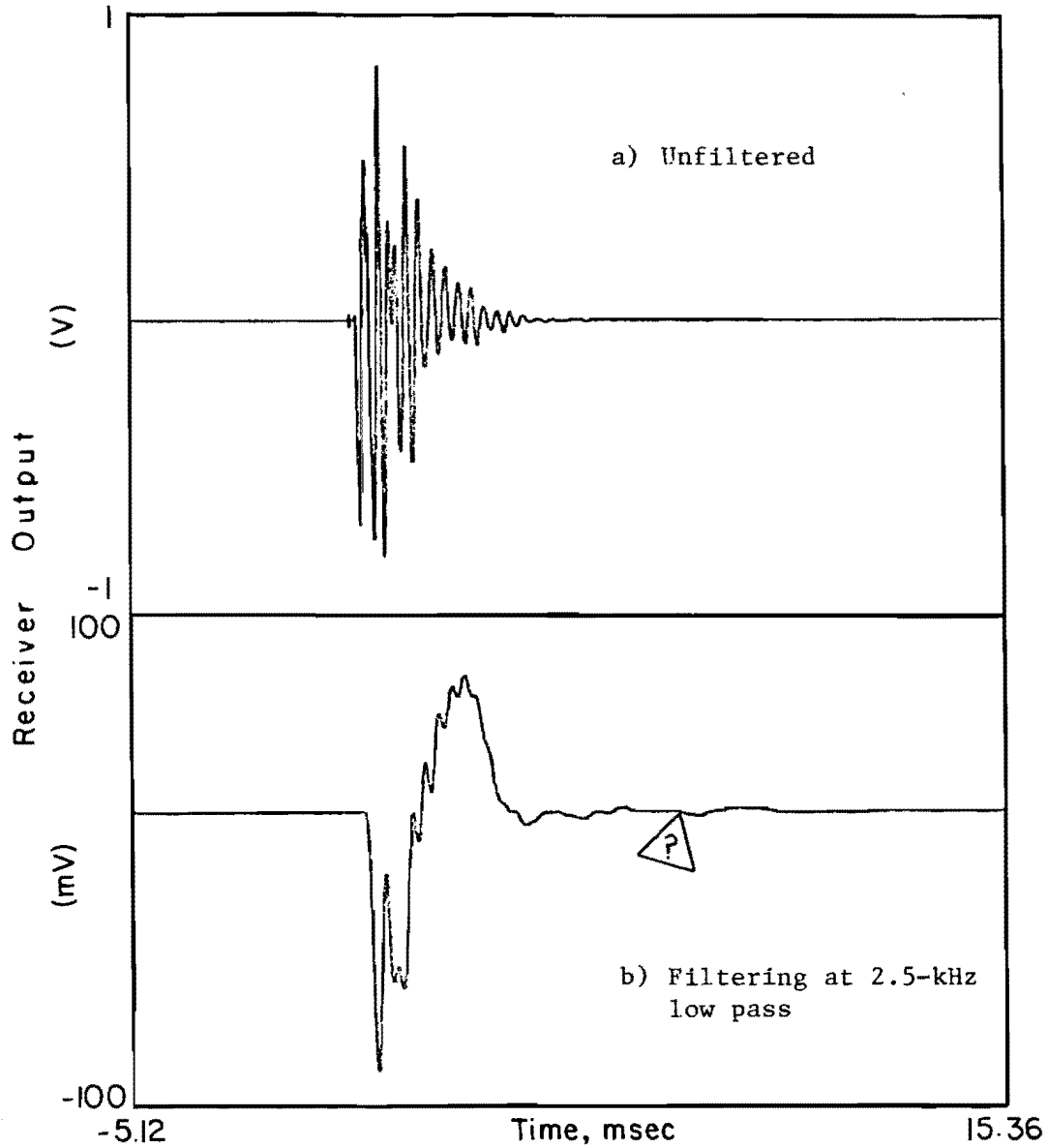


Fig. 6.17. WAPS test on Shaft A (Houston site) using hand-sledge-and embedded-nail source and a velocity transducer as a surface receiver.

their size and nature, material damping in the pier, surrounding soil conditions, and pier geometry.

For sound, straight-sided drilled piers of good quality concrete, the major sources of wave attenuation are attributable to the characteristics of the embedment materials. Drilled piers surrounded by hard soils have been found to exhibit higher P-wave attenuation than similar piers in soft soils. Although it is difficult to quantify the influence of soil along the shaft of the pier on wave attenuation, theoretical consideration can be given to the wave reflection boundary provided by the pier bottom. As the downward propagating P-wave encounters the concrete-soil interface at the bottom of the pier, a certain amount of wave energy is transmitted into the underlying soil, while the remaining energy is reflected as a tension wave. For a plane wave, the ratio of reflected-to-incident compression wave amplitudes depends on the density and P-wave velocity contrasts between the concrete and soil at the base of the pier (Richart et al, 1970). This wave amplitude ratio is expressed as follows:

$$\frac{C}{A} = \frac{(\rho_1/\rho_2)(V_{c1}/V_{c2}) - 1}{(\rho_1/\rho_2)(V_{c1}/V_{c2}) + 1}$$

where

A = incident P-wave amplitude,

C = reflected P-wave amplitude,

ρ_1 = mass density of concrete,

ρ_2 = mass density of underlying soil,

V_{c1} = Pwave velocity in concrete, and

V_{c2} = P-wave velocity in underlying soil.

This theoretical relationship is graphically illustrated in Fig. 6.18. It can be seen from the figure that the greater the contrast in material properties at the reflecting boundary, the greater will be the ratio of reflected-to-incident wave amplitude. Therefore, for sound drilled piers, the amount of wave energy reflected from the concrete-soil interface at the pier bottom is dependent upon the material properties on both sides of the interface, while total reflection of wave energy should occur at the concrete-air interface at the top of the pier.

Measurements

To study wave attenuation in sound and defective drilled piers, the test piers constructed at the Houston site were instrumented with numerous embedded velocity transducers. Results of wave propagation attenuation studies on Shaft A are presented in this section. Wave attenuation studies conducted on the defective piers are discussed in Chapter 7.

To better understand wave attenuation in drilled piers, a single waveform will initially be analyzed. This wave signature is shown in Fig. 6.19. This signature was recorded at the 10 ft (3.1 m) embedded velocity transducer in Shaft A using a 15 lb (6.8 kg) drop hammer. In this signature, the wave reflections off the bottom and top are both identifiable, the reflections denoted by R_b and R_t , respectively. The amplitudes of the direct and reflected wave energy are directly measured from the generated waveform, and are provided in the figure.

As revealed in Fig. 6.19, a large percentage of the direct wave arrival energy (a) has been attenuated by the time the reflected wave passes the receiver (b). Using the amplitudes provided in the figure, the amount of wave attenuation during this period is approximately 94 percent. Because the pier has previously been deemed sound, (excellent concrete quality and no

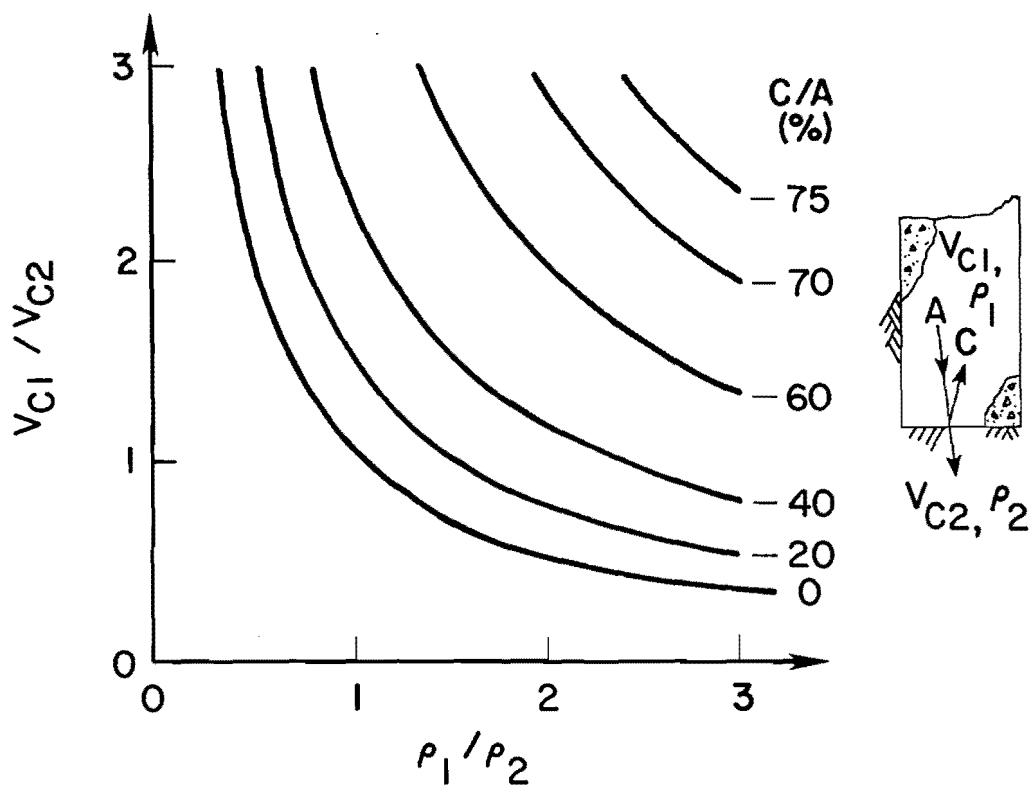
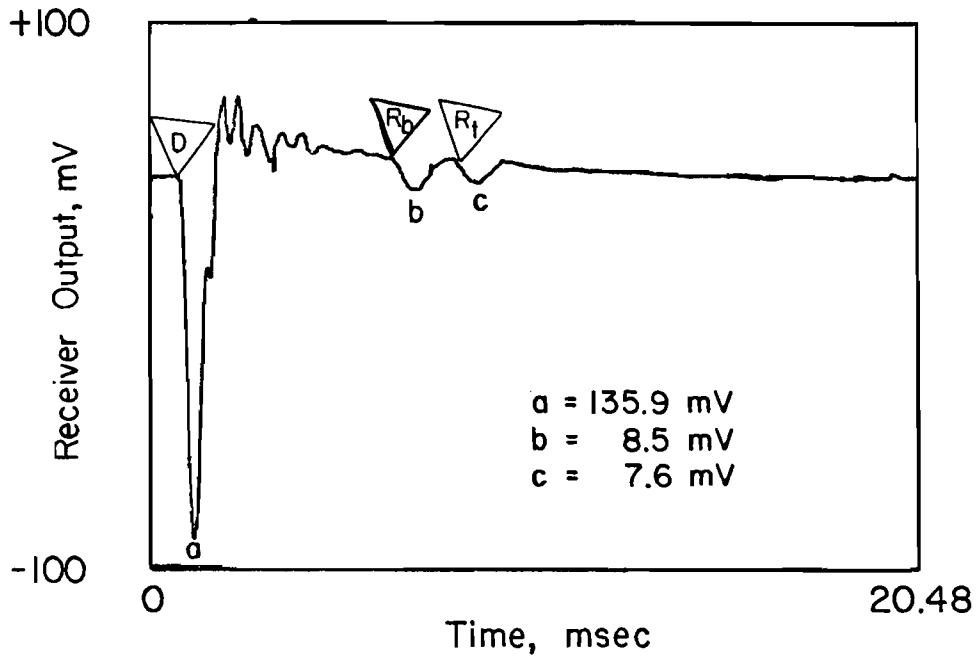


Fig. 6.18. Theoretical relationship for reflected/incident P-wave amplitude (C/A) (from Hearne et al, 1981).



D = Direct Wave Arrival

R_b = Reflected Wave Arrival Off Bottom

R_t = Reflected Wave Arrival Off Top

Receiver Depth = 10 ft (3.0 m)

Pier Length = 50 ft (15.2 m)

Pier Diameter = 32 in. (81.3 cm)

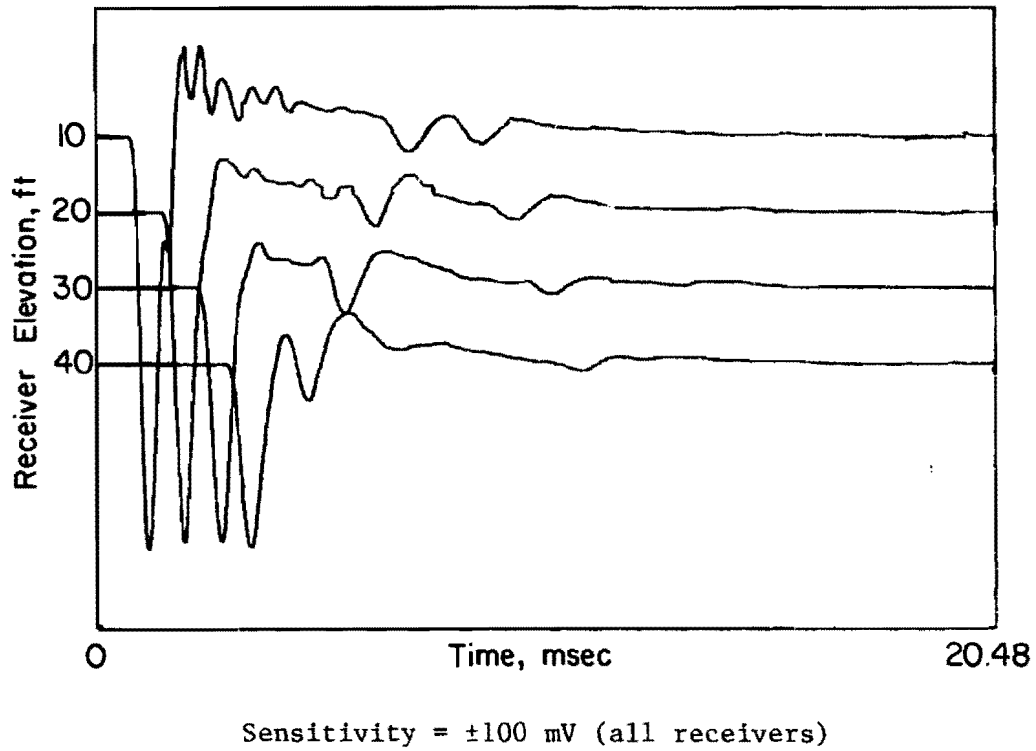
Fig. 6.19. Attenuation of single receiver output from WAPER test conducted on Shaft A (Houston site).

defects), this high percentage of wave attenuation is largely attributable to the surrounding soil conditions and the reflection characteristics of the pier bottom. The difference in wave amplitudes of the reflected waves off the top (R_t) and bottom (R_b) of the pier is small, confirming the theory that nearly total reflection occurs at the concrete-soil interface at the top of the pier.

The wave signature shown in Fig. 6.19 and the findings presented above illustrate the importance of receiver location on the success of wave propagation measurements in determining pier integrity. For very long, sound piers, the reflected wave arrival off the bottom of the pier may be indistinguishable in the recorded output of shallow embedded receivers due to significant wave attenuation. Two or more receivers, embedded at strategic locations near the top and bottom of the pier, eliminate this problem by allowing comparison between wave arrival amplitudes. Unfortunately, no simple solution exists for monitoring highly attenuated waves with a surface receiver.

The advantages of using multiple receivers for wave attenuation studies are illustrated in Figs. 6.20 and 6.21. In Fig. 6.20, the outputs recorded at the 10-, 20-, 30-, and 40-ft (3.1-, 6.1-, 9.1-, and 12.2-m) velocity transducers embedded in Shaft A are shown. The output has been positioned in equal voltage increments along the ordinate to simulate the actual positioning of the receivers within the pier. To obtain comparative amplitude data in the four embedded receivers, the wave signatures all had to be generated by a single impact. This required that two digital oscilloscopes be used for wave monitoring purposes, as shown in Fig. 4.2.

A review of Fig. 6.20 reveals that the reflected wave arrivals off both the bottom and top of the pier are distinguishable. By viewing multiple



Pier Length = 50 ft (15.2 m)

Pier Diameter = 32 in. (81.3 cm)

Fig. 6.20. Attenuation study of multiple receiver outputs from WAPER test conducted on Shaft A (Houston site).

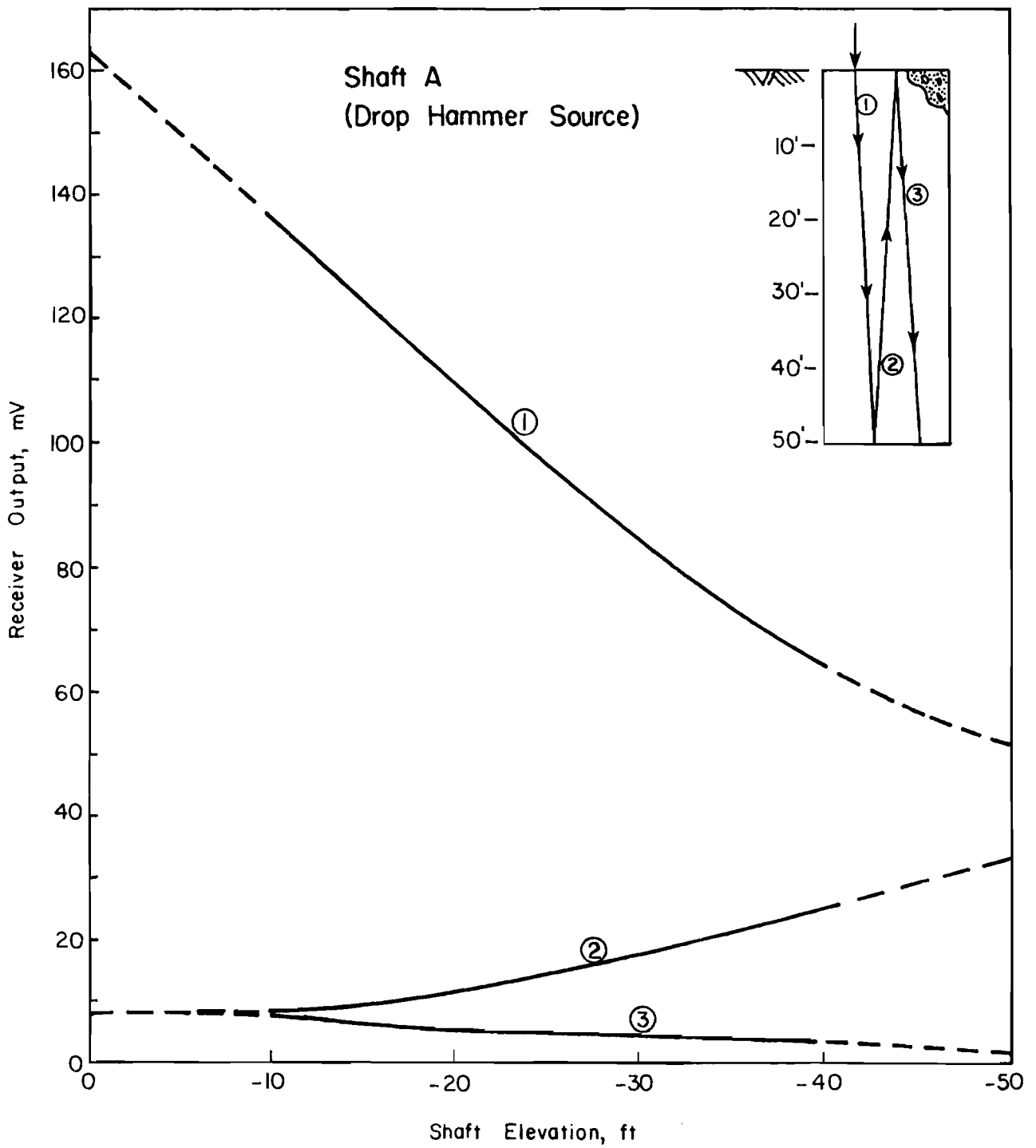


Fig. 6.21. Attenuation of P-wave in Shaft A (Houston site).

receiver outputs in this manner, the viewer can "visually" see the compression wave attenuate as it propagates down and up the pier. The direct and reflected wave amplitudes shown in Fig. 6.20 have been graphically presented in Fig. 6.21. As shown in this figure, wave amplitude is attenuated rapidly during the initial pass of the P-wave down the pier. Upon arrival at the pier bottom, a certain amount of wave energy is transmitted to the underlying soil, while the remaining energy is reflected. Assuming P-wave velocities of 13,600 ft/sec (4,150 m/sec) and 5,000 ft/sec (1,520 m/sec) for the concrete and underlying soil (assumed saturated), respectively, and unit weights of 150 lbs/ft (2405 kg/m) and 120 lbs/ft (1925 kg/m) for the concrete and soil, respectively, the computed reflected-to-incident amplitude ratio (C/A) is 55 percent. From Fig. 6.21, the ratio of C/A is approximately 62 percent. In light of the assumptions and the extrapolation of the plotted data, the measured reflection-to-incident amplitude ratio compares favorably with the theoretical value.

Similar results were obtained for the hand-sledge-and-embedded-nail source, as shown in Figs. 6.22 and 6.23. In Fig. 6.22, WAPER output recorded at the multiple velocity transducers embedded in Shaft A has been presented in the same manner as the output shown in Fig. 6.20. A 5 lb (2.3 kg) hand sledge source striking a 61d embedded nail was used to generate the P-wave impulse. As before, reflected wave arrivals off both the bottom and top of the pier are distinguishable, allowing assessment of wave attenuation as the P-wave propagates down and up the pier. The direct and reflected wave arrivals for the hand sledge shown in Fig. 6.22 are graphically presented in Fig. 6.23. The wave attenuation curves shown in Fig. 6.23 have the same general shape as those generated with the drop hammer presented in Fig. 6.21. The computed reflected-to-incident amplitude ratio (C/A) for the wave energy

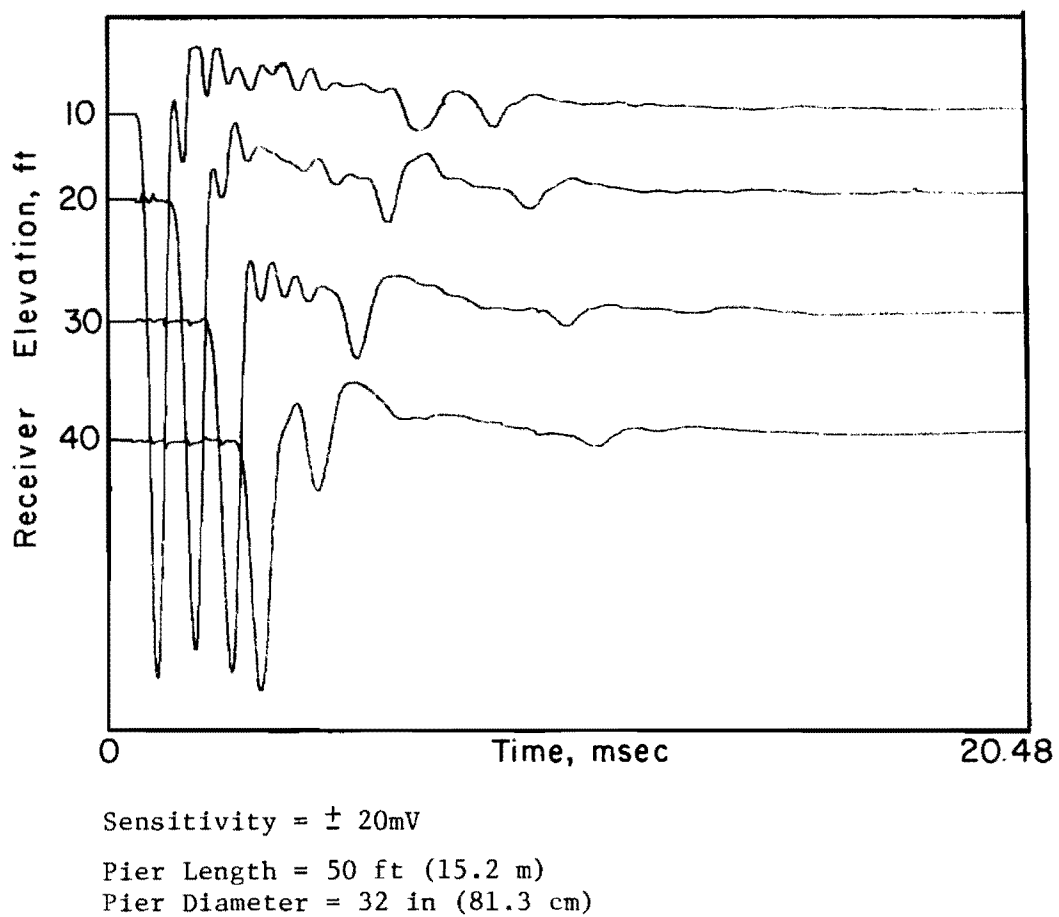


Fig. 6.22. Attenuation study of multiple receiver output from WAPER test conducted on Shaft A (Houston site) using hand sledge and embedded nail source.

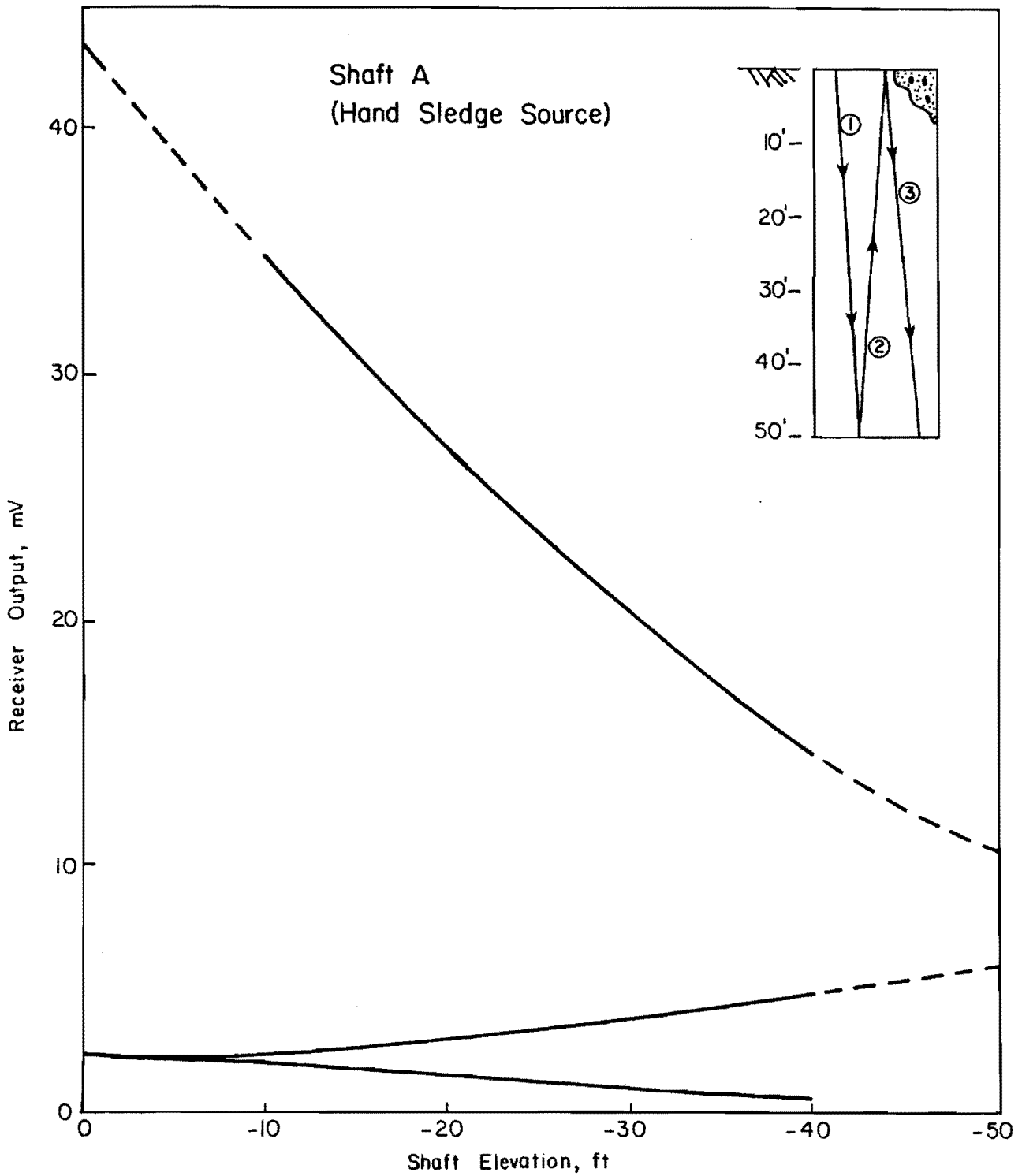


Fig. 6.23. Attenuation of P-wave in Shaft A (Houston site).

at the bottom of the pier in Fig. 6.23 is 56 percent, comparing favorably with the amplitude ratio computed from the drop hammer and the theoretical value.

For comparison purposes, the wave attenuation curves presented in Figs. 6.21 and 6.23 have been normalized and tabulated in Table 6.2. From Table 6.2, it can be seen that the higher amplitude signal provided by the drop hammer resulted in a slight decrease in wave attenuation when compared with that generated by the hand-sledge-and-embedded-nail source. For graphical comparison, polynomial regression analyses were performed using only the direct P-wave amplitudes in Table 6.2. Direct P-wave arrivals were selected for several reasons, including: (1) ease of interpretation, (2) accuracy of determination of wave amplitude, (3) unaffected by material properties and reflection coefficient at the bottom of the pier, and (4) general application to a variety of drilled pier lengths and subsurface conditions. The normalized wave attenuation data for both sources are presented in Fig. 6.24. The dashed portions of the normalized curves represent extrapolated data to be verified by piers longer than those included in this study.

The normalized attenuation curves in Fig. 6.24 can be used to evaluate the integrity of piers drilled in cohesive soils and instrumented with two or more embedded receivers. As a check, WAPER output recorded at a test site in Beaumont, Texas was evaluated for wave attenuation (see Fig. 6.23). The drilled pier was a 36 in. (91.4 cm) in diameter, 92 ft (28 m) in length, straight sided, and instrumented with vertical velocity transducers embedded at depths of 30-, 55- and 75 ft (9.1-, 16.8- and 22.9 m) below the top of the shaft. The subsurface conditions at the site were similar to those shown in Fig. 3.5(a). A 15 lb (6.8 kg) drop hammer was used as the P-wave source. Based on the output shown in Fig. 6.25, the drilled pier had been

Table 6.2. Source comparison of wave attenuation
in Shaft A (Houston site)

<u>CHANGE IN OUTPUT, PERCENT</u>		
(Normalized to 10 ft (3.0 m) receiver)		
<u>Receiver</u>	<u>Drop Hammer</u>	<u>Hand sledge</u>
20	80.1	75.3
30	61.4	59.2
40	47.3	41.5
40	18.5	13.5
30	13.7	11.2
20	7.6	8.2
10	6.3	6.8
10	5.6	5.8
20	3.6	3.7
30	2.8	2.9
40	1.7	1.5

previously deemed sound. Because three receivers were used to monitor wave propagation within the drilled pier, a regression analysis was possible of the direct P-wave amplitude data. The normalized attenuation data is plotted in Fig. 6.24. Wave attenuation exhibited by this pier correlates well with the data obtained for Shaft A (sound pier).

Fig. 6.24. If only two receivers were available in the pier in Beaumont, say the 30 and 75 ft (9.1 and 22.9 m) velocity transducers, the normalized curves of Fig. 6.24 are still helpful in evaluating pier integrity. The percent reduction in wave energy between the 30 and 75 ft (9.1 and 22.9 m) receivers can be compared with the reduction shown in the normalized data. A large variation in attenuation should signal the possibility of a pier discontinuity or irregularity.

Use of Fig. 6.24 requires that a minimum of two, and preferably more, embedded receivers be positioned in the drilled pier. The embedded receivers should be positioned as far apart as possible to increase the chances of irregularity detection. For optimum results, one receiver should be positioned about 10 ft (3.0 m) below the top of the shaft and one receiver should be positioned about 10 to 15 ft (3.0 to 4.6 m) above the bottom of the shaft.

One final point is that the data provided in Fig. 6.24 appears to be applicable only to small-diameter piers. A check of a 72 in. (183 cm) diameter, 92 ft (28 m) long, drilled pier constructed at the Beaumont site and evaluated as structurally sound showed considerable deviation from the extrapolated data in Fig. 6.24. Additional research will be required to determine the exact limits of the normalized data.

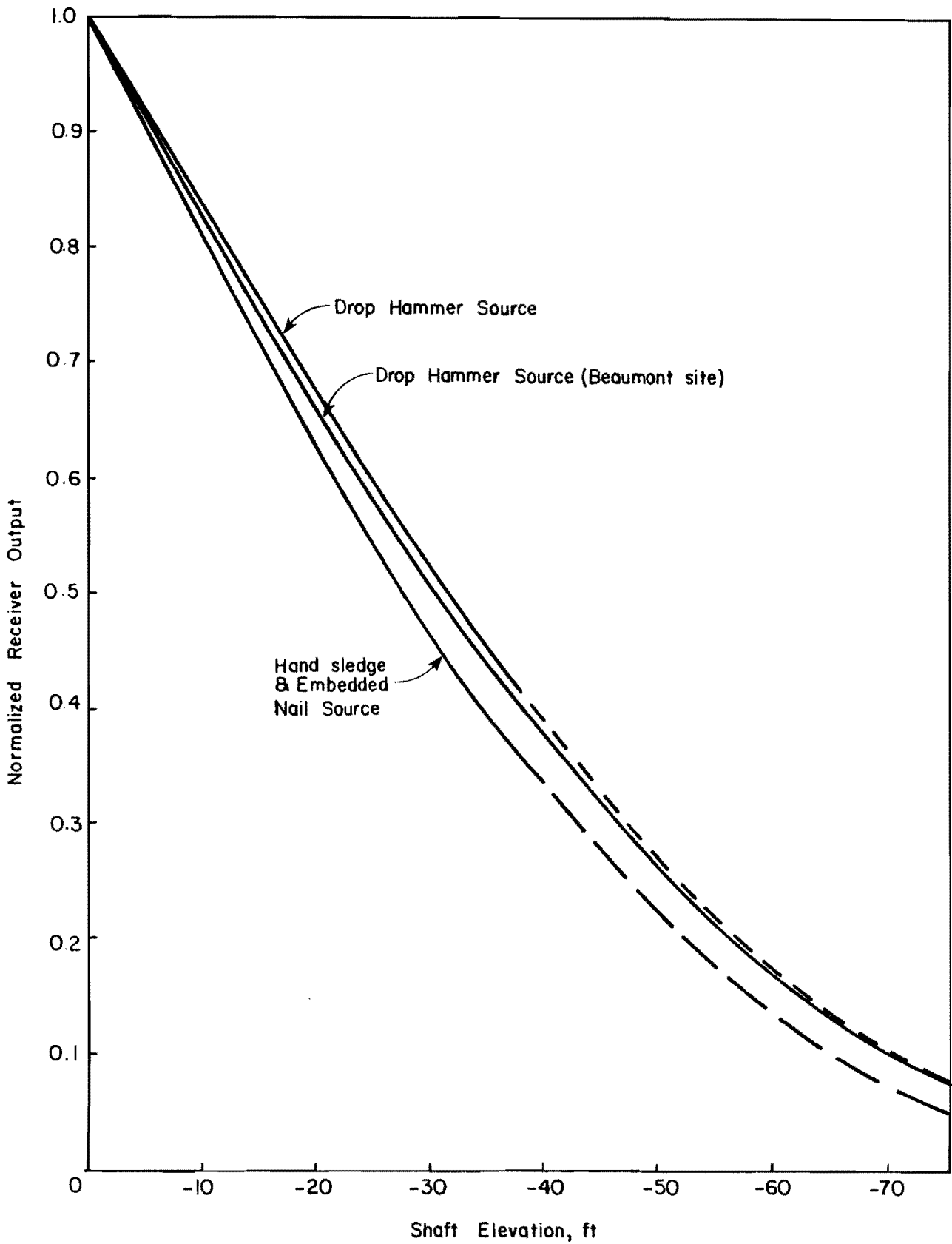
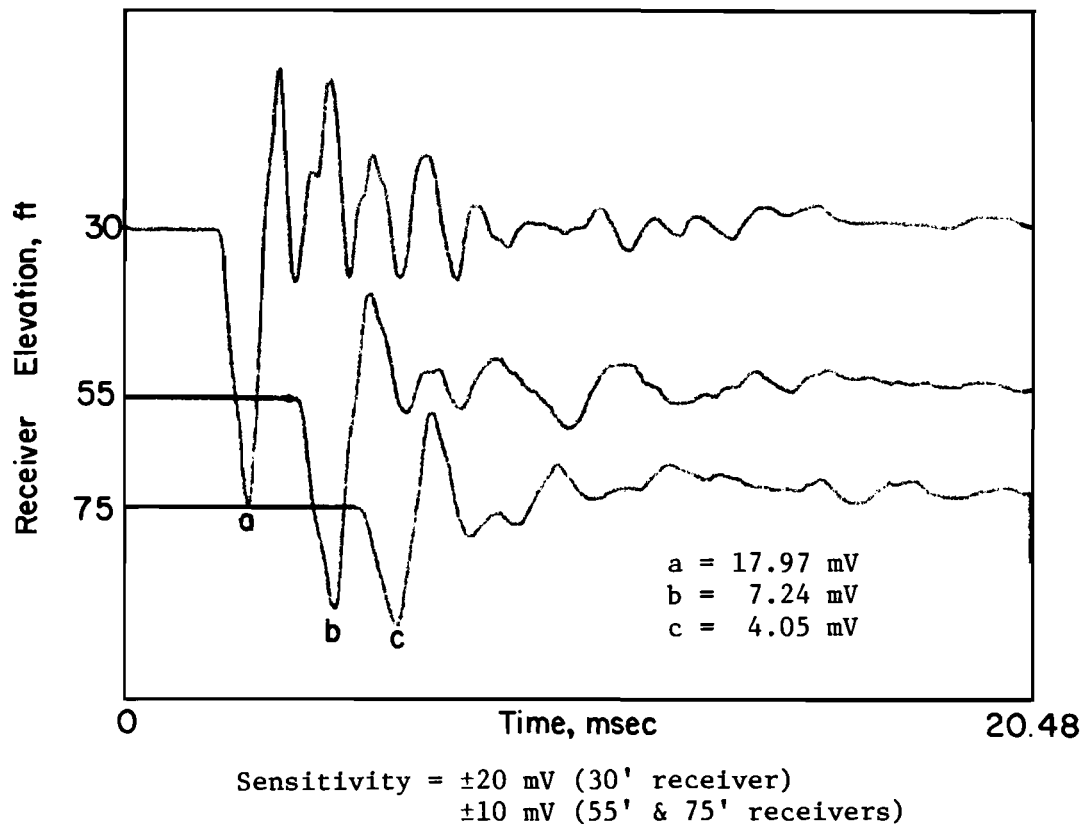


Fig. 6.24. Normalized attenuation of direct P-wave in Shaft A (Houston site).



Pier Length = 92 ft (28 m)

Pier Diameter = 36 in. (91.1 cm)

Fig. 6.25. Attenuation of multiple receiver output from WAPER test (Beaumont, Texas)

SOURCES

Various surface sources were experimented with in an attempt to obtain clearer and more easily interpretable wave records. The various sources included drop hammers, sledge hammer and chisel combinations, steel rods, steel balls, and an impact gun. In conjunction with the various sources, different triggering surfaces consisting of metal plates, bars, rods, balls, and nails were examined. Results of the tests varied considerably, and only the significant findings will be addressed in this section.

WAPER Tests. As revealed in the wave excitation records presented in the earlier sections of this chapter, the drop hammer consistently provided ample wave energy and interpretable wave signatures. The same is true for the hand-held, sledge hammer. However, the hand-sledge-and-embedded-nail configuration provided the optimum wave signature in regard to clarity and ease of assessment of WAPER test records. This observation is shown in Fig. 6.26, where wave signatures for both the drop hammer and hand sledge/embedded nail sources are compared. The output shown in Fig. 6.26 is wave excitation recorded at the 30 ft (9.1 m) embedded velocity transducer in Shaft B. The reflected wave arrivals off the pier bottom, top, and bottom again are easily recognizable in both traces, indicating the suitability of both hammers as sources. Wave amplitudes are also sufficient in both signatures, further confirming their suitability. However, the drop hammer creates more ringing in the waveform, as shown in the initial portion of the lower wave signature in Fig. 6.26. Although reflected wave arrivals off the bottom are distinguishable in both records, wave arrivals occurring a short time after the arrival of the direct wave may be "masked" in the record generated with the drop hammer. The absence of ringing in the record generated with the hand sledge/embedded nail increases the chances of detecting additional

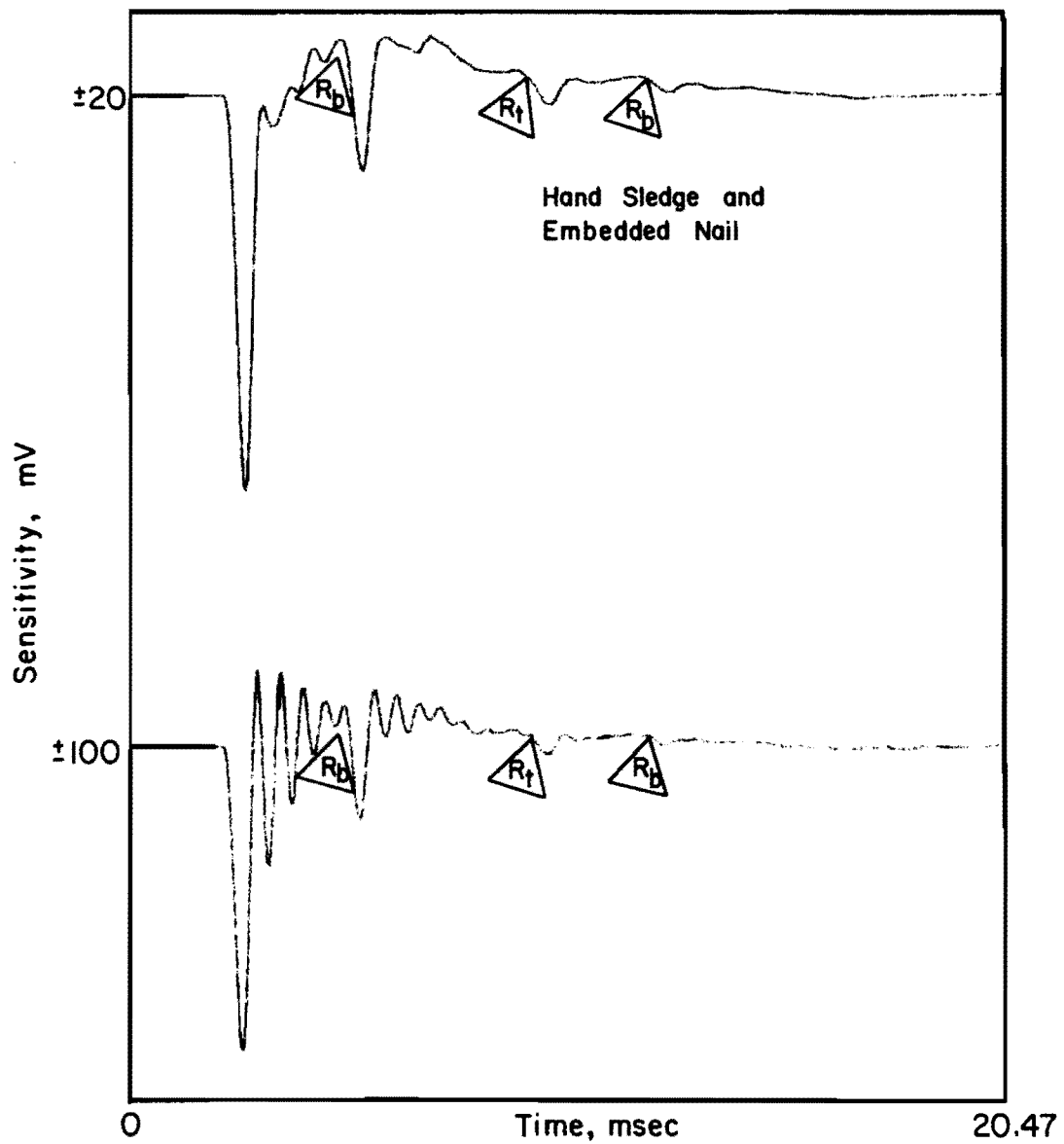


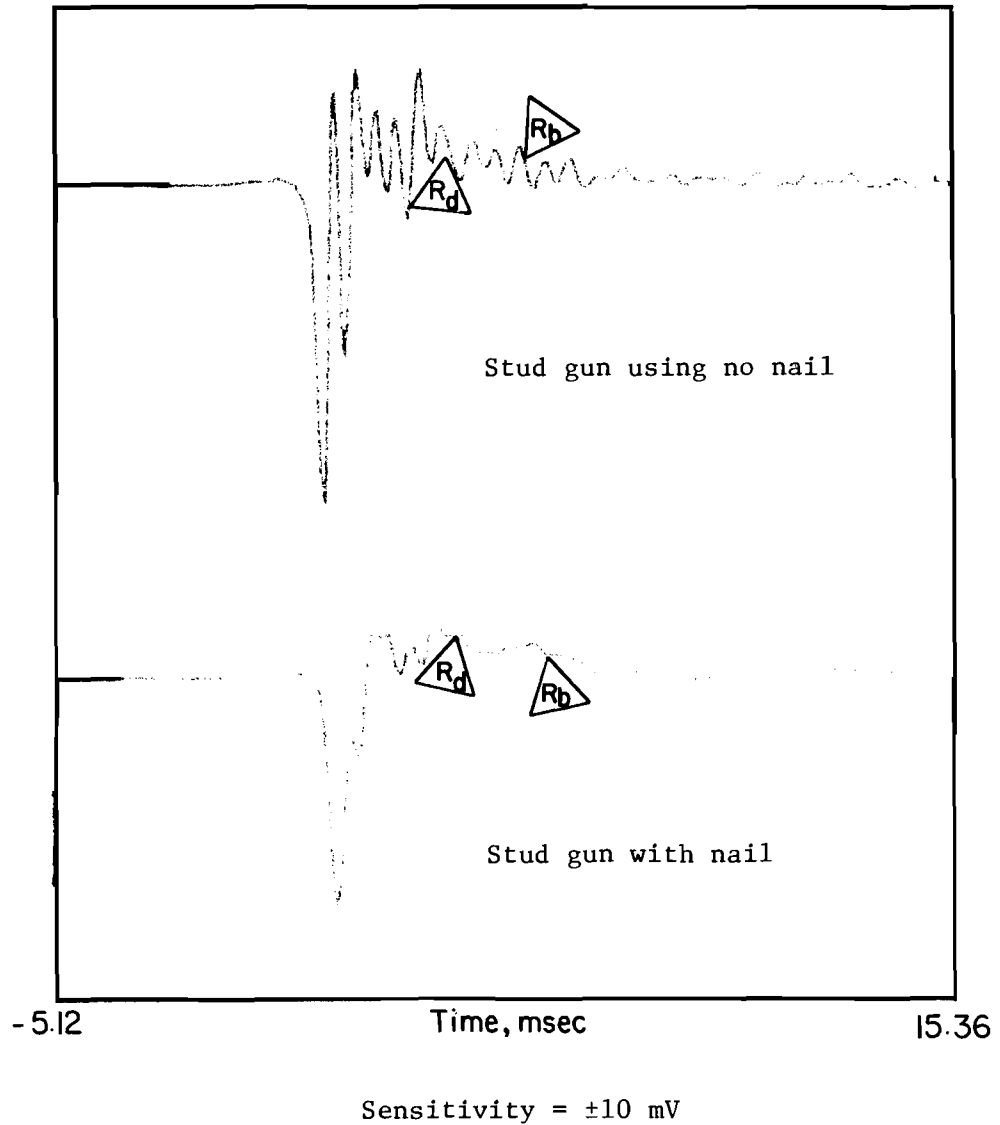
Fig. 6.26. Comparison of records generated with various sources; hand sledge and embedded nail versus drop hammer (Shaft A).

reflected waves in the record. Reflected wave energy off a defect in the general proximity of the embedded receiver would only be realized in the drop hammer trace in Fig. 6.26 by analyzing the attenuation of the direct wave arrivals.

Of interest are WAPER tests performed using the stud gun as a surface source. The stud gun was included in this study in an attempt to generate compression waves with higher frequencies. It was reasoned that higher frequency waves, thus shorter wavelength P-waves, would effectively sample smaller regions of the pier, possibly resulting in the detection of smaller defects.

Results of wave propagation tests conducted on Shaft C using the stud gun as the source are shown in Figs. 6.27 and 6.28. In Fig. 6.27, output recorded at the 10 ft (3.1 m) embedded velocity transducer is shown. The wave energy was supplied by the stud gun fired directly on the concrete surface of the pier, in one instance without a nail (Fig. 6.27(a)) and the other with a nail (Fig. 6.27(b)). Due to the nature of the source, triggering of the oscilloscope was provided by a velocity transducer on top of the pier. A review of Figs. 6.27(a) and (b) reveals that the stud gun without nail source provided the most interpretable record, although both records are of poorer quality than those generated with the drop hammer or sledge hammer sources. In Fig. 6.27, reflected wave arrivals resulting from the planned defect and pier bottom are barely visible and would most likely go undetected under normal circumstances.

The same is not true of the receiver output presented in Fig. 6.28. Here, the stud gun has been utilized in its proper manner, that is to secure wooden boards to concrete by shooting nails through the boards into the concrete. Both filtered and unfiltered wave signatures are included in Fig. 6.28. By taking into account time delays resulting from the surface receiver



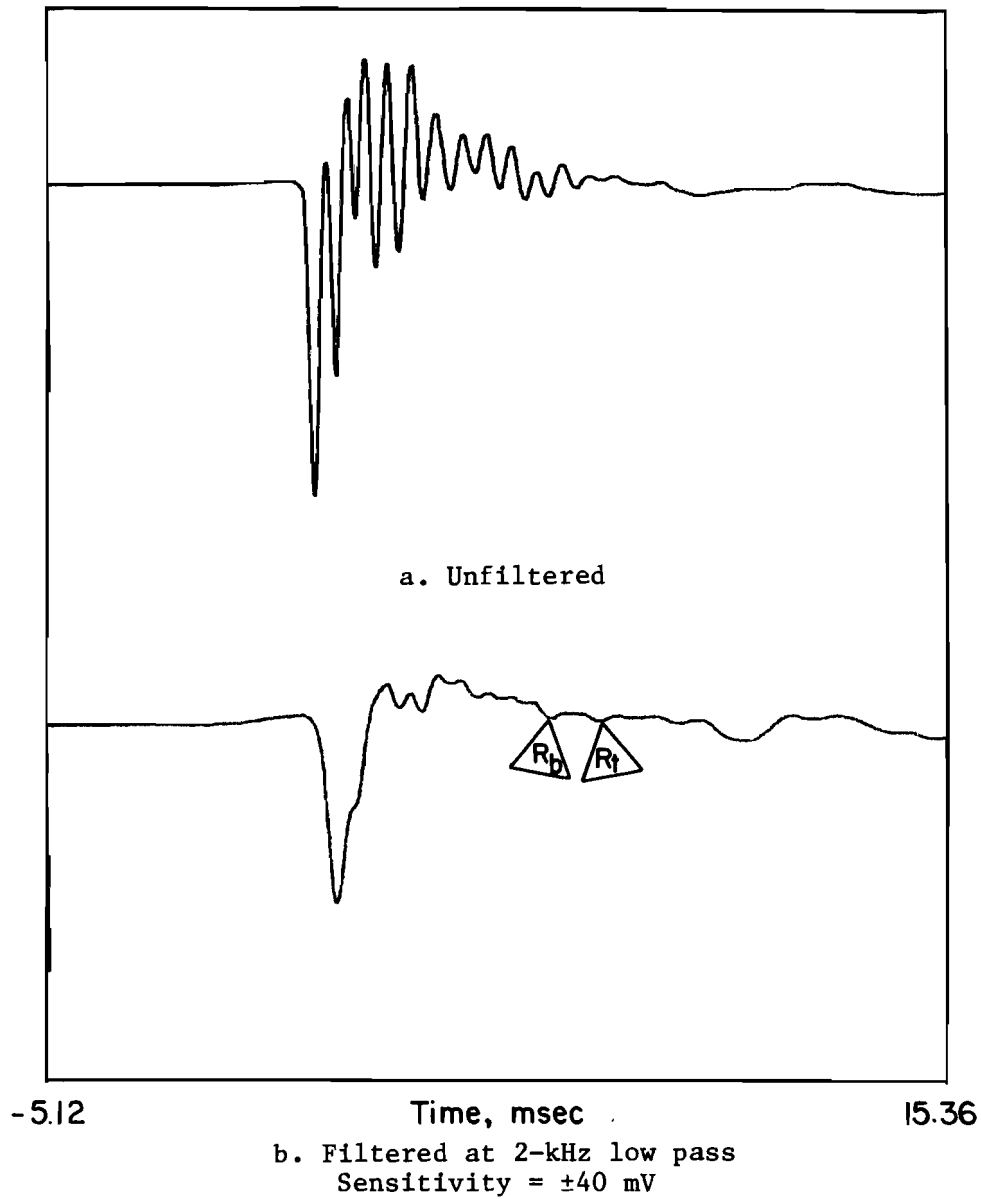
R_d = Reflected wave arrival off planned defect

Receiver Depth = 10 ft (3.0 m)

Pier Length = 50 ft (15.2 m)

Pier Diameter = 32 in. (81.3 cm)

Fig. 6.27. Source evaluation using stud gun fired directly on concrete at top of Shaft C.



R_d = Reflected wave arrival off planned defect

Receiver Depth = 10 ft (3.0 m)

Pier Length = 50 ft (15.2 m)

Pier Diameter = 32 in. (81.3 cm)

Fig. 6.28. Source evaluation using stud gun firing nail through 2X4 board into concrete at top of Shaft C.

triggering system and the affects of filtering (discussed in Chapter 4), reasonably well defined wave signatures are obtained. However, problems associated with oscilloscope triggering and waveform filtering are a nuisance in these evaluations, rendering this source less desirable than the other hammer sources.

SUMMARY

Wave propagation measurements using both embedded receiver (WAPER) and surface receiver (WAPS) methods have been shown to be effective in assessing the integrity of sound drilled piers. Although both methods were successful in assessing pier integrity, the WAPER method allows a more thorough investigation of pier integrity. For example, compression wave velocities, computed directly from wave signatures, provide a general indication of concrete quality. Furthermore, instrumentation of the piers utilizing multiple embedded receivers provides information concerning attenuation of wave amplitude, an important factor when reflected wave arrivals are "masked" in the receiver output by spurious noise.

With regard to equipment modifications, the digital oscilloscope was found to be superior to older analog storage oscilloscopes. Advantages of the digital oscilloscope include higher resolution, waveform expansion and superposition, and magnetic disk storage capabilities. Of the various sources tested, the hand-sledge-and-embedded-nail configuration consistently provided clean, easily interpretable wave signatures. Piezoelectric ceramic transducers were shown to be effective monitors of wave propagation within drilled piers, although vertical velocity transducers are still considered superior receivers due to waveform clarity and ease of interpretation.

Accelerometers are considered to be the best choice of receivers for WAPS tests.

WAPER tests performed on the sound pier at the Granger site confirmed the results obtained by Arias. Measurements performed on the sound pier at the Houston site further substantiated the suitability of wave propagation tests in assessing pier integrity. Assuming certain soil parameters, the attenuation study performed on the Houston pier provided field data that correlated well with theory. Wave attenuation for similar diameter sound piers founded in clay was also shown to correlate well for two different sites located in Texas.

CHAPTER 7. WAVE PROPAGATION MEASUREMENTS ON DEFECTIVE DRILLED PIERS

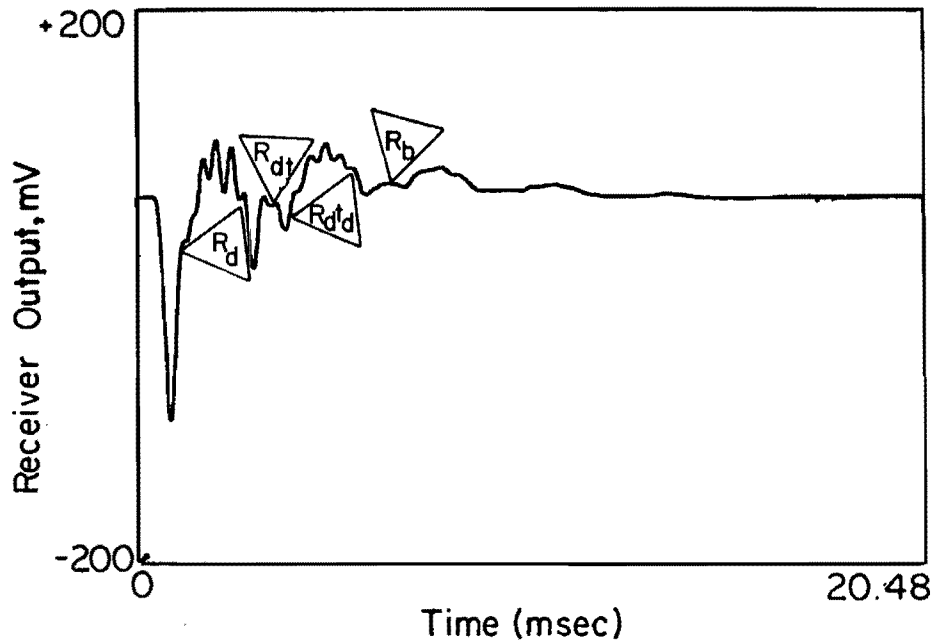
INTRODUCTION

In this chapter, the results of wave propagation conducted on the defective piers at both the Granger and Houston sites are presented. Measurements performed on the defective piers include both embedded receiver (WAPER) and surface receiver (WAPS) tests. In addition, attenuation studies were conducted on the test piers at the Houston site.

TIME DOMAIN MEASUREMENTS AT GRANGER SITE

Wave propagation tests were conducted on the defective test piers constructed at this site principally to evaluate the performance of the new equipment. The tests also allowed comparison with results obtained by Arias. Only WAPER tests were performed on these piers.

The wave signature for a WAPER test conducted on Shaft 2 is shown in Fig. 7.1. For review purposes, Shaft 2 is a 39 ft (11.9 m) long pier constructed with a 2 ft (0.61 m) thick combination clay-and-styrofoam defect at a depth of 20.2 ft (6.2 m) below the top of the pier. The direct wave generated by the drop hammer resulted in an arrival which occurred at 0.42 msec, resulting in a P-wave velocity of 12,380 ft/sec (3,770 m/sec). A second major excursion in the record (denoted R_d) can be seen arriving at a time of 2.83 msec. Using the computed P-wave velocity, this arrival time



R_d = Reflected Wave Arrival Off Defect, 2.83 msec

R_{dt} = Reflected Wave Arrival Off Defect, Then
Top of Pier, 3.63 msec

R_{dtd} = Reflected Wave Arrival Off Defect, Pier
Top, then Defect, 6.03 msec

R_b = Reflected Wave Arrival Off Pier Bottom, 6.66 msec

Receiver Elevation = 5.2 ft (1.6 m)

Pier Length = 39 ft (11.9 m)

Pier Diameter = 30 in. (76.2 cm)

Fig. 7.1. Wave signature recorded in Shaft 2 (Granger site) showing reflected wave arrivals off the 20.2 ft (6.2 m) deep defect.

corresponds to a total travel distance past the 5.2 ft (1.6 m) deep receiver of 35 ft (10.7 m), resulting in a computed reflection boundary at 20.1 ft (6.1 m) below the top of the pier. This location compares favorably with the actual defect location, proving the WAPER method to be effective in assessing drilled pier integrity. Shortly after the arrival of the reflection off the defect, another excursion in the wave signature occurs (denoted R_{dt}). The arrival of this reflection occurs at an approximate time of 3.63 msec, which represents wave energy reflected off the defect and then reflected off the top of the pier.

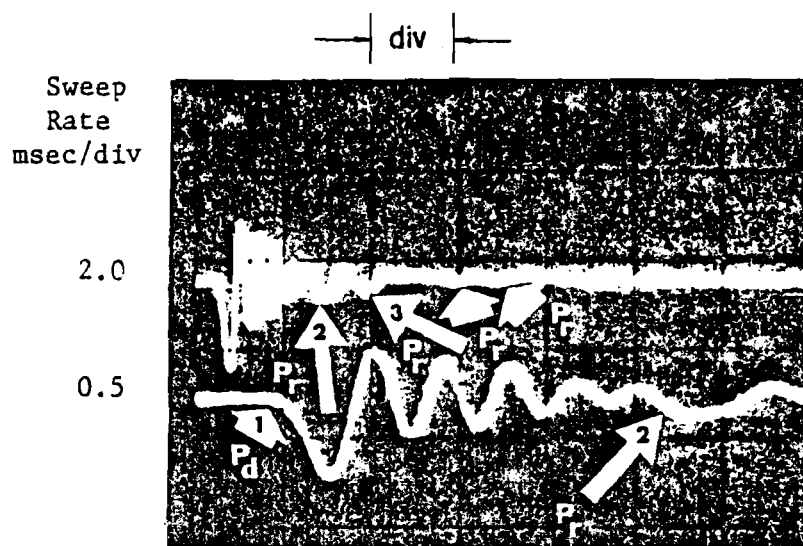
As presented in the discussion of Fig. 3.6(b), the defect in Shaft 2 is located at a depth such that the reflection from the bottom of the pier closely corresponds with the second reflected wave arrival from the defect. Using the direct P-wave velocity of 12,380 ft/sec (3,770 m/sec), the travel time for the P-wave reflection off the bottom of the pier is 5.88 msec. Using the same P-wave velocity, the travel time for the P-wave to reflect off the defect, back off the top of the pier, and then back off the defect to the 5.2 ft (1.6 m) deep receiver is 6.11 msec. Both arrival times correspond closely with the arrival time of the wave shown in Fig. 7.1 as R_{dtd} . However, for the P-wave to reflect from the pier bottom to the receiver, it must first pass through the soil defect. The clay defect has a much slower P-wave velocity than concrete, consequently causing a delay in the P-wave arrival. Assuming a P-wave of 5,000 ft/sec (1,520 m/sec) for the clay defect (assuming saturated conditions), the travel time of the reflected wave from the pier bottom would be increased by approximately 0.8 msec, for a modified arrival time of 6.68 msec. This time corresponds to the arrival time of the bottom reflected wave which is denoted as R_b in the figure.

The wave signature shown in Fig. 7.1 illustrates the importance of correctly assessing early wave arrivals in the receiver output. The example also supports the value of having two or more receivers embedded in the drilled pier. Due to the thickness of the planned defect, the increase in travel time would be reflected in the direct wave arrival of a receiver located below the defect, resulting in a lower P-wave velocity. This was substantiated in Arias' study, as a direct P-wave velocity of 11,000 ft/sec (3,350 m/sec) was reported for output recorded at the 38.5 ft (11.7 m) receiver in Shaft 2, compared with 12,380 ft/sec (3,770 m/sec) obtained at the 5.2 ft (1.6 m) receiver.

For comparison purposes, the output recorded and presented in Arias' report for the 5.2 ft (1.6 m) embedded receiver in Shaft 2 is shown in Fig. 7.2. Again, the superiority of recording with the digital oscilloscope is shown by comparing Figs. 7.1 and 7.2.

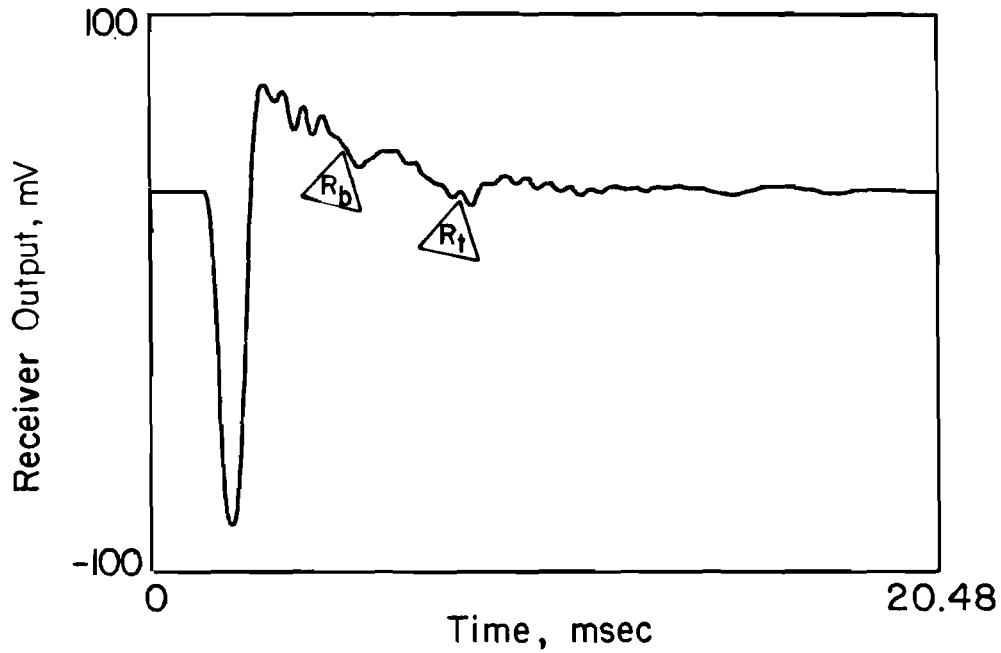
A typical wave signature for a WAPER test performed on Shaft 3 is shown in Fig. 7.3. As described in Chapter 5, Shaft 3 is a 39 ft (11.9 m) long drilled pier implanted with a 1.5 ft (0.46 m) diameter, by 1.5 ft (0.46 m) thick soil inclusion located at a depth of 8 ft (2.1 m) below the top of the pier, and a 3 ft (0.91 m) thick, full cross-sectional sand and gravel "washout" located at the bottom of the pier. The output shown in Fig. 7.3 is recorded from the 18.2 ft (5.5 m) embedded velocity transducer. A 15 lb (6.8 kg) drop hammer was used to excite the compression wave. For comparison purposes, receiver output presented in Arias' report for the same pier and receiver is provided in Fig. 7.4.

For this pier, the possibility exists for a decrease in computed direct P-wave velocity at the 18.2 ft (5.5 m) receiver, due to the effective cross-sectional area occupied by the overlying soil inclusion. Arias reported a



Sensitivity = 50 mv/div

Fig. 7.2. Signature of stress waves recorded by the vertical transducer embedded in Shaft 2 (Arias, 1977).



Receiver Elevation = 18.2 ft (5.5 m)

Defect Elevations = 8 ft (2.1 m) (soil inclusion)
 36 ft (11 m) (sand and
 gravel washout)

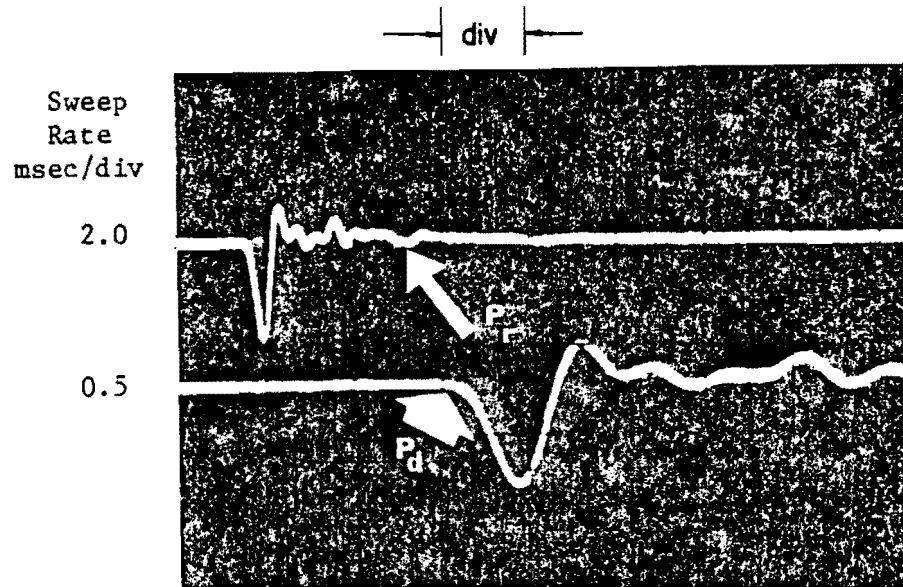
R_b = Reflected wave from bottom of pier, 4.88 msec

$R_{t?}$ = Possible reflected wave from top of pier

Pier Length = 39 ft (11.9 m) (soil inclusion)

Pier Diameter = 30 in. (76.2 cm)

Fig. 7.3. Wave signature recorded at 18.2 ft (5.5 m) embedded receiver in Shaft 3 (Granger site) showing reflected wave arrivals.



P_d = Direct wave arrival

P_r = Reflected wave from bottom of pier

Fig. 7.4. Signature of stress waves recorded by the vertical transducer embedded in Shaft 3 at a depth of 18.2 ft (4.8 m) showing reflections (Arias, 1977).

direct P-wave velocity of 11,970 ft/sec (3,650 m/sec) at the 18.2 ft (5.5 m) receiver, an indication that the soil inclusion defect occupying approximately 36 percent of the pier cross-sectional area did affect the travel time of the compression wave. However, the direct wave arrival in Fig. 7.3 occurs at 1.45 msec, resulting in a direct P-wave velocity of 12,550 ft/sec (3,830 m/sec). This P-wave velocity is fairly typical of average values computed for Shafts 1 and 2, and tends to contradict the findings of both Arias and Steinbach (1971).

Further examination of the wave signature shown in Fig. 7.3 reveals that an early arrival of a wave reflection does not occur as the result of the sand and gravel defect at the bottom of the pier. The reflected wave arrival denoted by R_p in Fig. 7.3 occurs at an approximate time of 4.88 msec. Using the computed direct P-wave velocity, the wave reflection off the bottom of a concrete pier 39 ft long should arrive at 4.76 msec, which is close to the actual measured time. Although no apparent wave reflection off the sand and gravel defect is discernable in Fig. 7.3, the difference in the measured and predicted wave travel times is most likely attributable to the slower P-wave velocity associated with the defect and provides a slight, but nonetheless measurable, indication of the existence of the discontinuity. In addition, by comparing ratios of direct-to-reflected wave amplitudes for this output and that recorded by the 17.9 ft (5.5 m) receiver in Shaft 1 (sound pier), a further indication of a possible defect in Shaft 3 is realized. This example illustrates the importance of performing an attenuation study in conjunction with wave travel time analyses. Both comparisons of multiple receiver output in a single pier and single receiver output with output from a pier deemed sound are valuable in assessing pier integrity.

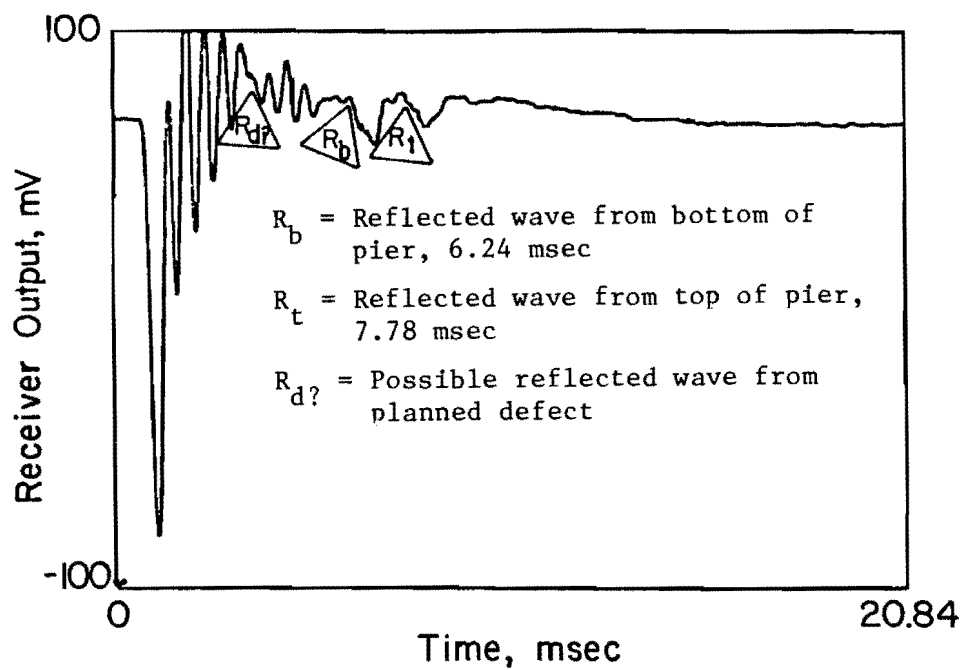
It is interesting to note that in Fig. 7.3 no reflected wave from the bag of soil implanted in this pier is visible in the wave signature at suitable times. It is understandable that reflections involving both defects are not seen, due to the strong attenuation encountered in the bottom defect. However, it was felt that the stress wave path of defect-to-top-of-pier-to-receiver would yield sufficient wave energy to register at the receiver. The bag of soil seems to either attenuate the wave energy prior to arrival of the reflected wave or to reflect little energy.

TIME DOMAIN MEASUREMENTS AT HOUSTON SITE

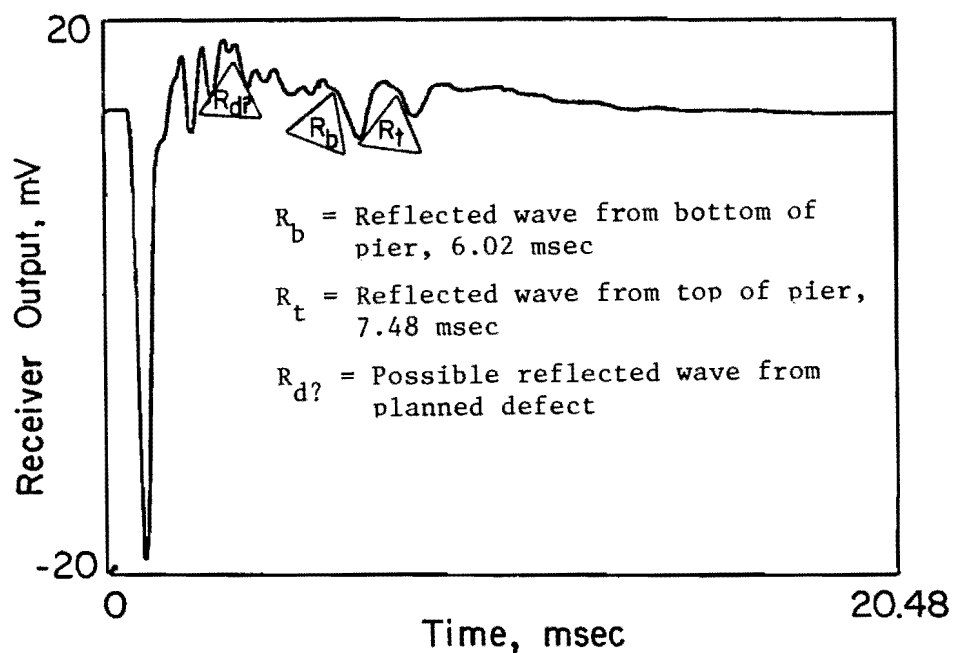
As mentioned previously, three of the four piers at the Houston site possess soil inclusions of varying cross-sectional area. Wave propagation tests were performed on the test piers to evaluate further the defect detection capabilities of the WAPER and WAPS methods, particularly concentrating on the influence of cross-sectional areas of the defects. Results and interpretations of the findings are presented in the following sections.

Shaft B

WAPER Method. Wave signatures from wave propagation with embedded receivers conducted on Shaft B are shown in Fig. 7.5. For review, Shaft B contained a planned soil inclusion at a depth of 32 to 33 ft (9.8 to 10.1 m) below the top of the pier. The defect consisted of a burlap bag filled with soil and positioned in the pier by attachment to the reinforcing cage with bailing wire. The output shown in Fig. 7.5 is wave excitation monitored by the 10 ft (3.1 m) embedded velocity transducer. The wave signature shown in Fig. 7.5(a) was generated with a 15 lb (6.8 kg) drop hammer, while the



a. Drop hammer on concrete.



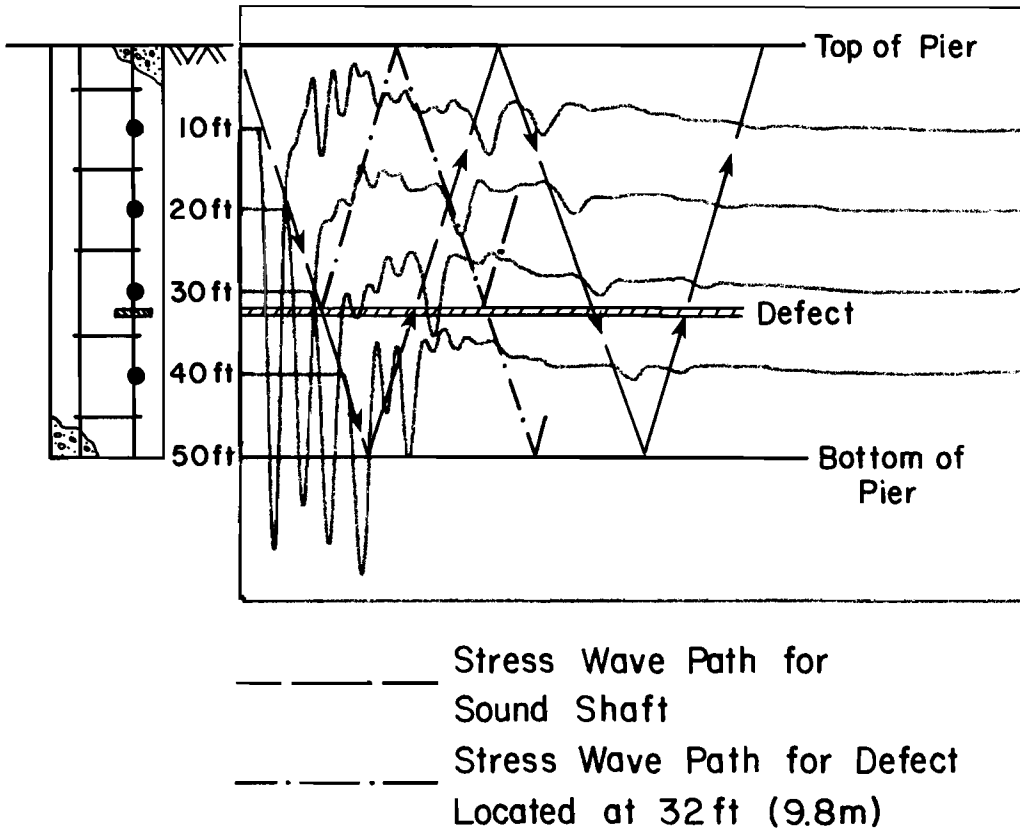
b. Hand sledge on embedded nail.

Fig. 7.5. Wave signatures for 10 ft (3.1 m) embedded velocity transducer in Shaft B (Houston site).

signature shown in Fig. 7.5(b) was produced using the 5 lb (2.3 kg) hand sledge/embedded nail source.

A review of both figures reveals that reflections off both the bottom and top of the pier are clearly visible in the recorded output, a reasonable indication that no large defects are present in the pier. No early wave arrivals resulting from the defect are clearly visible in these or any of the other records, further substantiating the erroneous conclusion that the pier is sound. The direct wave arrival in Fig. 7.5(a) occurs at 0.74 msec, resulting in a direct P-wave velocity of 13,510 ft/sec (4,120 m/sec). Using this P-wave velocity and the 54 ft (16.5 m) total travel distance of the reflected compression wave, the reflected wave arrival off the planned defect should occur at approximately 4.0 msec. Changes in wave excitation are visible in the wave signatures in the proximity of this time, denoted by R_d in Fig. 7.5. However, reflected wave energy is of such a small magnitude that the defect would most likely go undetected in an assessment of single receiver output.

In Chapter 6, a method of presenting wave signatures was discussed whereby reflected wave arrivals may be more clearly visible in the recorded output. The method requires the use of a digital oscilloscope capable of waveform superposition and recording multiple embedded receivers. By positioning the recorded waveforms in increments on the record corresponding to the embedded receiver configuration, the stress wave records can be more easily assessed for early reflections. The record in Fig. 7.6 illustrates this data presentation technique. In this figure, output recorded at the 10-, 20-, 30-, and 40-ft (3.1-, 6.1-, 9.1-, and 12.2-m) velocity transducers embedded in Shaft B have been plotted. For illustrative purposes, the drilled pier with embedded receivers and planned defect has been drawn to correlate



Pier Length = 50 ft (15.2 m)

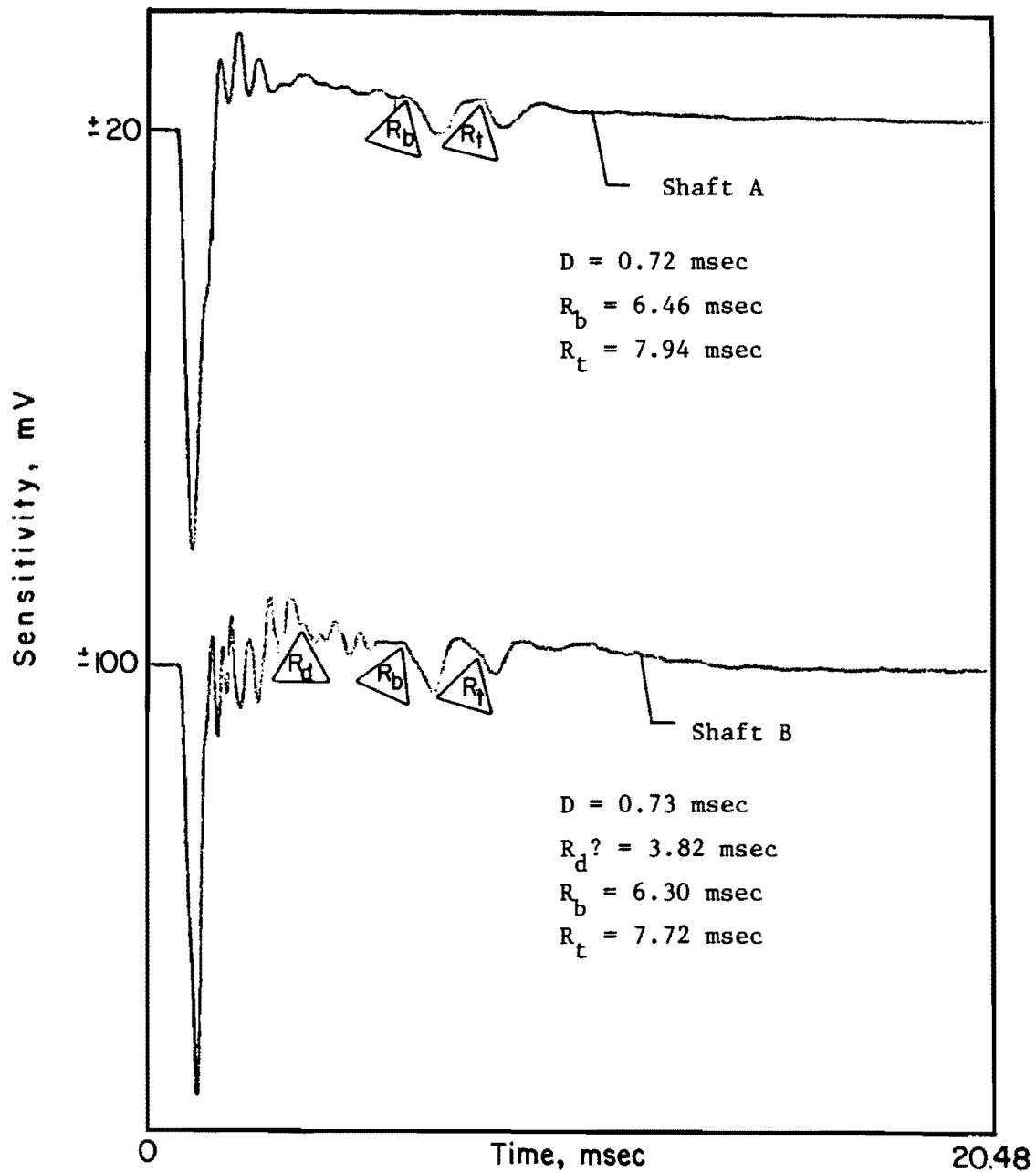
Pier Diameter = 32 in. (81.3 cm)

Fig 7.6. Wave signatures for WAPER method test showing wave reflections in Shaft B (Houston site) constructed with 1/4 cross-sectional area soil inclusion defect.

with the positioning of the corresponding receivers. The paths for wave reflections off both the top and bottom of the pier (denoted by the dashed lines) are easily traced, indicating a pier of sound integrity. However, a closer examination of the recorded output reveals a general trend of reflected wave energy corresponding to the stress wave path of reflections off the defect (denoted by the dotted and dashed lines). This method of data presentation provides a better means of identifying wave arrivals in receiver output that may go unrecognized if only a single receiver is used.

For comparison purposes, wave excitation recorded at the 10 ft (3.0 m) embedded velocity transducer in Shaft B has been plotted in Fig. 7.7 along with output recorded at the 10 ft (3.0 m) embedded receiver in Shaft A. Wave arrivals of the piers are nearly identical in the wave signatures. With regard to early reflected wave arrivals, a noticeable difference in wave excitation is visible around 4.0 msec in the wave signature for Shaft B, the arrival time computed for the reflected wave from the 1/4 cross-sectional-area defect. However, this wave excitation is not clearly defined and would most likely go undetected under normal evaluation circumstances. Still, the visual differences in the wave signatures presented in this figure illustrates the value of comparing recorded output of piers suspected of being defective on a given project with those deemed sound.

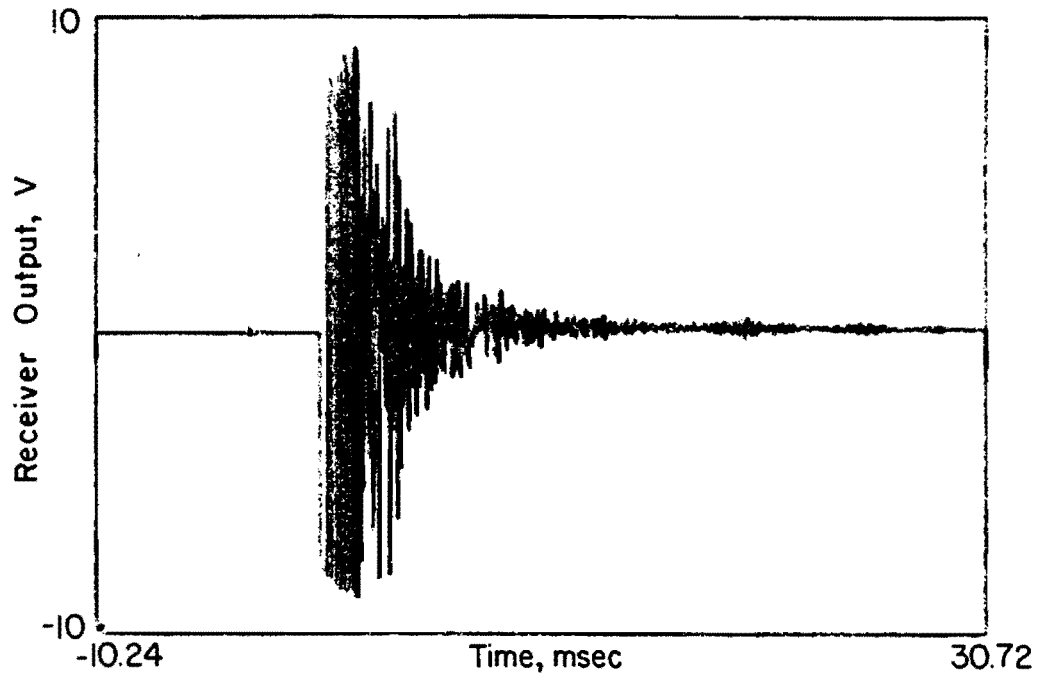
WAPS Method. WAPS tests were also conducted on Shaft B to assess the ability of a surface receiver to detect effectively drilled pier discontinuities. The unfiltered and filtered wave signatures recorded for one such test are shown in Fig. 7.8. A 15 lb (6.8 kg) drop hammer was used as the source, and an accelerometer was used as the surface receiver to capture the resulting wave excitation.



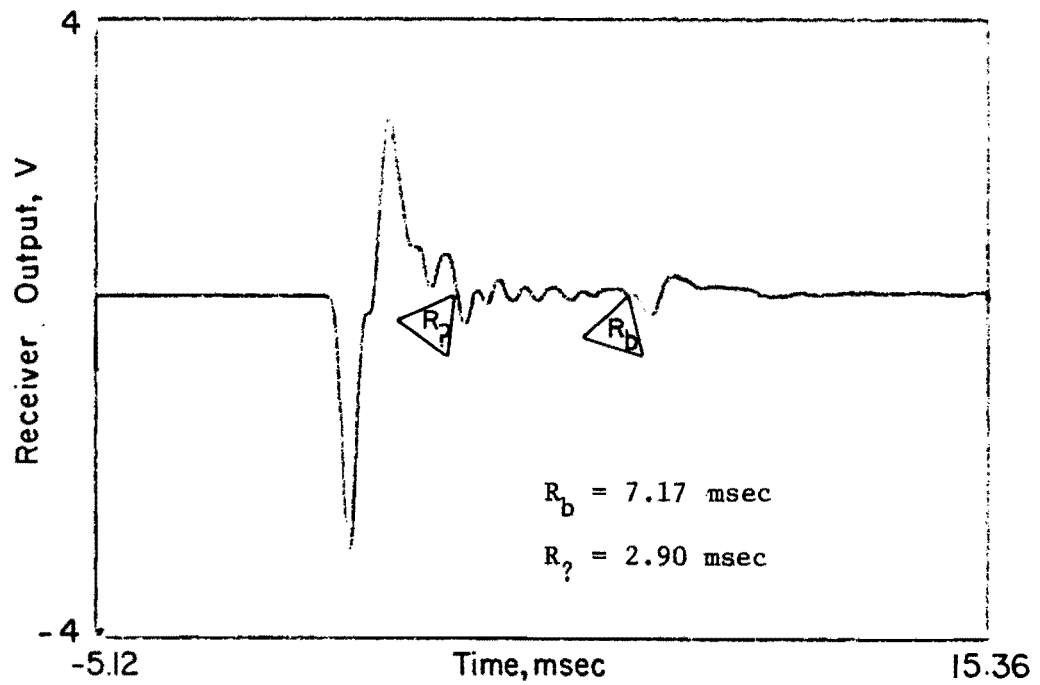
R_b = Reflected wave off bottom of pier
 R_t = Reflected wave off top of pier
 $R_d?$ = Possible reflected wave from defect

Receiver Elevation = 10 ft (3.0 m) (both records)
 Pier length = 50 ft (15.2 m)
 Pier Diameter = 32 in (81.3 cm)

Fig. 7.7. Comparison of reflection records from 10 ft (3.0 m) velocity transducers in Shafts A and B (Houston site).



a. Unfiltered



b. Filtered at 1.8 kHz low pass

Fig. 7.8. WAPS test on Shaft B (Houston site) using drop hammer source and accelerometer surface receiver.

An examination of Fig. 7.8 reveals that no reflected wave arrivals are discernable in the unfiltered output due to the source-induced surface waves which tend to complicate the wave signature. Use of a filter greatly enhances the recorded signal by eliminating the undesirable surface wave excitation, as illustrated in Fig. 7.8(b). The lower waveform was recorded using a 1.8-kHz low-pass filter. The mid-signal trigger feature of the digital oscilloscope was utilized for this trace. As mentioned previously, this feature is extremely valuable when evaluating filtered output, due to the affects of filtering on time domain measurements.

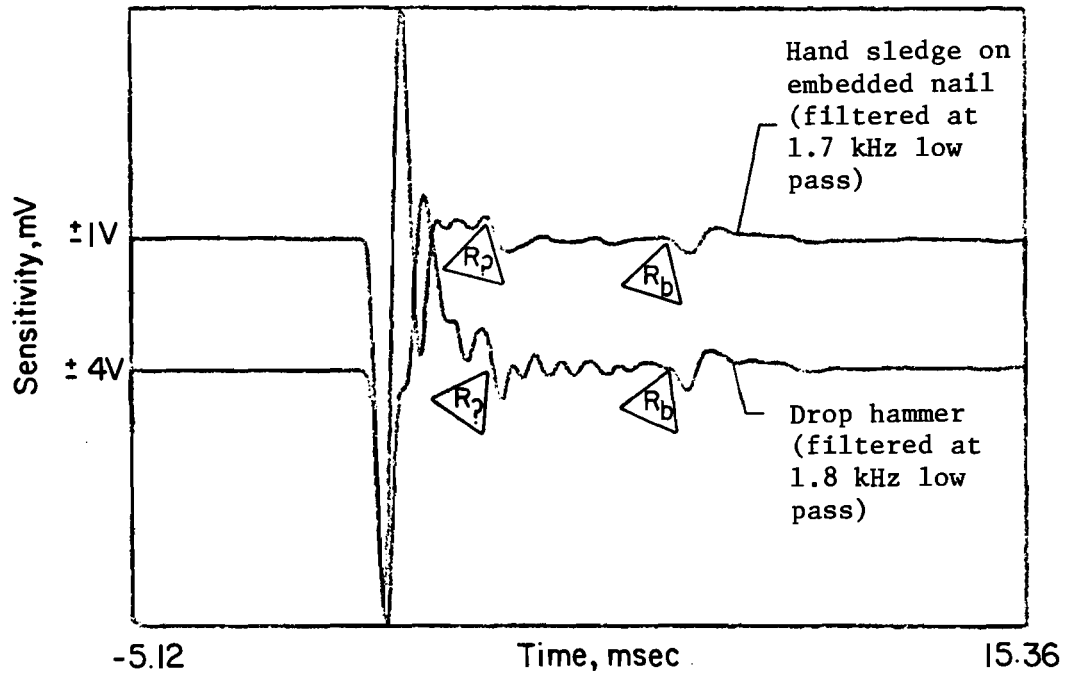
The filtering process effectively eliminated a majority of the surface wave "noise" in the wave signature, allowing identification of a reflected wave, denoted by R_b in the filtered trace. The reflected wave arrival occurs at approximately 7.17 msec in the filtered record, the arrival time representing the 2L travel time of the compression wave. Using an average P-wave velocity of 13,800 ft/sec (4,210 m/sec), which accounts for the increase in P-wave velocity with depth within the pier, a 2L travel distance of 99 ft (30.2 m) is obtained. This travel distance corresponds to a pier length of 49.5 ft (15.1 m), comparing favorably with the actual pier length. As noted before, small differences in actual and computed pier length can be attributable to the inaccuracy in determining exact reflected wave arrivals and to the effects of filtering.

Unfortunately, no early reflected wave arrivals resulting from the 1/4 cross-sectional area defect present in Shaft B are clearly visible in the filtered trace of Fig. 7.8. Again using an average P-wave velocity of 13,800 ft/sec (4,210 m/sec), a reflected wave from the 32 ft (9.8 m) defect should arrive at the surface receiver at an approximate time of 4.64 msec. No reflected wave arrival is clearly visible at the computed time, although a

distinct oscillation (denoted by R_7) does occur in the wave signature at approximately 2.9 msec. Using Eq. 3.6 and an initial arrival time of zero for the surface receiver configuration, this travel time corresponds to a pier reflection boundary of 20 ft (6.1 m). Since a velocity transducer and two piezoelectric ceramic transducers were the only instruments positioned at this depth in Shaft B, and because no corresponding excursions were visible in the previously shown WAPER records, an explanation for the early oscillation in the filtered output of Fig. 7.8 is not readily apparent.

To verify that the absence of the anticipated early reflected wave arrival in the wave signature was not source dependent, various sources were used in the WAPS testing of Shaft B. Receiver output from one such test, using the 5 lb (2.3 kg) hand-sledge-and-embedded-nail source, is presented for comparison with the receiver output associated with the drop hammer source in Fig. 7.9. Again, the reflected wave from the bottom of the pier is easily identified in the record using the hand sledge/embedded nail source, but no reflected wave arrival from the planned defect is readily distinguishable in the waveform. It is interesting to note that the inexplicable oscillation (R_7) is again identifiable in the record with the hand sledge/embedded nail source.

Based on the WAPER and WAPS test records presented in Figs. 7.5 through 7.9, it is concluded that wave energy reflected from the defect is low in magnitude and effectively attenuated prior to its arrival at the surface receiver, or, more likely, that the 1/4 cross-sectional area defect is of such small magnitude that it presents no distinguishable boundary for the reflection of wave energy. Because the reflected waves from the bottom of the pier are clearly visible in all receiver output, Shaft B would most likely be erroneously deemed sound under normal testing circumstances.



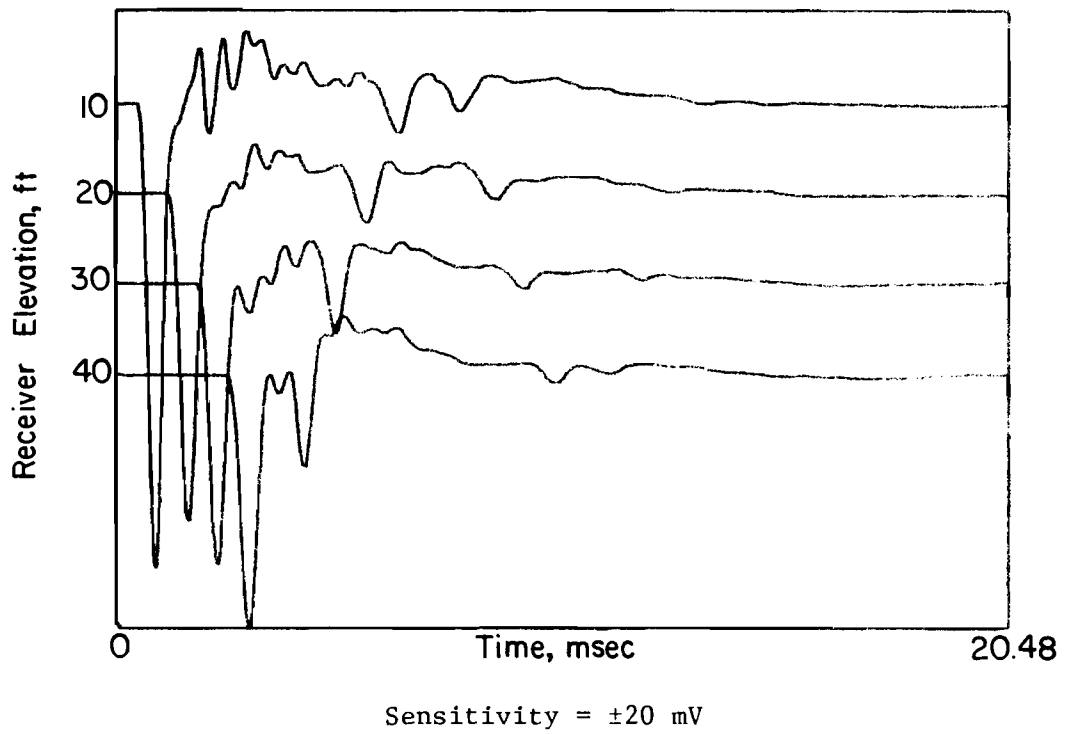
R_b = Reflected wave from bottom of pier, 7.18 msec
 Pier length = 50 ft (15.2 m)
 Pier Diameter = 32 in (81.3 cm)

Fig. 7.9. Comparison of drop hammer and hand sledge/embedded nail sources for WAPS tests conducted on Shaft B (Houston site).

Attenuation. As discussed in Chapter 6, wave energy dissipates as the P-wave propagates through a sound pier. The degree of attenuation is dependent upon the properties of the concrete, surrounding soil, and reflection boundaries. The presence of one or more defects in a pier acts as additional reflection boundaries, increasing wave attenuation.

Using the same setup as described for measurements on Shaft A, an attenuation study was performed of waves propagating in Shaft B. Multiple embedded receivers were monitored with two oscilloscopes connected in series shown in Fig. 4.2. The output shown in Fig. 7.10 is the same as that previously analyzed for reflected wave arrivals (Fig. 7.6). Examination of the direct and reflected wave amplitudes reveals that the P-wave attenuates fairly rapidly. This is graphically illustrated in Fig. 7.11, where the direct and reflected wave amplitudes have been plotted for the respective receivers. Receiver output for Shaft A (sound pier) has also been provided in the figure for comparison purposes.

Because the plotted data are for different piers and, therefore, were the result of differing impulses, only the slopes of the lines are of importance. It can be seen that the general slopes of the lines are quite similar from the 10 ft (3.0 m) to the 30 ft (9.1 m) receivers. At this point, the data contradicts what is expected to happen. Due to the overlying planned defect, the wave amplitude should be slightly attenuated in the 40 ft (12.2 m) receiver in Shaft B compared to that recorded in Shaft A. However, as shown in Fig. 7.11, the output recorded at this receiver is greater in Shaft B than in Shaft A. Upon reflection of the P-wave at the concrete-soil interface at the bottom of the pier, the wave energy in Shaft B attenuates at a slightly faster rate than the wave energy in Shaft A, as expected, until the two gradually became equivalent at low output levels.



Pier Length = 50 ft (15.2 cm)

Pier Diameter = 32 in (81.3 cm)

Fig. 7.10. Attenuation study of multiple receiver output from WAPER test conducted on Shaft B (Houston site).

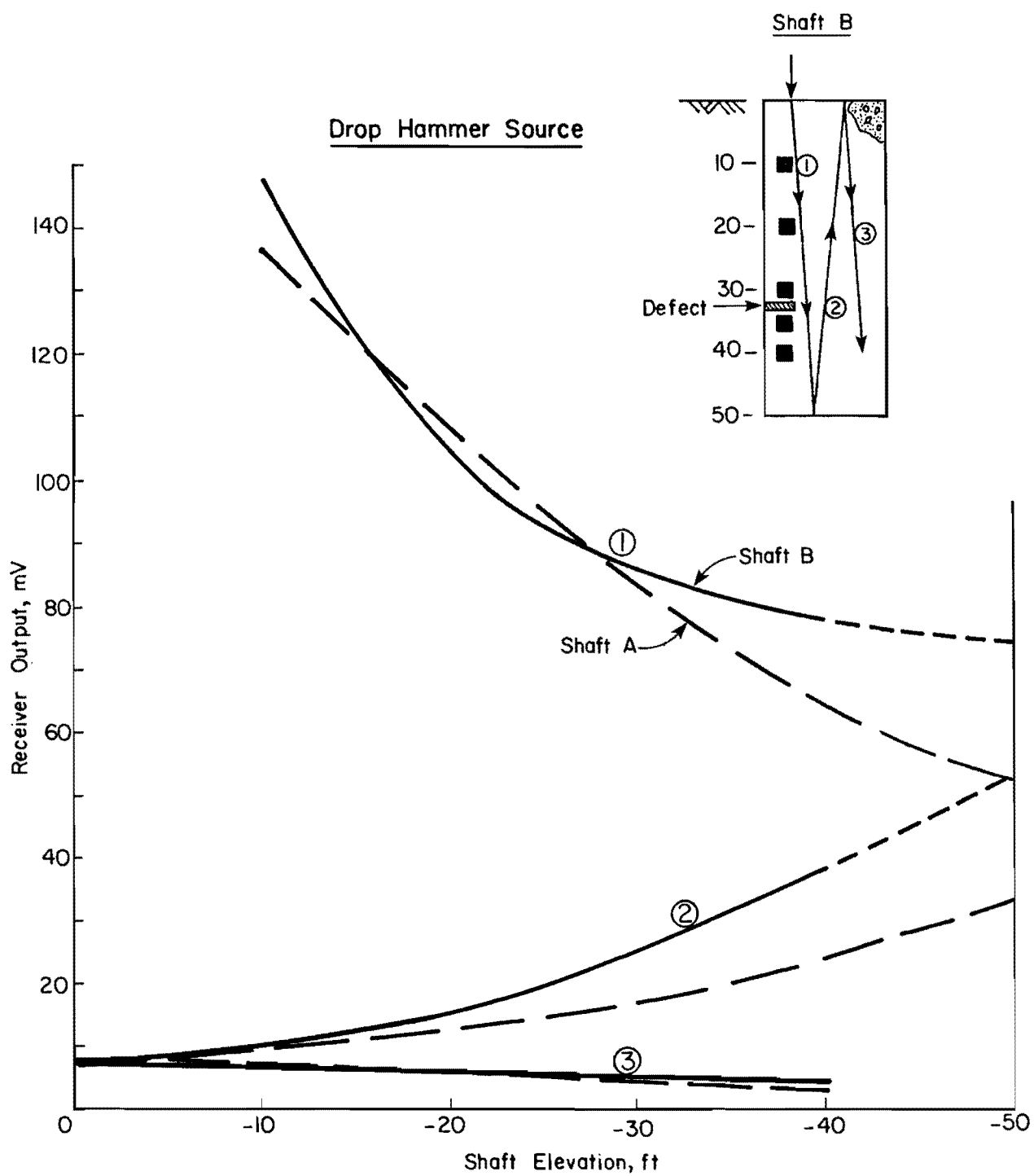


Fig. 7.11. Attenuation of P-wave in Shaft B (Houston site).

To determine if the results shown in Fig. 7.11 were repeatable and not dependent upon some indirect component such as type of source, additional tests were performed utilizing the hand sledge/embedded nail source configuration. The results of the wave amplitude attenuation study using this source are plotted in Fig. 7.12. Although the magnitude of wave output differs between the two figures, wave attenuation is very similar, tending to dispel the notion of source induced effects on wave attenuation. A possible explanation for this phenomenon may lie in the defect itself. It is possible that the small magnitude of the defect and its location in relation to the monitored receiver affects the amplitude of the receiver output. Further research is warranted regarding wave attenuation to investigate this observation.

As in Chapter 6, the data presented in Figs. 7.11 and 7.12 have been normalized with respect to the 10 ft (3.0 m) receiver for comparison purposes. The normalized output is tabulated in Table 7.1. Again, the output for the two sources compares favorably, indicating no apparent source induced attenuation phenomenon affecting the dissipation of wave energy. Furthermore, receiver output decreases continuously as the P-wave propagates up and down the pier, an indication of no appreciable pier discontinuity. As will be shown for Shafts C and D, waves reflected from both the pier top and bottom and any discontinuity present in the pier coincide at times as they propagate up and down the shaft, with the summation of the overlapping tensile and compressive wave energy reflected as greater output at receivers located at any points of coincidence.

The normalized receiver output for the direct P-wave arrival tabulated in Table 7.1 has been graphically presented in Fig. 7.13. The normalized direct P-wave output for Shaft A (sound pier) plotted in Fig. 6.24 has been

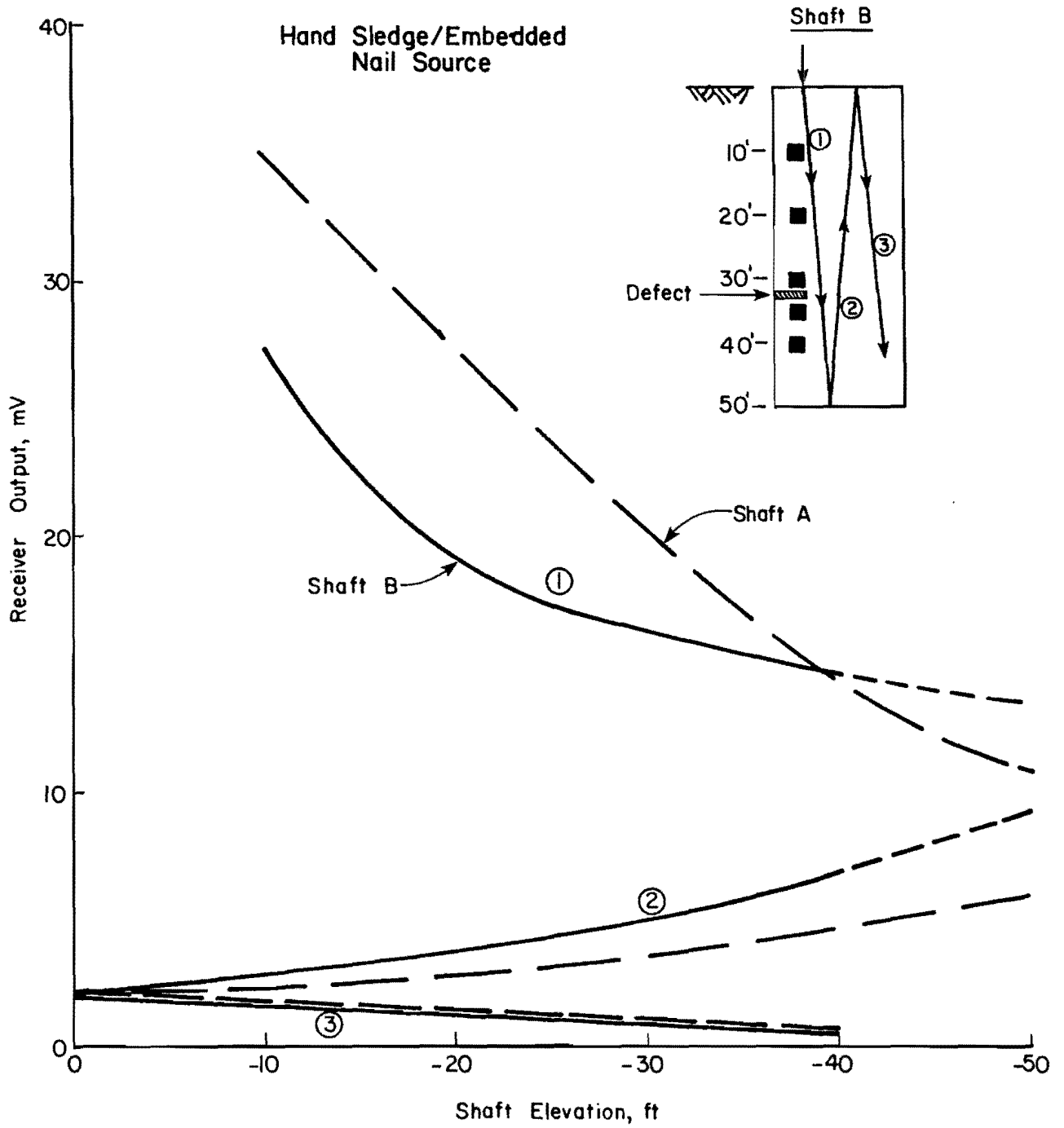


Fig. 7.12. Attenuation of P-wave in Shaft B (Houston site).

Table 7.1. SOURCE COMPARISON OF WAVE ATTENUATION
IN SHAFT B (HOUSTON SITE).

	<u>RECEIVER</u>	<u>CHANGE IN OUTPUT, PERCENT</u> <u>(NORMALIZED TO 10 ft (3.0 m) RECEIVER)</u>	
		<u>DROP HAMMER</u>	<u>HAND SLEDGE</u>
①	20	70.6	69.3
	30	57.8	59.6
	40	52.7	53.7
②	40	27.1	29.8
	30	19.2	18.6
	20	9.5	13.0
	10	7.0	9.6
③	10	3.5	5.9
	20	3.4	5.2
	30	3.2	3.2
	40	2.7	2.3

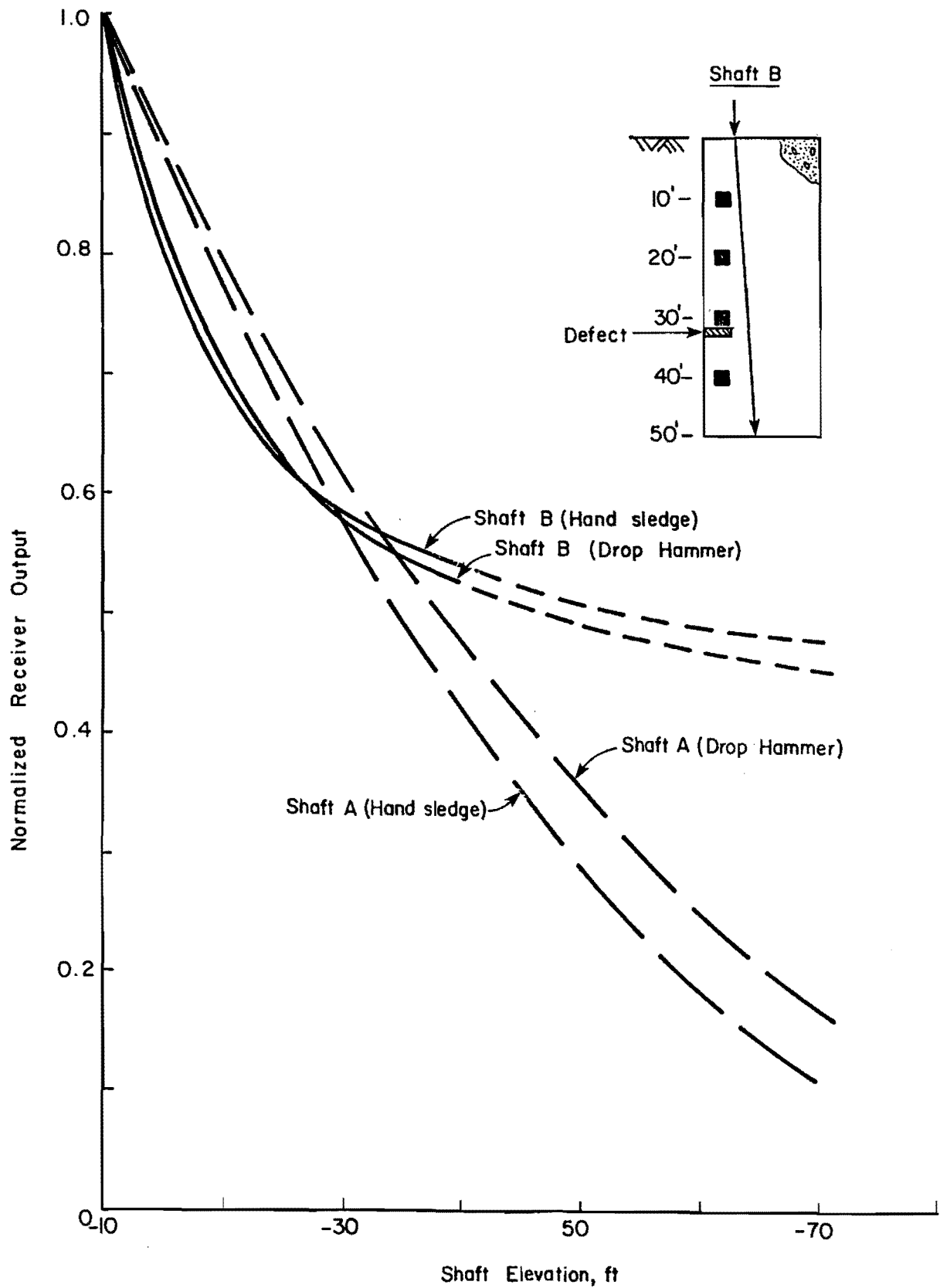
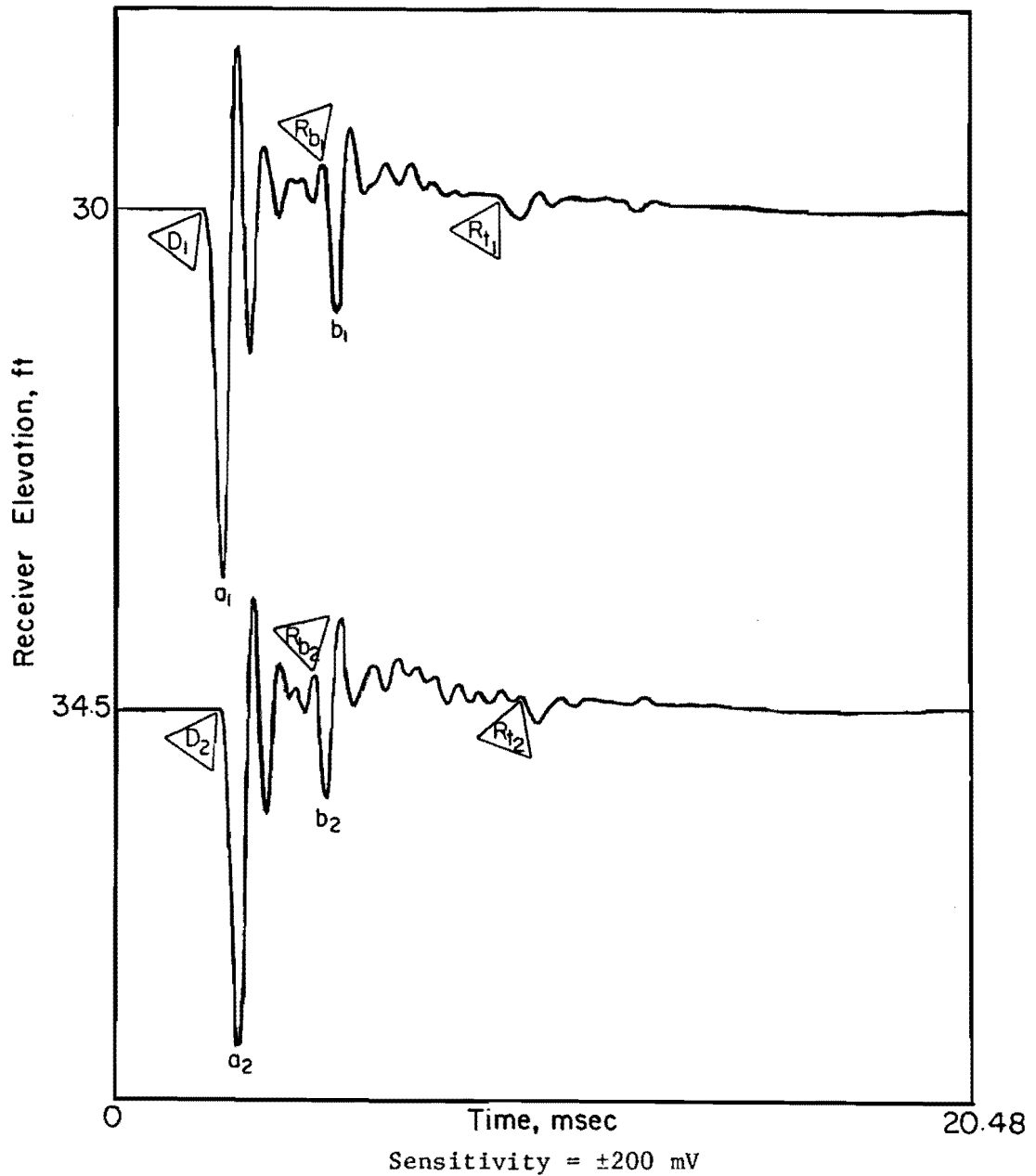


Fig. 7.13. Normalized attenuation of direct P-wave in Shaft B (Houston site).

included in Fig. 7.13 for comparison purposes. A review of Fig. 7.13 reveals that P-wave energy attenuates at a slightly faster rate in the upper 30 ft (9.1 m) of Shaft B when compared to Shaft A. Below this depth, the reverse is true. The difference in wave attenuation in the upper regions of the piers is not readily apparent, although it is thought that the difference may be attributable to differences in embedment surroundings. Shaft B is positioned between Shafts A and C, with a close center-to-center spacing of $2D$, whereas wave propagation in Shaft A is influenced by only one adjacent pier. However, due to the increased amount of concrete adjacent to Shaft B, it would appear that wave attenuation in Shaft B might be less than attenuation in Shaft A, which is not the case. Irregardless, the attenuation curves presented in Fig. 7.13 differ significantly, signaling the possible presence of irregularities in Shaft B, although no conclusion can be clearly drawn from the tabulated or plotted data.

In an attempt to obtain additional wave propagation data concerning the effect of defect cross-sectional area on wave attenuation, additional velocity transducers were positioned in the vicinity of the planned defect. As illustrated in Fig. 5.7, one receiver was positioned just below the planned defect at a depth of 34.5 ft (10.5 m), while two additional receivers were positioned opposite the defect at 30 ft (9.1 m) and 34.5 ft (10.5 m).

A comparison of the wave signatures recorded at the receivers directly above [30 ft (9.1 m) transducer] and below [34.5 ft (10.5 m) transducer] the planned $1/4$ cross-sectional area soil inclusion is provided in Fig. 7.14. The 15 lb (6.8 kg) drop hammer source was used to generate the P-wave energy recorded in these signatures. A comparison of the direct P-wave velocities for the two records reveals that the velocity is slightly reduced by the intermittent defect, decreasing from a value of 13,890 ft/sec (4,230 m/sec)



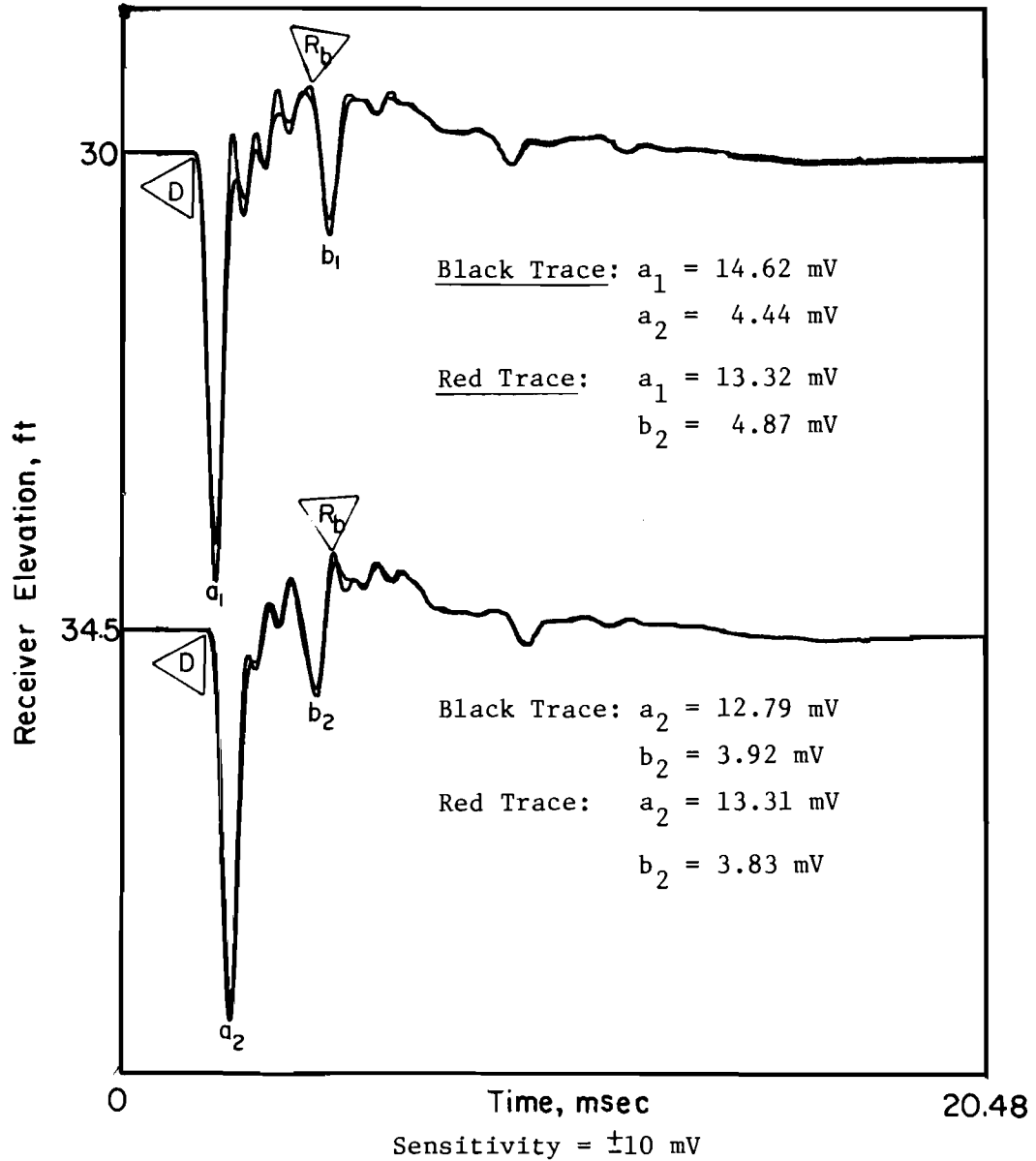
- D_1 = Direct wave arrival at 30 ft (9.1 m) receiver, 2.16 msec
 D_2 = Direct wave arrival at 34.5 ft (10.5 m) receiver, 2.50 msec
 R_{b1} = Reflected wave from bottom of pier to 30 ft (9.1 m) receiver, 5.04 msec
 R_{b2} = Reflected wave from bottom of pier to 34.5 ft (10.5 m) receiver, 4.74 msec
 R_{t1} = Reflected wave from top of pier to 30 ft (9.1 m) receiver, 9.31 msec
 R_{t2} = Reflected wave from top of pier to 34.5 ft (10.5 m) receiver, 9.74 msec
 Pier Length = 50 ft (15.2 m)
 Pier Diameter = 32 in (81.3 cm)

Fig. 7.14. Comparison of wave signatures for 30 ft (9.1 m) and 34.5 ft (10.5 m) velocity transducers directly overlying and underlying defect in Shaft B (Houston site).

at the 30 ft (9.1 m) receiver to 13,800 ft/sec (1,210 m/sec) at the 34.5 ft (10.5 m) receiver. Assuming a P-wave velocity of 5000 ft/sec (1,520 m/sec) (saturated condition) in the 1 ft (0.3 m) thick soil inclusion defect, it can be shown that the defect results in the reduction in direct P-wave velocity. However, the reduction in P-wave velocity is so small that it would likely go unnoticed or be deemed insignificant under normal circumstances.

With regard to wave attenuation, the direct wave amplitudes measured by the 30 ft (9.1 m) and 34.5 ft (10.5 m) receivers in Fig. 7.14 are 130.6 and 117.4 mV, respectively. The direct P-wave arrivals are selected for comparison due to their ease of interpretation and, consequently, reliability. The ratio of amplitudes between these two receivers is 89.9 percent, which compares favorably with ratios computed using values obtained for the appropriate receivers in Fig. 7.11, giving no clear indication of the planned defect located between the receivers. Furthermore, wave reflections from the bottom of the pier are clearly identifiable in the receiver output, further substantiating the absence of significant discontinuities in the pier.

Similar results were obtained for the receiver output presented in Fig. 7.15. In this figure, receiver output from the 30 ft (9.1 m) and 34.5 ft (10.5 m) velocity transducers located above and below and opposite the planned defect in Shaft B are shown. To obtain comparable output, the equipment set-up shown in Fig. 4.2 was utilized for recording purposes. A single impulse of the 5 lb (2.3 kg) hand sledge was used to generate all four signatures in Fig. 7.15. As before, only a slight indication of the planned defect is afforded in an assessment of the direct P-wave velocities. As expected, the direct P-wave velocities for the two 30 ft (9.1 m) receivers and the 34.5 ft (10.5 m) receiver opposite the defect are very similar,



D = Direct wave arrival

R_b = Reflected wave from bottom of pier

Pier Length = 50 ft (15.2 m)

Pier Diameter = 32 in (81.3 cm)

Black Traces: Receivers located directly above and below
planned defect

Red Traces: Receivers located opposite the planned defect

Fig. 7.15. Comparison of output for 30 ft (9.1 m) and 34.5 ft (10.5 m) velocity transducer receivers located above and below and opposite the planned defect in Shaft B (Houston site).

averaging 13,910 ft/sec (4,210 m/sec), whereas the velocity for the 34.5 ft (10.5 m) receiver located directly below the defect is a slightly slower 13,750 ft/sec (4,190 m/sec). Again, the reduction in direct P-wave velocity resulting from the planned defect is of such small magnitude that the defect would most likely go undetected under normal testing conditions.

With regard to wave attenuation in the signatures shown in Fig. 7.15, the direct wave amplitude ratio for the receivers located directly above and below the planned defect is 87.5 percent, again comparing favorably with the data in Fig. 7.11. In comparing the two 30 ft (9.1 m) receivers, the direct wave amplitude of the receiver located directly above the defect was approximately 9 percent greater than the amplitude of the corresponding receiver opposite the defect. This difference is most likely attributable to the close proximity of the overhead receiver to the defect and wave reflection off the defect. As discussed in Chapter 3, a compression wave is reflected from a pier discontinuity as a tension wave. Due to the proximity of the overhead receiver and defect, the velocity transducer is still undergoing its initial downward excursion resulting from the direct P-wave as the tension wave is reflected from the defect to the receiver. By coupling the "pushing" and "pulling" actions of the P-wave, a greater downward excursion of the direct wave arrival results. Although the small difference in direct wave amplitudes for the 30 ft (9.1 m) receivers may be an indication of defect magnitude, it is possible that the receiver opposite the defect was affected to some degree by the reflected wave energy from the defect.

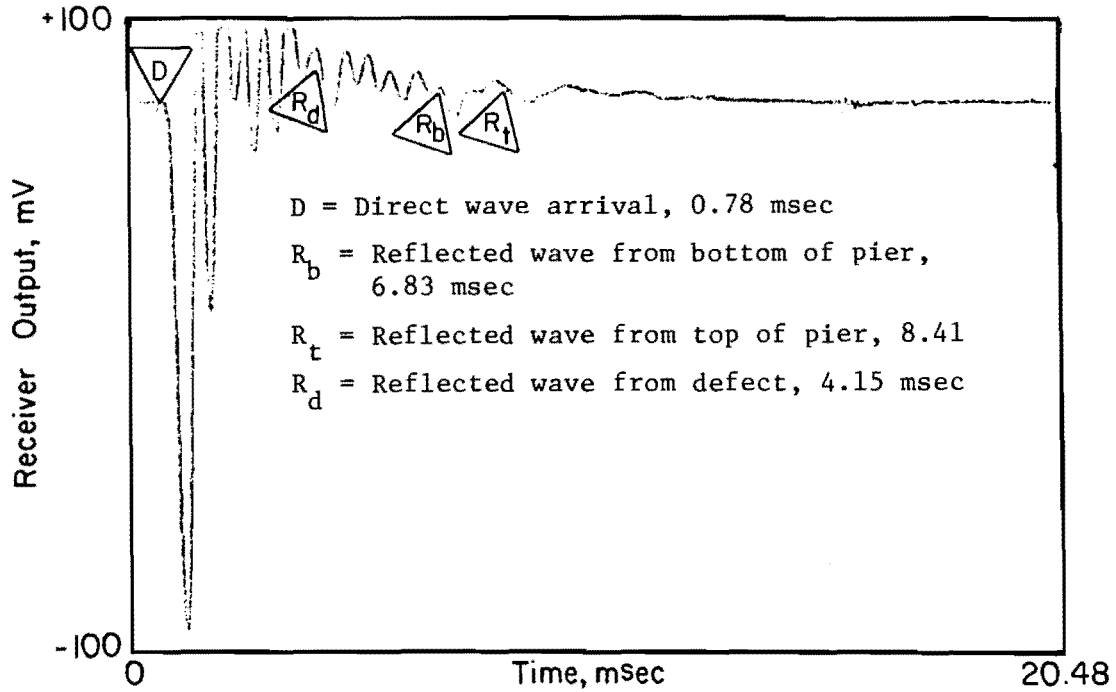
No significant conclusions concerning the planned defect are provided by the small difference in the direct wave amplitudes of the 34.5 ft (10.5 m) receivers.

Shaft C.

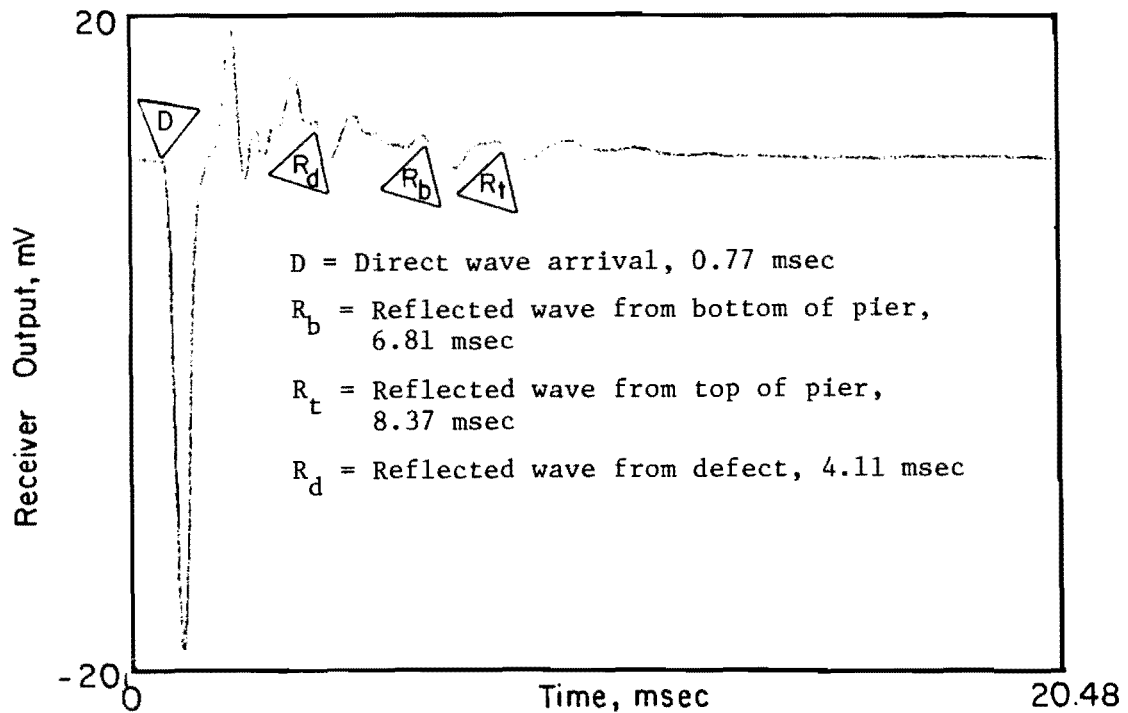
WAPER Method. Typical wave signatures for WAPER tests conducted on Shaft C are shown in Fig. 7.16. Shaft C has a simulated soil inclusion consisting of burlap bags filled with soil and attached to the reinforcing cage at a depth of 32 ft (9.8 m) below the top of the pier. A sufficient number of bags were attached to the reinforcing cage to construct a defect occupying approximately 1/2 of the cross-sectional area of the pier. The wave signatures shown in Fig. 7.16 were recorded at the 10 ft (3.0 m) velocity transducer and were generated by a drop hammer source, Fig. 7.16(a), and a hand sledge and embedded nail source, Fig. 7.16(b).

The direct wave arrival times for the signatures occur at 0.77 and 0.78 msec, resulting in P-wave velocities of 12,990 and 12,820 ft/sec (3960 and 3910 m/sec), respectively. Using an average value of 12,900 ft/sec (3930 m/sec) for the P-wave velocity and Eq. 3.6 to assess the early reflected wave arrivals in the signatures (denoted by R_d), a reflection boundary of some type would be estimated to exist at a depth of 31.5 to 31.8 ft (9.6 to 9.7 m) below the top of the pier. This location compares extremely well with the actual depth of 32 ft (9.8 m) of the planned defect. Similar computations indicate that the second pair of wave arrivals visible in the signatures are the P-wave reflections off the bottom and top of the pier, denoted by R_b and R_t , respectively.

Several important points are illustrated in Fig. 7.16. First, the reflected wave arrivals off of the 1/2 cross-sectional area defect are easily recognizable in the single wave signatures. This was not true for the defect of 1/4 cross-sectional area in Shaft B, where multiple receiver output was required to "identify" the planned defect. Secondly, the amplitudes of the reflected stress waves off the bottom and top of the pier are visibly smaller



a. Drop hammer on concrete



b. Hand sledge on embedded nail

Fig. 7.16. Wave signatures for 10 ft (3.0 m) embedded velocity transducer in Shaft C (Houston site).

than those reported in Shaft A, indicating the possibility of a defect in the drilled pier causing a certain amount of attenuation of the P-wave. If wave attenuation is great or if the piers are very long, waveform expansion and signal amplification may be necessary to allow identification of wave arrivals to reach conclusions concerning the characteristics of the possible defect. Wave attenuation in Shaft C will be discussed later in this chapter. Finally, although both wave signatures clearly show reflected waves from both the pier bottom and top and the planned defect, the hand sledge/embedded nail record is again found to be superior in waveform clarity.

Wave propagation output recorded by the string of velocity transducers has been prepared for optimum analysis of the time domain measurements in Fig. 7.17. In the figure, the reflected wave arrivals off the top and bottom of the pier are visible, but the wave amplitudes are somewhat low and erratic, two good indicators of possible pier defects. Furthermore, reflections off the planned defect are visible only for a short period of time after encountering the defect, suggesting that the defect is of sufficient magnitude to attenuate appreciably any wave energy passing it.

Further evidence of the effects of the 1/2 cross-sectional area defect on wave propagation measurements is illustrated in Fig. 7.18. In this figure, a comparison is made of records from the 10 ft (3.1 m) embedded velocity transducers in Shaft A (sound pier) and Shaft C. Besides the obvious fact that the piers are different (sound compared with defective), the differences in direct and reflected wave arrival times in the wave signatures are predominantly the result of different testing dates and the accompanying increase in concrete stiffness and, consequently, increase in P-wave velocity which occurred during the time interval between tests. The longer travel times of the reflected waves in Shaft C could also be due in

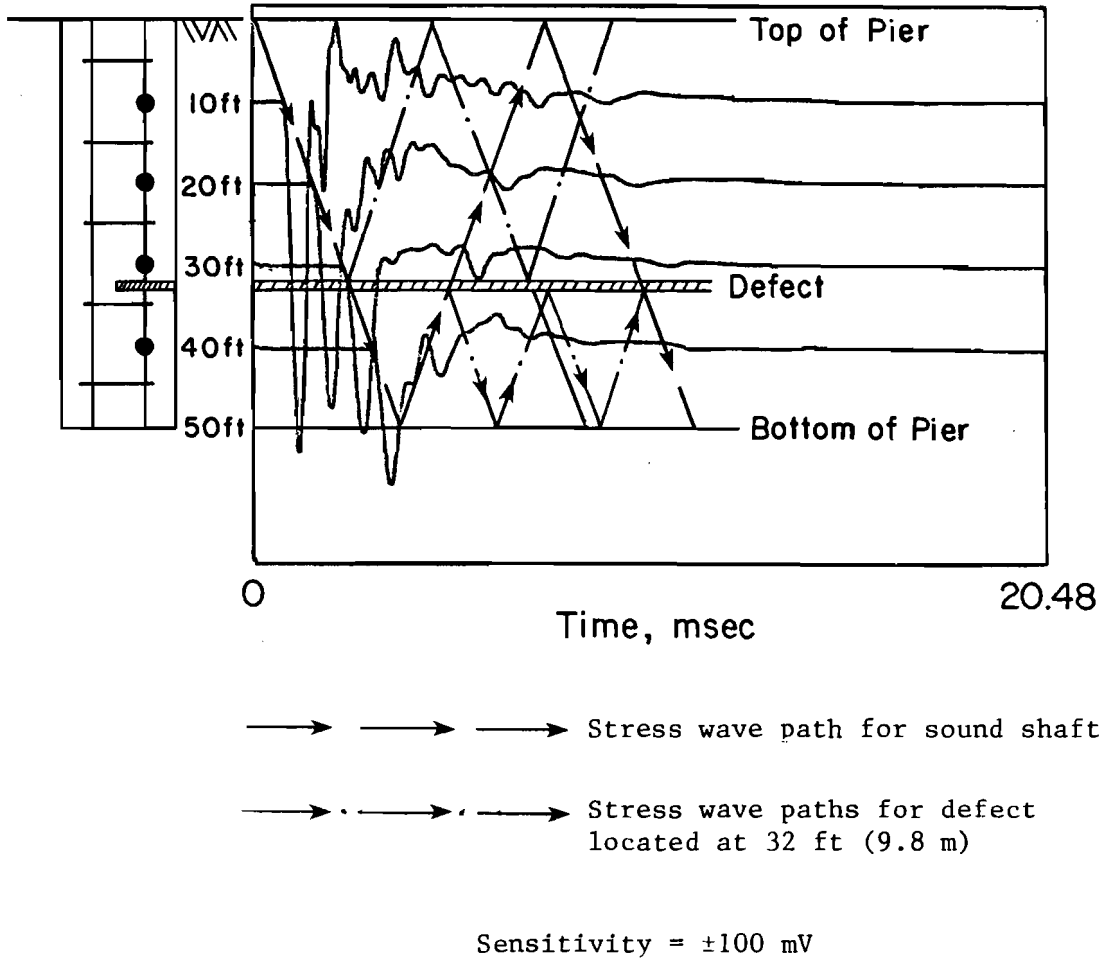
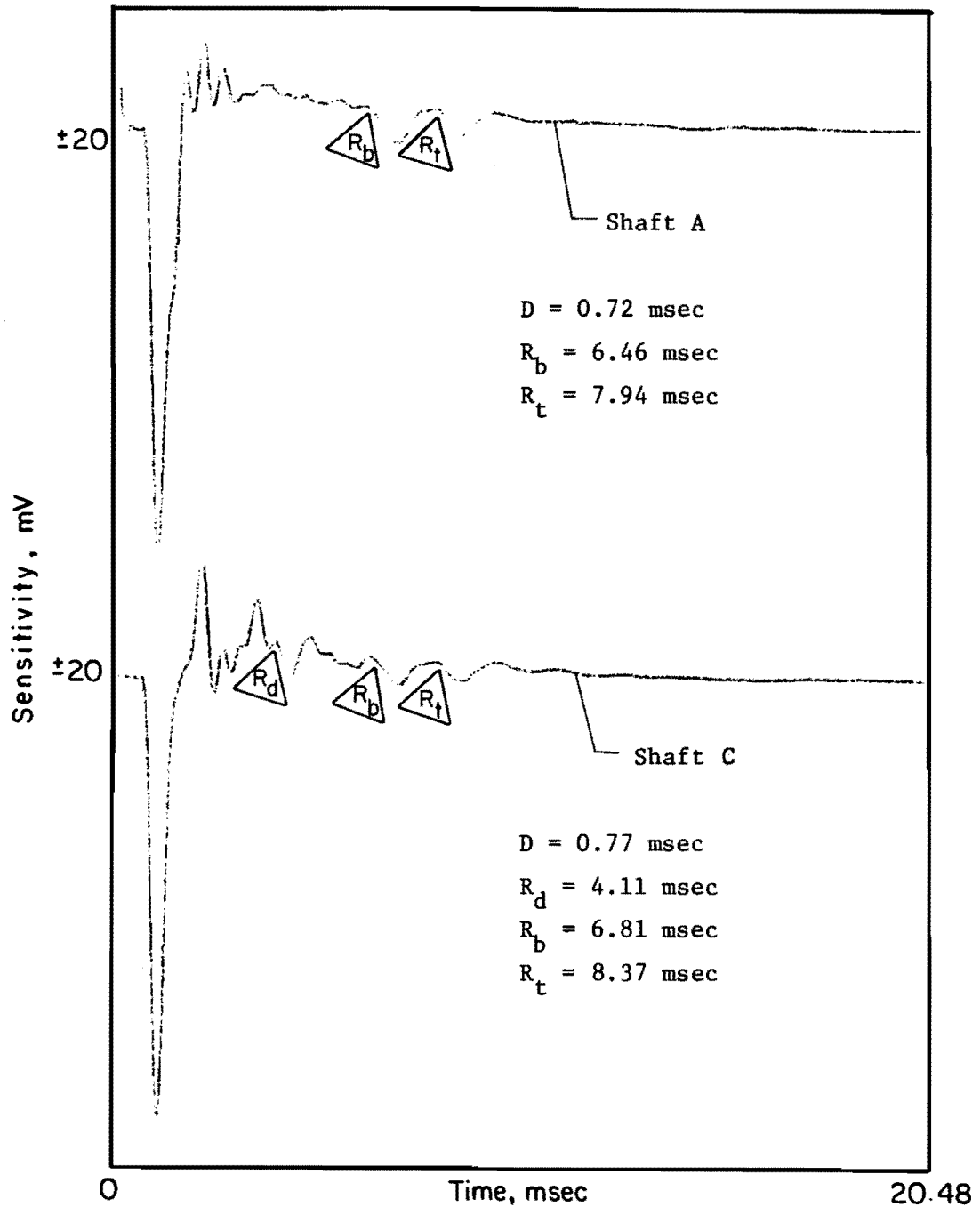


Fig. 7.17. Wave signatures for WAPER test showing wave reflections in Shaft C (Houston site) constructed with 1/2 cross-sectional area soil inclusion.



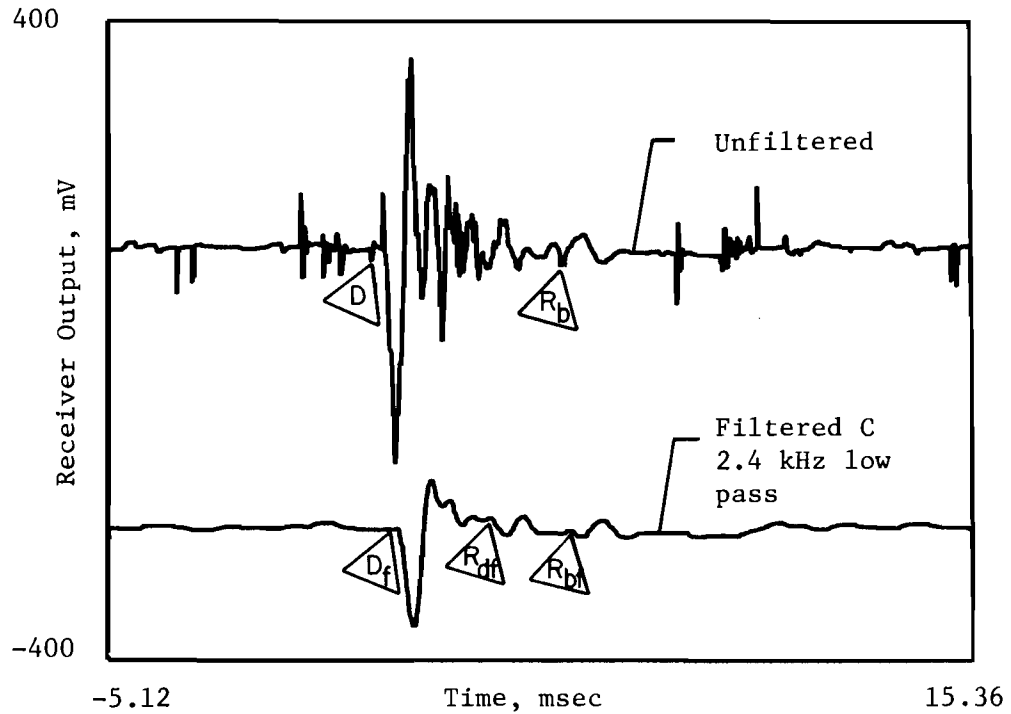
R_b = Reflected wave from bottom of pier
 R_t = Reflected wave from top of pier
 R_d = Reflected wave from defect
 Pier Length = 50 ft (15.2 m)
 Pier Diameter = 32 in (81.3 cm)

Fig. 7.18. Comparison of reflection records from 10 ft (3.0 m) velocity transducers in Shafts A and C (Houston site).

part to the decrease in velocity as the P-wave passes through the partial cross-sectional defect. Irregardless, a basic comparison of the wave signatures reveals a distinct change in waveform configuration in the record for Shaft C at a time corresponding to the reflected wave arrival of the planned defect which is absent from the record for Shaft A. Unfortunately, due to wave amplitude attenuation, no other wave arrivals resulting from the defect are clearly visible in the wave signature for Shaft C.

WAPER tests were also conducted using the various piezoelectric ceramic transducers positioned in Shaft C at a depth of 20 ft (6.1 m) below the top of the pier. Wave signatures resulting from one such test are presented in Fig. 7.19. In this figure, filtered and unfiltered output recorded by the 1/2 in. by 1/4 in. by 1 in. (1.27 cm by 0.64 cm by 2.51 cm) LTZ-2 piezoelectric transducer is presented. A 15 lb (6.8 kg) drop hammer was used to generate the P-wave impulse.

Several important points can be made concerning wave propagation testing of drilled piers by examining the output in Fig. 7.19. It should be noted that although the receiver output shown in Fig. 7.19 was recorded by a piezoelectric transducer, the following discussion also pertains to velocity transducer receivers. First, extraneous noise can be seen intermittently throughout the unfiltered wave signature. The extraneous noise was the result of equipment vibrations from adjacent roadway repair operations in progress at the time of testing. Due to the nature of the testing environment and the continuous sequence of project activities, extraneous noise such as that exhibited in Fig. 7.19 is not uncommon on many construction projects. Should extraneous noise be discovered in receiver output during initial testing, it may prove advantageous to use the mid-signal trigger of the digital oscilloscope for future testing, as was done in



D = Direct wave arrival, 1.45 msec
 D_s = Filtered direct wave arrival, 1.70 msec
 R_b = Reflected wave from bottom of pier, 5.75 msec
 R_{bf} = Filtered reflected wave from bottom of pier, 6.01 msec.
 R_{df} = Filtered reflected wave from defect, 3.50 msec.
 Receiver Elevation = 20 ft (6.1 m)
 Pier Length = 50 ft (15.2 m)
 Pier Diameter = 32 in (81.3 cm)

Fig. 7.19. WAPER test on Shaft C (Houston site) using drop hammer source and 1/2 in. x 1/4 in. 1 in. LTZ-2 piezoelectric ceramic transducer.

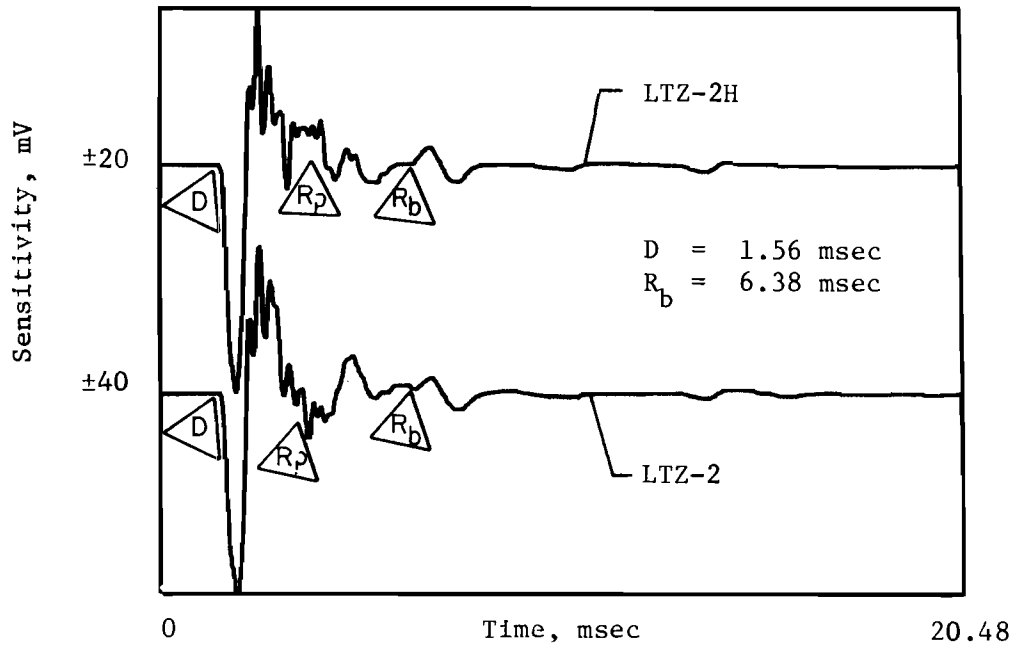
the output of Fig. 7.19. Use of the mid-signal trigger allows assessment of receiver excitation prior to the arrival of the generated P-wave, providing valuable information for proper wave signature evaluation.

In some instances, the extraneous noise can be of such magnitude and frequency that it can "mask" the direct and reflected wave arrivals in the wave signature, rendering integrity evaluation impossible. In these instances, a filter is required to eliminate the undesirable noise from the recorded output. The effects of filtering the receiver output are shown in the lower trace of Fig. 7.19. The extraneous noise present in the upper trace has been eliminated by filtering the output using a 2.4-kHz low-pass filter. The reflected wave from the bottom of the pier as well as the wave reflections off the planned defect are clearly visible in the lower trace as a result of filtering.

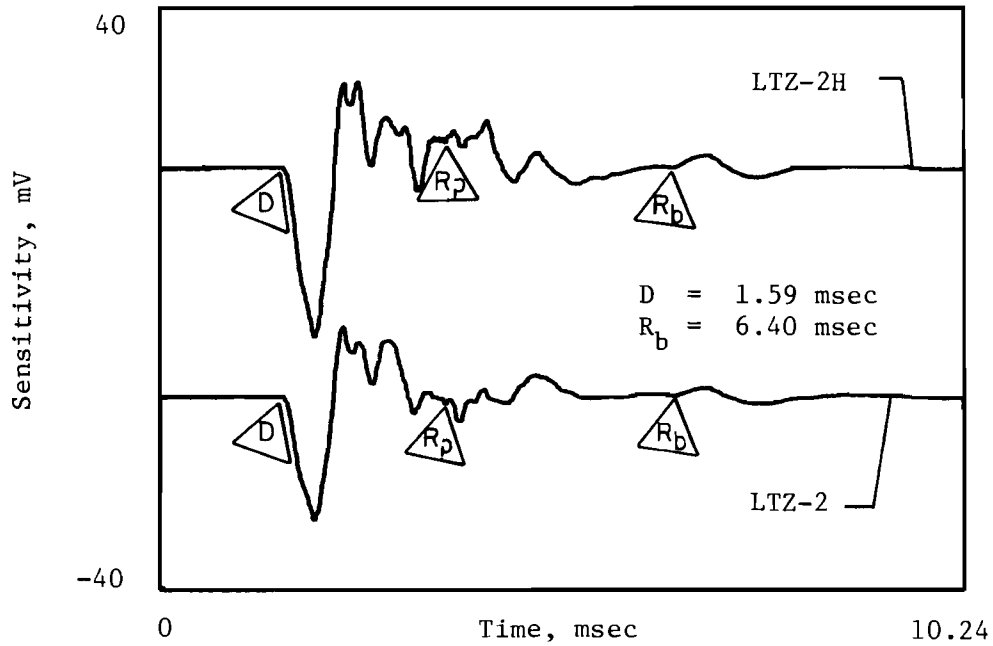
Unfortunately, filtering of receiver output can alter travel times and wave amplitudes of receiver output. Failure to recognize the influence of filtering on time domain measurements could result in erroneous assessment of P-wave velocities and reflection boundaries and, consequently, drilled pier integrity. This fact is illustrated in an assessment of the wave signatures presented in Fig. 7.19. A review of the signatures reveals that filtering of the receiver output caused a delay of 0.25 msec in direct P-wave travel times. A comparison of arrival times of the wave reflection from the bottom of the pier reveals that the delay in travel times is reflected throughout the filtered record. The direct P-wave velocity associated with the filtered output is 11,760 ft/sec (3,580 m/sec), compared to the P-wave velocity of 13,790 ft/sec (4,200 m/sec) computed using the direct wave travel time associated with the unfiltered signature. Use of the slower P-wave velocity in assessing reflected wave arrivals in filtered output will result in

erroneously long travel times and incorrect reflecting boundaries. Proper assessment of filtered output requires the use of an accurate P-wave velocity and elimination of time delays from computations of reflecting boundaries. Elimination of time delays is accomplished by using Eq. 3.7 for computational purposes, which reflects only the travel time subsequent to the direct arrival of the P-wave at the receiver. With regard to the wave reflection referred to as R_{df} in the filtered wave signature in Fig. 7.19, the use of Eq. 3.7 results in a reflection boundary located at 12.4 ft (3.8 m) below either the top of the pier or the monitoring receiver. The latter situation results in a reflection boundary location of 32.4 ft (9.9 m) below the top of the pier, which corresponds favorably with the known elevation of the planned defect in Shaft C. Similarly, the travel time of the wave reflection denoted as R_{bf} in Fig. 7.19 results in a reflection boundary of 49.7 ft (15.2 m), which compares well with the pier length of 50 ft (15.2 m). Because proper assessment of filtered output requires an accurate P-wave velocity for the member being evaluated, it is important that an unfiltered signature be recorded in conjunction with the filtered records, with emphasis placed on obtaining a clearly defined direct P-wave arrival.

Wave signatures for four of the piezoelectric ceramic transducers positioned in Shaft C are presented in Fig. 7.20. A basic comparison of the wave signatures reveals that wave reflections from the bottom of the pier are clearly visible in all four records. As discussed previously, the wave arrival from the bottom of the pier is distinguished in the signatures as an upward excursion of the waveform, the upward excursion resulting from the reflected tension wave and the transverse compression polarization of the piezoceramic transducer. Identification of the wave reflection from the bottom of the pier is an indication of a non-defective drilled pier or a pier



a. V₂ in. x 1/4 in. x 1 in ceramic.



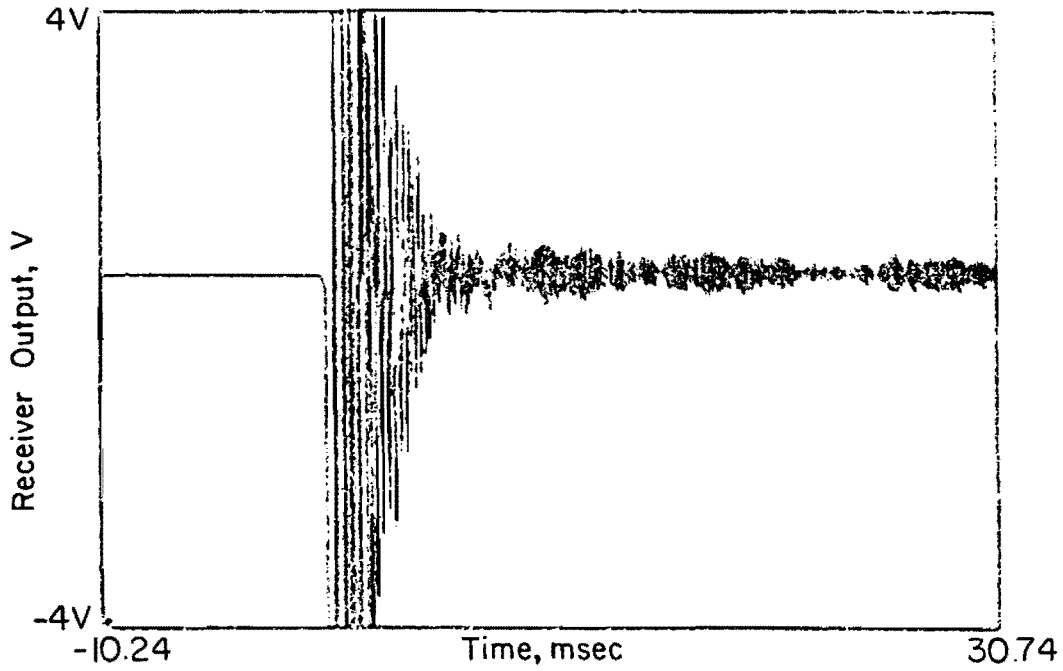
b. 1/2 in. x 1/8 in. ceramic.

Fig. 7.20. WAPER tests on Shaft C (Houston site) using drop hammer source and 20 ft (6.1 in) piezoelectric ceramic transducers.

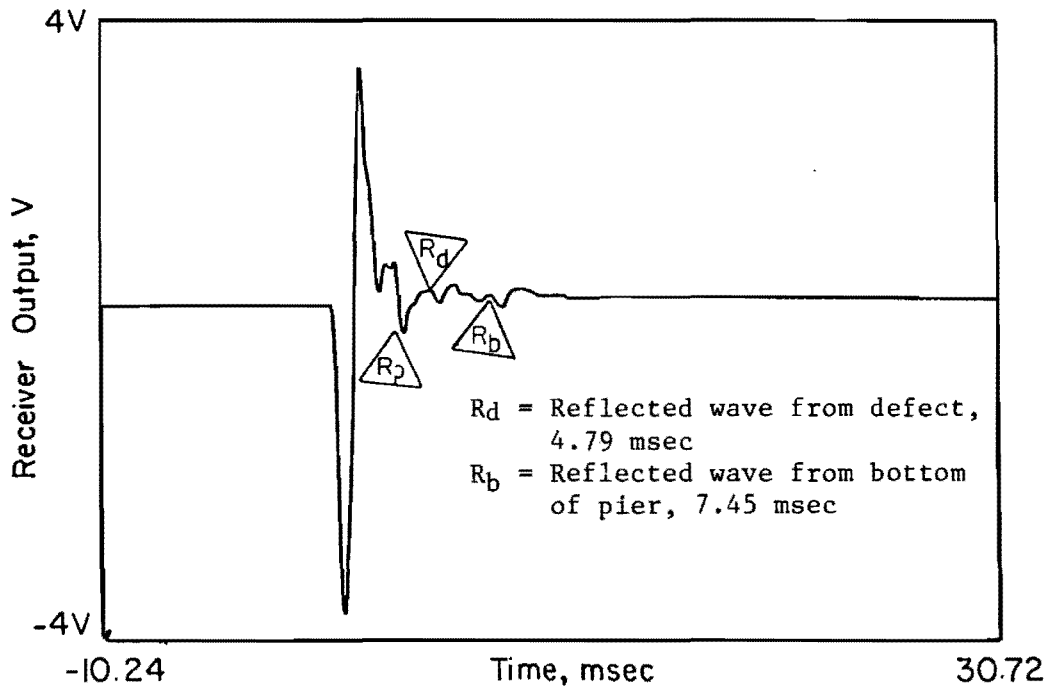
containing defects of negligible magnitude or consequence. This erroneous conclusion is further substantiated by the absence of clearly distinguishable early reflected wave arrivals in the wave records. The arrows denoted as R_7 in Fig. 7.20 are positioned at the estimated arrival times of the wave reflection off the 1/2 cross-sectional area defect in Shaft C, the arrival times estimated using the known travel distance and P-wave velocities. Unlike the wave signatures recorded using the velocity transducers in Shaft C, no evidence of wave reflections off the planned defect is apparent in the vicinities of the estimated wave arrival times. Failure to monitor early wave reflections off defects considered to be major in magnitude, and the nuisance of interpreting polarization dependent output renders piezoelectric ceramic transducer less than desirable as recording devices in integrity testing of drilled piers using wave propagation methods.

WAPS Method. Typical WAPS tests conducted on Shaft C are presented in Fig. 7.21. Both filtered and unfiltered receiver output is shown in the figure. A 15 lb (6.8 kg) drop hammer was used to generate the P-waves.

The filtered and unfiltered wave signatures are similar to those presented previously for Shafts A and B. Again, no wave reflections are discernable in the unfiltered wave signature due to the "noise" created by the surface waves propagating back and forth across the top of the pier. Filtering greatly enhances the clarity of the waveform, as revealed in Fig. 7.21(b). Using an average P-wave velocity of 13,300 ft/sec (4,050 m/sec), which accounts for increases in P-wave velocity with depth within the pier, the wave reflection from the bottom of Shaft C is estimated to arrive at the surface receiver approximately 7.51 msec after the initial impulse. A review of Fig. 7.21(b) reveals a wave arrival (denoted by R_b) at approximately 7.45 msec, correlating well with the computed arrival time of the reflected wave



a. Unfiltered.



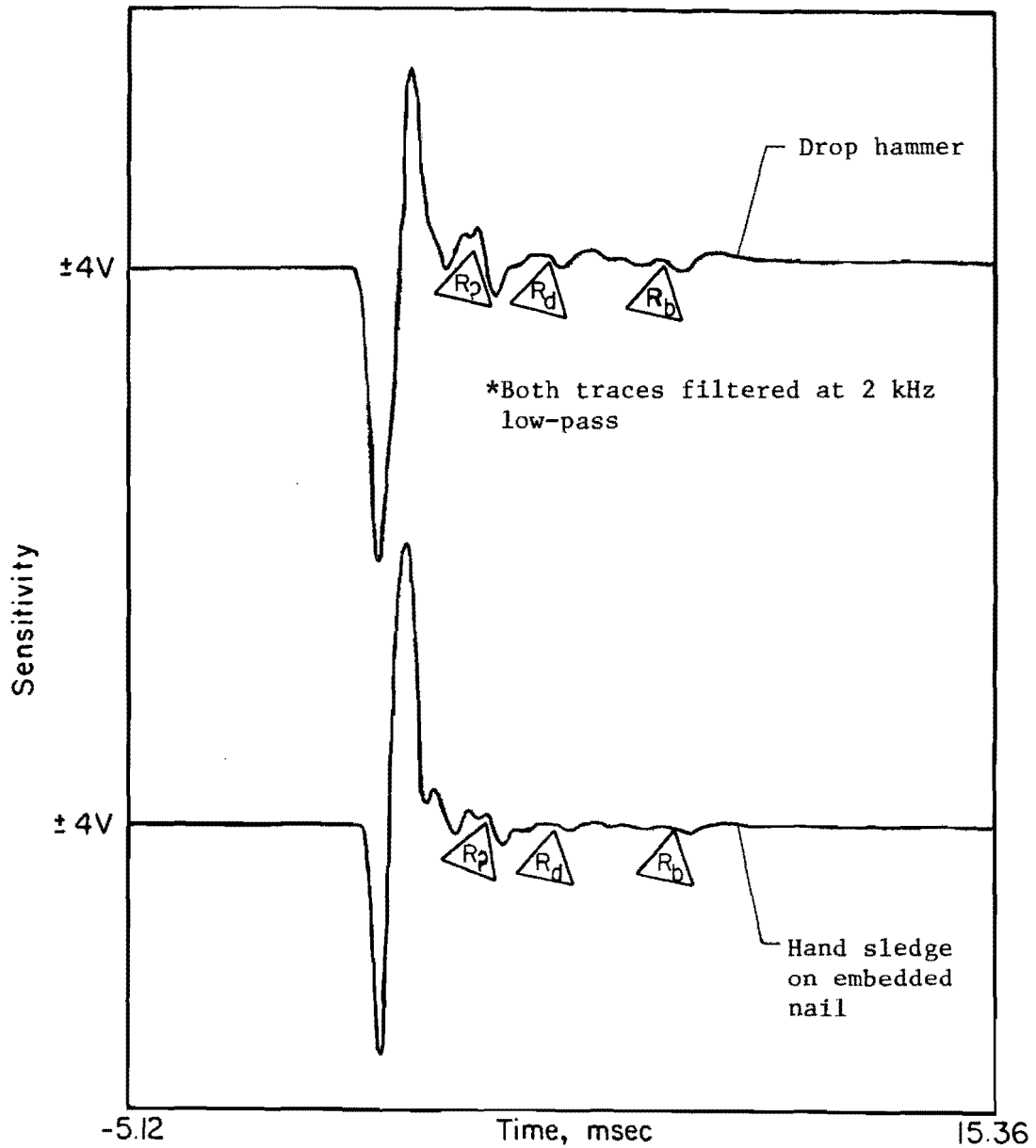
b. Filtered c 2.0 kHz Low-pass.

Fig. 7.21. WAPS Test on Shaft C (Houston site) using drop hammer source and accelerometer surface receiver.

considering the effects filtering can have on time domain measurements.

A closer examination of the wave signature in Fig. 7.21(b) reveals two additional downward excursions of the waveform (denoted by R_d and R_s) occurring prior to the arrival of the wave reflection from the bottom of the pier. The travel time of the wave arrival referred to as R_d is 4.79 msec. Again using the average P-wave velocity of 13,300 ft/sec (4,050 m/sec) and Eq. 3.6 (with initial arrival time equal to zero), the reflection boundary is computed to be at a depth of 31.9 ft (9.7 m) below the top of the pier. The computed reflection boundary compares extremely well with the actual depth of the planned defect in Shaft C. The travel time of the apparent wave arrival denoted by R_s is 3.15 msec, which corresponds to a reflection boundary at a depth of 20.9 ft (6.4 m) below the top of the pier. Because a similar wave arrival occurred in the WAPS receiver output for Shaft B in Fig. 7.9, it is concluded that the wave arrival referred to as R_s is the result of the surface wave, which is source induced.

Wave signatures for WAPS tests conducted on Shaft C using both drop hammer and hand sledge/embedded nail sources are presented in Fig. 7.22. An analysis of travel times of reflected wave arrivals visible and denoted in the wave signatures results in conclusions identical to those drawn for the receiver output in Fig. 7.21(b). A basic examination of the waveforms reveals that wave reflections from the bottom of the pier and the planned defect are identifiable in both records, although the signature associated with the drop hammer source is slightly superior to that generated with the hand sledge in regard to clarity and definition. Unfortunately, as with the WAPS data presented for Shaft B, the wave arrival denoted by R_s would most likely be evaluated erroneously under normal circumstances as a pier defect located at a depth of approximately 20 ft (6.1 m), rendering the WAPS method



R_d = Reflected wave from defect, 4.78 msec

R_b = Reflected wave from bottom of pier, 7.45 msec

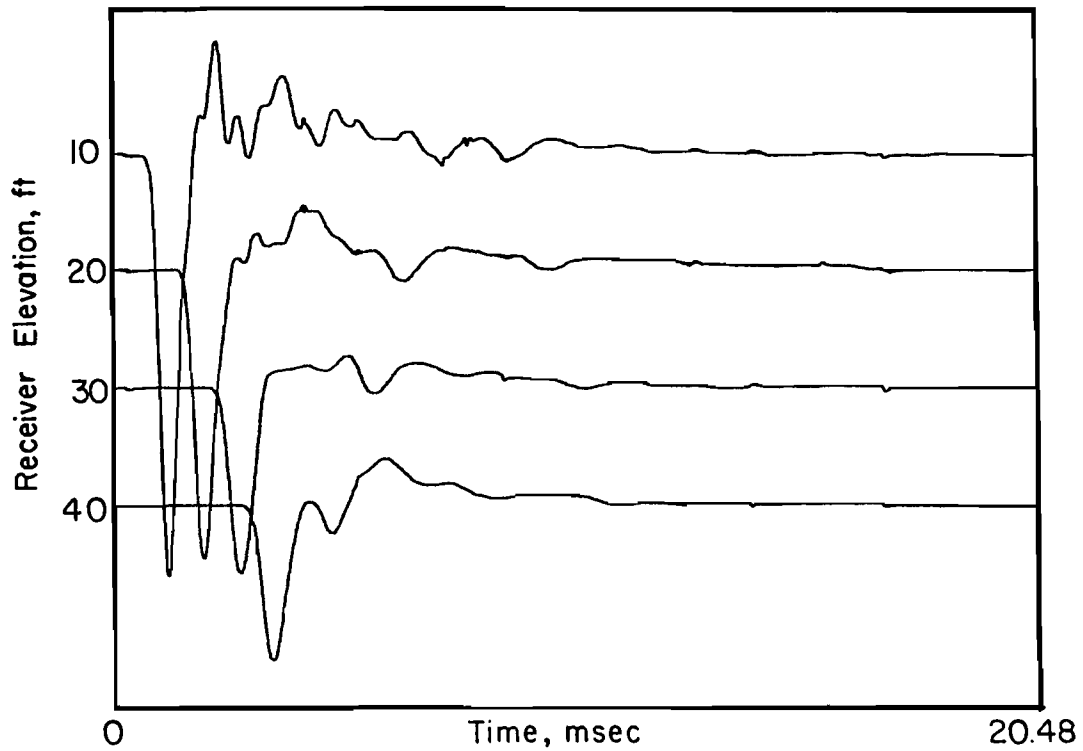
Pier Length = 50 ft (15.2 m)

Pier Diameter = 32 in (81.3 cm)

Fig. 7.22 Comparison of drop hammer and hand sledge/embedded nail sources for WAPS tests conducted on Shaft C (Houston site).

of pier evaluation questionable. However, one possibility (which was not tried) would be to take several records at various cut-off frequencies to see if the arrival denoted by R_2 shifts. If shifting is noted, the arrival probably is due to surface interference.

Attenuation. Multiple receiver output recorded in Shaft C for the attenuation study are shown in Figs. 7.23 and 7.24. The dual oscilloscope setup shown in Fig. 4.2 was utilized for recording purposes and a single impulse from both the drop hammer and hand-sledge-with-embedded-nail sources was used to generate the wave excitation recorded in Figs. 7.23 and 7.24, respectively. Wave amplitudes measured directly from the recorded output corresponding to the direct and reflected waves from the top and bottom of the pier are graphically illustrated in Figs. 7.25 and 7.26.

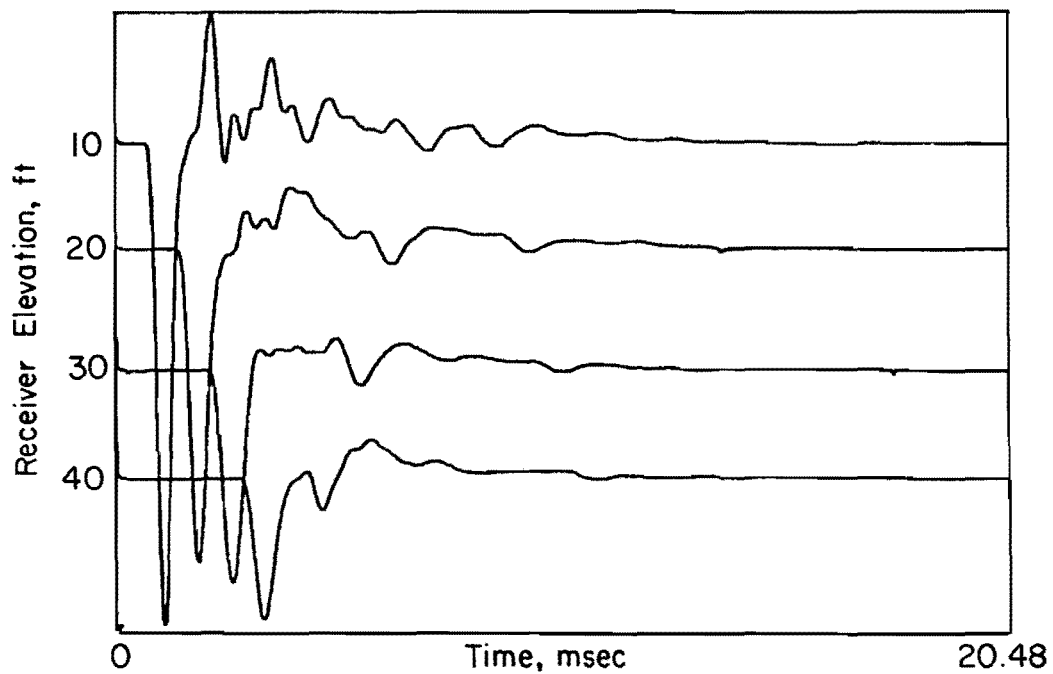


Sensitivity = \pm 200mV

Pier Length = 50 ft (15.2 m)

Pier Diameter = 32 in.(81.3 cm)

Fig. 7.23. Attenuation study of multiple receiver output from WAPER Test conducted on Shaft C (Houston site) using drop hammer source.



Sensitivity = \pm 20mV

Pier Length = 50 ft (15.2 m)

Pier Diameter = 32 in.(81.3 cm)

Fig. 7.24. Attenuation study of multiple receiver output from WAPER Test conducted on Shaft C (Houston site) using hand sledge and embedded nail source.

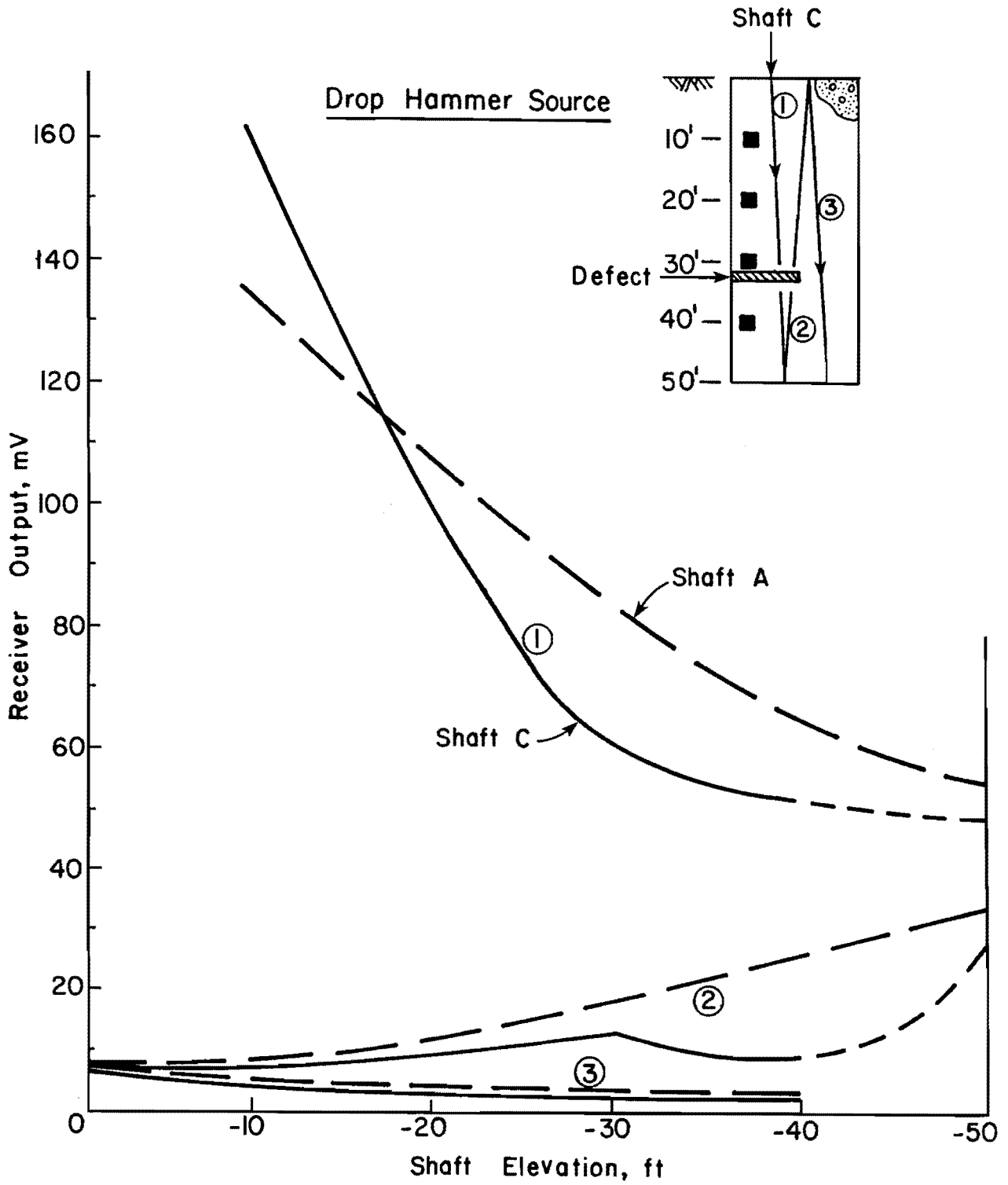


Fig. 7.25. Attenuation of P-wave in Shaft C (Houston site).

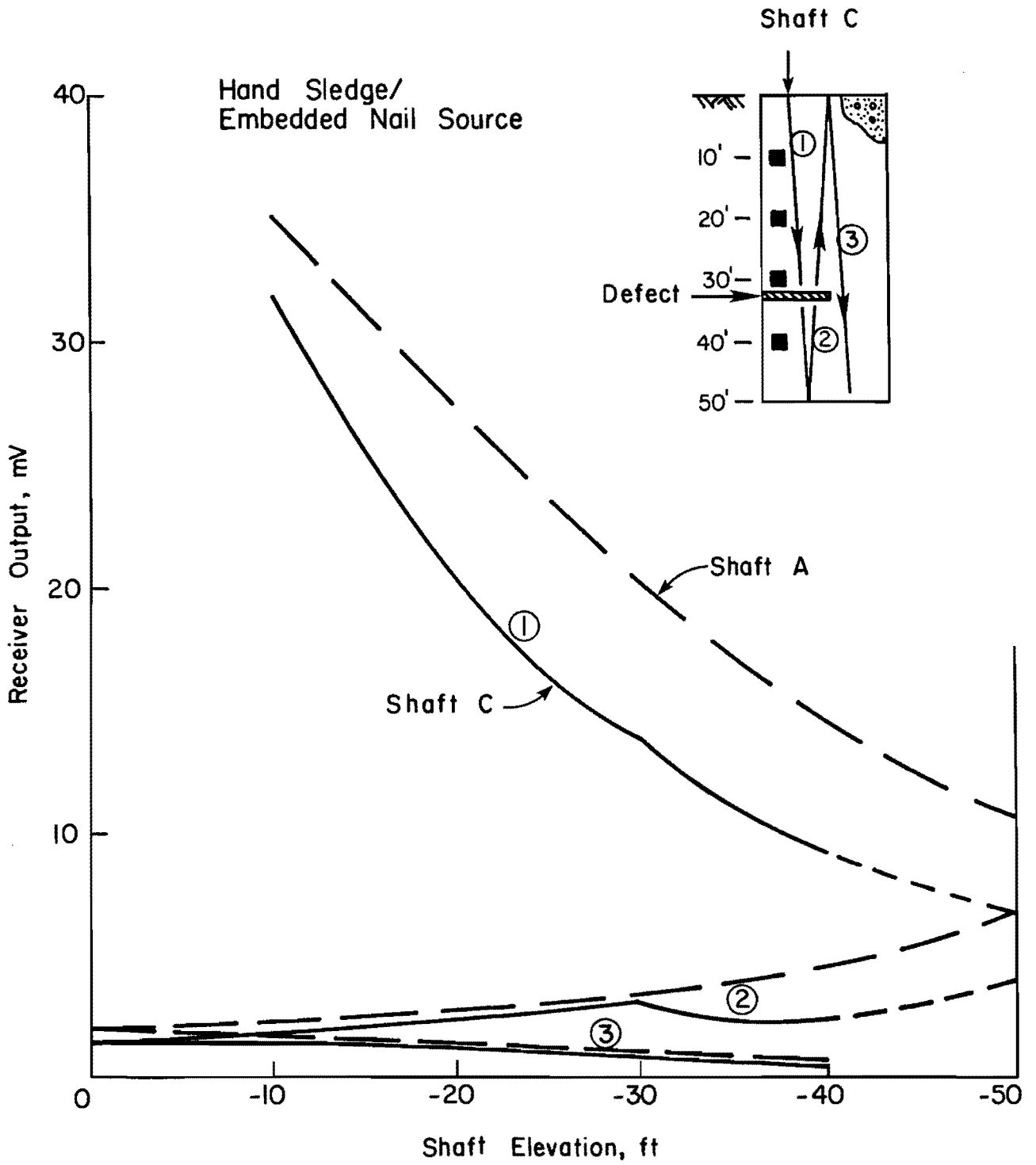


Fig. 7.26. Attenuation of P-wave in Shaft C (Houston site).

A review of Fig. 7.25 reveals that the P-wave generated with the drop hammer in Shaft C attenuates in a manner similar to that found in Shaft B; that is, the wave attenuation in the upper 30 ft (9.1 m) of Shaft C is greater than that measured in Shaft A, while the wave attenuation below the planned defect in Shaft C is slightly less than that corresponding to Shaft A. Again, this phenomenon contradicts what is expected for wave attenuation in a defective drilled pier. An explanation for the greater wave attenuation in the upper half of Shaft C is not readily apparent, although slight differences in concrete mix and quality and the previously discussed differences in surrounding environment may be some of the causes.

Similarly, unexplainable behavior occurs in the measured attenuation of the wave reflection from the bottom of the pier. It can be seen in Fig. 7.25 that wave energy is greater at the 30 ft (9.1 m) receiver than at the 40 ft (12.2 m) receiver, even though the travel distance is greater to the 30 ft (9.1 m) receiver. Again, the measured data contradicts what is expected to happen, that being that the planned defect would further attenuate what little wave energy remains after reflection at the bottom of the pier. A review of Fig. 7.17 confirms that no apparent reflected wave energy coincides at the travel time associated with the arrival of the wave reflection at the 30 ft (9.1 m) receiver from the bottom of the pier. While the amplitudes of reflected waves in receiver output are often vague and subject to the one's interpretation, the repeatability of the results shown in Fig. 7.25 tend to suggest some unknown wave attenuation phenomenon occurring in the vicinity of the 1/2-cross-sectional-area defect.

Somewhat different results were obtained for wave attenuation data presented in Fig. 7.26 and associated with the hand-sledge-and-embedded-nail source. Attenuation of the direct P-wave traveling in Shaft C correlates

fairly well with wave attenuation measured in Shaft A. A slight excursion of the attenuation data associated with Shaft C can be seen at the direct arrival of the P-wave at the 30 ft (9.1 m) receiver. The slight increase in wave energy at this particular receiver is associated with the concurrence of the direct P-wave and reflected tensile wave off the nearby planned defect, a small but nonetheless visible indication of the pier defect.

Attenuation of the wave reflected from the bottom of the pier exhibited the same contradictory phenomenon as that described for the drop hammer data, with wave energy measured at the 30 ft (9.1 m) receiver greater than that measured at the 40 ft (12.2 m) receiver. In the lower range of the receiver output, wave attenuation in Shaft C closely resembles that measured in Shaft A.

Evaluation of the attenuation data presented in Figs. 7.25 and 7.26 affords no clearly defined indication of the 1/2 cross-sectional area defect implanted in Shaft C. For the drop hammer source, differences in attenuation rates when comparing wave propagation in Shafts A and C are the only indication of possible pier differences, although no conclusions can be drawn from these differences concerning pier integrity. With the hand-sledge-and-embedded-nail source, a slight indication of the presence of the planned defect is revealed as a small increase in the wave amplitude at the 30 ft (9.1 m) receiver, although the magnitude of this increase would most likely go undetected under normal circumstances. This is particularly true for typical testing utilizing fewer embedded receivers and possibly less than ideal receiver positioning.

To eliminate possible source or impact-induced effects on wave attenuation, the receiver output presented in Figs. 7.23 and 7.24 have been normalized with respect to the 10 ft (3.0 m) receiver and tabulated in Table

7.2. In Table 7.2, it can be seen that the normalized output decreases continuously as the wave propagates up and down the pier, with exception of the previously discussed increase in reflected wave amplitude from the bottom of the pier at the 30 ft (9.1 m) receiver. Again, the cause of this fluctuation in wave amplitude is not readily apparent, although it is noted that assessment of reflected wave amplitudes are subject to interpretation.

Normalization of the outputs from the multiple receivers also resulted in eliminating the differences in output apparently caused by the differences in source impact. This is shown in Fig. 7.27 where the normalized output of the direct P-wave tabulated in Table 7.2 has been graphically plotted. Normalized output measured in Shaft A is included in the figure for comparison purposes. In this figure, wave attenuation in Shaft C for the two differing sources is nearly identical. Wave propagation in the upper half of Shaft C is seen to attenuate at a faster rate than wave propagation in Shaft A, presumably due to differences in the surrounding environment. Below 30 ft (9.1 m) in Shaft C, the opposite is true. Other than these general differences in wave attenuation, no indication of the presence of the 1/2-cross-sectional area defect in Shaft C is obvious.

As in Shaft B, additional vertical velocity transducers were positioned in Shaft C in the vicinity of the soil defect. The purpose of the additional receivers was to provide information concerning the effects on wave propagation of defects occupying only part of the cross-sectional area. Wave signatures recorded by receivers directly overlying (30 ft (9.1 m)) and underlying (34.5 ft (10.5 m)) the planned defect in Shaft C are presented in Fig. 7.28. The receiver output was recorded for a single drop hammer impulse.

Table 7.2. SOURCE COMPARISON OF WAVE ATTENUATION
IN SHAFT C (HOUSTON SITE).

<u>RECEIVER</u>	<u>CHANGE IN OUTPUT, PERCENT</u> <u>(NORMALIZED TO 10 ft (3.0 m) RECEIVER)</u>		
	<u>DROP HAMMER</u>	<u>HAND SLEDGE</u>	
①	20	62.7	63.9
	30	37.4	39.0
	40	31.8	32.7
②	40	5.1	6.9
	30	8.0	9.3
	20	5.7	4.5
	10	5.0	4.1
③	10	3.2	2.1
	20	2.8	1.9
	30	1.6	1.3
	40	1.2	1.1

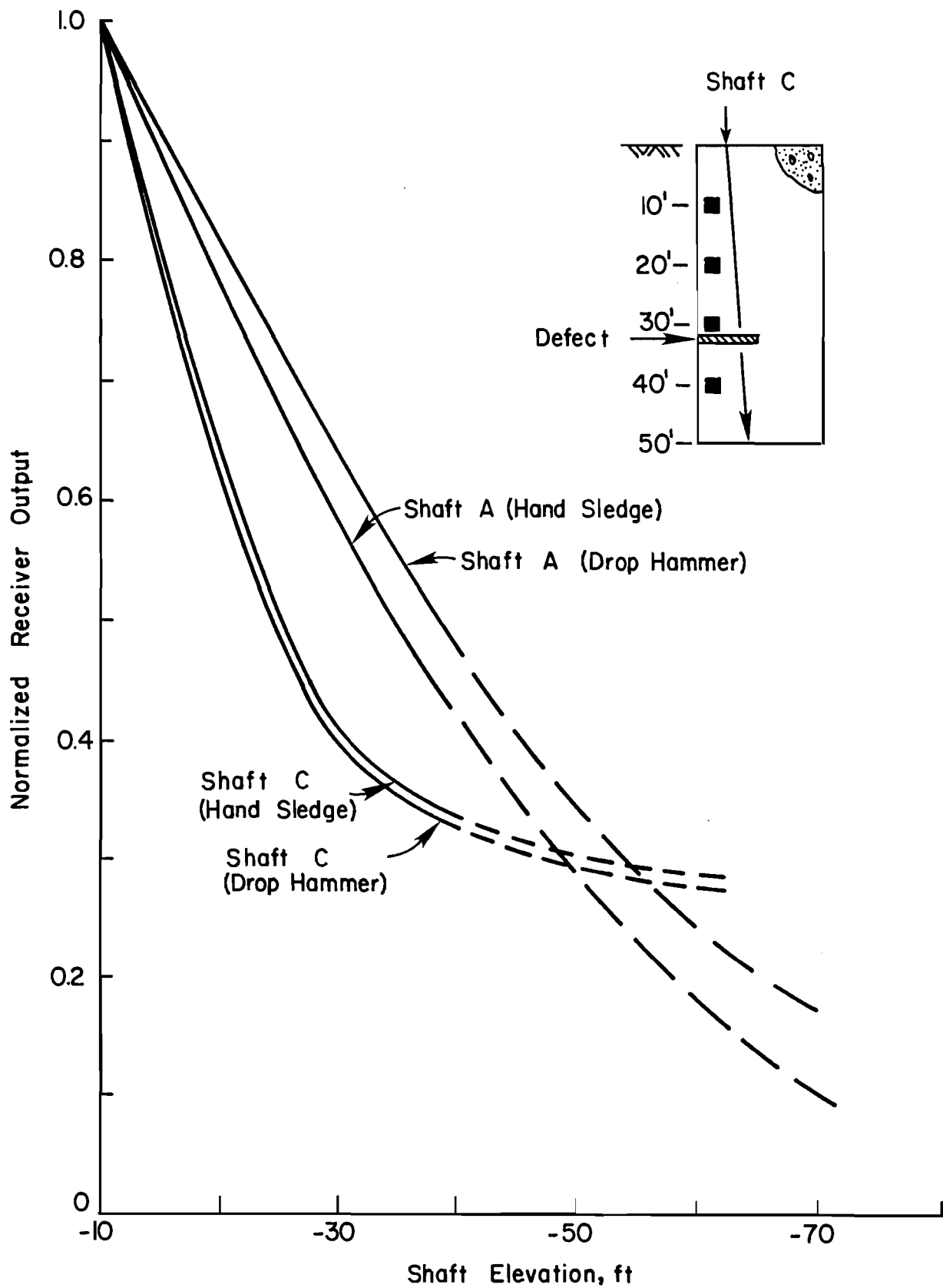
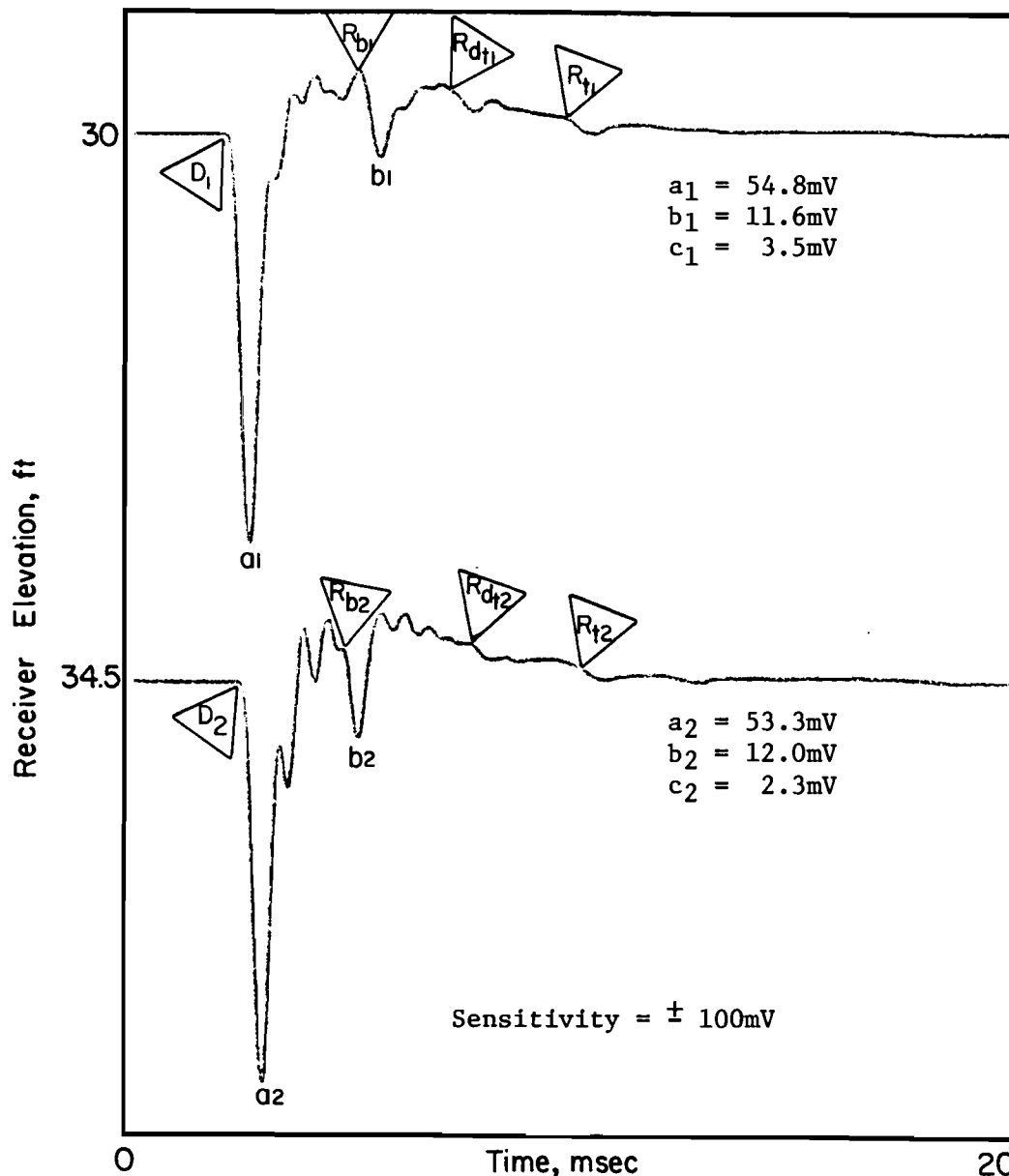


Fig. 7.27. Normalized attenuation of direct P-wave in Shaft C (Houston site).



- D_1 = Direct wave arrival @ 30 ft (9.1 m) receiver, 2.30 msec
 D_2 = Direct wave arrival @ 34.5 ft (10.5 m) receiver, 2.65 msec
 R_{b1} = Reflected wave from bottom of pier to 30 ft (9.1 m) receiver, 5.40 msec
 R_{b2} = Reflected wave from bottom of pier to 34.5 ft (10.5 m) receiver, 5.00 msec
 R_{t1} = Reflected wave from top of pier to 30 ft (9.1 m) receiver, 10.09 msec
 R_{t2} = Reflected wave from top of pier to 34.5 ft (10.5 m) receiver, 10.13 msec
 R_{dt1} = Reflected wave off defect and then top of pier to 30 ft (9.1 m) receiver, 7.35 msec
 R_{dt2} = Reflected wave off defect and then top of pier to 34.5 ft (10.5 m) receiver, 7.75 msec
Pier Length = 50 ft (15.2 m)
Pier Diameter = 32 in (81.3 cm)

Fig. 7.28. Comparison of wave signatures for 30 ft (9.1 m) and 34.5 ft (10.5 m) velocity transducers directly overlying and underlying defect in Shaft C (Houston site)

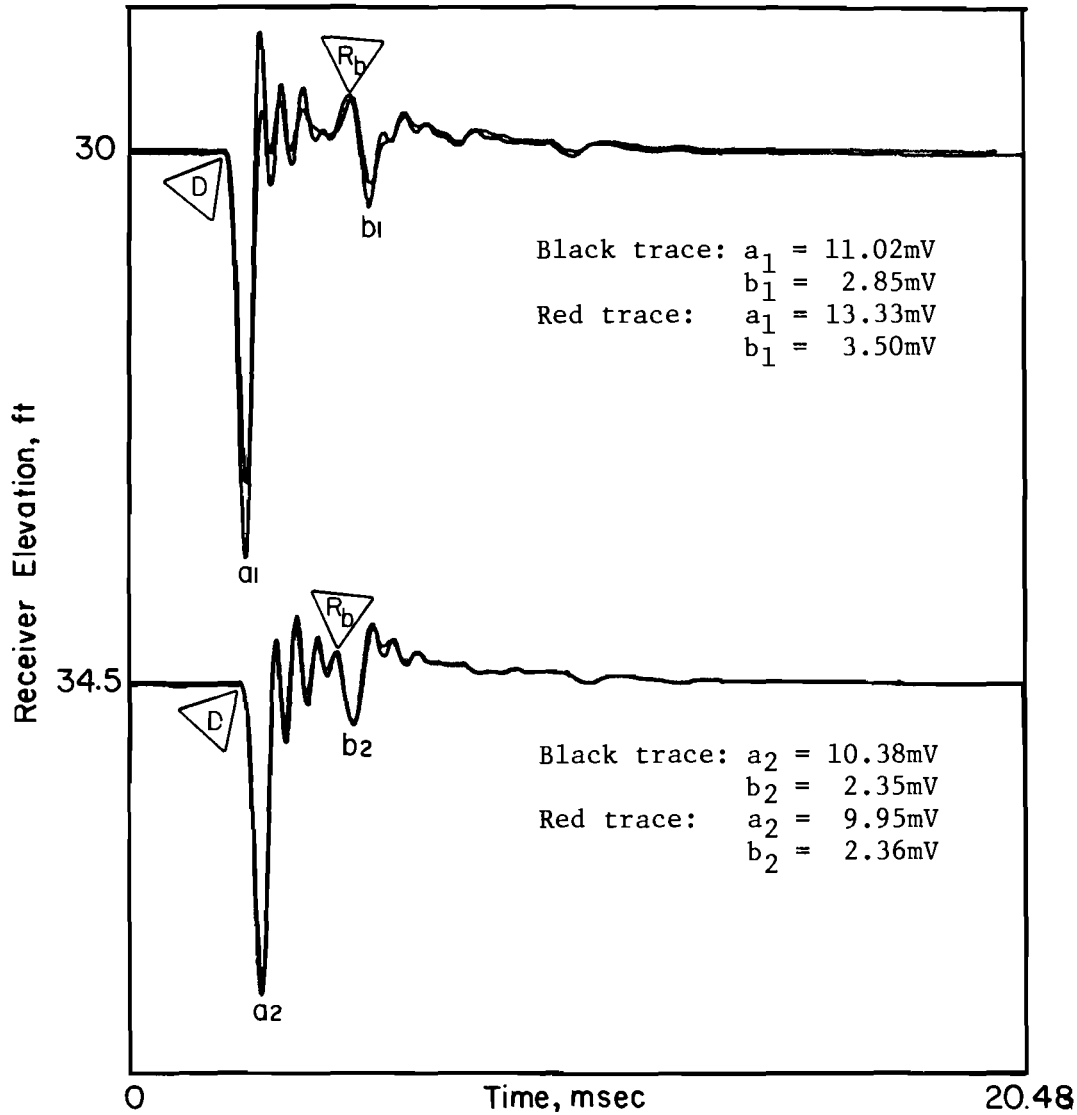
Several important points can be made by evaluating the receiver output in Fig. 7.28. First, the direct P-wave velocities are nearly identical for the wave signatures (13,040 ft/sec (3980 m/sec) for the 30 ft (9.1 m) receiver compared to 13,020 ft/sec (3970 m/sec) for the 34.5 ft (10.5 m) receiver). As such, an erroneous indication that no defect exists between the two receivers would be made. This erroneous conclusion is further substantiated by the presence of clearly defined wave reflections in the signatures from the top and bottom of the pier.

Similar conclusions are drawn by assessing wave attenuation in the receiver output. The direct wave amplitudes from the 30 ft (9.1 m) and 34.5 ft (10.5-m) receivers in Fig. 7.28 are 54.8 and 53.3 mV, respectively. The ratio of direct P-wave amplitudes between these two receivers is 97.2 percent, somewhat larger than that measured for the sound pier (Shaft A), but nonetheless indicative of a sound pier or a pier containing negligible defects.

It is interesting to note that although the planned defect in Shaft C is not discernable by assessing P-wave velocities and wave attenuation in the receiver output shown in Fig. 7.28 reflections off the defect and then the top of the pier are easily identified in both wave signatures. A general comparison of the amplitudes of wave reflections from the bottom of the pier with wave reflections off the defect and then the top of the pier indicates that the defect is of moderate magnitude, most likely not a full cross-sectional defect due to the ability to identify reflections from the top and bottom pier. This example illustrates the importance of assessing wave signatures for P-wave velocity, reflected wave arrivals and wave attenuation. Failure to assess all three characteristics could result in undetected pier irregularities.

In addition to the velocity transducers located directly above and below the 1/2-cross-sectional-area defect in Shaft C, velocity transducers were positioned in the pier opposite the defect and at the same receiver elevations. As in Shaft B, these additional receivers were positioned in the vicinity of the partial defect to determine its effect on wave propagation. Output recorded at the four receivers located above and below and opposite the planned defect is presented in Fig. 7.29. The dual oscilloscope setup shown in Fig. 4.2 was utilized for recording purposes. A single impulse of the handsledge/embedded nail source was used to generate the wave excitation.

As expected, the direct travel times of the P-wave determined from the 30 ft (9.1 m) receivers were identical, with the time of 2.28 msec resulting in a direct P-wave velocity of 13,160 ft/sec (4010 m/sec). Unexpectedly, the direct P-wave travel times to the 34.5 ft (10.5 m) receivers were also identical (2.59 msec), resulting in a direct P-wave velocity of 13,320 ft/sec (4060 m/sec). As shown in the recorded output for Shaft B, the presence of the pier discontinuity would seem to result in a longer direct travel time to the 34.5 ft (10.5 m) receiver underlying the defect than to the receiver positioned opposite the defect. The identical travel times of the direct wave registered at the 34.5 ft (10.5 m) receivers located directly below and opposite the planned defect along with the increase in P-wave velocity between the 30- (9.1-) and 34.5-ft (10.5-m) receivers, would lead one to the erroneous conclusion that no discontinuity exists at this depth in Shaft C. It is not readily apparent why the 1/4-cross-sectional area defect in Shaft B affected wave propagation travel times and, thus, P-wave velocities, and the larger defect present in Shaft C showed no apparent effects on these parameters.



Sensitivity = $\pm 10\text{mV}$

D = Direct wave arrival

R_b = Reflected wave from bottom of pier

Pier Length = 50 ft (15.2 m)

Pier Diameter = 32 in (81.3 cm)

Black traces: Receivers located directly above and below
planned defect

Red traces: Receivers located opposite the planned defect

Fig. 7.29. Comparison of output for 30 ft (9.1 m) and 34.5 ft (10.5 m) velocity transducer receivers located above and below and opposite the planned defect in Shaft C (Houston site).

The unexpected behavior exhibited in the travel times and wave velocities of the receivers presented in Fig. 7.29 was also found to exist in an assessment of wave attenuation. A review of the direct wave amplitudes for the 30 ft (9.1 m) receiver shown in Fig. 7.29 reveals that the wave amplitude for the receiver opposite the defect is greater than the amplitude associated with the receiver overlying the defect. This behavior contradicts what is expected to occur in practice. As discussed in the attenuation study for Shaft B, coincidence of the direct P-wave with the tension wave reflected from the defect should result in a larger wave amplitude recorded at the receiver directly overlying the defect than that recorded at the receiver opposite the defect. A possible explanation for the reversed situation measured in Shaft C could be that the 30 ft (10.5 m) receiver overlying the defect was not functioning properly, although the clearly defined direct and reflected wave arrivals in the wave signature and the reasonable travel times associated with these wave arrivals tends to refute this explanation. More likely, the nonuniform shape of the defect could result in variations in wave reflections off the defect, with the 30 ft (10.5 m) receiver positioned opposite the defect monitoring larger wave motion. As measured in Shaft B, no significant conclusions concerning the planned defect in Shaft C are provided by the small difference in the direct wave amplitudes of the 34.5-ft (10.5 m) receivers.

The receiver output presented in Figs. 7.28 and 7.29 should not be considered erroneous due to its nonuniformity with established wave propagation theory. The effects of pier irregularities, especially partial defects, are complicated at best, and the repeatability of the recorded data tends to indicate that some wave propagation phenomenon was in effect.

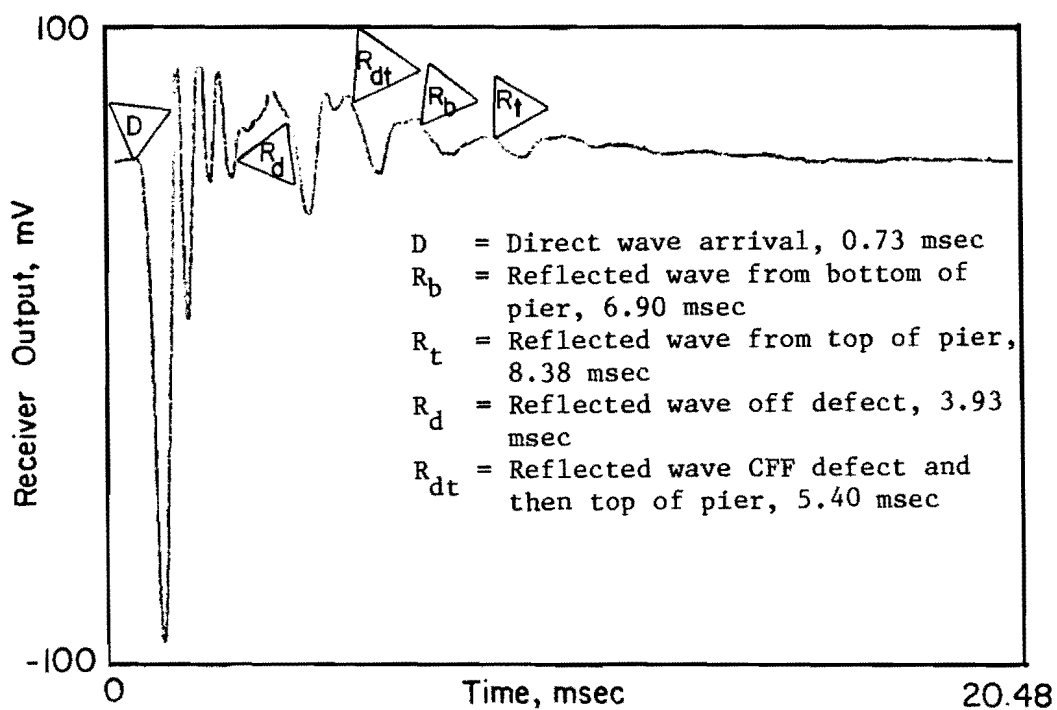
Further research in this area is required to ascertain the effects of attenuation on wave propagation measurements.

Shaft D

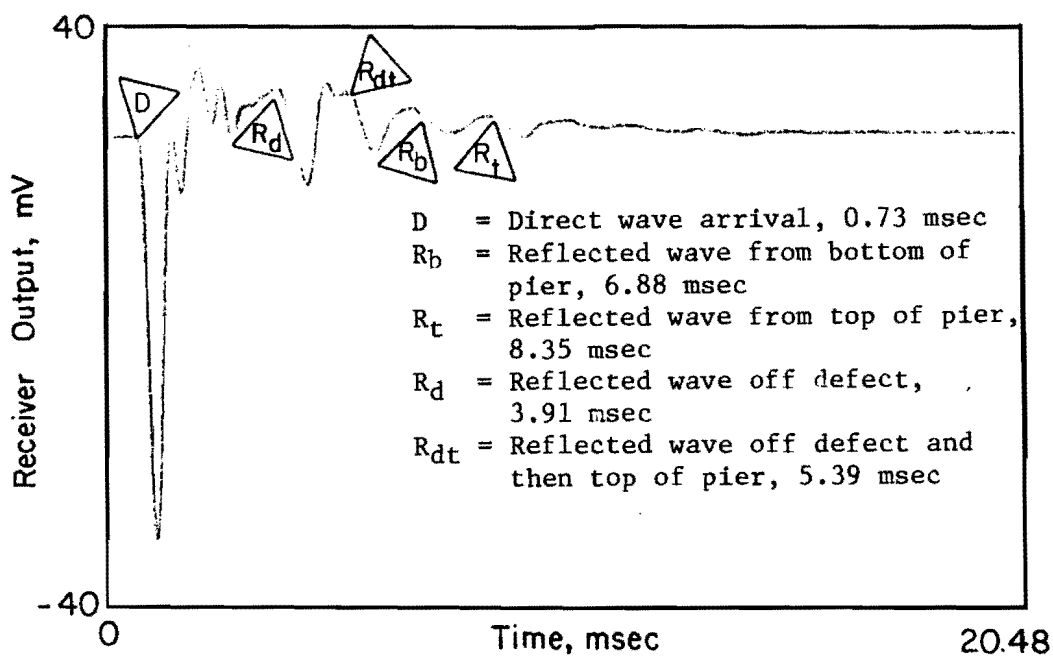
WAPER Method. Typical wave signatures for WAPER tests conducted on Shaft D using both drop hammer and hand-sledge-with-embedded-nail sources are shown in Fig. 7.30. For review, Shaft D was implemented with a nearly full cross-sectional soil inclusion located at a depth of 32 ft (9.2 m) below the top of the pier. The receiver output shown in Fig. 7.32 was recorded by the 10 ft (3.0 m) velocity transducer.

Examination of the receiver output presented in Fig. 7.30 shows that both impulse sources provide sufficient P-wave energy for well defined waveforms, although the hand-sledge-and-embedded-nail configuration was again judged to provide the superior signature. With regard to Fig. 7.30(b), the direct P-wave arrival occurs at 0.73 msec, resulting in a P-wave velocity of 13,700 ft/sec (4,180 m/sec). A high amplitude reflection off the defect (denoted as R_d) is clearly visible in the time domain record, with the wave arrival occurring at a time of 3.91 msec. Using the computed direct P-wave velocity and Eq. 3.6, the reflection boundary is computed to be located at a depth of 31.8 ft (9.7 m). This depth compares favorably with the 32 ft (9.8 m) actual depth of the defect.

Further evaluation of the wave signatures in Fig. 7.30 reveals that the initial P-wave energy was of sufficient magnitude to result in three later reflected wave arrivals. Regarding the three later arrivals, one corresponds to the wave reflection off the top of the pier as a result of the planned defect (denoted by R_{dt}) and the other two represent the original P-wave energy reflected from the bottom and top of the pier, denoted by R_b and R_t , respectively.



a. Drop hammer on concrete



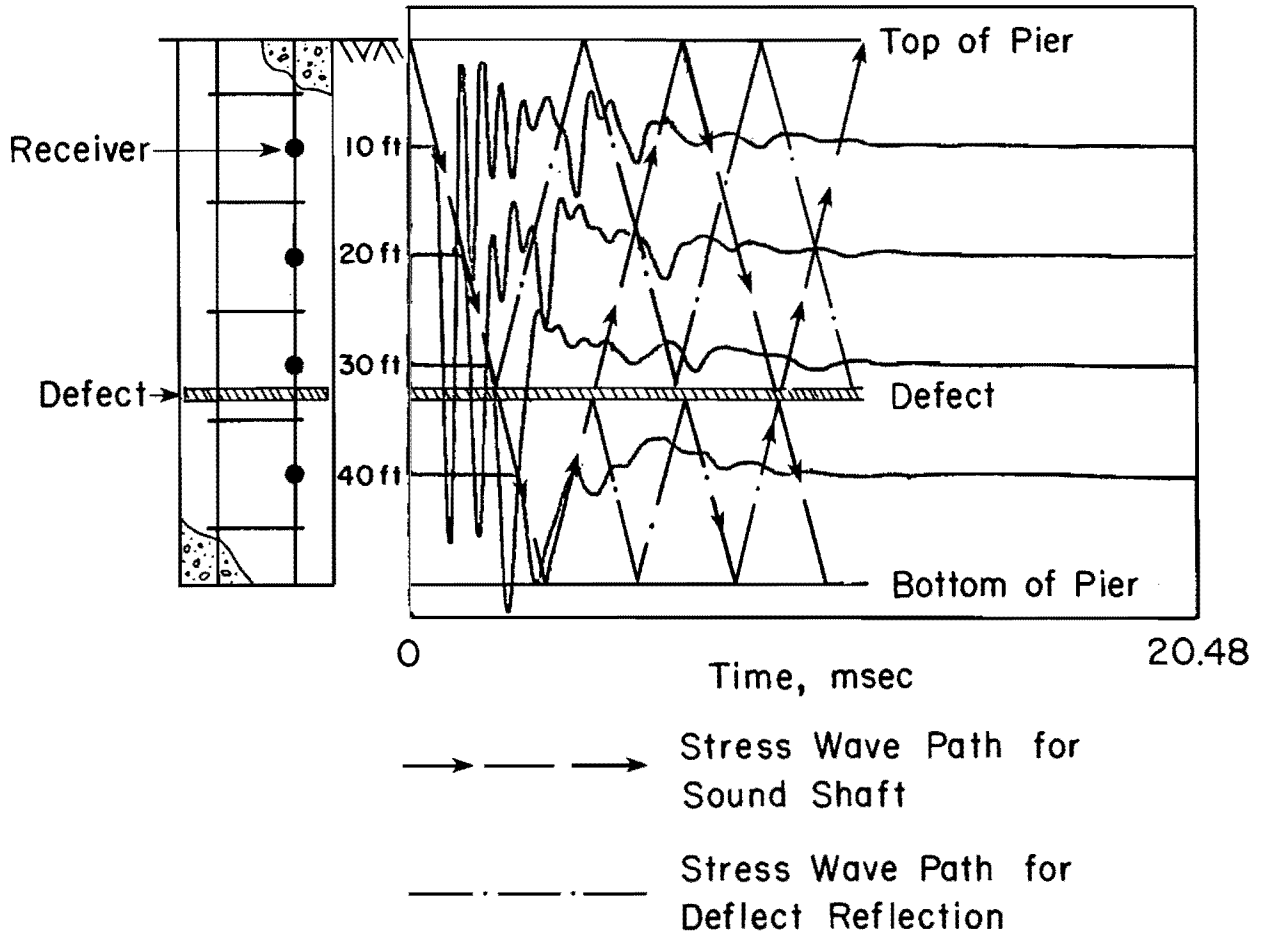
b. Hand sledge on embedded nail

Fig. 7.30. Wave signatures for 10 ft (3.0 m) embedded velocity transducer in Shaft D (Houston site).

Of interest in Fig. 7.30 is the ability to identify reflected waves off the concrete-soil interface at the bottom of the pier. Similar results were obtained for WAPER tests conducted on Shaft 2 at the Granger site, which also contained a full cross-sectional defect (see Fig. 7.1). To register this reflection, the P-wave had to twice propagate through the 1 ft (0.3 m) thick, full cross-sectional area defect present in Shaft D at the Houston site. It should be noted that this unexpected receiver response may be due in part to the 1 in. (2.5 cm) thick annular ring of concrete which is present along the side of the defect. This concrete ring, a result of the oversized hole required for casing the drilled pier during construction, may allow a larger percentage of P-wave energy to be reflected back up the pier than would be true for a full cross-sectional defect. Nonetheless, this ability to monitor successfully attenuated wave arrivals shows promise for this method in testing very long piers suspected of being defective.

For a detailed analysis of wave propagation in defective piers, multiple receiver output recorded in Shaft D is presented in Fig. 7.31. As before, receiver output has been plotted in equal voltage increments along the ordinate scale to simulate the actual positioning of the receivers in the pier. The drilled pier has been graphically presented alongside the wave records, the pier scaled to show the embedded receivers opposite their respective wave signatures. Reflection boundaries in the pier, consisting of the natural interfaces at the top and bottom of the pier and the additional boundary resulting from the planned defect, have been superimposed on the wave record to illustrate the wave paths in the pier.

A review of Fig. 7.31 shows a clear pattern of waves reflecting from the planned defect (denoted by the dot-and-dashed lines in the figure). Wave energy is of sufficient amplitude to show three significant reflections off



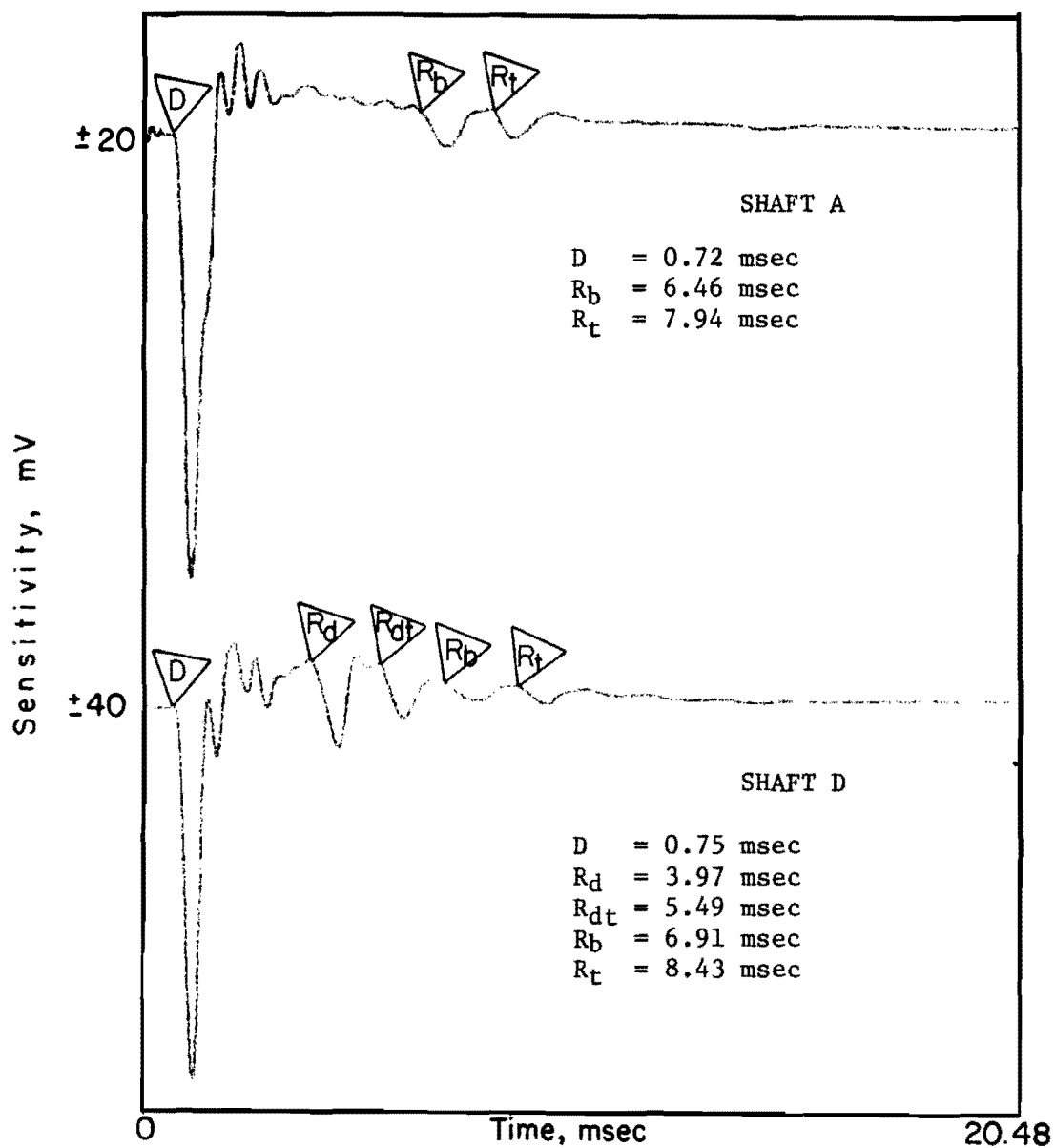
Sensitivity = \pm 20mV

Fig. 7.31. Wave signatures for WAPER test showing wave reflection in Shaft D (Houston site) constructed with full cross-sectional area defect.

the defect. Similarly, P-wave energy reflected at the concrete-soil interface at the bottom of the pier is also visible, as denoted by dashed lines in the figure. However, wave energy reflecting from the bottom of the pier has been highly attenuated by the defect and is not clearly visible in the wave signatures upon reflection at the top of the pier. Again, by reviewing multiple receiver output in this manner, patterns setup by the stress waves in the pier permit easy assessment of pier integrity.

For comparison purposes, output recorded at the 10 ft (3.1 m) embedded receivers in Shafts A (sound pier) and D is presented in Fig. 7.32. Relative comparison of receiver output in this manner may allow detection of certain discrepancies in the recorded waveforms, with these discrepancies possibly attributable to pier irregularities. In Fig. 7.32 the early reflected wave arrivals previously identified in Shaft D are accentuated upon comparing with the wave signature from Shaft A. Of further interest in this figure is a comparison of the reflections off both the bottom and top of the piers. While the reflected wave arrivals for the top and bottom pier boundaries in Shaft A are relatively sharp and distinct, the corresponding reflections in Shaft D are less well defined. The reduced definition of these reflections in Shaft D is obviously the result of attenuation imposed by the planned defect. The full cross-sectional defect in Shaft D also effectively increases wave propagation travel time, as revealed by comparison of the wave reflections from the bottom and top of Shafts A and C, denoted as R_b and R_t , respectively, in Fig. 7.32. Such comparisons may prove to be extremely useful in applications where extraneous noise in the monitored receiver output tends to mask early reflected wave arrivals.

Floating Receivers. As a final note, WAPER tests were performed utilizing the "floating" velocity transducer embedded in Shaft D. As



D = Direct wave arrival
 R_b = Reflected wave from bottom of pier
 R_t = Reflected wave from top of pier
 R_d = Reflected wave off defect
 R_{dt} = Reflected wave off defect and then top of pier

Receiver Elevation = 10 ft (3.0 m)

Pier Length = 50 ft (15.2 m)

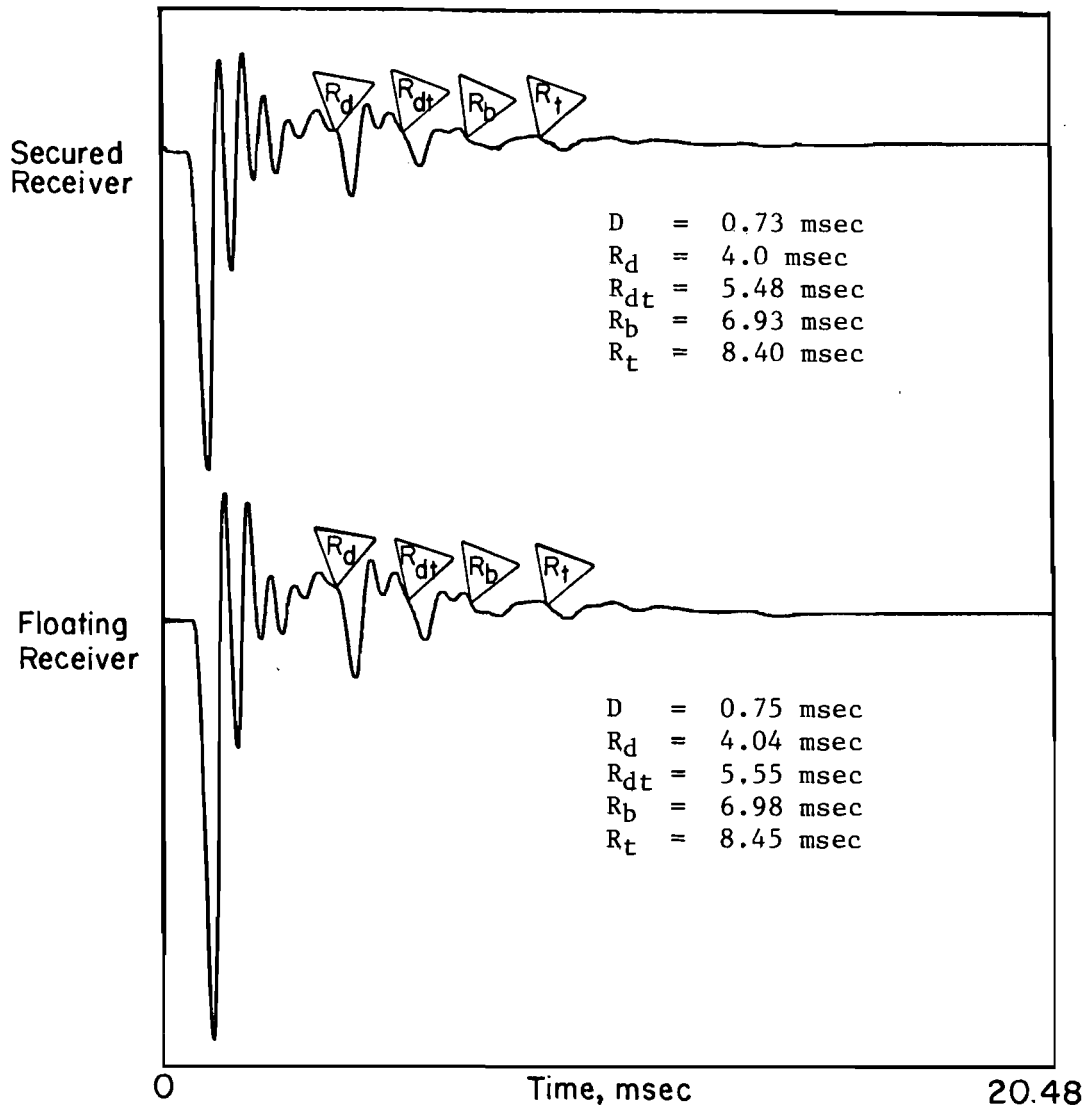
Pier Diameter = 32 in (81.3 cm)

Fig. 7.32. Comparison of reflection records from 10 ft (3.0 m) velocity transducers in Shafts A and D (Houston site).

mentioned previously, vertical velocity transducers were attached to special sleeves and positioned at a depth of 10 ft (3.0 m) in shafts B and D by use of the pier drilling rig. The purpose of including these "floating" receivers in this study was to assess the possibility of making measurements in unreinforced drilled piers. Shafts B and D were selected for study due to the size of defects present in these piers. WAPER tests conducted utilizing the floating velocity transducer in Shaft B have previously been presented under the discussion of Shaft B in this chapter.

A typical wave signature for a WAPER test conducted on Shaft D utilizing the floating velocity transducer is presented in Fig. 7.33. Receiver output for the corresponding velocity transducer attached to the reinforcing steel in Shaft D at a depth of 10 ft (3.0 m) is also included in Fig. 7.33 for the purpose of comparison. An examination of the figure shows the waveforms to be nearly identical in definition and clarity. Wave reflections off the defect as well as the top and bottom of the pier are clearly identifiable in the signature of the floating receiver. Travel times and, therefore, P-wave velocities for the direct and reflected waves are also nearly identical in each record. Based on these findings and those presented for Shaft B, it can be concluded that floating velocity transducers monitor wave propagation in drilled piers as well as velocity transducers affixed to the reinforcing steel and, thus, monitoring of wave propagation in unreinforced drilled piers is possible.

WAPS Method. A typical wave signature for a WAPS test conducted on Shaft D is presented in Fig. 7.34. The source-receiver configuration utilized for this test consisted of a 15 lb (6.8 kg) drop hammer and an accelerometer bonded to the concrete surface. A 1800-Hz low-pass filter was used during recording of the wave signature.



Sensitivity = $\pm 10\text{mV}$ (both traces)

D = Direct wave arrival

R_b = Reflected wave from bottom of pier

R_t = Reflected wave from top of pier

R_d = Reflected wave off defect of pier

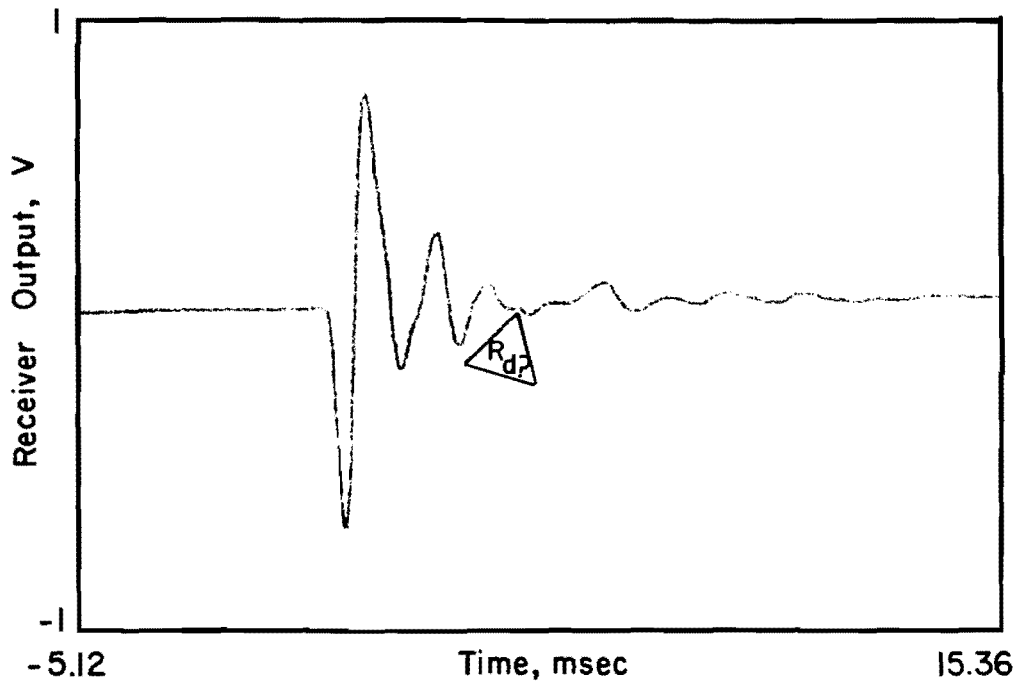
R_{dt} = Reflected wave off defect and then top of pier

Receiver Elevation = 10 ft (3.0 m)

Pier Length = 50 ft (15.2 m)

Pier Diameter = 32 in (81.3 cm)

Fig. 7.33. Comparison of WAPER output recorded by secured and floating velocity transducers in Shaft D (Houston site).



$R_d?$ = possible reflected wave from defect, 4.54 msec

Pier length = 50 ft (15.2 m)

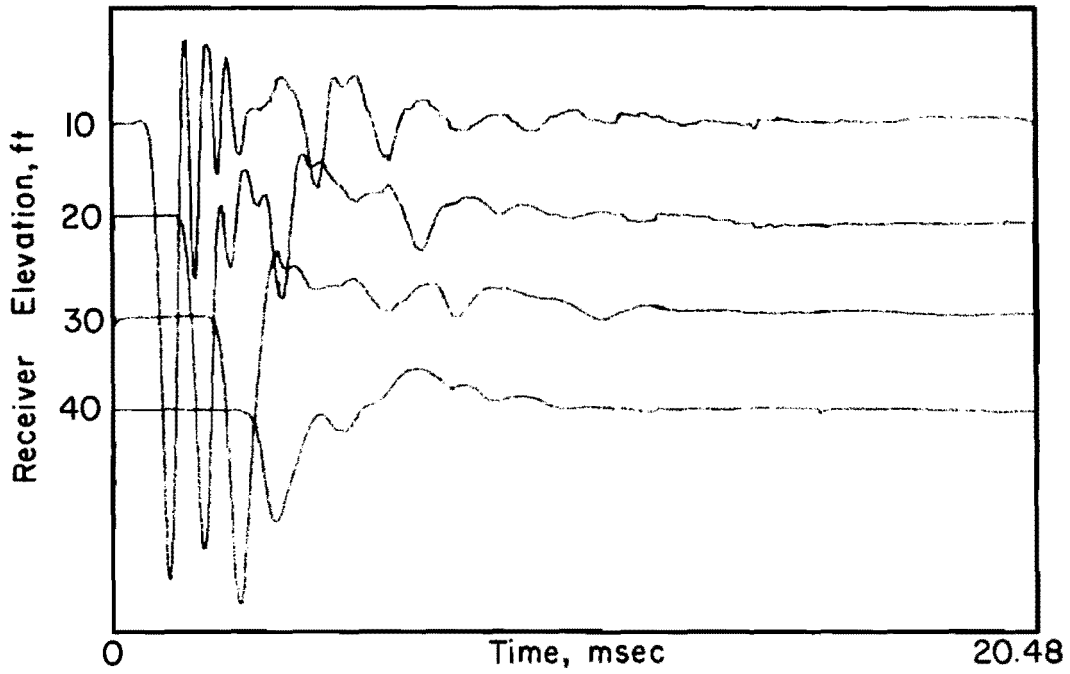
Pier diameter = 32 in. (81.3 cm)

Fig. 7.34. WAPS test on Shaft D (Houston site) using drop hammer source and surface accelerometer filtered @ 1800 Hz low pass

A review of Fig. 7.34 reveals that no wave reflection from the full cross-sectional defect is clearly identifiable in the record. The symbol denoted by R_d in the figure has been positioned at the expected time of arrival of the wave reflection from the defect. It was apparent at the time of testing that the surface waves produced by the source were of sufficient magnitude to mask effectively identification of the reflection off the defect. In an attempt to obtain a wave signature exhibiting the proper wave reflection various filter settings ranging from 1000 to 3000 Hz were tried to eliminate the undesirable surface wave excitation. Unfortunately, the results of the variable filter tests were similar to the findings shown in Fig. 7.34.

The only indication provided by the receiver output shown in Fig. 7.34 of the presence of a large defect existing in Shaft D is the absence of a definitive wave reflection from the bottom of the pier. However, identification of the wave reflection off the bottom of sound piers is often difficult, if not impossible, for WAPS tests conducted on long piers or in instances when the material properties at the concrete-soil interface at the bottom of the pier are similar. Therefore, to assess properly the significance of the indistinguishable wave reflection off the bottom of Shaft D, the questionable receiver output must be compared with output recorded for a pier previously deemed sound. In comparing WAPS signatures for Shafts A and D, the clearly defined wave reflection from the bottom of Shaft A in the receiver output would indicate the possible presence of a large discontinuity in Shaft D. Unfortunately, no other information concerning the nature and depth of the defect is provided in the wave signature shown in Fig. 7.34.

Attenuation. Wave signatures recorded for attenuation studies of wave propagation in Shaft D are presented in Figs. 7.35 and 7.36. The dual

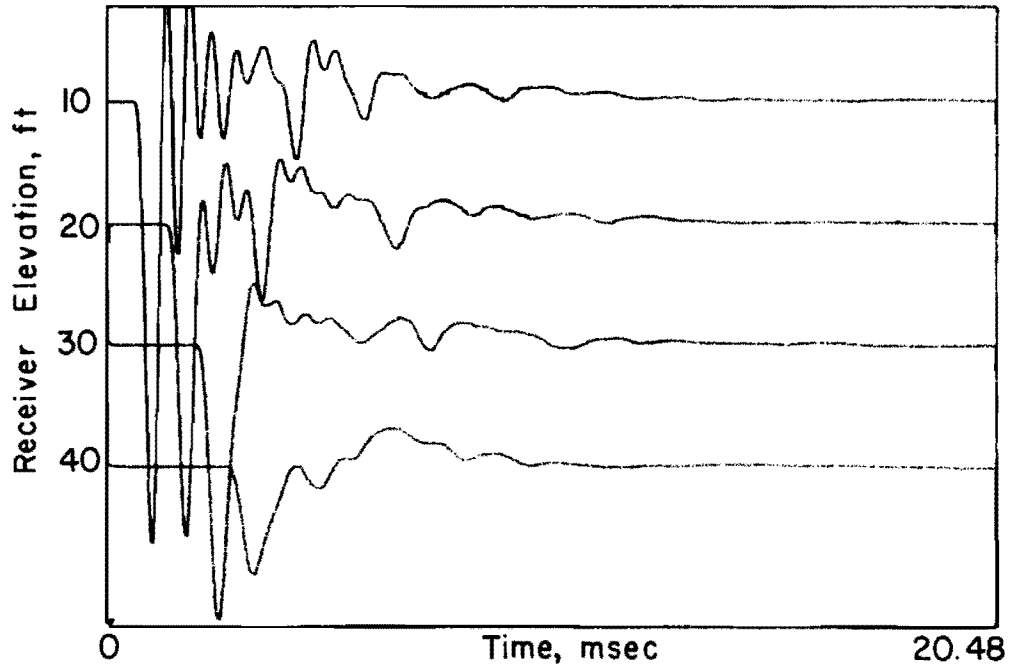


Sensitivity = $\pm 100\text{mV}$

Pier Length = 50 ft (15.2 m)

Pier Diameter = 32 in. (81.3 cm)

Fig. 7.35. Attenuation study of multiple receiver output from WAPER Test conducted on Shaft D (Houston site) using drop hammer source.



Sensitivity = $\pm 20\text{mV}$

Pier Length = 50 ft (15.2 m)

Pier Diameter = 32 in. (81.3 cm)

Fig. 7.36. Attenuation study of multiple receiver output from WAPER Test conducted on Shaft D (Houston site) using hand sledge and embedded nail source.

oscilloscope setup pictured in Fig. 4.2 was used for recording purposes, with the output shown in Fig. 7.35 associated with the drop hammer source and the output in Fig. 7.36 associated with the hand-sledge-and-embedded-nail source. Wave amplitudes of both direct and reflected waves off the top and bottom of Shaft D have been plotted in Figs. 7.37 and 7.38, respectively. Results of the attenuation study in Shaft A have also been included in Figs. 7.37 and 7.38 for comparison purposes.

As expected, a review of Figs. 7.37 and 7.38 reveals that the receiver output for Shaft D does not correlate well with that for Shaft A. However, the results for Shaft D do correspond favorably with what is predicted in wave propagation theory. For comparison purposes, it has been shown for the previous discussions that normalization of the wave attenuation data greatly enhances data interpretation. This procedure has been accomplished for the data tabulated in Table 7.3, where the direct and reflected wave output plotted in Figs. 7.37 and 7.38 have been normalized with respect to the 10 ft (3.0 m) receiver. The normalized attenuation data in Table 7.3 associated with the direct P-wave have been plotted in Fig. 7.39, along with the corresponding normalized data for Shaft A.

From wave propagation theory, it is expected that the direct wave amplitude at the 40 ft (12.2 m) receiver would be significantly reduced as a result of the attenuation effects of the overlying defect. This is shown in Fig. 7.39, where the 40 ft (12.2 m) receiver output for Shaft D is approximately $1/2$ of that registered at the same receiver in Shaft A. Furthermore, due to the proximity of the 30 ft (9.1 m) receiver to the defect, a larger direct wave amplitude is expected for this receiver. The larger receiver output would be due to the cumulative actions of the direct compression wave and reflected tension wave occurring at approximately the

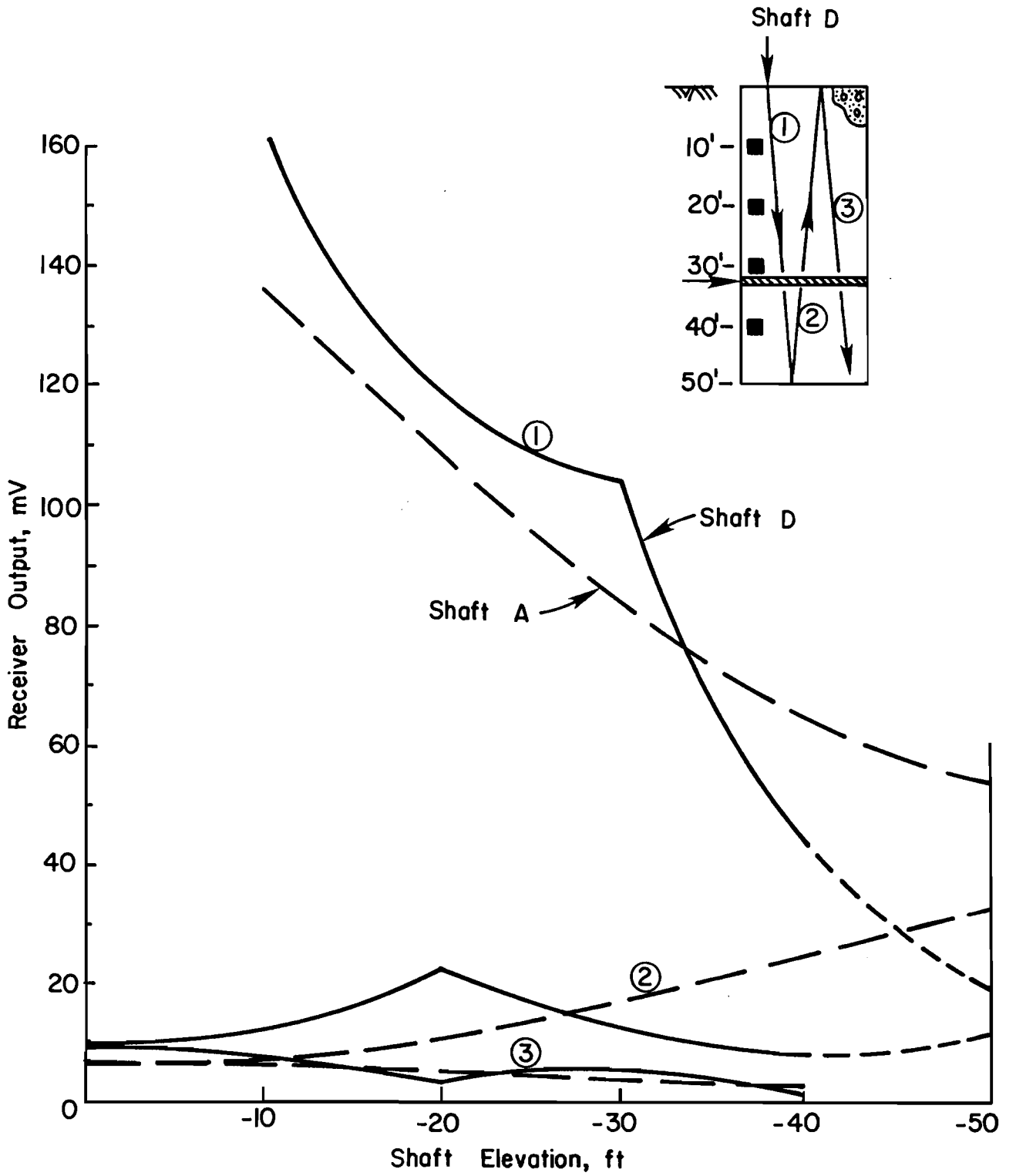


Fig. 7.37. Attenuation of P-wave in Shaft D (Houston site).

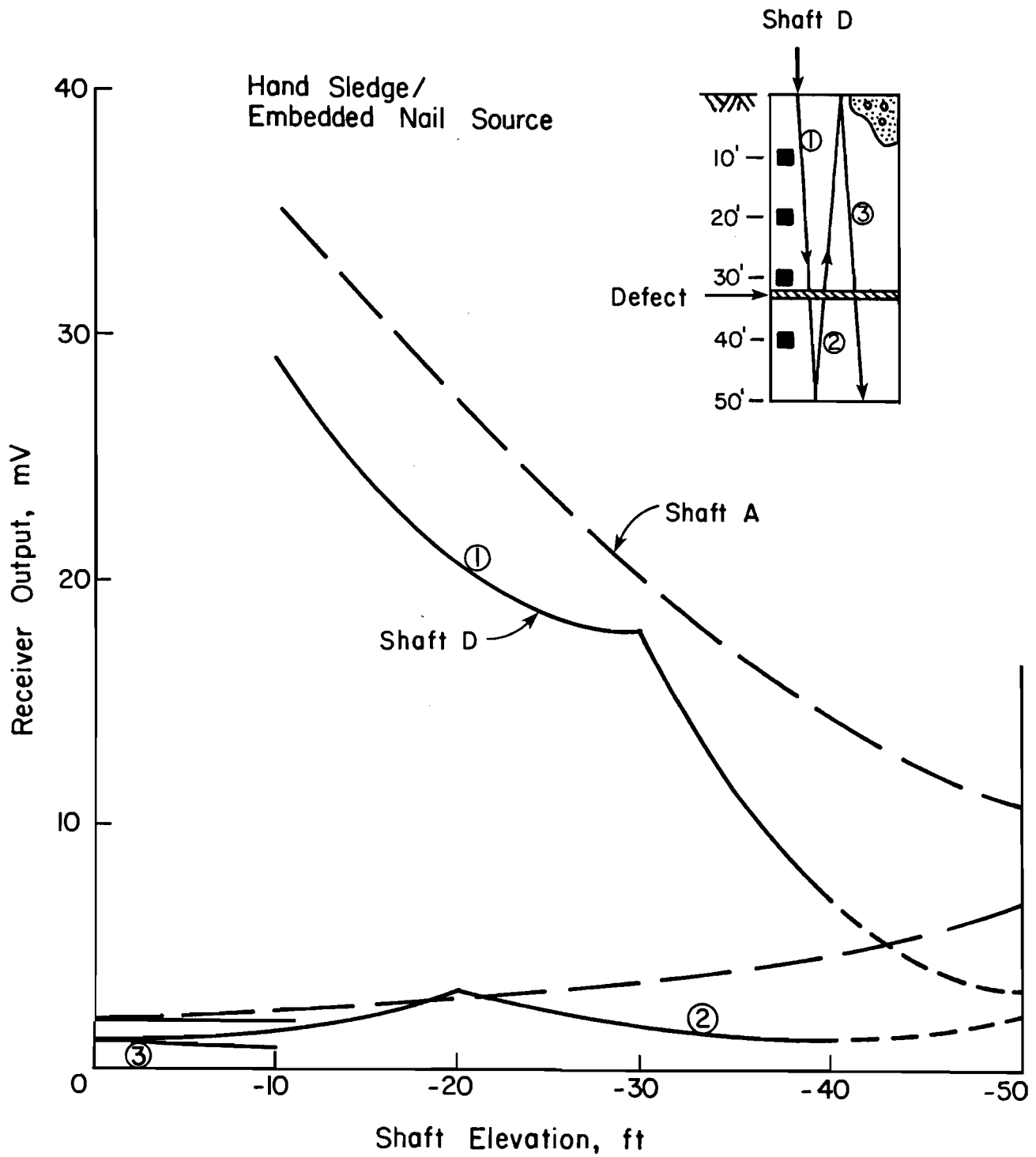


Fig. 7.38. Attenuation of P-wave in Shaft D (Houston site).

Table 7.3. SOURCE COMPARISON OF WAVE ATTENUATION
IN SHAFT D (HOUSTON SITE).

RECEIVER	CHANGE IN OUTPUT, PERCENT NORMALIZED TO 10 ft (3.0 m) RECEIVER)		
	<u>DROP HAMMER</u>	<u>HAND SLEDGE</u>	
①	20	73.5	69.2
	30	65.0	59.9
	40	26.3	23.1
②	40	4.5	4.9
	30	7.8	6.5
	20	13.7	10.6
	10	7.6	5.4
③	10	4.4	2.9
	20	2.0	1.4
	30	3.2	2.0
	40	0.6	—

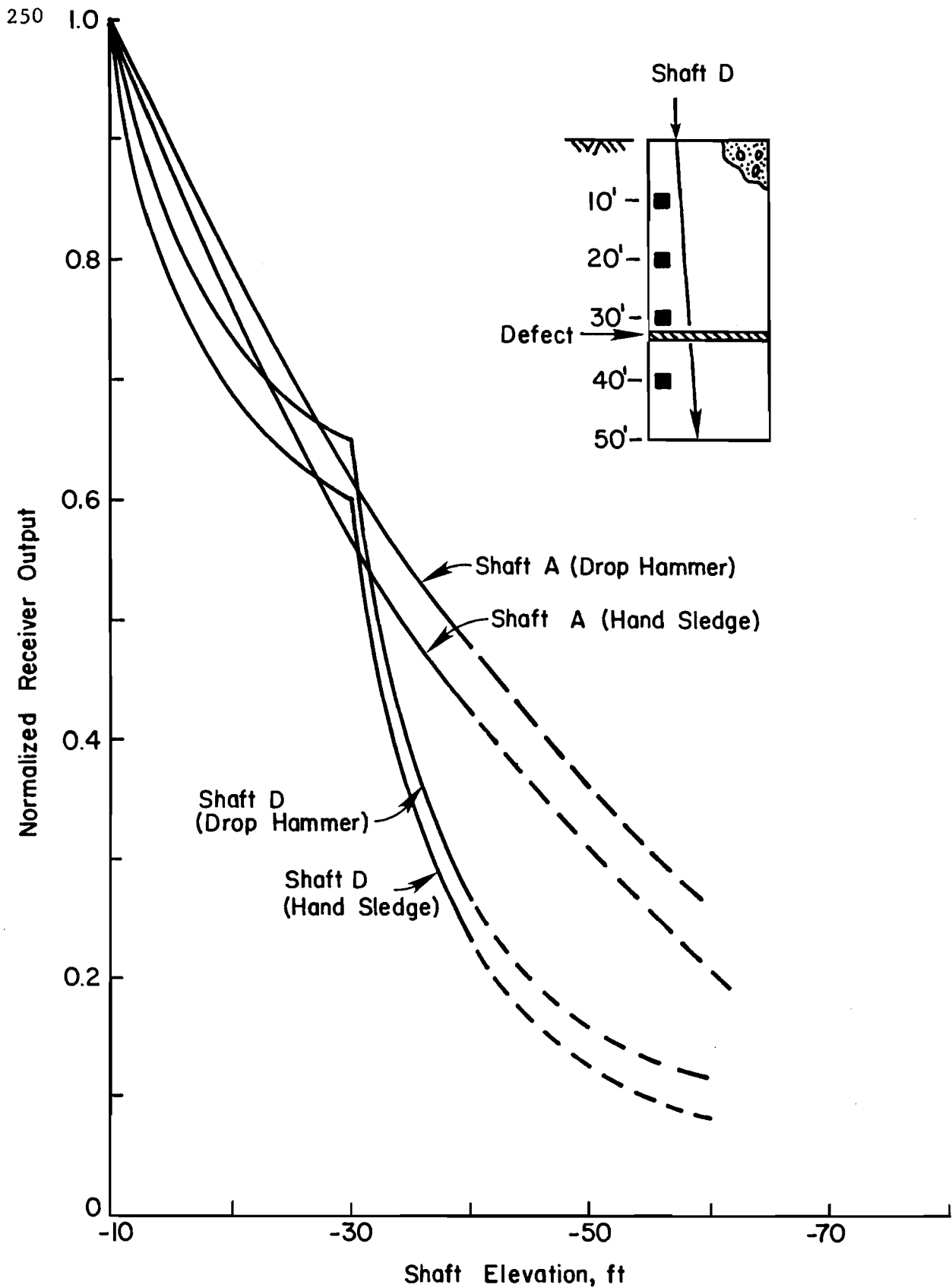


Fig. 7.39. Normalized attenuation of direct P-wave in Shaft D (Houston site).

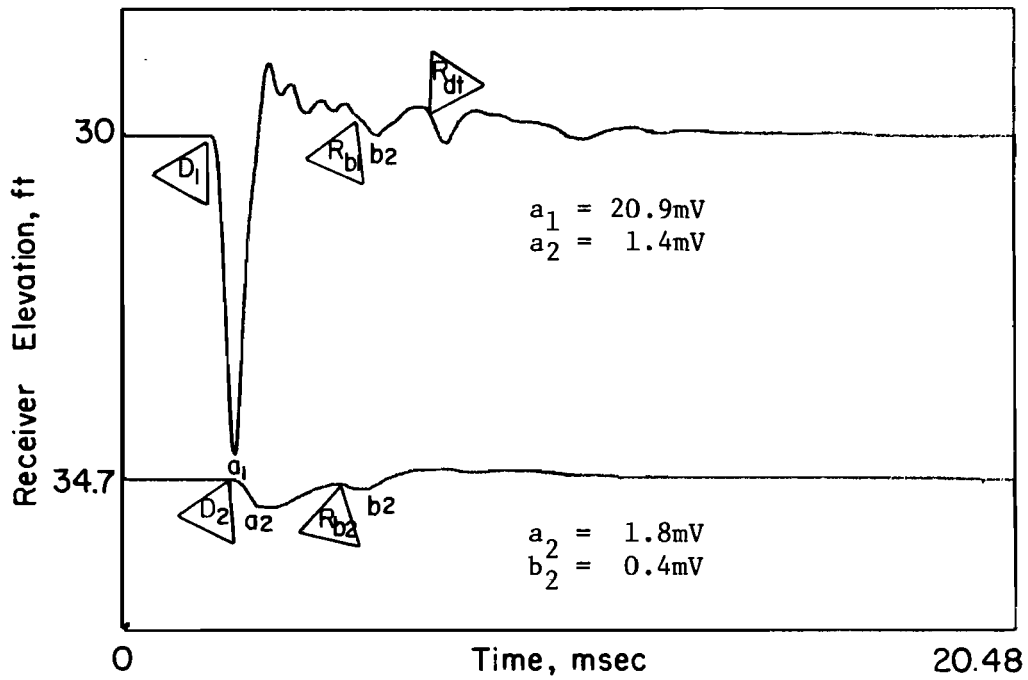
same time in the time domain measurement. This is also shown in Fig. 7.39, where the receiver output for Shaft D is slightly larger (approximately 6 percent) than output for the same receiver in Shaft A.

This phenomenon of overlapping compression and tension waves occurs again at further points in time in the wave propagation process. The first occurrence is registered at the 20 ft (6.1 m) receiver, as shown in Fig. 7.31 where the action of the tension wave reflected off the bottom of the pier occurs at the same time (approximately 6 msec in the time records) as compression wave energy reflected from the top of the pier. The summation of tension and compression wave amplitudes registered at the 20 ft (6.1 m) receiver is graphically shown in the receiver output associated with the wave reflection off the bottom of the pier in Figs. 7.37 and 7.38 and confirmed by the sudden increase in wave amplitude in the normalized data tabulated in Table 7.3.

The overlapping phenomenon is seen to occur again at approximately 10 msec in Fig. 7.31, in the wave signature associated with the 30 ft (9.1 m) receiver. Interpretation of the receiver output becomes complicated at this late time in the time domain record, due to the multiple wave reflections propagating within the pier. A review of Fig. 7.31 shows that wave excitation recorded at the 30 ft (9.1 m) receiver at approximately 10 msec subsequent to the initial impulse is the result of four wave reflections, these being: 1) the compression wave reflection from the bottom and then top of the pier; 2) the tension wave reflection from the bottom of the pier, the top of the pier, and then off the defect; 3) the tension wave reflected off the defect, the top of the pier, and then the bottom of the pier; and 4) the tension wave reflection resulting from wave reflections propagating between the defect and the bottom of the pier. Although contributing differing wave amplitudes due to variable degrees of wave attenuation, all of these wave

reflections provide some measure of excitation at the designated time at the 30 ft (9.1 m) receiver due to the coincidence of the above mentioned wave reflections. This point is shown in the graphical and tabulated data of Figs. 7.37 and 7.38 and Table 7.3.

The effects of the full cross-sectional area defect on wave propagation measurements are further illustrated in Figs. 7.40 and 7.41. In Fig. 7.40, wave excitation recorded at the 30 ft (9.1 m) and 34.5 ft (10.5 m) receivers are compared, while output recorded at the 30 ft (9.1 m) and 40 ft (12.2 m) receivers are presented in Fig. 7.41. It is interesting to note the changes in direct P-wave velocity caused by the defect. A direct P-wave travel time of 2.09 msec was recorded at the 30 ft (9.1 m) receiver, resulting in a direct P-wave velocity of 14,350 ft/sec (4,380 m/sec). The increase in P-wave velocity in this record in comparison with values computed in previous records presented in this chapter is attributable to differences in testing dates and the previously discussed fact that concrete stiffness and strength are both functions of time. The direct travel time of the P-wave at the 34.5 ft (10.5 m) receiver is approximately 2.60 msec, resulting in a direct P-wave velocity of 13,270 ft/sec (4,040 m/sec). As expected, the slower P-wave velocity associated with the soil inclusion resulted in an overall reduction in the direct travel time and, consequently, the velocity of the P-wave. However, the P-wave velocity computed using the direct travel time at the 40 ft (12.2 m) receiver is 14,230 ft/sec (4,340 m/sec), which compares favorably with the direct P-wave velocity computed for the 30 ft (9.1 m) receiver. The similarity in direct P-wave velocities for these two receivers is most likely attributable to the positioning of the 40 ft (12.2 m) receiver relative to the defect and the fact that the defect did not occupy the full cross-section of the pier. Nonetheless, this example illustrates



Sensitivity = $\pm 20\text{mV}$

D_1 = Direct wave arrival @ 30 ft (9.1 m) receiver, 2.09 msec

D_2 = Direct wave arrival @ 34.5 ft (10.5 m) receiver, 2.60 msec

R_{b1} = Reflected wave from bottom of pier to 30 ft (9.1 m) receiver, 5.35 msec

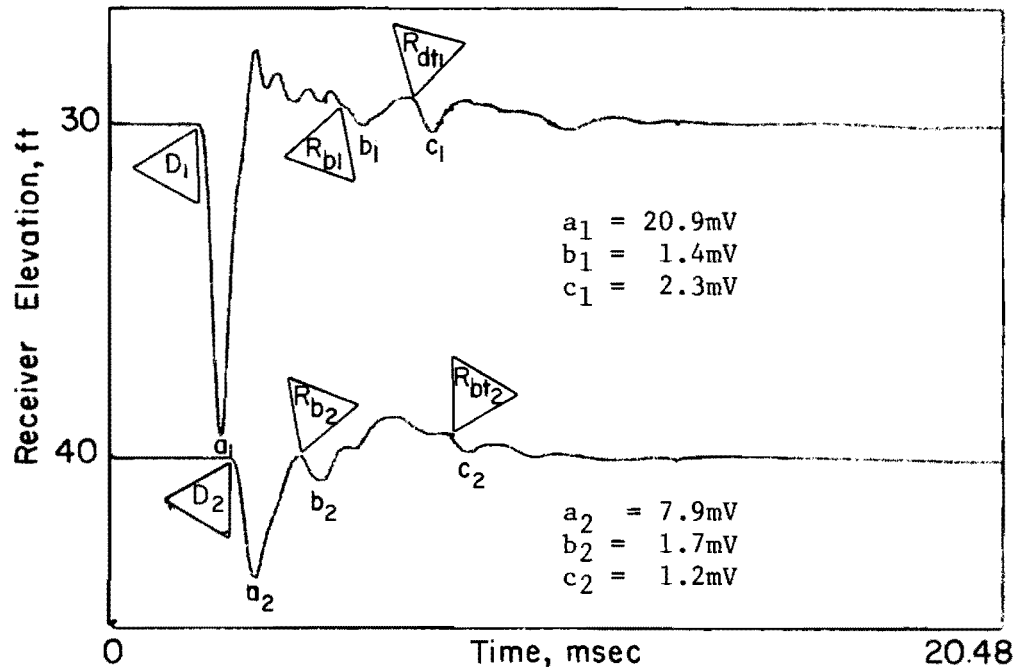
R_{b2} = Reflected wave from bottom of pier to 34.5 ft (10.5 m) receiver, 4.85 msec

R_{dt} = Reflected wave off defect and then top of pier, 6.65 msec

Pier Length = 50 ft (15.2 m)

Pier Diameter = 32 in (81.3 cm)

Fig. 7.40. Comparison of wave signatures for 30 ft (9.1 m) and 34.5 (10.5 m) velocity transducers in Shaft D (Houston site)



Sensitivity = $\pm 20\text{mV}$

- D_1 = Direct wave arrival @ 30 ft (9.1 m) receiver, 2.09 msec
 D_2 = Direct wave arrival @ 40 ft (12.2 m) receiver, 2.81 msec
 R_{b1} = Reflected wave from bottom of pier to 30 ft (9.1 m) receiver, 5.35 msec
 R_{b2} = Reflected wave from bottom of pier to 40 ft (12.2 m) receiver, 4.30 msec
 R_{dt1} = Reflected wave off defect and then top of pier to 30 ft (9.1 m) receiver, 6.65 msec
 R_{dt2} = Reflected wave off defect and then top of pier to 40 ft (12.2 m) receiver, 7.45 msec

Pier Length = 50 ft (15.2 m)
 Pier Diameter = 32 in (81.3 cm)

Fig. 7.41. Comparison of wave signatures for 30 ft (9.1 m) and 40 ft (12.2 m) velocity transducers in Shaft D (Houston site).

the need to assess both reflected wave arrivals and wave attenuation in conjunction with direct P-wave velocities. With the 34.5 ft (10.5 m) receiver eliminated, assessment of P-wave velocities only could have resulted in an erroneous conclusion of the integrity of the pier, even for a defect as large as that in Shaft D.

With regard to wave attenuation, the amplitude of the direct P-wave arrival at the 30 ft (9.1 m) receiver has been increased due to the previously mentioned cumulative action of the direct and reflected stress waves. Conversely, corresponding wave output recorded by the receivers located below the defect has been significantly attenuated, with the output recorded by the 34.5 ft (10.5 m) receiver distorted almost beyond recognition. Again, the unexpected increase in the output of the 40 ft (12.2-m) receiver in comparison to the 34.5 ft (10.5 m) receiver appears to be the positioning of the receivers in relation to the defect and the nearly full cross-sectional area of the defect.

SUMMARY

Measurements of wave propagation with embedded receivers were performed on the defective drilled piers at both the Granger and Houston sites. WAPER tests performed at the Granger site basically confirmed the findings of Arias. The full cross-section soil and styrofoam defect in Shaft 2 is easily identified in the recorded output and confirmed by assessing travel times of the wave reflections. With regard to Shaft 3, no early reflected wave arrivals resulting from either of the defects located within the pier were observed with the 18 ft (5.5 m) receiver. However, an indication of the existence of the sand and gravel defect is provided by assessing the measured and predicted travel times of the wave reflection off the bottom of the pier,

combined with the slower P-wave velocity associated with the bottom defect. In addition, the amplitude of the wave reflection from the bottom of the pier is small when compared to that obtained in Shaft 1 (sound pier), indicating the possibility of a pier defect or irregularity. A proper attenuation study employing multiple embedded receivers strategically located in the pier may have resulted in more positive identification of pier integrity.

Regarding the tests conducted on the defective drilled piers at the Houston site, several important points were determined. It was found that soil inclusions of a size on the order of 20 to 25 percent of the pier cross-sectional area may not be determined utilizing conventional wave propagation techniques. However, by viewing multiple receiver output on a single record, with the output positioned in the record in a manner similar to the positioning of the receivers in the pier, stress wave propagation patterns may become evident in the recorded output indicating possible additional reflection boundaries. The soil inclusions occupying one-half and the full cross-sectional areas in Shafts C and D, respectively, were identified by an assessment of the time domain records, although early reflected wave arrivals from the defect in Shaft C were not as prominent as expected.

An attention study of multiple receiver outputs is recommended in conjunction with travel time assessments. Normalization of the direct wave amplitudes of multiple receiver outputs was shown to be an effective method of assessing wave propagation attenuation in drilled piers founded in cohesive soils. With regard to the defective drilled piers at the Houston site, normalization of the multiple receiver output with the 10 ft (3.0 m) receiver resulted in several significant findings. In comparison with the corresponding output for Shaft A (sound pier), wave energy was found to attenuate at a faster rate in the initial 30 ft (9.1 m) of wave travel in

Shafts B and C. Below 30-ft (9.1-m) in Shafts B and C, wave attenuation decreased with respect to that measured in Shaft A. This phenomenon seems to contradict wave attenuation theory, in that the defects are expected to act as boundaries for wave reflection, reducing the energy of the incident wave and, thus, resulting in a decreased output at the 40-ft (12.2-m) receivers. Possible causes for this effect include differences in materials surrounding the piers, including adjacent piers, and frequency discrepancies. Wave attenuation in Shaft D correlates well with that predicted by theory.

WAPS tests conducted on Shafts B and C successfully monitored wave reflection from the bottom of the piers, allowing determination of the pier lengths. However, receiver output for the WAPS tests conducted on Shaft B showed no indication of the 1/4 cross-sectional area defect present in the pier. Wave reflections off the 1/2 cross-sectional area defect were visible in the WAPS output for Shaft C. Based on these results, it is concluded that successful evaluation of drilled pier integrity is probable for pier defects occupying 1/2 or more of the cross-sectional area of the pier. The depth and nature of the defect influences the success of the method, as do the characteristics of the generated surface waves. The influence of surface waves were illustrated in the WAPS tests on Shaft D, where the surface waves were seen to propagate across the top of the pier for a sufficient period of time to mask the identification of the wave reflection off the full cross-sectional area defect. However, the absence of the wave reflection from the bottom of Shaft D provides an indication of the possible presence of a defect, the magnitude of the defect most likely large based on the degree of wave attenuation.

Similar to the results of the WAPS tests, piezoelectric ceramic

transducers were shown to monitor effectively wave reflections from the bottom of Shaft C, but no clearly defined wave reflections off the 1/2 cross-sectional area defect were apparent in the receiver output. Nevertheless, the successful monitoring of wave reflections from the bottom of the pier warrant further study of the capabilities of piezoelectric ceramic transducers as monitors of wave propagation in drilled piers.

Finally, wave propagation evaluation of the special case of unreinforced drilled piers was proven feasible. Wave signatures from "floating" velocity transducers attached to special sleeves and embedded at specified depths in Shafts B and D using the foundation drilling rig compared favorably with output recorded by conventional, reinforcing-attached receivers.

CHAPTER 8. CONCLUSIONS

In recent years, the construction industry has experienced an increase in the use of drilled pier foundations for the support of new buildings and bridges. The interest in drilled pier foundations appears to be the result of several factors, these being: the growth in population over the years, and the need for new multi-story structures and large highway systems; the advent of large, efficient crane-mounted drilling and excavation equipment capable of constructing large foundation members; and an increased number of documented case histories and experimentation focusing on drilled pier behavior.

The primary purpose of utilizing a drilled pier foundation for structural support is to transmit structural loads through shallow, undesirable subsurface conditions down to a firmer substratum, such as bedrock. Unfortunately, problems can occur when constructing through the weaker subsurface materials, attributable to either the subsurface conditions or the construction process, that can result in drilled piers of questionable integrity. Because defective drilled piers could have catastrophic effects on the ultimate performance of the supported structure, an effective, economical method is needed for assessing drilled pier integrity prior to loading of the foundation.

Various methods of evaluating drilled pier integrity are referenced in the literature. Test results utilizing these methods vary substantially, and each method appears to possess one disadvantage or another, whether it be

equipment setup, data interpretation, or costs. However, one method, simply referred to as the stress wave propagation method, has recently shown promise as an effective, economical technique of assessing pier integrity. In an attempt to improve upon the basic wave propagation testing technique and further assess the capabilities of this method, a research program at the Center for Transportation Research at The University of Texas at Austin was undertaken.

Wave propagation in drilled piers is theoretically described by the behavior of elastic waves propagating in rods. In general, piers in soil behave as free-ended members, that is, a compression wave is reflected from the end of the pier as a tension wave, and a tension wave is reflected as a compression wave. Because of embedded boundary constraints, total reflection of wave energy does not occur at the bottom of the pier. A certain percentage of the incident wave energy is transmitted into the bearing stratum, while the remaining wave energy is reflected back through the pier.

Two wave propagation methods previously established were used in this study, each method described by the receiver location. The wave-propagation-with-embedded-receiver method, or WAPER method, uses velocity transducers attached to the reinforcing cage at known elevations to monitor wave excitation. The wave-propagation-with-surface-receiver method, or WAPS method, uses a transducer or accelerometer bonded to the top of the pier to monitor wave excitation. Various hammer-type sources are used to generate the compression wave at the top of the pier, and an oscilloscope is used to monitor and store wave signatures.

Drilled piers constructed at two sites were tested in this research program. The first site, located near Granger, Texas, had three previously constructed drilled piers, one being sound and two having planned defects of

equipment setup, data interpretation, or costs. However, one method, simply referred to as the stress wave propagation method, has recently shown promise as an effective, economical technique of assessing pier integrity. In an attempt to improve upon the basic wave propagation testing technique and further assess the capabilities of this method, a research program at the Center for Transportation Research at The University of Texas at Austin was undertaken.

Wave propagation in drilled piers is theoretically described by the behavior of elastic wave propagating in rods. The pier-end behavior is considered free, that is, a compression wave is reflected from the end of the pier as a tension wave, and a tension wave is reflected as a compression wave. Because of embedded boundary constraints, total reflection of wave energy does not occur bottom of the pier. A certain percentage of the incident wave energy is transmitted into the bearing stratum, while the remaining wave energy is reflected back through the pier.

Two wave propagation methods previously established were used in this study, each method described by the receiver location. The wave propagation with embedded receiver, or WAPER, method uses velocity transducers attached to the reinforcing cage at known elevations to monitor wave excitation. The wave propagation with surface receiver method, or WAPS, uses a transducer or accelerometer bonded to the top of the pier to monitor wave excitation. Various hammer-type sources are used to generate the compression wave at the top of the pier, and an oscilloscope is used to monitor and store wave signatures.

Drilled piers constructed at two sites were tested in this research program. The first site, located near Granger, Texas, had three previously constructed drilled piers, one being sound and two having planned defects of

varying types and sizes. Tests were conducted on these piers to confirm the previously reported results and to evaluate the suitability of new test equipment. As a supplemental study, four drilled piers were constructed at a site in Houston, Texas. One of the piers had no planned defects, while the other three were constructed with soil inclusions varying in size between one-quarter to the full cross-sectional area of the pier. Tests were conducted on these piers to evaluate further equipment modifications and assess the effects of a defect on wave propagation measurements. Results of these test programs are presented in the following paragraphs.

In regard to equipment modifications, a digital oscilloscope proved to be far superior to the previously used analog storage oscilloscopes. Advantages of the digital oscilloscope in wave propagation measurements include high resolution, mid-signal triggering capabilities for assessing pre-trigger information, both waveform expansion and superposition capabilities, magnetic disk storage capabilities and the ability to produce hard copies. Concerning the source evaluation, the hand-sledge-and-embedded nail configuration provided consistently clear, interpretable wave signatures. Accelerometers provided optimum surface receiver data, and vertical velocity transducers are still considered the best embedded receivers.

In regard to the test methods, the WAPER method is considered superior to the WAPS method in assessing reflection boundaries in drilled piers. Use of the WAPER method allows direct computation of P-wave velocity and, when using two or more receivers, allows an attenuation study of wave amplitude. The major disadvantage of this method is that instrumentation must be installed in the pier prior to pier construction. The WAPS method is economical and easily implemented in the field. However, the method is

hampered by surface waves propagating across the top of the pier, which tend to mask reflected wave arrivals. It is, therefore, recommended that WAPS tests be used primarily to supplement WAPER tests of drilled piers on a project.

Concerning the measurements performed on the sound piers, the wave propagation technique was successful in concluding sound pier integrity. Of the defective piers, the full cross-sectional area defects of Shaft 2 (Granger) and Shaft D (Houston) as well as the 1/2 cross-sectional area defect of Shaft C (Houston) were easily identifiable in the recorded wave signatures. The sand and gravel defect at the bottom of Shaft 3 (Granger) was detected by assessing reflected wave arrivals and by observing the reduced amplitude of the reflection off the bottom of the shaft. These results confirmed the importance of utilizing multiple receivers and performing an attenuation study of the receiver output. The 1/4 cross-sectional area defect of Shaft B (Houston) was not distinguishable in an assessment of single receiver data. However, by using multiple receivers and by presenting the data in a format simulating the receiver locations, the wave paths of reflected waves off the small defect was visible. These results further confirmed the recommended use of multiple receivers for assessing pier integrity.

Attenuation studies of the four test piers in Houston revealed some interesting points. Wave attenuation in Shaft D correlated well with theory. Wave attenuation in Shaft B was similar to that of Shaft A, which is indicative of minimal effects of a small defect. However, attenuation results in Shaft C were somewhat erratic for the initial stages of wave propagation. Possible explanations for results include pier embedment conditions, frequency variations in source impulse, and improper receiver

performance. Additional research, utilizing frequency spectrum analysis, is recommended to assess the effects of frequency content on wave attenuation.

REFERENCES

1. Arias, R.P., "Evaluation of Drilled Shaft Integrity by Non-Destructive Methods," M.S. Thesis, The University of Texas at Austin, 1977.
2. Baker, C.N. and F. Khan, "Caisson Construction Problems and Correction in Chicago," Journal of the Soil Mechanics and Foundation Division, ASCE, February, 1971, Vol. 97, pp. 417-440.
3. Bancroft, D., "The Velocity of Longitudinal Waves in Cylindrical Bars," Physical Review, April, 1971, Vol. 59, pp. 588-593.
4. "Caisson Trouble Hits Chicago," Engineering News Record, September 29, 1966, p. 14.
5. Davies, R.M., "A Critical Study of the Hopkinson Pressure Bar," Philosophical Transactions of the Royal Society, January, 1948, Vol. 240, pp. 375-457.
6. Davis, A.G. and C.S. Dunn, "From Theory to Field Experience with the Non-Destructive Vibration Testing of Piles," Proceedings of the Institution of Civil Engineers, Part 2, December, 1974, 57, pp. 571-593.
7. Davis, A.G. and S.A. Robertson, "Vibration Testing of Piles," The Structural Engineer, June, 1976, pp. A7-A10.
8. Ewing, W.M., W.S. Jardetzky, and F. Press, Elastic Waves in Layered Media, McGraw-Hill Book Company, New York, NY, 1957.
9. Feld, J., Construction Failure, John Wiley and Sons Ltds., 1968, p. 78.
10. Gardner, R.P.M. and G.W. Moses, "Testing Bored Piles Formed in Laminated Clays," Civil Engineering and Public Works Review, January, 1973, pp. 60-63.

11. Hearne, T.M., Jr., "Evaluation of Drilled Shaft Integrity by Stress Wave Propagation Method," Ph.D. Dissertation in preparation, The University of Texas at Austin.
12. Hearn, T.M., Jr., K.H. Stokoe, II, and L.C. Reese, "Evaluation of Drilled Pier Integrity by Seismic Wave Propagation Method," Journal of the Geotechnical Engineering Division, ASCE, Vol. 107, No. GT10, October, 1981, pp. 1327-1344.
13. Hudson, G.E., "Dispersion of Elastic Waves in Solid Circular Cylinders," Physical Review, January, 1943, Vol. 63, pp. 46-51.
14. Kolsky, H., Stress Waves in Solids, Dover Publications, Inc., 1963.
15. Love, A.E.H., A Treatise on the Mathematical Theory of Elasticity, Dover Publications, Inc., New York, NY, 4th Edition, 1944, p. 287.
16. Malhotra, V.M., Testing Hardened Concrete: Non-Destructive Methods, Iowa State University Press, Ames, Iowa, and American Concrete Institute, Detroit, Michigan, 1976, p. 87.
17. Mitchell, J.M. "Assessing Large Diameter Piles," The Consulting Engineer, December, 1973, pp. 37-39.
18. Preiss, K., H. Weber, and A. Caiserman, "Integrity Testing of Bored Piles and Diaphragm Walls," The Civil Engineer in South Africa, August, 1978, pp. 191-196.
19. Reese, L.C., "Design and Construction of Drilled Shafts," Twelfth Terzaghi Lecture, National Meeting, ASCE, Philadelphia, PA, September, 1976.

20. Reese, L.C. and S.G. Wright, "Construction of Drilled Shafts and Design for Axial Loading," Drilled Shaft Design and Construction Guidelines Manual, Vol. 1, U.S. Dept. of Transportation, July, 1977.
21. Richart, F.E., Jr., J.R. Hall, Jr., and R.D. Woods, Vibrations of Soils and Foundations, Prentice-Hall, Inc., 1970, pp. 61-62.
22. Robertson, S.A., "Vibration Testing," The Consulting Engineer, January, 1976, pp. 36-38.
23. Shear, S.K. and A.B. Focke, "The Dispersion of Supersonic Waves in Cylindrical Rods of Polycrystalline Silver, Nickel and Magnesium," Physical Review, March, 1940, Vol. 57, pp. 532-537.
24. Soil Survey of Harris County, Texas, United States Department of Agriculture Soil Conservation Service, August, 1976, p. 19.
25. Steinbach, J., "Caisson Evaluation by the Stress Wave Propagation Method," Ph.D. Dissertation, Illinois Institute of Technology, 1971.
26. Steinbach, J. and E. Vey, "Caisson Evaluation by Stress Wave Propagation Method," Journal of the Geotechnical Engineering Division, ASCE, April, 1974, Vol. 101, pp. 361-378.
27. "Testing Halt John Hancock Work," Engineering News Record, August 18, 1966, p. 18.
28. Timoshenko, S.P. and J.N. Goodier, Theory of Elasticity, McGraw-Hill Book Company, Inc., 1934, pp. 492-496.
29. Whitaker, T., "Structural Integrity of Piles," Civil Engineering, June, 1974, pp. 20-23.

30. Van Koten, H. and P. Middendorp, "Investigation of Results from Integrity Tests and Dynamic Load Tests," Delft Netherlands, 1977.